



UNIL | Université de Lausanne

Unicentre

CH-1015 Lausanne

<http://serval.unil.ch>

Year : 2021

Radiolabeling and preclinical theranostic study of anti TEM-1 scFv-Fc fusion proteins in a mouse neuroblastoma model

Delage Judith

Delage Judith, 2021, Radiolabeling and preclinical theranostic study of anti TEM-1 scFv-Fc fusion proteins in a mouse neuroblastoma model

Originally published at : Thesis, University of Lausanne

Posted at the University of Lausanne Open Archive <http://serval.unil.ch>

Document URN : urn:nbn:ch:serval-BIB_817B796FD18C5

Droits d'auteur

L'Université de Lausanne attire expressément l'attention des utilisateurs sur le fait que tous les documents publiés dans l'Archive SERVAL sont protégés par le droit d'auteur, conformément à la loi fédérale sur le droit d'auteur et les droits voisins (LDA). A ce titre, il est indispensable d'obtenir le consentement préalable de l'auteur et/ou de l'éditeur avant toute utilisation d'une oeuvre ou d'une partie d'une oeuvre ne relevant pas d'une utilisation à des fins personnelles au sens de la LDA (art. 19, al. 1 lettre a). A défaut, tout contrevenant s'expose aux sanctions prévues par cette loi. Nous déclinons toute responsabilité en la matière.

Copyright

The University of Lausanne expressly draws the attention of users to the fact that all documents published in the SERVAL Archive are protected by copyright in accordance with federal law on copyright and similar rights (LDA). Accordingly it is indispensable to obtain prior consent from the author and/or publisher before any use of a work or part of a work for purposes other than personal use within the meaning of LDA (art. 19, para. 1 letter a). Failure to do so will expose offenders to the sanctions laid down by this law. We accept no liability in this respect.



UNIL | Université de Lausanne

Faculté de biologie
et de médecine

Département de Médecine nucléaire et imagerie moléculaire

Radiolabeling and preclinical theranostic study of
anti TEM-1 scFv-Fc fusion proteins in a mouse neuroblastoma model

Thèse de doctorat ès sciences de la vie (PhD)

présentée à la

Faculté de biologie et de médecine
de l'Université de Lausanne

par

Judith DELAGE

PharmD, Faculty of Medicine, Rouen, France
MSc (Cancerology) Faculty of Medicine University Paris XI - ENS Cachan, France

Jury

Prof. Sven Bergmann, Président
Prof. John O. Prior, Directeur de thèse
Prof. Alain Faivre-Chauvet, Co-directeur de thèse
Dre Nathalie Rizzo-Padoin, Experte
Prof. Farshid Sadeghipour, Expert

Lausanne 2021

Imprimatur

Vu le rapport présenté par le jury d'examen, composé de

Président·e	Monsieur	Prof.	Sven	Bergmann
Directeur·trice de thèse	Monsieur	Prof.	John O.	Prior
Co-directeur·trice	Monsieur	Prof.	Alain	Faivre-Chauvet
Expert·e·s	Madame	Dre	Nathalie	Rizzo-Padoin
	Monsieur	Prof.	Farshid	Sadeghipour

le Conseil de Faculté autorise l'impression de la thèse de

Madame Judith Anna Delage

Docteure en pharmacie, Faculté de Médecine de Rouen, France

intitulée

**Radiolabeling and preclinical theranostic study of
anti TEM-1 scFv-Fc fusion proteins in a mouse
neuroblastoma model**

Lausanne, le 17 décembre 2021

pour le Doyen
de la Faculté de biologie et de médecine



Prof. Sven Bergmann

Acknowledgements

Mes remerciements vont,

Au Professeur John Prior, directeur de thèse

John, je te remercie vivement pour ton écoute et ton soutien tout au long de ce projet de thèse. Merci pour la confiance que tu m'as accordée et de m'avoir donné les moyens de travailler sur ce projet de recherche épanouissant. Je souhaite que nous puissions continuer à développer des travaux innovants au cours de ces prochaines années.

Au Professeur Alain Faivre-Chauvet, co-directeur de thèse

Alain je te remercie infiniment pour ton aide et ton accompagnement sans relâche au cours de ce PhD. Merci pour le partage et la transmission d'une partie de tes très nombreuses connaissances dans le domaine de la radio-immunothérapie. Ces années ont été pour moi motivantes, riches de découvertes et m'ont donné l'envie de poursuivre des travaux de recherche sur la base de tes enseignements.

A mon jury de thèse,

Professeur Sven Bergman, président du jury,

Thank you very much for taking the time to read and assess my thesis manuscript and to organize my thesis defense.

Docteur Nathalie Rizzo-Padoin, Experte

Nathalie, je te remercie d'avoir accepté d'évaluer ce travail. C'est un réel honneur pour moi de bénéficier de ta grande expertise dans ce jury de thèse. Je souhaite vivement que nous puissions continuer à développer les échanges « Suisso-Caribéens » sur les radiopharmaceutiques que nous avons eus au cours de ces dernières années.

Professeur Farshid Sadeghipour, Expert

Farshid, je te remercie d'avoir accepté de faire partie des membres de mon jury. Je te suis reconnaissante de m'avoir encouragée durant toutes ces années et de m'avoir permis de réaliser ce travail en parallèle de mes fonctions de responsable d'unité. Merci pour ta bienveillance et ton soutien, c'est pour moi un réel plaisir de faire partie de ton service.

Je tiens également à remercier,

The L-AbCore team, especially Dr Steven Dunn and Dr Julie Fierle who produced and provided the antibody, which is the heart of this thesis. Thanks a lot for your help and all your advice. The collaboration between our two laboratories have been very stimulating and promising. I am sure we will continue to work together to develop optimal radio-immunoconjugates. Great perspectives for the future !

Les collaborateurs de l'équipe 13, unité Inserm 1232 du Centre de Recherche en Cancérologie et Immunologie Nantes-Angers (CRCINA) et de la plateforme d'imagerie CIMA pour leur excellent accueil lors de mes stages à Nantes qui ont été très riches et formateurs.

Je remercie Michel Chérel qui m'a permis de réaliser ces stages dans son équipe.

Je tiens à remercier particulièrement Patricia Remaud-Le Saëc et Séverine Marionneau- Lambot pour leur aide précieuse, le partage de leur expertise et leur gentillesse.

Je garde un excellent souvenir de mes expériences sur Nantes et souhaite vivement qu'un lien privilégié soit maintenu entre nos centres.

L'équipe du GIP Arronax et en particulier le Docteur Jacques Barbet pour son accompagnement et son précieux support pour la réalisation de modélisations pharmacocinétiques.

L'équipe du Translational Radiopharmaceutical Sciences Group, la Professeure Margret Schotellius pour les échanges fructueux que nous avons pu avoir et le Docteur David Viertel pour son soutien et sa formation aux techniques de biodistribution et d'imagerie.

L'ensemble des membres de l'équipe de radiopharmacie pour leur aide, leur motivation et leur travail de grande qualité qui permettent chaque jour à notre unité d'avancer vers de nouveaux défis.

L'ensemble de l'équipe du service de médecine nucléaire pour sa collaboration et particulièrement le Professeur Niklaus Schaefer pour son implication dans ce projet et le Docteur Silvano Gnesin pour son aide dans la réalisation d'études de dosimétrie.

Professor Georges Coukos for supporting this research work.

Mes amis pour leur présence et leurs constants encouragements.

Mes parents, ma sœur Carole et Alexis. Cette thèse marque la clôture de ma vie d'étudiante, un grand merci pour votre accompagnement sans faille.

Abstract

Antibodies recognizing specific tumor targets can be used to deliver therapeutic payloads with high degree of specificity. The simultaneous use of the same antibody, combined with different radionuclides for imaging and for therapy, an approach named “theranostics”, offers unique opportunities for personalizing therapy and rapidly assessing therapeutic response at a molecular level. Two major challenges in the field of theranostics have been the identification of suitable tumor-specific targets and the development of high-affinity antibodies.

For this project, we decided to target the tumor endothelial marker 1 (TEM-1), a type I single-pass transmembrane cell surface glycoprotein, described as an excellent therapeutic antigen, since it is tumor-specific and expressed in the neo-vasculature.

A panel of novel scFv-Fc fusion antibody constructs targeting murine and human TEM-1 have been developed by the LabCore laboratory (Ludwig Institute for Cancer Research, Lausanne). Among them, 1C1m-Fc was shown to be the best candidate and was selected to be extensively studied preclinically in this thesis work. 1C1m-Fc was conjugated to the chelator p-SCN-Bn-DOTA using different molar ratio and radiolabeled either with ^{64}Cu or ^{177}Lu . *In vitro* and *in vivo* characterization in xenograft models were performed to assess the immunoreactivity, the pharmacokinetic behavior and the dosimetry profile of our radiolabeled compound and to determine if this new radiolabeled probe is suitable for a theranostic application.

Our experimental results first highlighted the potential of [^{177}Lu]Lu-1C1m-Fc to target TEM-1. Then, we have shown that the number of DOTA per antibody plays a determining role in tumor targeting and that a high DOTA ratio has an impact on the biodistribution, the immunoreactivity and the pharmacokinetic behavior of our radiolabeled compound. The number of chelators has to be as low as possible to maintain a balance between these parameters and the radiochemical yield. We also demonstrated that [^{64}Cu]Cu-1C1m-Fc allows to visualize TEM-1 in positron emission tomography (PET-scan) with high quality images and could be an interesting companion of [^{177}Lu]Lu-1C1m-Fc therapy to predict its efficacy and safety.

Our findings have shed some light on the role of the DOTA conjugation on the *in vivo* behavior of a radiolabeled compound. This finding is an opportunity to further improve the biodistribution and imaging contrast of radiopharmaceuticals. Furthermore, our study highlights the interest of a theranostic targeting of TEM-1 with a new radiolabeled antibody. The promising results appear as a prelude to a future translation in patients.

Résumé

La reconnaissance spécifique de cibles tumorales par les anticorps peut être utilisée en thérapie anticancéreuse. L'utilisation simultanée du même anticorps combiné à différents radionucléides pour l'imagerie et la thérapie, une approche appelée "théranostique", offre des possibilités uniques de personnaliser le traitement des patients et d'évaluer rapidement la réponse thérapeutique au niveau moléculaire. Deux défis majeurs pour cette approche ont émergé : l'identification de cibles spécifiques des tumeurs et le développement d'anticorps à haute affinité. Pour ce projet, nous avons décidé de cibler le marqueur tumoral endothélial (TEM-1), glycoprotéine transmembranaire de type I, décrite comme un excellent antigène thérapeutique en raison de sa spécificité tumorale et de son expression dans les néo-vaisseaux.

Un panel de nouvelles protéines de fusion, scFv-Fc, ciblant le TEM-1 murin et humain a été développé par le laboratoire LabCore (Ludwig Institute for Cancer Research, Lausanne). Parmi ces anticorps, le 1C1m-Fc s'est avéré être le meilleur candidat et a été sélectionné et étudié précliniquement dans ce travail de thèse. Le 1C1m-Fc a été conjugué au chélateur p-SCN-Bn-DOTA en utilisant différents ratios moléculaires avant d'être radiomarqué avec du ^{64}Cu ou du ^{177}Lu . Une caractérisation *in vitro* et *in vivo* faisant appel à des modèles de xéno-greffes ont été réalisées pour évaluer l'immunoréactivité, le profil pharmacocinétique et dosimétrique de notre anticorps radiomarqué et pour déterminer si ce dernier était adéquat pour un usage théranostique.

Nos résultats expérimentaux ont tout d'abord permis de mettre en évidence le potentiel du [^{177}Lu]Lu-1C1m-Fc pour cibler TEM-1. Nous avons ensuite prouvé que le nombre de DOTA par anticorps joue un rôle déterminant dans le ciblage tumoral et qu'un nombre élevé de DOTA a un impact sur la biodistribution, l'immunoréactivité et le comportement pharmacocinétique de notre anticorps radiomarqué. Le nombre de chélateurs doit être aussi faible que possible pour maintenir un équilibre entre ces différents paramètres et le rendement radiochimique. Nous avons également démontré que le [^{64}Cu]Cu-1C1m-Fc permet de cibler le TEM-1 en tomographie par émission de positons (TEP-scan) avec des images de haute qualité et que la dosimétrie résultante pourrait être un indicateur prédictif de l'efficacité et de la sécurité d'un traitement au [^{177}Lu]Lu-1C1m-Fc.

Nos résultats ont mis en lumière le rôle de la conjugaison DOTA sur le comportement *in vivo* d'un composé radiomarqué. Cette découverte donne l'opportunité d'améliorer la biodistribution et le contraste en imagerie des radiopharmaceutiques. De plus, notre étude souligne l'intérêt d'un ciblage théranostique de TEM-1 avec un nouvel anticorps radiomarqué. Ces résultats prometteurs pourraient ouvrir la voie vers une future application chez les patients.

Table des matières

List of Figures/Tables	3
List of abbreviations	4
Introduction	6
1- Theranostic approach in nuclear medicine	6
1-1 Imaging in nuclear medicine	6
1-1-1 Background	6
1-1-2 Principles of SPECT and PET imaging	6
1-1-3 Quantitative imaging	8
1-2 Radiotheranostics in cancer diagnosis and management.....	9
1-2-1 Concept	9
1-2-2 Current Clinical applications	10
1-3 Optimization of RIT approach.....	15
1-3-1 Antibody engineering.....	15
1-3-2 Most appropriate isotopes and chelators for RIT	16
1-3-3 Protocol: Pretargeting and Fractionated Dose	17
2- TEM-1 (tumor endothelial marker 1).....	19
2-1 Background	19
2-2 Molecular characteristics.....	19
2-3 Gene regulation and binding partners of TEM-1	21
2-3-1 Gene regulation.....	21
2-3-2 TEM-1 interaction partners	21
2-4 Physiological expression of TEM-1	23
2-4-1 <i>In vitro</i> expression of TEM-1	23
2-4-2 TEM-1 expression during development	23
2-5 Pathological expression of TEM-1.....	24
2-5-1 TEM-1 expression during inflammation and fibrosis	24
2-5-2 TEM-1 expression in Cancer	25
3- Targeting TEM-1: Potential applications in clinic.....	28
3-1 Background	28
3-2 TEM-1 and neuroblastoma	28
3-3 Anti TEM-1 in clinical trials	29
3-4 TEM-1 targeting experimental therapeutics	30
3-4-1 Antibody-drug conjugates	30
3-4-2 Specific DNA vaccination	32

3-4-3 TEM-1 Imaging	33
3-4-4 First fully human anti-TEM-1 sc-Fv	34
3-4-5 1C1m-Fc a novel anti TEM-1 fusion protein antibody	36
4- Conclusion	37
Summary of results	38
Chapter 1: ¹⁷⁷ Lu radiolabeling and preclinical theranostic study of 1C1m-Fc: an anti-TEM-1 scFv-Fc fusion protein in soft tissue sarcoma	38
Chapter 2: Impact of DOTA Conjugation on Pharmacokinetics and Immunoreactivity of [¹⁷⁷ Lu]Lu-1C1m-Fc, an Anti TEM-1 Fusion Protein Antibody in a TEM-1 Positive Tumor Mouse Model	42
Chapter 3: Copper-64-labeled 1C1m-Fc, a new tool for TEM-1 PET imaging and prediction of Lutetium-177-labeled 1C1m-Fc therapy efficacy and safety.....	46
Discussion	50
1- Main findings of the project	50
1-1 Interest of a new type of fusion protein antibody	50
1-2 Validation of the radionuclide used for theranostic approach	51
1-3 Determination of the dose and of the condition of pre-saturation.....	52
1-4 Impact of the conjugation.....	52
1-5 Interest of pharmacokinetic modeling.....	53
2 - Perspectives of this study	54
2-1 Optimisation of the radioimmunoconjugate	54
2-1-1 New fusion protein antibody	54
2-1-2 Site specific conjugation	54
2-1-3 Test of new bifunctional ligands.....	55
2-1-4 Test of other radionuclides	56
2-2 Complementary experiments necessary for human translation study	56
2-2-1 Preclinical therapeutic experiment.....	56
2-2-2 Dosimetric study with human extrapolation.....	57
2-3 From bench to bedside	57
Conclusion.....	59
References.....	60
Appendix : Articles.....	70
Article 1 : Delage, J. A., et al. " ¹⁷⁷ Lu radiolabeling and preclinical theranostic study of 1C1m-Fc: an anti-TEM-1 scFv-Fc fusion protein in soft tissue sarcoma." EJNMMI Res 2020	71
Article 2: Delage, J. A., et al. "Impact of DOTA Conjugation on Pharmacokinetics and Immunoreactivity of [(177)Lu]Lu-1C1m-Fc, an Anti TEM-1 Fusion Protein Antibody in a TEM-1 Positive Tumor Mouse Model." Pharmaceutics 2021	86
Article 3: Delage, J. A., et al. "Copper-64-labeled 1C1m-Fc, a new tool for TEM-1 PET imaging and prediction of Lutetium-177-labeled 1C1m-Fc therapy efficacy and safety." Cancers 2021.....	106

List of Figures/Tables

Figure 1: SPECT imaging principle. Figure adapted from (6).	7
Figure 2: Schematic representation of PET imaging principle. Figure adapted from (6, 7).....	8
Figure 3: Overview of several radiotheranostic constructs. Figure from (23).....	11
Figure 4: Endosialin/TEM-1 structure and sequence homology with thrombomodulin and C1qRp/CD93. Figure from (101).	20
Figure 5: TEM-1 interaction with binding partners. Figure from (90).....	22
Figure 6: TEM-1 patterns of expression.....	27
Figure 7: Structure of an ADC. Figure from (150).	31
Figure 8: Proposed mechanism for TEM-1-TT fusion DNA experimental vaccine. Figure from (160).....	33
Figure 9: scFv-Fc format was obtained by fusing the scFv (in red) to the constant domain of human IgG1 (in blue).	35
Figure 10: Biodistribution at 24 hours of [¹⁷⁷ Lu]Lu-1C1m-Fc non-glycosylated form in Balb/c nu mice bearing TEM-1 positive tumor with or without Kiovig® pre-injection.	40
Figure 11: Biodistribution at 24 hours of [¹⁷⁷ Lu]Lu-1C1m-Fc non-glycosylated form conjugated with 2 or 5 DOTA in Balb/c nu mice bearing TEM-1 positive tumor.	40
Figure 12: [¹⁷⁷ Lu]Lu-1C1m-Fc dorsal view SPECT/CT fusion maximum intensity projection imaging on mice with TEM-1 positive tumor (SK-N-AS, left flank, red arrow) and TEM-1 negative tumor (HT-1080, right flank, white arrow), (a) at 24 h, (b) at 48 h, (c) at 72 h.....	41
Figure 13: Ratio between the tumor and the liver uptake at 24 h with respect to the number of DOTA per [¹⁷⁷ Lu]Lu-1C1m-Fc in Balb/c mice bearing TEM-1 positive tumor. Spearman test gives a rho = -0.99, p < 0.0001.....	43
Figure 14: Comparison between the results obtained by biodistribution (in grey) and pharmacokinetic modeling (in red) at 24 h for [¹⁷⁷ Lu]Lu-1C1m-Fc conjugated with 1 to 11 DOTA in Balb/c nu mice bearing TEM-1 positive tumor.	44
Figure 15: [⁶⁴ Cu]Cu-1C1m-Fc dorsal view PET/CT fusion maximum intensity projection on mouse bearing TEM-1 positive tumor (SK-N-AS, left flank, red arrow), (a) at 4 h, (b) at 24 h, (c) at 48 h.....	47
Figure 16: Biodistribution of [⁶⁴ Cu]Cu-1C1m-Fc (a) in Balb/c nude mice bearing TEM-1 positive tumor (group 1). Data are shown as mean ± SD.	48
Table 1: Comparison between SPECT and PET	8

List of abbreviations

ADC	antibody-drug conjugate
APC	antigen-presenting cell
BFCA	bifunctional chelating agent
C1qRp	complement receptor
CT	computed tomography
CTL	cytotoxic T lymphocyte
CTLD	C-type lectin-like domains
CRPC	castration-resistant prostate cancer
cDNA	complementary deoxyribonucleic acid
DNA	deoxyribonucleic acid
DOTA	1,4,7,10-tetraazacyclododecane-tetraacetic acid
DTPA	diethylenetriaminepentaacetic acid
ECM	extracellular matrix
EGF	epidermal growth factor
Fab	antigen binding fragment
FAP	fibroblast activation protein
Fc	fragment crystallizable
FcRn	neonatal Fc receptor
Fv	variable fragment
FDA	Food and Drug Administration
HIF	hypoxia inducible factor
HPLC	high performance liquid chromatography
HRE	hypoxia-responsive elements
HUVEC	human umbilical vein endothelial cells
KO	knockout
LET	linear energy transfer
LOR	line of response
mAb	monoclonal antibody
MMP	matrix metalloproteinase
MMRN2	multimerin-2
MRI	magnetic resonance imaging

NaI(Tl)	thallium activated sodium iodide
NET	neuroendocrine tumors
NHL	non-Hodgkin lymphoma
NIR	near infrared
nTAC	normalized time-activity curves
PARP	poly(ADP-ribose)polymerase
PCR	polymerase chain reaction
PET	positron emission tomography
PPRT	peptide receptor radionuclide therapy
PSMA	prostate-specific membrane antigen
RIT	radioimmunotherapy
RNA	ribonucleic acid
scFv	single-chain variable fragment
SPECT	single photon emission computed tomography
SSTR	somatostatin receptor
STS	soft tissue sarcoma
TCO	trans-cyclooctene
TEM-1	tumor endothelial marker 1
TT	tetanus toxoid
Tz	tetrazine
VH	variable heavy
VL	variable light
VSMC	vascular smooth muscle cell

Introduction

1- Theranostic approach in nuclear medicine

1-1 Imaging in nuclear medicine

1-1-1 Background

Molecular imaging in the field of nuclear medicine is defined by the non-invasive recognition and visualization of biological process at molecular and cellular level relative to changes and interaction in the living body. Diagnosis radiolabeled probes are injected into the patients and accumulate in the target tissues where the radioisotope, which is not stable, decays with emission of radiation (1).

Molecular imaging modalities currently available in nuclear medicine are the gamma scintigraphy, single photon emission computed tomography (SPECT), and the positron emission tomography (PET). These two techniques combined with computed tomography (CT) have gained a central role particularly for the diagnosis and therapy monitoring of oncological pathologies (2).

1-1-2 Principles of SPECT and PET imaging

SPECT and PET are noninvasive techniques, which provide 3-dimensional functional information, allow the identification of the disease at the early stage and enable physicians to personalize patient care. These techniques are able to visualize biological alteration in tumors in contrast to healthy tissues. The principle of SPECT or PET is based on the detection of specific radioligands. The emission produced by decay of a radioactive tracer in the targeted tissue will give information on the location of the decay and, thus, on the dynamic biodistribution of this one.

Nevertheless, radionuclides used for these two modalities are different. SPECT detects radionuclides that decay with photons emission (gamma-ray) through the patient's body while PET detects annihilation radiation from positron emitting radionuclides (β^+ emission). The annihilation process corresponds to the collision between the emitted positron and an electron to generate two photons of 511 KeV, each in opposite direction (3).

This difference in emission results in technical adaptations for the dedicated cameras. For SPECT imaging, a detector, sensitive to the position, allows the photon detection.

Nevertheless, as it detects monophotonic emissions, it does not provide the path along which the photon travels and the incoming location of the photon. To have this information, a collimator is placed between the patient and the detector to shape the stream of emitted photons into a beam. This way, each location on the detector is associated to a line called the line of response (LOR). This line is located into a space where the decay occurred. The collimator only lets pass photons that approach the detector with certain angles; other photons are discarded. Thus, an image is formed despite the rejection of most of the emitted photons. Indeed, the sensitivity constraint imposed by the collimator is the most important factor limiting the performance of the SPECT (4) (Fig. 1).

The projections of the emitting body are made by rotating the camera around the patient (4, 5). Then, the electromagnetic signal is converted into an electronic signal using a scintillator coupled to photomultiplier tubes.

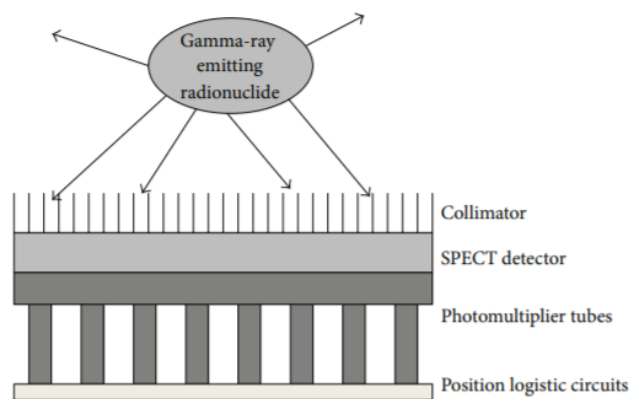


Figure 1: SPECT imaging principle. Figure adapted from (6).

For PET imaging, scintillation crystals are used to detect the gamma rays generated by the electron-positron annihilations. They allow converting the high-energy gamma rays into low energy visible photons. Then, a photosensor converts the light signal into an electrical signal. A modular detector is used to build a detecting ring to record three electronic signals: the time when the gamma ray hits the detector, the position where the gamma ray hits the detector, and the energy of the gamma ray (3, 7). These electronic signals are then processed through the coincidence unit to obtain the true events generated by the same annihilation which occur along the LOR. Finally, the raw data of thousands of LORs is used to generate the PET image through image corrections and reconstructions (3) (Fig. 2).

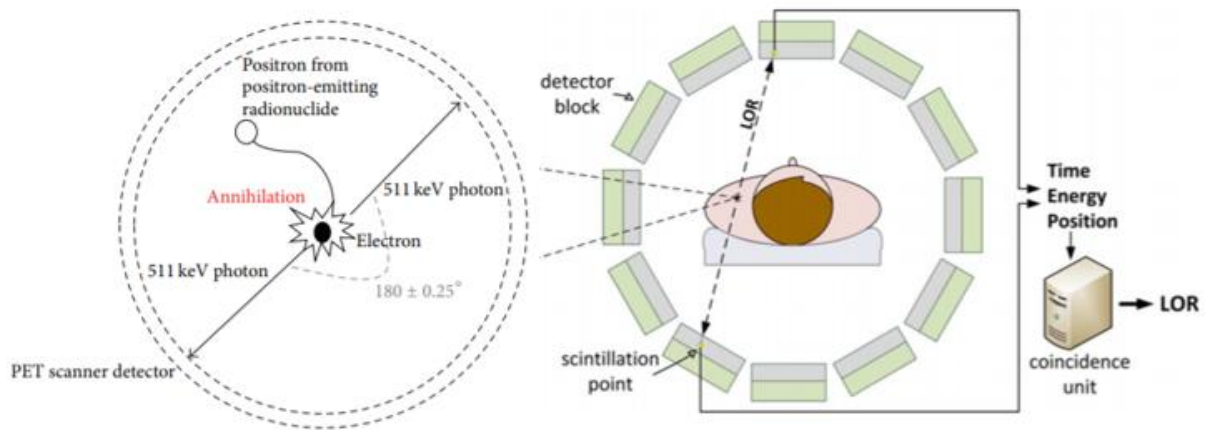


Figure 2: Schematic representation of PET imaging principle. Figure adapted from (6, 7).

Unlike in SPECT, a collimator is not necessary for PET imaging. Indeed the LORs are determined by coincident detection of two photons. Therefore, PET has a much higher sensitivity than SPECT but also a better resolution and a true potential for quantitative imaging (4).

The major differences between SPECT and PET are summarized in table 1.

SPECT	PET
Gamma ray detection	Positron detection
Collimator system	No collimator
Lower resolution	Higher resolution

Table 1: Comparison between SPECT and PET

1-1-3 Quantitative imaging

Currently, the evaluation of the images is performed by qualitative analysis. Nevertheless, in oncology, nuclear medicine techniques enable to quantify the uptake of the radiotracers in cancer cells. Quantitative imaging data shows the distribution of the radiolabeled probes within the patients' bodies and provides information for diagnosis lesions, such as expression levels of target molecules (1). The possibility to visualize, with non-invasive methods, a biological process at a molecular and cellular level *in vivo*, allows to detect oncological pathologies at once at the baseline and during therapy. Furthermore, a better characterization of oncological lesions have become possible by the increased sensitivity and resolution of the molecular imaging system (such as three-dimensional acquisition (8), resolution recovery strategies in image reconstruction) combined with the higher resolution of CT system (9) offered by current generation hybrid SPECT/PET/CT system (2). PET can also

be used simultaneously with magnetic resonance imaging (MRI) modality. PET/MRI combines MRI, which provides high soft tissue contrast, essential for local tumor staging, with the excellent sensitivity of PET for nodal and distant metastatic disease. PET/MRI provides the functional and anatomic information necessary for accurate whole-body and local tumor staging in a single examination (10).

Processing methods can be applied to SPECT or PET images to retrieve quantitative or semi-quantitative parameters from oncological lesions that can be used as *in vivo* biomarkers (11). Several strategies have been implemented to increase the accuracy of the quantitation. Indeed, a better quantitation allows the identification of accurate biomarkers for predicting therapy outcome (2, 12).

1-2 Radiotheranostics in cancer diagnosis and management

1-2-1 Concept

Precision medicine is based on specific targeting of cancer cells or of its environment. Progress in the understanding of cancer biology, advances in diagnostic technologies and developments of new therapeutic options have concurred to the concept of personalized care (13).

“Theranostics” is the association from the word therapeutics and diagnostics. The term of theranostics have been created in 1998 by J. Funkhouser, who developed a test for monitoring the efficacy of a new anticoagulant drug (14). This approach includes an imaging component that can detect the lesions followed by the administration of a companion agent that is able to treat the same lesions (13). Although theranostics is involving a growing number of scientific disciplines, especially in the field of nanotechnology (15), this innovative medical approach is deeply connected to nuclear medicine (16), especially in oncology. Radionuclide imaging offers an interesting opportunity to detect and quantify the expression of a specific tumor biomarker through the use of a certain radiopharmaceutical labeled either with isotopes emitting radiations suitable for imaging or with another radionuclide emitting alpha, beta particles or Auger electrons to obtain an anti-tumoral effect (17). Identifying the right target is crucial, since there is heterogeneity between tumor cells in an individual tumor and/or its metastases (18). Radiotheranostic approach offers also the possibility to use two probes with equivalent pharmacokinetics. Another way to follow therapeutic effects of tumor treatments or to propose theranostic probes is represented by tumor environment targeting as mentioned by Hanahan et al. (19).

With quantitative analysis of the diagnosis imaging data, the absorbed radiation dose can be estimated in the lesion sites but also in the normal tissues. Therefore, this data analysis enables to predict the therapeutic effects in the lesions as well as the side effects in normal tissues. This approach can greatly improve the personalized medicine because it allows a selection of patients, a determination of the most appropriate anti-tumoral therapy and an optimization of drug doses.

1-2-2 Current Clinical applications

Radiotheranostics seems to be the most clinically advanced application of theranostics, with several developments and emerging opportunities.

The concept of radiotheranostics has been employed for the last 70 years. The first theranostic approach was the use of different forms of radioactive iodine isotopes to diagnose (^{123}I , gamma emission, half-life = 13.2 hours) and treat (^{131}I , beta minus and gamma emission, half-life = 8.1 days) differentiated thyroid cancer (20, 21). Indeed, iodine is crucial in physiologic metabolism and function of the thyroid gland. After thyroidectomy, ^{131}I administration results in the ablation of residual differential thyroid cancer by incorporation of radioactive iodine and may treat potential distant metastases. With radioactive iodine, metastatic thyroid cancer was transformed from a disease with a poor outcome to a disease with about 85% overall survival (22).

Nowadays, radiotheranostics is at a tipping point, and is moving into the mainstream of cancer therapeutics. The main goals of theranostic indications have been to stabilize end-stage diseases that are refractive to other therapeutics and to improve the patients' quality of life. Current and future objectives consist to treat early-stage cancer through targeted intervention and to reduce the side effects of systemic radiotherapy (23).

In the past few years, several developments have been made. Theranostics radiopharmaceuticals carry alpha or beta minus emitters to the target by attaching ligands such as small molecules, peptides or antibodies, to chelators that complex radioisotopes for systemic delivery. Radioactive particles are also used to perform catheter-based intra-arterial therapy (Fig. 3).

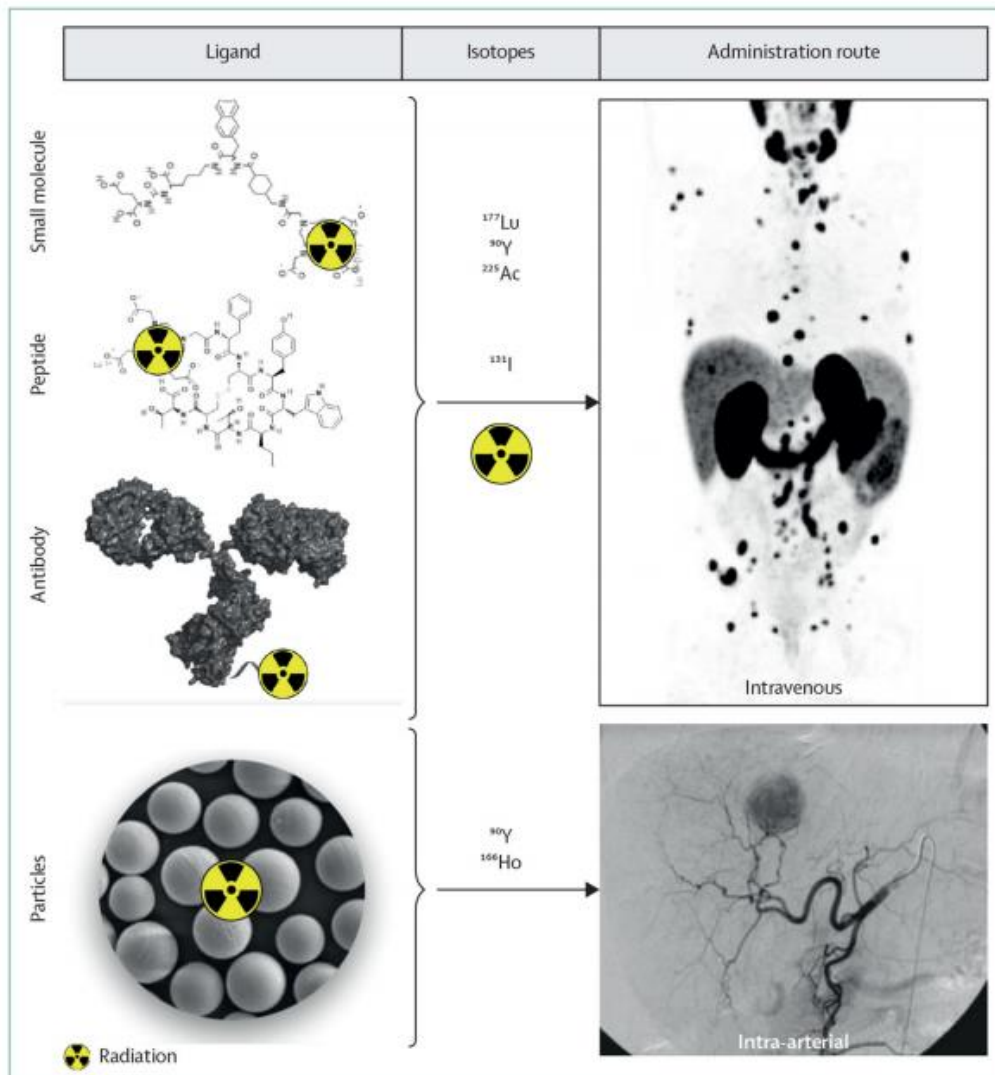


Figure 3: Overview of several radiotheranostic constructs. Figure from (23).

Some non-exhaustive examples of current clinical applications are given below.

One of the radiotheranostic approach currently used for neuroendocrine tumors and prostate cancer is the peptide receptor radionuclide therapy (PPRT). Peptides have a short blood clearance which is often desirable for imaging and have a good tumor penetration.

Imaging with peptides began with agonist of somatostatin receptor (SSTR). Neuroendocrine tumors (NET) often express high levels of SSTR, in particular SST2R at the cell surface (24, 25) and can be treated by agonist that inhibit MAP-Kinase activity resulting in an arrest of the tumor growth and in tumor cells apoptosis (26, 27). The two most common SSTR-targeting agents for neuroendocrine tumors are DOTATATE and DOTATOC. These peptides, associated to a radiometal, are receptor agonists. They stimulate SSTR as does the somatostatin that is the natural ligand and the internalization seems to be important for the long intratumoral retention of radiolabeled SSTR ligand (28). To allow a targeted radiometal tumor

delivery for imaging and therapy, chelators were conjugated to these peptides. For imaging, ^{68}Ga , a positron emitting radiometal, has increasingly been used this last years (29, 30). ^{68}Ga -DOTATOC was designated by the Food and Drug Administration (FDA) as an orphan drug in 2013 and in 2016, the FDA approved ^{68}Ga -DOTATATE for imaging NET. ^{68}Ga -DOTATOC and ^{68}Ga -DOTATATE are currently commercialized under the name of Somakit® and Netspot®.

With respect to therapy, beta-emitter PPRT was introduced and an increasing number of studies have demonstrated the efficacy of PPRT over the years (13, 31). ^{90}Y -DOTATOC and more recently ^{177}Lu -DOTATATE have been used. Both provided a significant rate of objective response in NET with a tolerable profile of toxicity. It has been shown that therapy with ^{90}Y or ^{90}Y plus ^{177}Lu entailed further side effects such as a higher nephrotoxicity than therapy with ^{177}Lu alone (32).

The cornerstone in PPRT studies has been represented by the phase 3 clinical trial NETTER-1 (33). 229 patients affected by well-differentiated metastatic midgut NET received PPRT plus best supportive care consisting in octreotide treatment. This study showed longer progression-free survival and a significantly higher response than participants treated with high-dose of octreotide. Furthermore, patients had a longer sustained function in health-related quality of life (34). ^{177}Lu -DOTATATE received the approval of the FDA and of the European Medicines Agency in 2018. ^{225}Ac -DOTATATE targeted alpha therapy was also studied in patients who were refractory to ^{177}Lu -DOTATATE with promising results (35).

Currently, SSTR antagonists are in development. Antagonists may have advantage over the agonists as SSTR have several conformations and agonists can only bind to active conformations (36). Nevertheless, there are up to 100 times more SSTR in inactive conformations on the cell surface and antagonists are also able to bind to receptors that are in inactive states (28, 37).

A more advanced PPRT indication is the prostate cancer that represents one of the most common malignancies in men and a leading cause of cancer death in male (16).

In this case, the aim is to target the prostate-specific membrane antigen (PSMA). PSMA is a transmembrane protein with glutamate-carboxypeptidase activity involved in the intestinal uptake of folate, the modulation of the neuronal signal transduction and the communication between neurons and support cells (38). In addition to its enzymatic functions, PSMA is expressed in all types of prostatic tissues and was found overexpressed (1000-fold more than physiologic levels) in 90 to 100% of prostate cancer lesions as well as in lymph nodes and metastasis from prostate cancer (39). PSMA was evaluated as a target of interest for imaging

and therapy in prostate cancer. Several anti-PSMA probes, labeled with different isotopes, were developed both for imaging and therapy, showing from moderate to high affinity for PSMA. Therefore, anti PSMA radiopharmaceuticals has entered in the routine theranostic approach (2, 40). The chelators have to bind to the Lys-Urea-Glu moiety to maintain the specificity for the PSMA enzymatic pocket (41). A turning point in prostate cancer theranostics was achieved by the development of ^{68}Ga -PSMA HBED-CC, PSMA-11. This peptide is a PSMA-inhibitor and can bind to the extracellular portion of PSMA (42). PET-CT imaging with ^{68}Ga -PSMA HBED-CC has been demonstrated to be able to detect at least one lesion with characteristic suggestive of recurrent prostate cancer in 79.5% of the examined subjects (43).

For therapy, two other peptides, PSMA-617 and PSMA I&T, that have a slower tracer kinetics than PSMA-11 are used. Published clinical results with PSMA-based radioligand therapy have been encouraging (44-46). Indeed, the first interpretable results of the randomized phase 3 trial (VISION) for metastatic castration-resistant prostate cancer (CRPC) in third line post novel androgen therapy and post taxane therapy are positive. Indeed, a 40% reduction of the risk of death was observed and an improvement in overall survival was also reported (47). The primary endpoints evaluated by this study are overall survival and progression-free survival.

Another theranostic approach consists to use antibodies against cell antigens to target the radionuclide to cancer cells. In radioimmunotherapy (RIT), the radiation-induced biological effects may be combined with the antibody cytotoxic effect.

The first ^{131}I -labeled polyclonal antibodies against cancer cell antigen were used in 1953. In 1988, the first clinical trial focused on the treatment of hematological malignancies using ^{131}I -labeled or ^{67}Cu -labeled Lym-1 (anti-HLA-DR) monoclonal antibodies (mAbs) (48). And in 1993 it was followed by the use of ^{131}I labeled anti CD20 antibodies for treatments of patients with non-Hodgkin lymphoma (NHL) (49).

It took until 2002 before two radiopharmaceuticals for RIT were approved by the FDA for the treatment of relapsed or refractory low-grade, follicular, or transformed B-cell lymphoma: Zevalin®, ^{90}Y -ibritumomab tiuxetan; and Bexxar®, ^{131}I -tositumomab (50, 51). NHL is the disease on which RIT has the highest success rates. Indeed, the complete response rate ranged between 20 and 49%, the overall response rate from 60 to 80% with mild toxicity and the superiority of labeled versus unlabeled mAbs was demonstrated in patients with recurrent follicular lymphoma (52). Since the licensing of these radioimmunoconjugates, several radionuclides have been vectorized by mAb derivatives to treat, diagnose or manage

cancer (53). For example, an anti-PSMA immunoglobulin (J591) has also been radiolabeled with ^{177}Lu and studied in phase 1 and 2 in patients with CRPC. The size and the biodistribution of this form differ from that of radioligand therapy. J591 does not target the expression of PSMA in healthy tissues such as renal tubules and salivary glands. This represents an advantage as it decreases the risk of renal adverse effect or of xerostomia found with radiolabeled peptides. The long circulation time of the immunoglobulin is an advantage for the continuous delivery of the radionuclide to the tumor during several days; but on the contrary, regarding the myelosuppression it is a disadvantage as it exposes the bone marrow to high radiation for a long time (54, 55).

Over the last 15 years, small molecules with a low molecular weight have also been developed for theranostic approach. Among them fibroblast activation protein (FAP) inhibitors have been radiolabeled and tested in preclinical and clinical studies (28). FAPIs bind to the FAP, a serine protease that is highly expressed on the cell surface of activated fibroblasts (56). ^{68}Ga -FAPI-04 have been used for imaging of patients with metastatic tumors and an excellent imaging contrast was obtained (57). ^{90}Y -FAPI-04 was studied for therapeutic approach in patient with advanced breast cancer. Despite the high accumulation of this radiolabeled compound in the tumor, a fast clearance from the tumor tissue was observed, limiting the effectiveness of this radiopharmaceutical. Optimizations are necessary to obtain a longer retention in the tumor tissue (28).

Radiolabeled poly(ADP-ribose)polymerase (PARP) inhibitors have also been studied for imaging and therapy. Indeed, PARP is an essential deoxyribonucleic acid (DNA) repair protein that has been found overexpressed in various type of cancer and has emerged as an interesting target for cancer therapy (58). Phase 1 trials are ongoing with the PARPi ^{18}F FTT in ovarian cancer patients (59) or with ^{18}F PARPi in head and neck cancer patients (60). Furthermore, recent clinical data has demonstrated that ^{18}F PARPi imaging can also be useful for the treatment monitoring of brain cancer (61).

This type of small molecules are also promising for the development of theranostic approach in nuclear medicine.

The field of theranostic has a rapid development and the accumulated evidence thus far is encouraging. From the classic and continuing clinical use of radioiodine in thyroid diseases to the more recent developments for prostate cancer and neuroendocrine tumors, the number of new agents and indications will certainly grow in the near future. Additional investigations are

needed to determine the most optimal diagnostic treatment algorithms that incorporate radiotheranostics (13).

1-3 Optimization of RIT approach

Even if RIT has been successful for hematological disorders, solid tumors constitute a big challenge. Indeed, solid tumors are less sensitive to radiation and are less accessible to large size vectors. Moreover, the slow diffusion rate, the long distance of diffusion in poorly vascularized tumors; the disorganized structure of neo-vessels are the main reasons for the insufficient tumor localization of radioimmunoconjugates and could explain the limited success of RIT for solid tumors (62).

Different strategies described in the next sections can be used to improve RIT success.

1-3-1 Antibody engineering

The first generated antibodies were full-length mouse mAb, but these proteins were not successful due to a low efficacy and a fast clearance. Mouse antibodies induce human antibody response leading to enhanced elimination in case of repeated administrations, thereby limiting the frequency of administrations and their effectiveness (62, 63). Afterwards, new developments conducted to synthesize chimeric and then humanized mAbs that reduce the immunogenicity and increase the therapeutic efficiency (64). This improvement allowed important developments in oncological immunotherapy (65).

Other points to consider are the tumor penetration and the blood clearance of the antibody. These two factors play a major role in the efficacy of RIT. Indeed, most RIT trials are based on the intravenous injection of a whole radiolabeled mAbs.

Intact immunoglobulins, which have a large molecular size (150 kDa) have a prolonged serum half-life causing a dose-limiting radiotoxicity to non-target organs and the important size of the protein limits the diffusion into the tumor. Immunoconjugates derivatives have thus been made. The use of mAb fragment with a smaller size and pharmacokinetic half-lives such as single-chain variable fragment (scFv) (25 kDa), antigen binding fragment Fab (50 kDa) or Fab'2 (100 kDa) improves the tumor to background ratio (66, 67). These smaller protein fragments have reduced immunogenicity. They give an improved efficacy with a better tumor penetration and a binding to cryptic epitopes that are unreachable by full-size mAbs (68). They also have a faster blood clearance time and a rapid excretion, reducing the tumor uptake and possibly leading to renal radiotoxicity (62). Thus, a compromise must be found between small and large mAb molecular size to improve tumor penetration and blood clearance. Intermediate-size

fragments such as minibodies are in assessment. This field seems to be promising for theranostic approach and many developments are in evaluation (69).

1-3-2 Most appropriate isotopes and chelators for RIT

The choice of the best vector is determined by the target, while the one of the radionuclide depends of the approach (imaging or therapy). This selection is driven by practical considerations, emission type and physical half-life (70).

The half-life of the radionuclide must match the antibody pharmacokinetics to deliver the highest absorbed dose to the target after injection and to optimize the tumor retention time. Therefore, radionuclides with a long half-life are preferred for intact monoclonal antibodies or for vectors with long tumor residence time and radionuclides with a shorter half-life are more appropriate for antibody fragments or for imaging proposes.

For diagnosis, in the majority of cases positron-emitting isotopes (β^+), suitable for PET imaging are preferred since PET presents higher spatial resolution than SPECT, also providing the opportunity of carrying out accurate quantitative information. The positron emitters with low β^+ energy are the most interesting due to a short distance between the emission site and the annihilation site that increase the resolution. Among them, ^{68}Ga is a short half-life isotope which can be conjugated to rapidly clearing immunoconjugates such as small fragments of antibodies or in pretargeting protocols (53). Isotopes with longer half-lives, ^{64}Cu or ^{89}Zr can be used for immuno-PET using vectors with a slower clearance (71, 72).

For therapeutic application the choice of the radionuclide is dependent of its tumor retention time as well as its low linear energy transfer (LET). The tumor retention time is determined by the ability of the tumor cell to excrete the radionuclide. For example, for an antibody radiolabeled with ^{131}I , a de-iodination can occur in the cell leading to an elimination of I ion in the extracellular media. Conversely, for ^{177}Lu , the radionuclide is sequestered into the cell. Even if ^{177}Lu has a lower half life than ^{131}I , the resulting absorbed dose will be nearly the same between the two radionuclides due to these sequestration/excretion processes. The LET criteria is related to the energy released by the radiation per unit of distance ($\text{keV}/\mu\text{m}$). Radionuclides are arbitrarily divided into low- and high-LET radiation emitters. Two types of radionuclides are used : beta minus (β^-) and alpha (α) emitters (62).

Beta minus radionuclides emit low LET radiation compared to alpha emitters with an energy deposit on a few millimeters. Among them ^{131}I , ^{90}Y and ^{177}Lu are currently the most used. Choice and efficacy of the radionuclide will depend of the size of the tumor. For example, ^{90}Y have a range of 12 mm and may provide better coverage for larger metastases whereas ^{177}Lu

have a range of 2 mm and is more appropriate for treatment of minimal disease. A combination of these two radionuclides have been studied (32). The efficacy ^{177}Lu was shown in various hematological or solid tumors and this radionuclide is currently considered of choice for RIT (73, 74).

Conversely, alpha emitters such as ^{225}Ac , ^{213}Bi , ^{212}Pb or ^{211}At are much more ionizing along their track than beta. Indeed, they have a smaller depth of penetration in tissue (50-100 μm) which increases the damage to tumor cells. These lesions are poorly repairable and thus, alpha particles are highly cytotoxic and very attractive candidates for overcoming radio-resistance of solid tumors (75). These isotopes have already been used to treat patients with hematological malignancies, solid tumors and for targeting tumor vascular antigens. Nevertheless, despite encouraging results, clinical translation will probably take more time than for beta minus emitters because of logistical challenges (e.g. production, cost, waste management, and half-life) and the potential for more severe toxic side-effects (23).

A bifunctional chelating agent (BFCA) is required to stabilize the radiometal by chelation and to covalently link the radionuclide complex to the antibody. In most cases, the ligand is first graft on the immunoconjugate. The modified immunoconjugate is then purified and characterized before to be combined with the radionuclide during the radiolabeling process. Chelating agents must lead to thermodynamically stable and kinetically inert complexes (76). Radioactive metals are currently conjugated to monoclonal antibodies utilizing stable coordination complexes. The most used are linear (diethylenetriaminepentaacetic acid, DTPA) or macrocyclic (1,4,7,10-tetraazacyclododecane-tetraacetic acid, DOTA).

1-3-3 Protocol: Pretargeting and Fractionated Dose

A particular aspect of RIT is the possible synergic role of unlabeled drugs. Pretargeting protocols have been developed to increase the tumor to healthy tissue ratio and to limit the irradiation of the healthy tissue. Indeed, the prolonged circulation time of radioimmunoconjugates contribute to a high irradiation dose to healthy tissues. Pretargeting relies upon performing radiosynthesis within the body. The antibody is injected prior the radionuclide and the two components will combine at the tumor site. The radioactivity is delivered to target tissues with a short circulating time. This technique either facilitates the use of short half-lives radionuclides that are normally incompatible with vectors with long pharmacokinetic half-lives (77) or, on the contrary, allows the administration of long half-lives

radionuclides which will have a long tumor-specific retention time and a short circulating time (78).

This approach can be done by the administration of the therapeutic mAbs conjugated to avidin or streptavidin followed later by the injection of radiolabeled biotin with a fast clearance (79). Another technique consists to inject non-radioactive bispecific antibody and then a radiolabeled bivalent hapten peptide. The bispecific antibody will bind to tumor cells and after determining the best delay, the hapten can be injected and will bind rapidly with the tumor-bound specific antibody. Any unbound hapten is rapidly cleared from the circulation via the renal system (53). The administration of radiolabeled molecules with a fast blood clearance when all unbound mAbs are cleared from the blood allows the administration of higher activities to increase the tumor-absorbed dose, while minimizing the absorbed dose to healthy organs. This method has been successfully used in hematological disorders or solid tumors but needs complex clinical assessments to define the best protocol (80-83).

The click-chemistry approach seems also to be promising for SPECT, PET or radioimmunotherapy. This technique is based on the rapid and bioorthogonal inverse electron demand Diels-Alder reaction between trans-cyclooctene (TCO) and 1,2,4,5-tetrazine (Tz).

First a TCO-bearing immunoconjugate is administrated, then the antibody will accumulates in the target tissues and will be cleared from the blood during a multi-day periode. After, the radiolabeled tetrazine will be administrated to allow the *in vivo* click ligation between the two components followed by the rapid clearance of any unreacted radioligand (84).

For therapeutic application, it has also been described that the usage of a fractionated dose instead of a single dose limits the hematological toxicity. With this type of protocol the bone marrow regenerates more quickly than tumor cells (85).

2- TEM-1 (tumor endothelial marker 1)

2-1 Background

TEM-1, also named endosialin or CD248, is a transmembrane cell surface glycoprotein expressed on pericytes and fibroblasts during tissue development, tumor neovascularization and inflammation (86).

TEM-1 was first identified in 1992 as an antigen of FB5 monoclonal antibody generated by immunizing mice with activated fetal mesenchymal fibroblasts (87).

Immunohistochemical analyses where the FB5 resultant antibody was applied to various tissues revealed that FB5 reacted strongly with vascular cells in 67% of malignant tumor specimens and weakly with stromal fibroblast in a subset of other specimens (86). TEM-1 expression was shown to be restricted to the endothelial cells of these solid tumors and was lacking overall in the blood vessels of normal tissues. This study highlighted that TEM-1 is a tumor-specific antigen and more specifically a potential antiangiogenic target.

Subsequent studies revealed that TEM-1 is expressed by perivascular cells, stromal fibroblasts (especially in cancer and inflammation), mesenchymal stem cells and some tumor cells but not on healthy tissues or adult endothelium (88-90).

However, in humans and mice, the TEM-1 transcript was found to be ubiquitously expressed in normal tissues and in somatic tissues (91). Tissues with high TEM-1 transcript levels expressed the protein, while tissue with lower levels of transcript were negative for the protein (86). High TEM-1 was detected in fibroblasts and pericytes in human thymus, lymph nodes and spleen during lymphoid tissue development but was mostly absent in the adult (92). In normal adults, TEM-1 protein expression appears to be limited to normal endometrial stroma and occasional fibroblasts (86, 93).

The exact role of TEM-1 is not fully understood but based on its pattern of expression and its limitation to pathologic conditions, TEM-1 is considered by the research community as a potential therapeutic target (94, 95).

2-2 Molecular characteristics

The human gene for TEM-1 is localized on the long arm of the chromosome 11, while the corresponding murine gene is on chromosome 19. In mice, TEM-1 shares 77.5% overall amino acid sequence homology to human TEM-1 (91).

The molecular cloning of TEM-1 led to its further characterization as a type I cell surface glycoprotein of 757 amino acids with a predicted molecular mass of 80.9 kDa (96).

TEM-1 is classified as a C-type lectin-like domains (CTLD) protein and is composed of an extracellular region and a transmembrane region with a cytoplasmic tail. The N-terminal portion of the protein corresponds to the signal leader peptide required for the transport into the endoplasmic reticulum. The signal leader peptide is followed by five globular extracellular domains; a c-type lectin domain followed by a sushi domain and three epidermal growth factor (EGF) repeats; and is separated from the membrane by a mucin domain (97). The extracellular domain may function in cell-cell interactions (98). The cytoplasmic tail of TEM-1 contains putative PDZ binding domains (99). These domains are involved in a number of protein-protein interactions and contribute to modulate intracellular signaling pathways (94, 100) (Fig. 4).

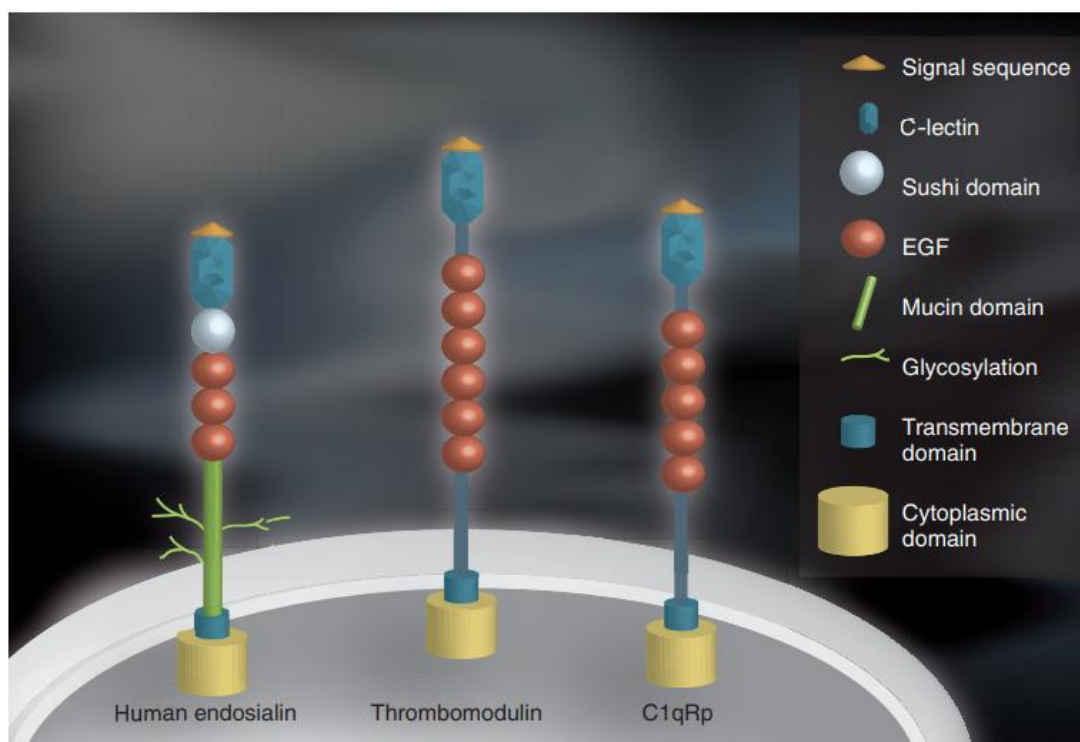


Figure 4: Endosialin/TEM-1 structure and sequence homology with thrombomodulin and C1qRp/CD93. Figure from (101).

Transgenic animals' expression TEM-1 with deletion of the cytoplasmic tail develop significantly smaller tumors following subcutaneous injection of fibrosarcoma cells T241 than wild type animals (99). Thus, the cytoplasmic tail of TEM-1 seems to be important for the growth of some tumor types (94).

The N-terminal residue of TEM-1 is most closely related to two others CTLD: thrombomodulin (39% sequence homology) and the complement receptor (C1qRp) (33% sequence homology) (96, 102, 103).

TEM-1, thrombomodulin and C1qRp are involved in the angiogenesis process and may be overexpressed under pathological conditions or participate to physiological vascular functions (thrombomodulin, C1qRp). Similar to TEM-1, thrombomodulin has also been detected in malignant tissues. Thrombomodulin and C1qRp are known for their function in immune responses (104, 105), yet the role of TEM-1 in this context has not been thoroughly investigated. The similarities in protein structure between TEM-1, thrombomodulin and C1qRp suggest that this line of research may hold value in further elucidating the function of TEM-1.

2-3 Gene regulation and binding partners of TEM-1

2-3-1 Gene regulation

Although the structure of TEM-1 is well characterized its function has not been fully elucidated.

The rapid proliferation of cancer cells promotes hypoxia as it overtakes the development of the blood vessels. With an inadequate delivery of oxygen, hypoxia inducible transcription factor (HIF) is upregulated and induces a vascular remodeling (106). As angiogenesis in tumors and in embryo development is stimulated by a low oxygenation, it was supposed that hypoxia might influence TEM-1 expression. This hypothesis was validated as it was shown that the transcription of TEM-1 gene is upregulated *in vitro* in the context of hypoxia (107). The promoter region of the gene contains several hypoxia-responsive elements (HRE) that constitute binding sites for HIF.

It also has been demonstrated that expression of TEM-1 is modified by the cell density in mouse models expressing TEM-1 (91). The density in human cells has an effect and it may be partially mediated by pericellular hypoxia, which occurs in cells growing to high density (108). The response of TEM-1 to high cell density is mediated, at least in part, by the binding of the transcription factor SP1 to the promoter. SP1 may also be upregulated by HIF and provides a molecular link between hypoxia and cell density mediated upregulation of TEM-1. Nevertheless, the cell density can affect the TEM-1 expression under both normoxic and hypoxic conditions (107).

2-3-2 TEM-1 interaction partners

The multidomain architecture of the TEM-1 extracellular domain suggests that it may have multiple protein partners. Several TEM-1 ligands have been identified (Fig. 5).

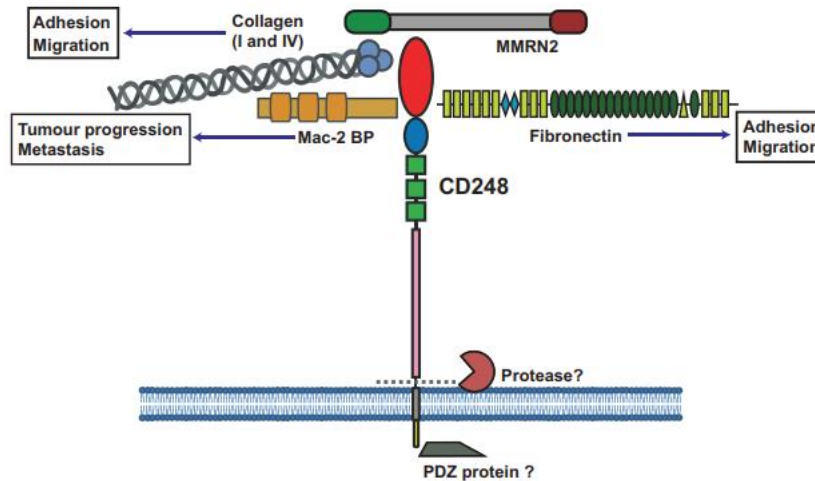


Figure 5: TEM-1 interaction with binding partners. Figure from (90).

It has been demonstrated that the extracellular matrix (ECM) proteins fibronectin and collagen types I and IV bind to the extracellular domain of TEM-1. This binding may play an important role in the cells attachment and migration during tumor invasion. TEM-1 knockdown resulted in a decrease of migration and proliferation of fibroblasts, reinforcing a supposed role in adhesion (109). This binding also promotes the release of active matrix metalloproteinase (MMP)-9, implicating TEM-1 in ECM degradation, a key step in angiogenesis, tumor metastasis and invasion (110).

Recently a direct interaction of TEM-1 with the endothelial ECM protein multimerin-2 (MMRN2) has been shown having a role in the binding to endothelial ECM, angiogenesis and tumor progression (111).

The Mac-2 binding protein has also been identified as a TEM-1 ligand and may promote metastatic spread of tumor cells (112). This protein is weakly expressed in the small intestine, stomach, colon, ovary and kidneys but strong staining was observed on several tumor tissues including adenocarcinoma of the uterus and colon, carcinoma of the small intestine and renal cell carcinomas (113).

TEM-1-Mac-2 interaction occurred during tumorigenesis and a correlation has been demonstrated between the level of Mac-2 in the circulation and the frequency of metastasis (86).

The removal of the interaction between TEM-1 and these proteins could be a target for the future development of therapeutics.

Currently, no interacting partner has been described for the cytoplasmic domain of TEM-1 but this structure is crucial for facilitating an inflammatory response in models of arthritis and for promoting tumor growth in mouse model (95, 99, 114).

2-4 Physiological expression of TEM-1

2-4-1 *In vitro* expression of TEM-1

The first studies identified TEM-1 as a marker of tumor endothelium. However, it was demonstrated later that TEM-1 is primarily expressed by cultured embryonic fibroblasts, pericytes and smooth muscle cells; but not by human umbilical vein cells (HUVEC); primary blood vessel endothelial cells, cells of lymphatic endothelium or epithelial cells (88, 93, 94). After immunohistochemical analysis, TEM-1 expression has been shown in mesenchymal cells, whereas in healthy tissues only low level of TEM-1 was found. TEM-1 expression was also detected in mesenchymal stem cells originating from bone marrow (94, 115). This expression is very interesting as cells of the mesenchymal lineage conserve multipotent differentiation capacity and may differentiate into a variety of cell types such as chondrocytes, osteoblasts or adipocytes. Depending on the microenvironment of tumors, the mesenchymal stem cells could differentiate into activated synovial fibroblasts, cancer-associated fibroblasts or pericytes that promote fibrovascular network expansion, progression of inflammatory lesion or tumor development (95, 116, 117).

2-4-2 TEM-1 expression during development

In non-pathological conditions, TEM-1 is expressed during development, at a high level in the embryo and decreases progressively postnatally. Indeed, in mice embryos, transcripts are detectable at embryonic day 9.5 (118) in the central nervous system, spleen, thymus and lymphatic nodes (92). Then, TEM-1 expression remains high throughout fetal development. After, TEM-1 is diminishes in postnatal organs except for the perivascular cells in lung, the stromal cells of the uterus, the endometrium and ovaries, the kidney glomeruli, the bone marrow fibroblast and the red pulp of the spleen (119). In a healthy adult organism, TEM-1 is expressed in tissues in need of active angiogenesis, during wound healing.

Although TEM-1 is a marker of mesenchymal and stromal cells, it is also selectively expressed by the surface of naïve CD8⁺ T-lymphocytes, as it probably negatively regulates their proliferation, ensuring they remain in a quiescent state and playing a role in suppressing T-cell proliferation (120).

TEM-1 knockout (KO) mice are viable and were unaffected with regard to embryonic development, phenotype and wound healing responses, suggesting that compensatory mechanisms may be employed during development (121).

2-5 Pathological expression of TEM-1

2-5-1 TEM-1 expression during inflammation and fibrosis

During inflammation an increase of TEM-1 expression was observed.

In psoriatic and rheumatoid arthritis, the synovium is transformed from a thin paucicellular tissue into an invasive and joint destructive tissue, characterized by hyperplasia, angiogenesis, immune and mesenchymal cell infiltration, and development of secondary lymphoid structures (86). Synovial tissue biopsy samples from rheumatoid and psoriatic arthritis showed that TEM-1 expression is upregulated in fibroblasts and pericytes of synovial tissue (114) and has been also observed in the sublining layer of a distinct subset of synovial fibroblasts (122). Compared to wild-type mice, a reduction in experimental arthritis, an important decrease in synovial inflammation with lower plasma levels of pro-inflammatory cell accumulation and a reduced leukocytes infiltration were observed with KO mice or mice lacking the cytoplasmic domain of TEM-1.

TEM-1 is also implicated in bone formation as it is expressed by osteoblasts but not by osteoclasts in mice and human (123). TEM-1 KO mice have a higher bone mass and superior mechanical properties compared to control mice probably due to an increase of mineral formation that would normally be inhibited by PDGF signaling which is disrupted in TEM-1 deficient cells. Targeting TEM-1 in rheumatoid arthritis may reduce the inflammation but also the bone loss associated to arthritis (90).

In healthy human and mouse kidney, TEM-1 is expressed in the mesangial cells of the glomerulus, in pericytes and fibroblasts. TEM-1 can be considered as a predictor of renal failure as it is overexpressed in chronic kidney disease (124) and as it was shown to have a potential role in the development of kidney fibrosis in mice (125). TEM-1 KO mice with renal damages were protected from microvascular rarefaction and fibrosis, probably due to less production of collagen by fibroblasts and to the absence of differentiation of the pericytes into myofibroblasts, that are involved in fibrosis (126).

TEM-1 was also upregulated in liver fibrosis. KO TEM-1 mice were protected against liver fibrosis following liver injury and an enhanced hepatocyte proliferation and a reduction of collagen expression was observed (127). TEM-1 expression was detected in human samples

of liver fibrosis, on myofibroblasts and perivascular cells and was elevated in human liver fibrosis samples compared to healthy controls as well as correlating with levels of collagen deposition (90).

High expression of TEM-1 was observed in idiopathic pulmonary fibrosis patients and may serve as a marker of the severity of the disease (128).

TEM-1 is expressed in vascular smooth muscle cells (VSMCs) and is implicated in the pathogenesis of atherosclerosis. TEM-1 KO mice exhibited marked reductions in macrophage infiltration into atherosclerotic plaques, due to reduced chemokine expression in VSMCs (129).

All these observations highlight the role of TEM-1 in inflammation and fibrosis. TEM-1 could be an interesting target for these diseases (90).

2-5-2 TEM-1 expression in Cancer

An important increase of TEM-1 expression levels on tumor-associated stroma have been reported in several primary tumor types such as glioma, colorectal carcinoma, melanoma as well as brain metastases (130, 131).

Immunohistochemistry studies showed that TEM-1 co-localizes with the pericyte marker NG2 in breast cancer specimens (86, 88, 132). TEM-1 is expressed in numerous tumor cell lines and clinical samples of sarcoma and neuroblastoma but is absent in cancer cells of epithelial origin (89).

Lack of TEM-1 in transgenic mice results in a slower tumor growth, suggesting that a TEM-1 positive stroma promotes malignancy. TEM-1 may also play a role in cell-cell adhesion and in adhesion to extracellular matrix protein (110, 133).

The first indication that TEM-1 may be expressed by malignant cells was in 1992, by Rettig et al. who reported immunoreactivity of FB5 anti TEM-1 antibody in several neuroblastoma and sarcoma cell lines (87). In 2005, Rouleau et al. analyzed 94 clinical sarcoma specimens and 84% of them were TEM-1 positive (89). More recently one, TEM-1 expression was evaluated in a group of 203 clinical sarcoma specimens and 96% of expression was reported (89, 134). A retrospective analysis of diagnostic reports showed that TEM-1 was detected in high-grade diseases and metastasis.

TEM-1 is expressed in stromal cells, endothelial cells and pericytes in several tumors. However, a few studies focused on expression in malignant cells. Dolznig et al. demonstrated that the TEM-1 protein was present in human sarcomas and showed the expression of the protein in malignant cells (119).

Amongst central nervous system tumors, glioblastoma is the most aggressive subclass. This type of tumor has massive neovascularization. Although TEM-1 is not expressed in normal adult brain, it is expressed in the angiogenic vasculature of high-grade glioma (86) and by the perivascular cells (135).

Metastasis process is linked on the interaction between the metastasizing tumor cells and the local microenvironment within tumor stroma, pericytes and myofibroblasts have upregulated TEM-1 expression. Studies in wild-type and TEM-1-deficient mice showed that stromal TEM-1 promoted spontaneous metastasis (136). TEM-1 expressing pericytes in the tumor facilitated distant site metastasis. Indeed, TEM-1 promotes the intravasation of tumor cells in a cell contact-dependent manner, resulting in higher circulating tumor cells. In independent cohorts of primary human breast cancers, upregulation of TEM-1 expression is correlated with increased metastasis (86).

To summarize, the presence of TEM-1 in a wide variety of cell types is associated with malignant diseases and validates TEM-1 as a potential therapeutic target (132). Furthermore, clinical studies have shown a direct correlation between TEM-1 transcript levels and patients' outcome. The degree of TEM-1 expression was correlated to the patients' prognosis, with elevated levels associated with nodal involvement and disease progression (137-139).

The landscape of cellular expression of TEM-1 is summarized in Fig. 6.

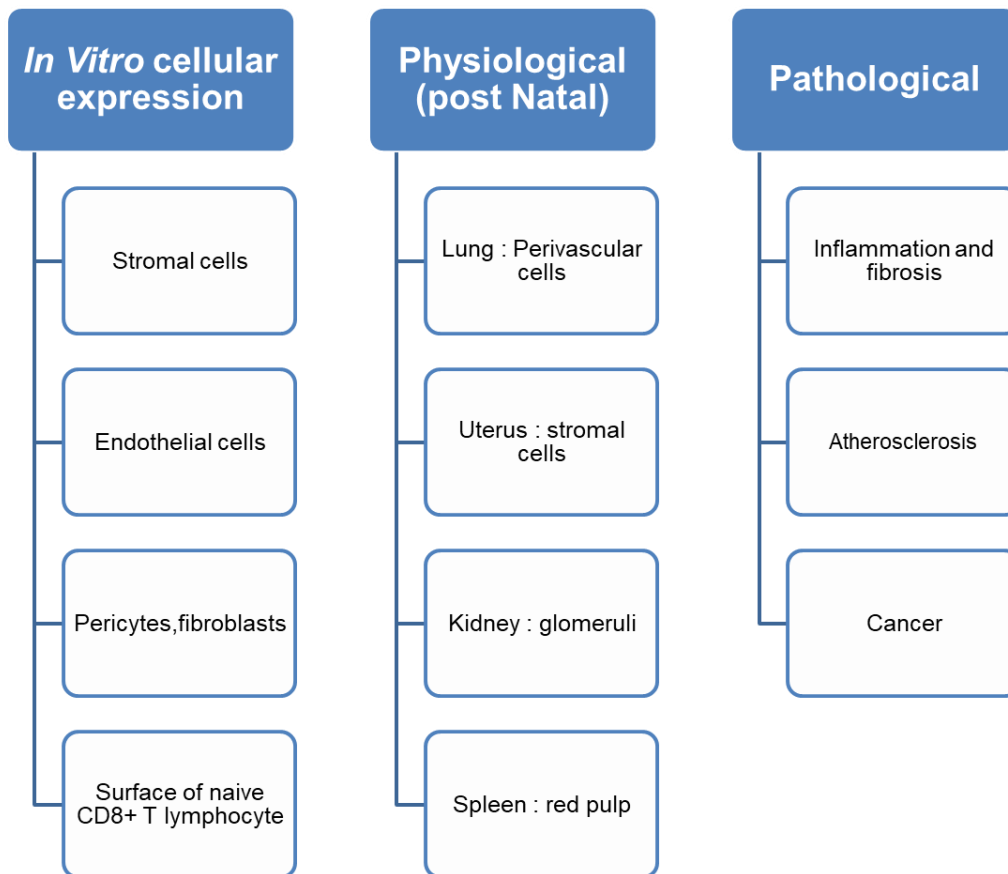


Figure 6: TEM-1 patterns of expression.

3- Targeting TEM-1: Potential applications in clinic

3-1 Background

Laboratory techniques for molecular biology have promoted a field of molecular-targeted therapies in oncology. By the identification of specific gene expression, it is possible to give to the patient drugs that are adapted to the molecular composition of their tumors and to select the treatment with the best efficacy.

The prevalence of TEM-1 in the vasculature and the stroma of solid tumors and in malignant cells of sarcomas suggests that an anti-TEM-1 therapy in combination with other modalities could have therapeutic benefits. The development of anti TEM-1 companion diagnostic may assist in the personalized medicine approach, whereby TEM-1 expression is exploited as a biomarker to select patients that would most benefit from a treatment directed towards the TEM-1 antigen (101).

3-2 TEM-1 and neuroblastoma

Neuroblastoma is the most common extra-cranial cancer in the childhood (140). This is a peripheral nervous system tumor derived from neural crest. Its pathobiology is various. Low-risk diseases can be cured with surgery, whereas high-risk diseases require intensive radiotherapy, chemotherapy and/or immunotherapy. Stage 4S neuroblastoma, which is defined by dissemination to liver and skin, cannot be treated and requires supportive care (141).

TEM-1 expression was studied in neuroblastoma. In this type of tumor, TEM-1 was not only expressed by tumor vasculature, but also by malignant cells (as it was observed for sarcomas) (142). A side population analysis was also done by Rouleau et al. to determine whether tumor stem cells could be detected in the neuroblastoma cell lines and whether the side population cells would express TEM-1. In both cell lines tested, levels of TEM-1 were similar in the total cell population and in the side population cells, showing that TEM-1 is a possible therapeutic target for neuroblastoma stem cell-like cells. On all cell lines tested in this study, the highest level of TEM-1 staining was observed in SK-N-AS tumors. Furthermore, when SK-N-AS cells were implanted subcutaneously in immunodeficient mice, the resulting tumors were TEM-1 positive. Therefore, they concluded that TEM-1 expression detected in cell culture was maintained *in vivo* and in different tissue environments (142).

The reported low level of expression of TEM-1 in normal tissue and the expression of TEM-1 on malignant cells and tumor vasculature in neuroblastoma suggests that TEM-1 may

be a suitable therapeutic target for advanced disseminated neuroblastoma, a disease with poor prognosis (141). In our studies, we have thus decided to work on murine neuroblastoma models with mice grafted with SK-N-AS positive cell lines.

3-3 Anti TEM-1 in clinical trials

A humanized anti-TEM-1 monoclonal antibody called Ontuxizumab (MORAb-004) has been tested in clinical studies for sarcoma. MORAb-004 is derived from antibody FB5 and was later humanized by grafting six complementarity determining regions into a human IgG1 framework (143).

MORAb-004 was the first agent to enter in clinical development for TEM-1 targeting. In the first-in human phase I study, the selected patients had solid tumors refractory to treatment. The antibody was administered intravenously one time per week in 4-week cycles (144). 36 patients were treated with antibody dose levels from 0.0625 to 16 mg/kg. During this study, preliminary antitumor activity was observed. Safety profile, pharmacokinetics and early antitumor activity suggested that MORAb-004 should be studied further for efficacy (144, 145).

In a second time, a randomized, placebo controlled, phase II study was performed to evaluate the safety and the efficacy of MORAb-004 in patients with chemo-refractory metastatic colorectal cancer (146). 126 patients received weekly intravenous injections of MORAb-004 (8 mg/kg) or a placebo plus best supportive care until progression or toxicity. No difference in progression-free survival, overall survival or overall response rate were observed between the Ontuxizumab and the placebo. The treatment-related adverse events were fatigue, nausea, decreased appetite and constipation. The antibody was well tolerated.

Another Phase II study was done in metastatic melanoma patients who had received at least one prior systemic treatment (147). The aim of this study was to evaluate progression-free survival, pharmacokinetics, and tolerability of two doses of MORAb-004. Patients received either 2 or 4 mg/kg of Ontuxizumab weekly, until disease progression. No difference was found on the progression-free survival between the two groups (8.3 weeks). The median overall survival was 31 weeks. The efficacy of Ontuxizumab as single treatment at this dose in melanoma was low.

A phase I trial was conducted in children with relapsed or refractory solid tumors (neuroblastoma, Ewing sarcoma, rhabdomyosarcoma and other tumors) (148). The antibody was administered intravenously weekly during 4 weeks at three dose levels (4, 8, and 12

mg/kg). 12 mg/kg was determined as the recommended dose for Phase II trial and was well tolerated.

Based on a Phase I study conducted in sarcoma patients, Ontuxizumab received FDA orphan drug designation for sarcoma (86).

A phase II study was performed to examine the safety and efficacy of Ontuxizumab in combination with gemcitabine and docetaxel in metastatic soft-tissue sarcomas (149). Ontuxizumab plus gemcitabine/docetaxel showed no enhanced activity over chemotherapy alone in soft-tissue sarcomas, whereas the safety profile of the combination was consistent with gemcitabine/docetaxel alone.

3-4 TEM-1 targeting experimental therapeutics

3-4-1 Antibody-drug conjugates

A few research groups have developed antibody-drug conjugates (ADCs) modality. ADCs are monoclonal antibodies conjugated to cytotoxic agents. They use antibodies that are specific to tumor cell-surface proteins and have tumor specificity and potency not achievable with traditional drugs. Antitumor activity is reached by conjugating antibodies with different effector molecules that promote cell death after antibody binding and internalization. These effector molecules include cytotoxic agents, bacterial or plant protein toxins (immunotoxins) (150) (Fig. 7). The optimal ADC has antigen recognition that is similar from the unconjugated antibody. The linker connects the cytotoxic part to the monoclonal antibody and maintains the stability of the ADC in the circulation. Most linkers are labile in the intracellular environment, resulting in the release of the cytotoxic payload after internalization (151, 152). Other linkers need intracellular enzymatic cleavage for the release of the cytotoxic payload. A stable linker reduces non-specific systemic release of the cytotoxic drug. This point is determinant for the ADC safety (150). ADCs usually include 2 to 4 highly potent anticancer agent small molecule drugs.

The requirement for an ADC is to have a target expressed on the cell surface and to be internalized into the cell along with the target protein to enable delivery to the cytotoxic drug payload (153).

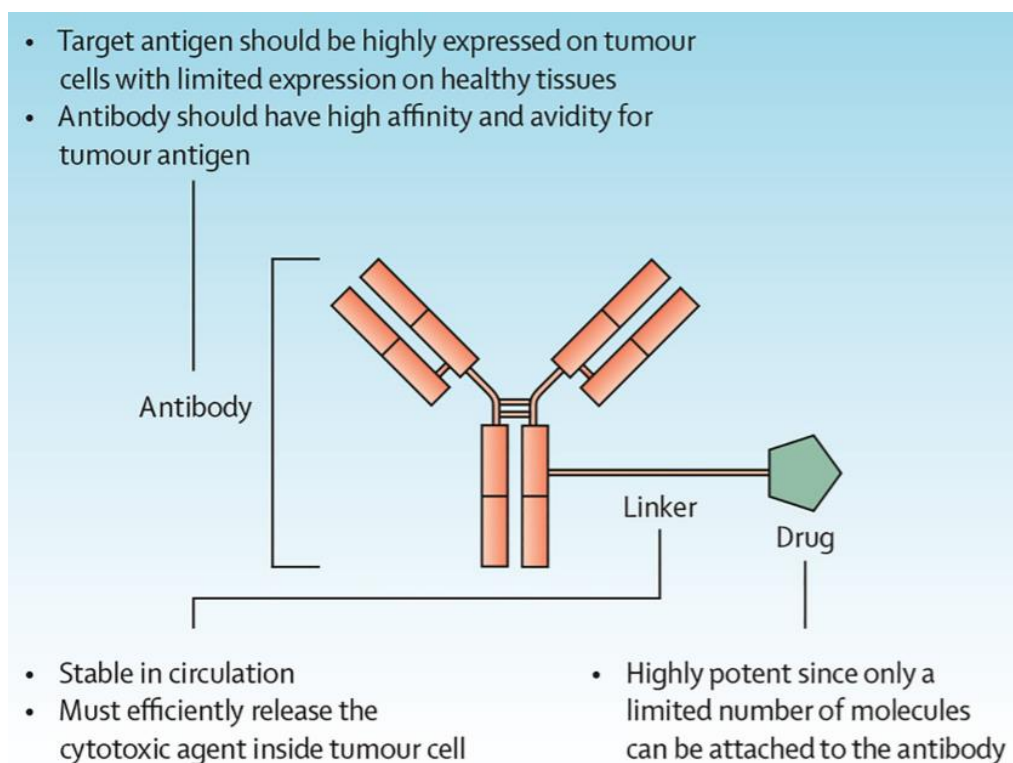


Figure 7: Structure of an ADC. Figure from (150).

In the past few years, ADCs have benefited from several technological advancements. Early ADCs were mouse monoclonal antibodies covalently linked to anticancer drugs. Mouse antibodies were then replaced by humanized or fully human antibody to prevent immunogenicity. It is also necessary to note that as ADCs contain a protein component, an immune response can be induced after administration. Indeed, antibody responses may be directed against the mAb as we mentioned previously but also against the linker or the cytotoxic drug portion of the biotherapeutic (154). Immunogenicity assessment of these compounds is recommended for clinical development (155). Furthermore, careful target and antibody selection improved selectivity and efficiency of internalization (150).

The accessibility of TEM-1 as a cell surface antigen to antibodies and its high level of expression in sarcomas and neuroblastomas makes it a potentially suitable ADC target (95).

An anti-TEM-1 ADC, MC-VC-PABC-MMAE, was prepared and tested in cell culture and was found to be selectively cytotoxic to TEM-1. It also achieved a profound and durable antitumor efficacy in preclinical human tumor xenograft models in TEM-1 positive disease (153).

Another study, provided the evidence of the preclinical efficacy of a novel ADC. This ADC consisted of a humanized TEM-1 monoclonal antibody, named hMP-E-8.3, conjugated

to a duocarmycin derivative. In TEM-1 expressing cell lines, this ADC showed an important target-dependent killing activity. High expression of TEM-1 in cells correlated with efficient internalization and cytotoxic effect *in vitro*. In a cell line-based model of human osteosarcoma, efficacy studies demonstrated that this ADC treatment leads to a long tumor growth inhibition (156).

These studies demonstrated that TEM-1 is an interesting target and that ADCs have the potential to be developed as therapeutic agents.

3-4-2 Specific DNA vaccination

DNA vaccine approaches against TEM-1 have also been attempted preclinically.

Facciponte et al. generated a vaccine with murine TEM-1 cDNA fused to cDNA of the C fragment of tetanus toxoid (TT) (157). TEM-1-TT vaccination generated CD8+ and CD4+ T cell responses against immune dominant TEM-1 protein sequences. As an adjuvant TT may enhance immunogenicity (158, 159).

Prophylactic immunization with TEM-1-TT prevented or delayed tumor formation in mice. Vaccination of tumor bearing mice decreased tumor vascularity, increased T cell infiltration, and slowed tumor progression. The vaccination did not detrimentally affect wound healing and reproduction.

Antitumor effects were reported in both the prophylactic and therapeutic vaccine setting (157). The therapeutic effectiveness of this new vaccine can be summarized in three parts as schematically shown in Fig. 8.

Firstly, TEM-1-TT vaccine elicits cytotoxic T lymphocytes (CTLs) that specifically attack the tumor vasculature. TEM-1-TT vaccine modifies the tumor vessel architecture. As TEM-1 is expressed by tumor-vessels associated to pericytes cells, the vaccine may also target pericytes directly, with subsequent destabilization and inhibition of tumor endothelial cell network (157). TEM-1-TT vaccine functionally destabilizes the tumor vasculature, induces vessel collapse, as well as possibly impedes the assembly of new vasculature (160).

Secondly, authors supposed that the lack of a constant stream of metabolites and oxygen leads to an increased hypoxic and inflammatory tumor microenvironment that promotes tumor cell death. Indeed, an increase of apoptosis was shown in tumors cells from mice vaccinated with TEM-1-TT (160).

The last step of the TEM-1-TT therapeutic effectiveness was the ability of the vaccine to provide a secondary tumor-specific immune response. The events such as hypoxia, apoptosis can generate a source of antigenic determinants that can interact with antigen-presenting cells

(APCs) like dendritic cells and macrophages. These APCs are able to promote a secondary immune response against the tumor specific antigen (160, 161).

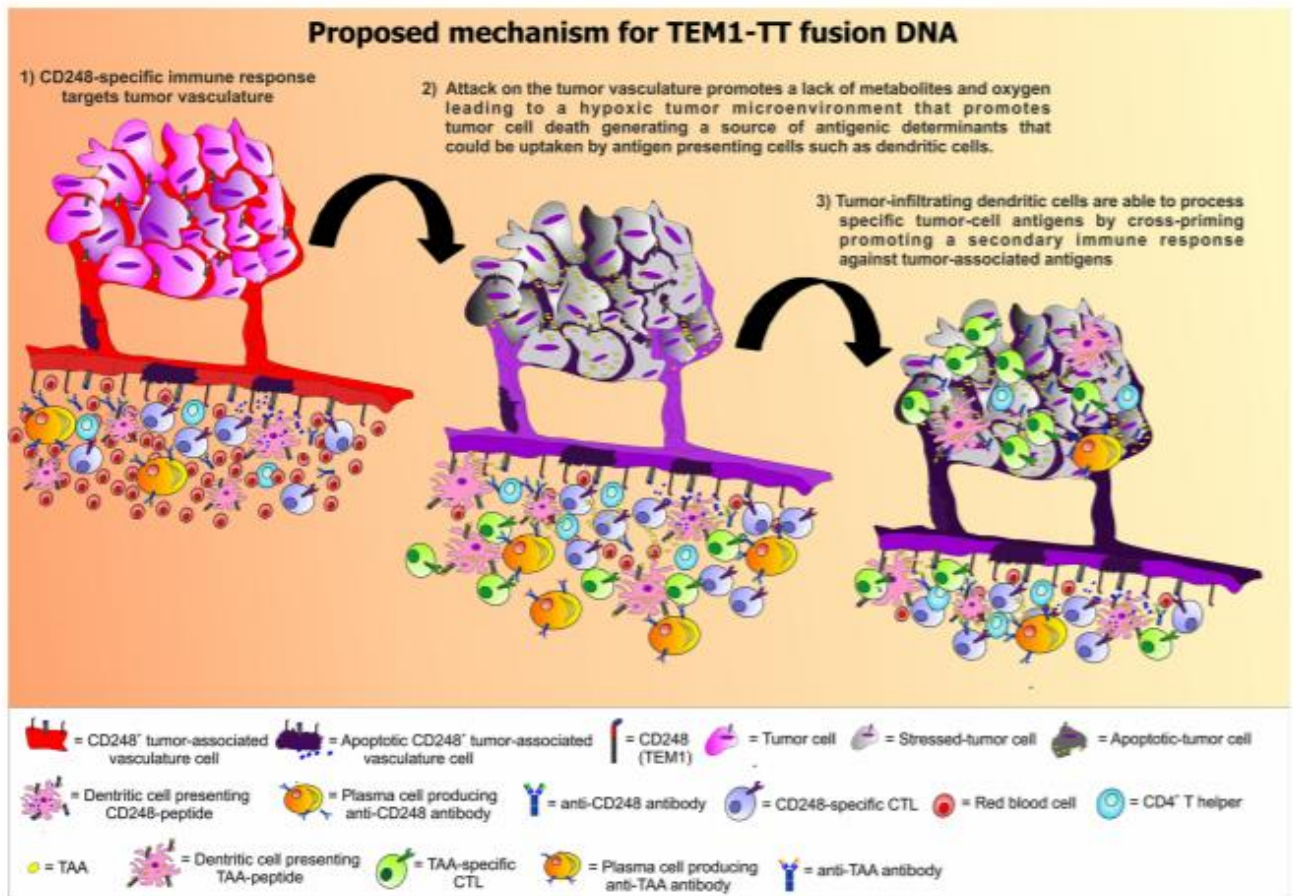


Figure 8: Proposed mechanism for TEM-1-TT fusion DNA experimental vaccine. Figure from (160).

Facciponte et al. also illustrate the safety of the vaccine in murine model. They showed that TEM-1-TT vaccine does not induce an immune response against physiological neoangiogenesis compared with other anti-angiogenic therapies that are associated with important safety concerns, including wound healing and pregnancy (162, 163).

TEM-1 could be considered as a new immunotherapeutic target for cancer treatment with an interest to develop translatable DNA based immunotherapy and further investigations are necessary (160).

3-4-3 TEM-1 Imaging

Currently, the ability to assess the clinical expression of TEM-1 in patients with metastatic disease relies on immunohistochemistry of biopsies of single lesions or primary tumors that may not represent true TEM-1 expression compared to the total tumor burden in a

patient. Negative staining for TEM-1 may represent an artifact of processing or a biopsy selection, while positive staining may only relate to the specific tumor that was biopsied and not the entire tumor burden (164).

To improve the screening of the patients, Ontuxizumab (MORAb-004) was radiolabeled and tested in preclinical and clinical studies. Indeed, antibody-based SPECT and PET are imaging modalities that provide a real-time non-invasive detection of pathologies. Although human and mouse TEM-1 share 87% homology, MORAb-004 binds to human and monkey TEM-1 but has no cross-reactivity with murine TEM-1 (110). This preclinical study requires chimeric graft models (143). Furthermore, in this case it is important to note that the uptake in the murine neo-vessels is not specific. This point has to be considered for the analysis of the biodistribution results.

This antibody has first been labeled with ^{124}I to evaluate the feasibility of using PET imaging to visualize TEM-1 in a cell line engineered to express high levels of this target (165). Biodistribution studies demonstrated a lower clearance of the radiolabeled antibody in TEM-1 positive tumors compared to negative and also a high uptake in tumors compared to normal tissues (165).

Others experiments were performed with Ontuxizumab radiolabeled with ^{89}Zr . Indeed, this radionuclide is known to be trapped inside cells after metabolism and to have the potential of generating images with higher quality (166). Lange et al. tested the ^{89}Zr -Ontuxizumab on non-engineered sarcoma cell lines to assess the clinical utility of this radiolabeled compound (164). Development of PET for TEM-1 expression may allow stratification of patients, potentially enhancing outcomes for patients with TEM-1 expressing tumors. Biodistribution studies in xenograft-bearing mice confirmed high tumor uptake of ^{89}Zr -Ontuxizumab that can be used to determine TEM-1 expression (164, 165, 167).

Furthermore, this data showed that a theranostic approach could be evaluated. Indeed, in addition to the effects of mAbs leading to an inhibition of tumors described above, delivery of isotopes emitting local radiation directed to either vascular or parenchymal tumor cells can be used. TEM-1 targeted radioimmunotherapy could lead to tumor destruction.

3-4-4 First fully human anti-TEM-1 sc-Fv

A novel single-chain variable fragment (scFv), 78scFv, against TEM-1 was isolated from a human display scFv-Fc library. This ScFv recognizes both human and murine TEM-1. The convenient human/murine cross-reactivity of this molecule was very promising for preclinical evaluation of the compound. Contrary to MORAb-004, the binding on both murine

and human TEM-1 has allowed bio-distribution studies evaluating the specificity of the antibody.

The scFv was fused to the fragment crystallizable (Fc) region of human IgG1, creating a dimeric protein (78Fc) (Fig. 9) which was conjugated with a fluorochrome for near-infrared (NIR) optical imaging (168, 169).

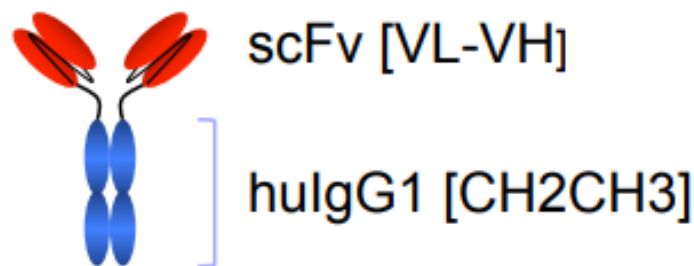


Figure 9: scFv-Fc format was obtained by fusing the scFv (in red) to the constant domain of human IgG1 (in blue).

The biodistribution of the selected Fc-fusion protein presented a minimal binding to normal organs. Nevertheless, an efficient 78Fc homing to tumors which express strongly TEM-1 in the vasculature and a weakly uptake in tumor cells *in vivo* were observed (134). 78Fc internalizes upon binding to cell-surface TEM-1 (170). The NIR imaging provided the first *in vivo* imaging data of TEM-1 expression in the mouse, which was consistent with the previously established expression profile of TEM-1 using *in situ* hybridization (171). Specific and sensitive tumor localization of 78Fc was confirmed with optical imaging in mouse tumor model that has highly endogenous mTEM-1 expression in the vasculature.

Optical imaging of TEM-1 could be interesting in clinical applications, including intraoperative imaging with NIR fluorescence dyes (172).

Based on this properties, Guo et al. theorized that 78Fc could also be an ideal candidate for drug delivery to TEM-1 positive sarcomas. They generated a scFv78-saporin immunoconjugate that exerted dose-dependent cytotoxicity with high specificity to TEM-1 positive cells *in vitro*.

78Fc was also studied preclinically after radiolabeling with ^{111}In and a specific uptake was observed in TEM-1 positive tumors (173).

All this data indicates that scFv78 presents advantages for the development of imaging probes or antibody-toxin conjugates for a large spectrum of human TEM-1 positive solid tumors (169).

3-4-5 1C1m-Fc a novel anti TEM-1 fusion protein antibody

A new fusion protein antibody, named 1C1m-Fc was produced by the LabCore laboratory, Ludwig Institute for Cancer Research, Lausanne.

1C1m-Fc was isolated from a naïve human antibody phage display. This fusion protein is composed of a scFv part, made bivalent by fusion to a human Fc domain (IgG1). The Fc part allows increasing the size, the avidity and the stability of the monovalent scFv antibody fragment *in vivo* leading to an improvement of the pharmacokinetic.

Furthermore, the interest of this new fusion protein is to bind to both human and murine TEM-1, enabling the evaluation of anti-TEM-1 theranostic approach in a mouse model.

1C1m-Fc presents a high affinity towards human TEM-1 (1nM) and murine TEM-1 (6nM) compared to 78Fc which has an affinity of 5.6 nM towards human TEM-1(168). The strong cross-reactivity of 1C1m towards murine TEM-1 is also directly compatible with translation in syngeneic models.

The specificity of 1C1m-Fc in staining has been evaluated by the LabCore laboratory within tissue sections. 1C1m-Fc was shown to co-localize with a proportion of neonatal pericytes but also in sections of Lewis lung carcinoma and MC38 colon carcinoma tissue. 1C1m-Fc staining signal co-localized with the pericyte marker NG2. All these characteristics made this antibody a promising candidate for preclinical and clinical testing. We thus decided to radiolabel it and to evaluate its theranostic potential in tumor mouse model.

4- Conclusion

Tumor vasculature and stroma targeting represents an effective strategy for early detection, diagnosis and treatment of many tumors (169). TEM-1 was proved to be an attractive surface molecule and a promising target. The universally high expression of TEM-1 in almost all types of solid tumors offers a variety of clinical applications, including molecular imaging.

Currently, only one anti-TEM-1 antibody, MORAb004, is under clinical development. This humanized antibody recognizes the fibronectin-binding domain of TEM-1. Unlike ScFv78, MORAb-004 does not cross-react with murine TEM-1. ScFv78 is the first fully human scFv antibody in the field and its properties including rapid internalization and specificity for mouse and human TEM-1, make it suitable for a variety of applications in tumor theranostics across a wide spectrum of solids tumors (169).

In our studies we explored the utility of targeting TEM-1 through a fusion protein antibody ScFv-Fc which could be used as imaging agents as well as delivery system for therapeutic payloads. Thus, a novel anti-TEM-1, 1C1m-Fc, isolated from phage display and made bivalent by fusion to a human Fc domain (IgG1) was radiolabeled with ^{64}Cu or ^{177}Lu and studied in preclinical investigations.

Summary of results

Chapter 1: ^{177}Lu radiolabeling and preclinical theranostic study of 1C1m-Fc: an anti-TEM-1 scFv-Fc fusion protein in soft tissue sarcoma

This article has been published in the European Journal of Nuclear Medicine Research, *EJNMMI Research* (2020) 10:98 (174).

I also presented a part of this work at the following congresses: European association of Nuclear Medicine Congress (EANM 2019, oral presentation), 4th Nuclear Technologies for Health Symposium (NTHS 2020, oral presentation), SwissTech Convention Center Symposium (SCCL 2019, poster presentation), and Swiss Association of Public Health Administration and Hospital Pharmacists Congress (GSASA 2020, poster presentation).

My contribution to this work was the definition of the methodology, the project administration (execution of the experiments) and the writing of the manuscript under the supervision of my director, Prof. Prior, and my co-director, Prof. Faivre-Chauvet.

The aim of this project was to study preclinically a novel scFv-Fc fusion protein antibody, 1C1m-Fc, which was radiolabeled with ^{177}Lu .

Prior to this work, five fusion protein antibodies (78-Fc, 2B11-Fc, 3B6-Fc, 1C1-Fc and 1C1m-Fc) were studied by high performance liquid chromatography (HPLC), flow cytometry analysis, immunoreactivity testing and their capacity to be radiolabeled was also evaluated. Following these experiments, 1C1m-Fc was shown to be the best candidate and was selected for this PhD work.

1C1m-Fc was isolated by phage display from a naïve human antibody phage display library by the LabCore laboratory, Ludwig Institute for Cancer Research, Lausanne.

In this study, 1C1m was first conjugated with three concentrations of DOTA; 10, 20 and 40 equivalents, corresponding respectively to 2, 3 and 6 DOTA added per antibody in mass spectrometry analysis. 1C1m-Fc and its conjugates were tested for binding to TEM-1 using flow cytometry analysis. A high percentage of binding was observed for 1C1m-Fc at each concentration tested and for each ratio used in the coupling reaction, showing that the conjugation does not affect the binding. Then, 1C1m-Fc was successfully radiolabeled with ^{177}Lu with a radiochemical purity release criterion of 95%. The ratio of 20 equivalents, thus 3

DOTA per antibody was selected to optimize the specific activity of the radiolabeling and was used for the experiments. The immunoreactivity following the radiolabeling was determined by Lindmo assay and was $86.2\% \pm 3.9\%$, showing that the conjugation with 3 DOTA and radiolabeling has no impact on the immunoreactivity.

After performing a dose escalation study (from 2.5 to 500 μg), the total injected dose of 50 μg was chosen for the biodistribution experiments. Indeed, this dose provides the best tumor-to-healthy tissues ratios and allows to have a sufficient specific activity for a therapeutic approach.

Biodistribution experiments were conducted in two groups of mice grafted with either TEM-1 positive tumors (SK-N-AS cell lines, from neuroblastoma) or TEM-1 negative tumors (HT-1080 cell lines, from fibrosarcoma) after injection of radiolabeled 1C1m-Fc conjugated with 3 DOTA. Mouse Fc receptors are highly abundant in mouse liver and spleen and these receptors are known to bind human Fc. Thus, to evaluate the impact of Fc receptor blocking on biodistribution and uptake, the first group received a pre-saturation with 200 μg of a commercial IgG, Kiovig®, followed 24 hours after by an injection of 2.5 μg of [^{177}Lu]Lu-1C1m-Fc and 47.5 μg of the non-radiolabeled antibody. The time point of the pre-saturation was chosen to allow the biodistribution of Kiovig® and its link to the Fc receptor. In this test, a significant uptake was shown in TEM-1 positive tumors compared to the negative ones. Furthermore, the uptake in the positive tumor remains constantly high ($15.8\% \pm 1.9 \text{ IA/g}$) 3 days after injection, demonstrating a retention of TEM-1 targeting antibody. The same test was performed in the second group but without Kiovig® pre-saturation and it was demonstrated that Kiovig® pre-injection had no influence on the biodistribution.

Another biodistribution experiment made in the same conditions, without Kiovig® saturation and with 1C1m-Fc conjugated with 6 DOTA, revealed a really high uptake in the liver and in the spleen $79\% \pm 12.5 \text{ IA/g}$ and $82\% \pm 40 \text{ IA/g}$ respectively, at 24 h.

As the pre-saturation had no impact on the biodistribution we hypothesized that other factors could be responsible of this high non-specific liver uptake; among them the glycosylation of the 1C1m-Fc and the number of DOTA attached per antibody.

To explore the glycosylation impact, biodistributions were done with a [^{177}Lu]Lu-1C1m-Fc non-glycosylated form. These results were not described in the published article.

The TEM-1 + tumor uptake with the non-glycosylated form (conjugated with 5 DOTA) was low ($<10\%$) whereas the spleen uptake in the liver was up to 30%. No difference was shown with or without saturation (Fig. 10).

This test excluded the glycosylation as the cause of liver uptake. A second biodistribution was done with non-glycosylated 1C1m-Fc conjugated with 2 and 5 DOTA (Fig. 11) and the tumor/liver ratio was improved by the 2 DOTA compound.

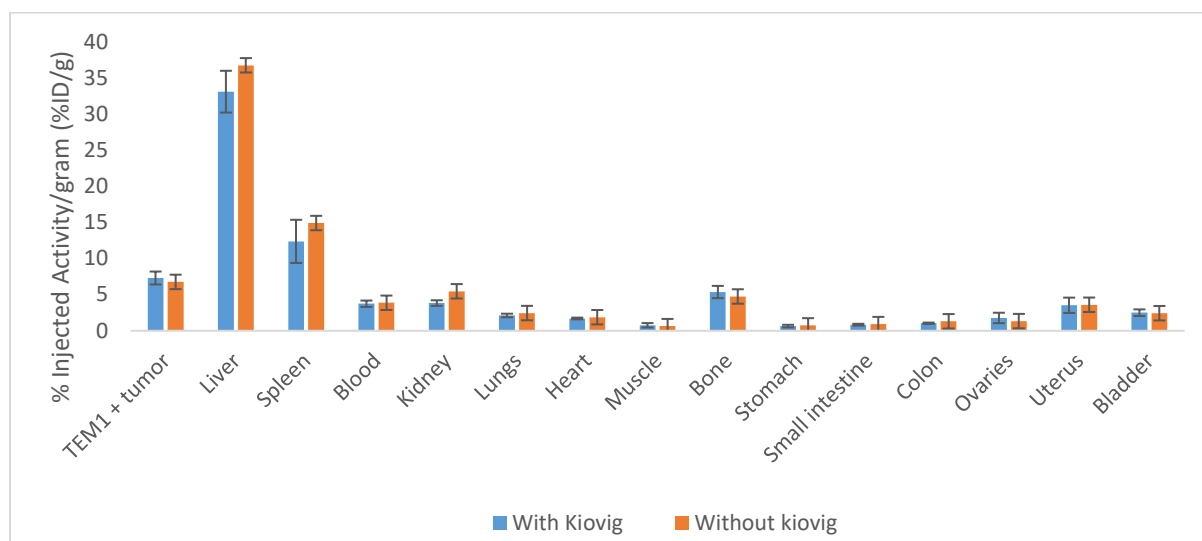


Figure 10: Biodistribution at 24 hours of [177Lu]Lu-1C1m-Fc non-glycosylated form in Balb/c nu mice bearing TEM-1 positive tumor with or without Kiovig® pre-injection.

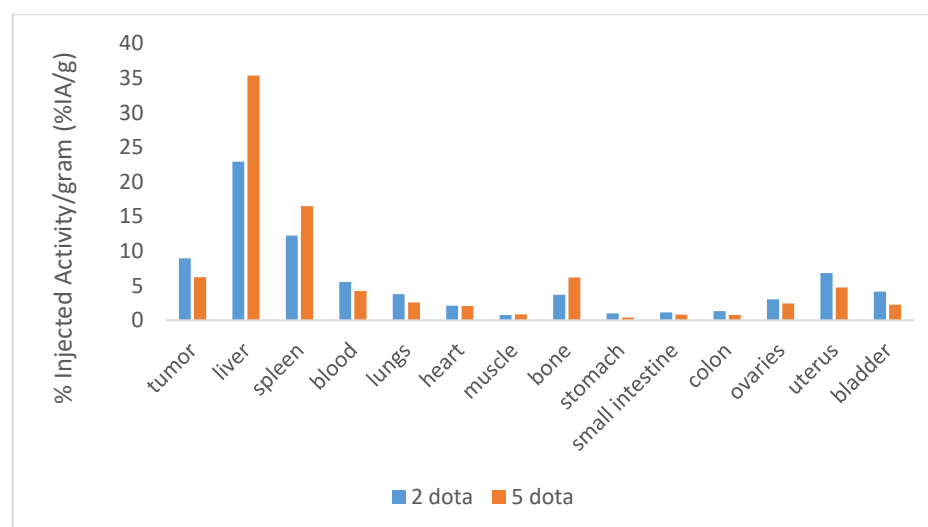


Figure 11: Biodistribution at 24 hours of [177Lu]Lu-1C1m-Fc non-glycosylated form conjugated with 2 or 5 DOTA in Balb/c nu mice bearing TEM-1 positive tumor.

These tests reinforce the hypothesis of the impact of the number of ligands attached to the antibody on the biodistribution.

A murine dosimetry has been done based on the biodistribution results between 4 hours and 6 days on SK-N-AS bearing mice injected with 2.5 µg of [177Lu]Lu-1C1m-Fc conjugated with 3 DOTA and 47.5 µg of the non-radiolabeled antibody. The organ receiving the highest absorbed dose was determined to be the liver (2.23 Gy/MBq), followed by the

uterus (1.5 Gy/MBq), the spleen (1.2 Gy/MBq) and the stomach (1.15 Gy/MBq). The total body dose was 0.4 Gy/MBq and the tumor dose was 1.82 Gy/MBq.

SPECT imaging was performed with mice bearing both TEM-1 positive and negative tumor at 24, 48 and 72 hours after injection of [¹⁷⁷Lu]Lu-1C1m-Fc conjugated with 3 DOTA (50 µg total antibody). The obtained images confirm the specificity of the uptake on TEM-1 positive tumor and validate our fusion protein antibody as a promising candidate for theranostic approach (Fig. 12).

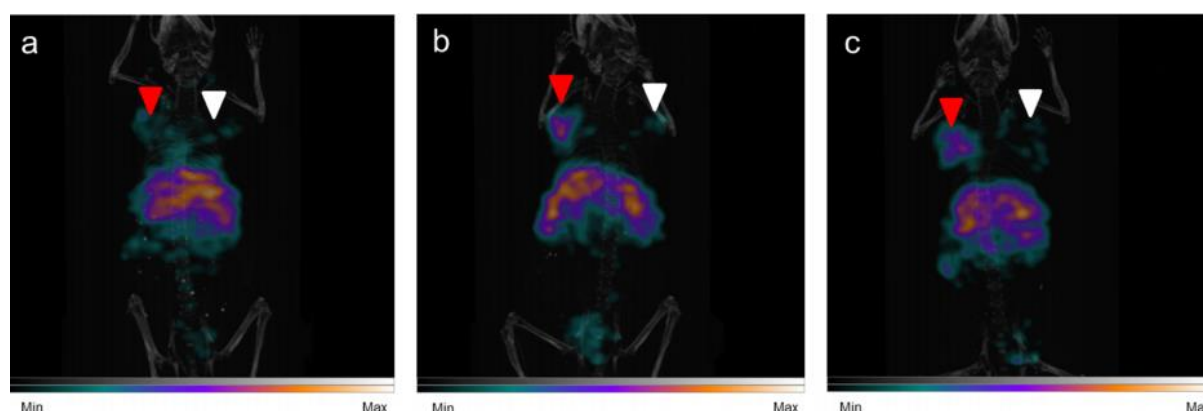


Figure 12: [¹⁷⁷Lu]Lu-1C1m-Fc dorsal view SPECT/CT fusion maximum intensity projection imaging on mice with TEM-1 positive tumor (SK-N-AS, left flank, red arrow) and TEM-1 negative tumor (HT-1080, right flank, white arrow), (a) at 24 h, (b) at 48 h, (c) at 72 h.

These experiments suggest that [¹⁷⁷Lu]Lu-1C1m-Fc is a potentially useful and safe tool for TEM-1 positive tumor therapy. SPECT imaging can also be used to monitor the therapeutic effect of this radiopharmaceutical. The number of DOTA molecules attached per 1C1m-Fc seems to have an impact on the biodistribution. The aim of our next experiments was thus to validate this hypothesis and to find the best ratio of DOTA per antibody to develop an optimal radiolabeled 1C1m-Fc suitable for theranostic application.

Chapter 2: Impact of DOTA Conjugation on Pharmacokinetics and Immunoreactivity of [¹⁷⁷Lu]Lu-1C1m-Fc, an Anti TEM-1 Fusion Protein Antibody in a TEM-1 Positive Tumor Mouse Model

This article has been published in *Pharmaceutics* Journal (2021), 13(1), 96 (175).

I also presented a part of this work at the following congresses: European association of Nuclear Medicine Congress (EANM 2020, oral presentation), SwissTech Convention Center Symposium (SCCL 2020, oral presentation) and Swiss Association of Public Health Administration and Hospital Pharmacists Congress (GSASA 2020, poster presentation).

My contribution to this work was the definition of the methodology, the project administration (execution of the experiments) and the writing of the manuscript under the supervision of my director, Prof. Prior, my co-director, Prof. Faivre-Chauvet and of Dr. Barbet who helped us to define a pharmacokinetic model.

The aim of this project was to validate the hypothesis emitted in my first article (174); namely the influence of the number of ligands on the biodistribution of the radiolabeled fusion protein antibody. Therefore, we evaluated the effect of coupling an increasing number of DOTA per 1C1m-Fc on the pharmacokinetic behavior, immunoreactivity, and dosimetry of the radiolabeled antibody complex to develop an optimal radiolabeled 1C1m-Fc suitable for theranostic application.

1C1m-Fc was conjugated to 6 concentrations of DOTA corresponding in mass spectrometry analysis to 1, 2.5, 3, 6, 8 and 11 DOTA attached to the antibody and the purity of each conjugate was analyzed by HPLC.

All these conjugates were radiolabeled with ¹⁷⁷Lu non carrier added and the immunoreactive fraction assessment was performed by Lindmo assay. The immunoreactivity was shown to not be affected by the conjugation up to 8.5 DOTA whereas a significant loss of immunoreactivity was obtained with the highest number of ligand (11 DOTA per 1C1m-Fc).

A biodistribution experiment was conducted with injection of a mixture of 2.5 µg of [¹⁷⁷Lu]Lu-1C1m-Fc conjugated with respectively 1, 2.5, 3, 6, 8, and 11 DOTA per 1C1m-Fc and 47.5 µg of native unlabeled 1C1m-Fc into the lateral tail vein of the mice bearing TEM-1 positive tumor. The mice were sacrificed for analysis 24 h after injection. The increasing number of DOTA led to a decrease of the tumor uptake, an accelerated blood clearance and a

increase of the liver uptake. An increase of spleen and bone uptake was also obtained with the highest ratio of DOTA. Finally, an inversed correlation of the tumor/liver ratio was observed (Fig. 13).

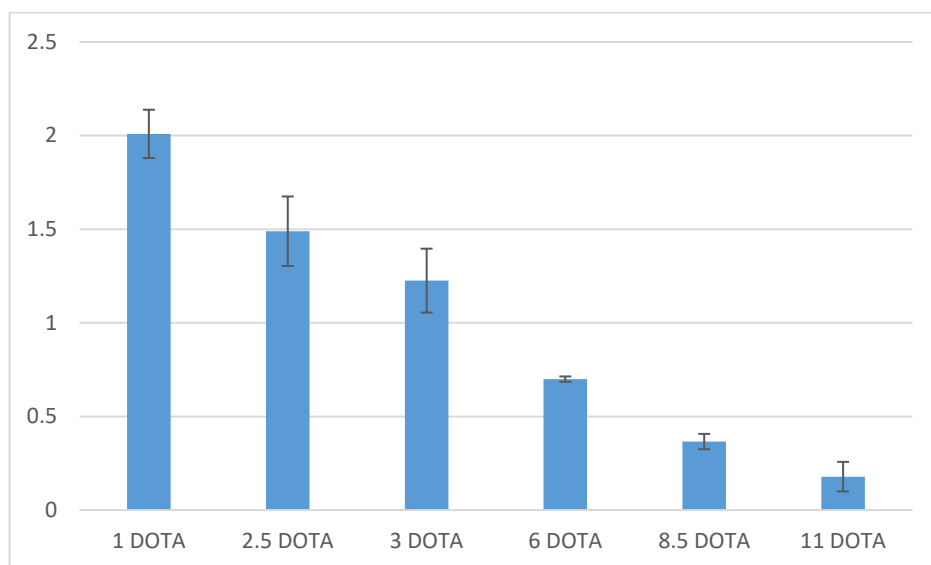


Figure 13: Ratio between the tumor and the liver uptake at 24 h with respect to the number of DOTA per [^{177}Lu]Lu-1C1m-Fc in Balb/c mice bearing TEM-1 positive tumor. Spearman test gives a $\rho = -0.99$, $p < 0.0001$.

For the [^{177}Lu]Lu-1C1m-Fc conjugated with 1 and 3 DOTA, complementary time points have been added for the biodistribution, and animals were euthanized 4, 24, 48, 72 h, and 6 days after injection. The uptake in TEM-1 positive tumors was unchanged between the two groups. However, in the case of [^{177}Lu]Lu-1C1m-Fc conjugated with 1 DOTA, the non-specific uptake in the liver was significantly lower than the one observed with 3 DOTA conjugated at 24 and 48 h ($p = 0.02$ and 0.01 respectively).

To ensure the consistency of the data, a multi-compartment pharmacokinetic model was defined. In this model, the injected antibody was distributed from a central compartment, representing the blood, into peripheric compartments corresponding to all investigated organs plus an additional compartment representing all uncounted tissues.

The following assumptions obtained regarding the data of the biodistribution were made: the rate of liver uptake is proportional to the number of DOTA per antibody and that the rates of uptake into tumor and uterus (a normal tissue expressing low amounts of antigen) increased linearly with the immunoreactivity. Conversely, the rates of spleen and bone uptake decrease linearly with the immunoreactivity. Then, all available biodistribution data, at all time-points for 1 and 3 DOTA per 1C1m-Fc, and at 24 h after injection for the other conjugates were fitted simultaneously using a single set of kinetic parameters.

Kinetics with 1C1m-Fc conjugated respectively with 1 and 3 DOTA were satisfactorily fitted by the model. More interestingly, the trends in 24 h biodistributions for the six different concentrations of DOTA were well replicated (Fig. 14).

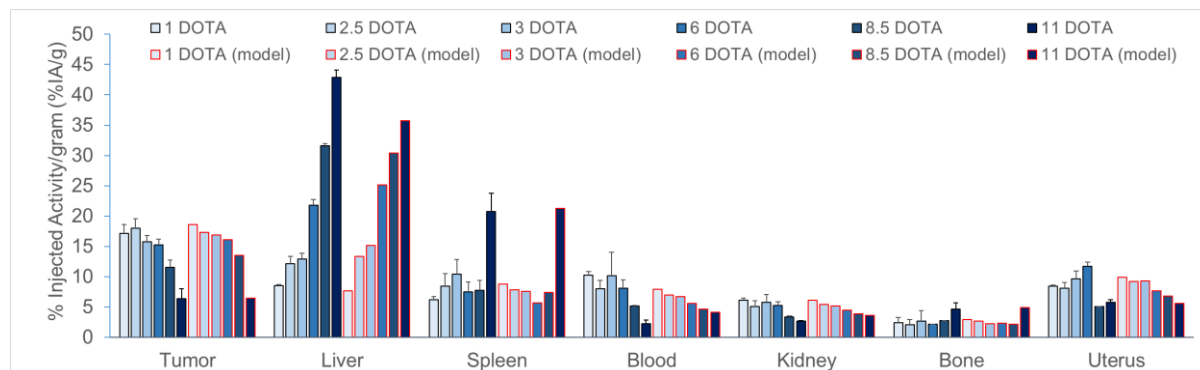


Figure 14: Comparison between the results obtained by biodistribution (in grey) and pharmacokinetic modeling (in red) at 24 h for $[^{177}\text{Lu}]\text{Lu-1C1m-Fc}$ conjugated with 1 to 11 DOTA in Balb/c nu mice bearing TEM-1 positive tumor.

The increased liver uptake at higher numbers of DOTA effectively decreases the amount of circulating $[^{177}\text{Lu}]\text{Lu-1C1m-Fc}$ and consequently the amount of $[^{177}\text{Lu}]\text{Lu-1C1m-Fc}$ in most of other organs. The loss of immunoreactivity explains the decrease of the TEM-1 specific uptake in the tumor and the uterus, especially at the two highest DOTA per antibody ratios. Finally, the increase of the spleen and bone uptake at the highest concentrations of DOTA is linked by a higher uptake of non-immunoreactive $[^{177}\text{Lu}]\text{Lu-1C1m-Fc}$.

This pharmacokinetic model allows to validate our hypothesis and to explain the observations made in the biodistribution experiments.

A murine dosimetry has been done based on the biodistribution results between 4 hours and 6 days on SK-N-AS bearing mice injected with 2.5 μg of $[^{177}\text{Lu}]\text{Lu-1C1m-Fc}$ and 47.5 μg of the non-radiolabeled antibody conjugated with 1 DOTA.

The organs that receive the highest absorbed dose was the uterus (1.83 ± 0.14 Gy/MBq), followed by the liver (1.79 ± 0.13 Gy/MBq), the stomach wall (1.66 ± 0.08 Gy/MBq) and the kidneys (1.32 ± 0.05 Gy/MBq). The total body dose was 0.55 ± 0.04 Gy/MBq and the tumor dose was 2.53 ± 0.25 Gy/MBq. Data was compared to the one obtained with radiolabeled 1C1m-Fc conjugated with 3 DOTA (published in (174)). The tumor/liver absorbed dose ratio increased from 0.8 for the $[^{177}\text{Lu}]\text{Lu-1C1m-Fc}$ conjugated to 3 DOTA to 1.4 for the $[^{177}\text{Lu}]\text{Lu-1C1m-Fc}$ conjugated to 1 DOTA. The non-specific uptake in the kidneys, the lungs and the specific uterus uptake was higher with the fusion protein conjugated with 1 DOTA showing again the impact of the number of ligands conjugated to the antibody.

In these experiments 1C1m-Fc appeared to be a very promising compound for a theranostic approach. We have demonstrated that the number of chelators per fusion protein antibody plays a significant role in determining successful tumor targeting. Thus, there is an opportunity to further improve the biodistribution and imaging contrast. [¹⁷⁷Lu]Lu-1C1m-Fc conjugated with 1 to 3 DOTA seem to be the best ratios to maintain a balance between the specific activity, immunoreactivity, and pharmacokinetic behavior and appear as interesting candidates for further theranostic development.

The aim of our next experiments was to use this candidate in a theranostic approach allowing imaging with ⁶⁴Cu and therapy with ¹⁷⁷Lu.

Chapter 3: Copper-64-labeled 1C1m-Fc, a new tool for TEM-1 PET imaging and prediction of Lutetium-177-labeled 1C1m-Fc therapy efficacy and safety

This article has been published in *Cancers Journal* (2021), 13(23), 5936.

My contribution to this work was the definition of the methodology, the project administration and the writing of the manuscript under the supervision of my director, Prof. Prior, my co-director, Prof. Faivre-Chauvet. The experiments have been performed in Lausanne and in Nantes with the help of the Équipe 13 (Recherche en oncologie nucléaire), CRCINA, UMR 1232 INSERM.

In our previous works we selected 1C1m-Fc, a fusion protein antibody, then radiolabeled it with ^{177}Lu and studied preclinically this radiolabeled compound. We demonstrated that [^{177}Lu]Lu-1C1m-Fc was a suitable tool for therapeutic approach and that the number of ligand per fusion protein antibody should be chosen carefully to have the best tracer biodistribution and pharmacokinetic.

In order to perform a complete theranostic application, 1C1m-Fc was radiolabeled with ^{64}Cu and studied preclinically. The aim of this work was to determine if [^{64}Cu]Cu-1C1m-Fc can be considered as a new tool for TEM-1 PET imaging and to predict the dosimetry of the [^{177}Lu]Lu-1C1m-Fc companion therapy.

1C1m-Fc was first conjugated to 3 to 4 DOTA. The DOTA ligand has been chosen to have the same chelator for imaging and therapy. The number of DOTA per antibody has been defined to have the capacity to radiolabel the fusion protein antibody, taking into account the variability of the specific activity of the copper source and to avoid a final purification. Furthermore, this number of DOTA offers sufficient specific activity for theranostic approach. Regarding our previous experiments this ratio of ligand per antibody was the best compromise to maintain an adequate balance between radiochemical yield, immunoreactivity and pharmacokinetic behavior.

1C1m-Fc was successfully radiolabeled with ^{64}Cu (release criteria > 95%). Immunoreactivity in serum media was assessed until 48 h and was up to 70%, meaning that the conjugation and the radiolabeling process do not affect the binding. ^{64}Cu has been selected as PET radionuclide as its half-life (12.7 h) was compatible with PET immuno-imaging and its

physical decay properties: low energy beta positive (17%, 0.655 MeV), beta minus particles (39%, 0.573 MeV) and electron capture (44%) made it suitable for theranostic applications.

Imaging studies were performed at 4, 24 and 48 h (Fig. 15). The best tumor to liver ratio was obtained 48 h after injection of the radiolabeled antibody.

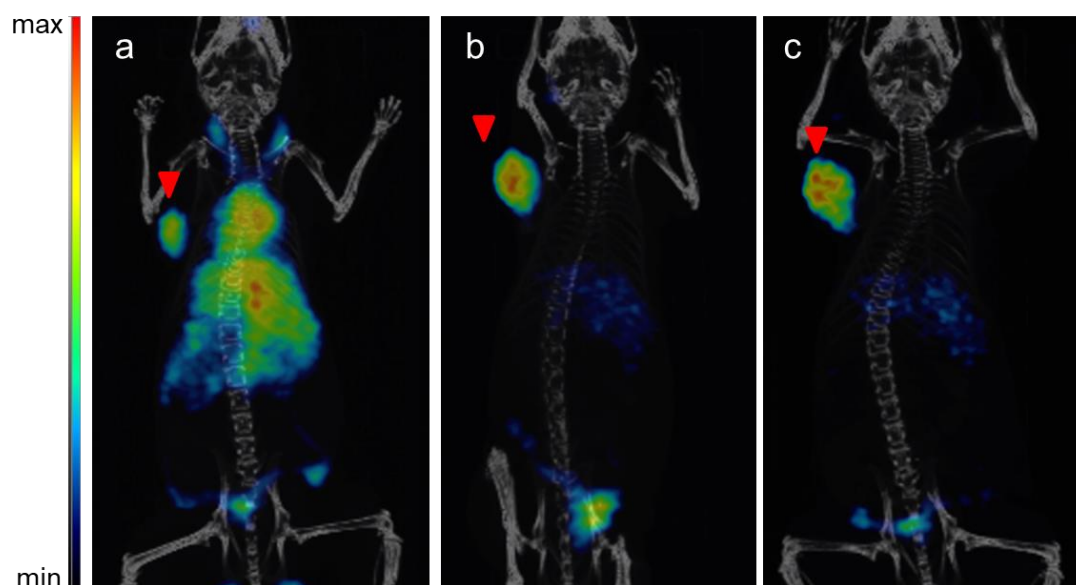


Figure 15: [^{64}Cu]Cu-1C1m-Fc dorsal view PET/CT fusion maximum intensity projection on mouse bearing TEM-1 positive tumor (SK-N-AS, left flank, red arrow), (a) at 4 h, (b) at 24 h, (c) at 48 h.

Furthermore, imaging with mice bearing both TEM-1 positive and negative tumors was done and confirmed the specific uptake in TEM-1 positive tumor contrary to control tumor. Nevertheless, a low uptake was observed in TEM-1 negative tumors, that can be due to the presence of TEM-1 in tumor stroma and neo-vessels and by the cross reactivity of our antibody for human and murine TEM-1.

Biodistribution experiments were conducted with two groups. For the first one, mice were grafted with TEM-1 positive tumor and sacrificed at around 4, 24 and 48 h after the injection of [^{64}Cu]Cu-1C1m-Fc (50 μg total antibody). (Fig. 16). An important specific uptake was observed in the tumor ($24.5 \pm 1.5\%$ IA/g) at 24 hours. The tumor to organ ratios were comprised between 1.6 (tumor to uterus) to 8 (tumor to muscle) at 24 hours.

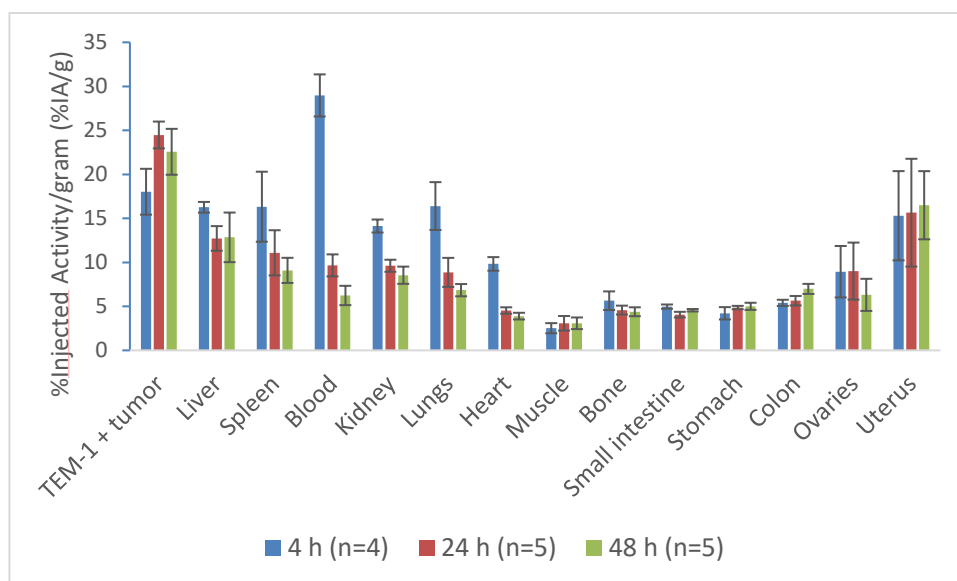


Figure 16: Biodistribution of [64Cu]Cu-1C1m-Fc (a) in Balb/c nude mice bearing TEM-1 positive tumor (group 1). Data are shown as mean ± SD.

The second biodistribution experiment was performed in the same conditions but in mice bearing both TEM-1 positive and negative tumors to ensure a control group. This test underlines the specific TEM-1 binding. The uptake in TEM-1 positive tumor was 2.4 times higher than the one in TEM-1 negative tumor. A high uptake in the uterus was also observed as this tissue expressed a low level of TEM-1 (91).

The biodistribution profile with [64Cu]Cu-1C1m-Fc was compared to the ones obtained with [177Lu]Lu-1C1m-Fc in our previous studies (174, 175). The profiles were very closed. Nevertheless, as the radionuclides differ in coordination geometry, number of DOTA and charges some differences were found.

A higher uptake in the tumor was observed with the 64Cu conjugate. This may be due to the difference in charges between the 3 DOTA 177Lu and 64Cu conjugates (176). The major discrepancy was the uptake in the gastrointestinal tract that was higher with the 64Cu compound. This can be explained as the hepatobiliary system is the most important excretion route for 64Cu compounds (177). Furthermore, the absence of excretion from the gastro intestinal tract and the liver between 24 and 48 h can be explained by the transchelation of [64Cu2+] ions due to the instability of the DOTA complexation.

The blood uptake was closer between [64Cu]Cu-1C1m-Fc and [177Lu]Lu-1C1m-Fc conjugated with 1 DOTA and conversely the hepatic uptake was closer to [177Lu]Lu-1C1m-Fc conjugated with 3 DOTA.

Dosimetry study was also performed. The organs which received the highest doses were the liver, the uterus, the heart, the kidneys and the lungs. The dose in the tumor was 225 mGy/MBq and exceeded the liver one by a factor of 1.2.

To determine if [^{64}Cu]Cu-1C1m-Fc is a good tool to predict the dosimetry of the [^{177}Lu]Lu-1C1m-Fc companion therapy, the absorbed doses obtained with ^{64}Cu were extrapolated to ^{177}Lu and compared to the absorbed doses obtained experimentally in our previous studies with [^{177}Lu]Lu-1C1m-Fc (1 and 3 DOTA chelation).

For parenchymal organs, the comparative between the extrapolated doses and the experimental doses obtained with [^{177}Lu]Lu-1C1m-Fc conjugated with 1 DOTA results were close (< 20% of discrepancies). The matching was inferior with the 3 DOTA form and correlates with the results of the biodistribution study. An overestimation is done by the extrapolated dose for the gastrointestinal tract, for the tumor and uterus. For the gastrointestinal tract, the potential origin of this high uptake has been described previously. Furthermore, for the uterus and the tumor the overestimation could also come from lack of later time acquisition point (> 50 h for the ^{177}Lu extrapolated biodistribution). In fact, for these tissues, the extrapolated ^{177}Lu effective normalized time activity curve (nTAC) is still not decreasing at 50 h post injection (the last measured time point). Indeed, the tail of the nTAC to infinite was assumed to follow the physical decay of ^{177}Lu possibly overestimating the actual value. An interesting perspective would be to use a radionuclide with a longer half-life such as ^{89}Zr (78.4 h).

In this study, we have demonstrated that [^{64}Cu]Cu-1C1m-Fc is a good tool to visualize TEM-1 expression with high resolution PET images. Furthermore, extrapolated dosimetry based on [^{64}Cu]Cu-1C1m-Fc data could be an indicator to predict the toxicity in parenchymal organs.

1C1m-Fc radiolabeled with ^{64}Cu appears as an interesting companion for therapeutic application with 1C1m radiolabeled with ^{177}Lu . To go further with this work, some improvements could be done, such as human extrapolation dosimetry or evaluation of the predictive potential of 1C1m-Fc radiolabeled with ^{89}Zr to determine the [^{177}Lu]Lu-1C1m-Fc dosimetry and safety.

Discussion

The current challenge in oncology is to give personalized medicine to the patients with a specific targeting of cancer cells. In this context, theranostic application plays a central role to increase the therapy efficiency, minimize the adverse effects and improve patient's outcome. The aim of this PhD work was then to select a promising target, TEM-1, and to explore a new ScFv-Fc fusion protein antibody, 1C1m-Fc, in a theranostic approach with dual radiolabeling: ^{64}Cu for imaging and ^{177}Lu for therapy.

1- Main findings of the project

1-1 Interest of a new type of fusion protein antibody

Several fusion protein antibodies were produced from a naïve human antibody phage display library by the LabCore laboratory (Ludwig Institute for Cancer Research, Lausanne). Among them 1C1m-Fc was selected regarding its *in vitro* properties (purity, immunoreactivity, flow cytometry profile).

The interest of this new fusion protein antibody lies first in its structure. Indeed, the major defect of the monovalent scFv antibody fragments was to have a short half-life associated with a relative *in vivo* instability (178). 1C1m-Fc results of the fusion of ScFvs to IgG constants domain. This construct leads to an improved blood kinetics with an increase stability. This point is relevant for therapeutic approach as long half-life nuclides are requested.

Furthermore, 1C1m-Fc has the ability to cross-react to murine and human TEM-1. Thus, 1C1m-Fc presents a superiority to other TEM-1 antibodies currently studied in clinic such as MORAb-004 (143). Indeed, this cross reactivity allows the evaluation of TEM-1 in xenograft mouse models. In this case, the fusion protein antibody can not only target the TEM-1 expressed by the human cancer cells but also the physiological expression of TEM-1 in mice and the neoangiogenic vasculature of the tumors. Due to these properties, in our experiments we have been able to observe a specific uptake of our radiolabeled compound in TEM-1 positive tumor, in the uterus (normal tissue with TEM-1 expression (86)) but also an uptake in TEM-1 negative tumor due to the neo-angiogenesis (as negative tumors used in our mouse model were highly vascularized). The uptake in the uterus will have to be considered in perspective of a human therapy. Further investigations will have to be done to define if this uptake will be a limiting factor for therapy development.

1-2 Validation of the radionuclide used for theranostic approach

Theranostics in nuclear medicine is relative to the synergic use of a radionuclide pair coupled to a vector for imaging and therapy. Companion nuclear imaging radiopharmaceuticals based on the same platform as therapeutic ones allow the selection and the monitoring of the patients as well as the optimization of the therapeutic doses (77).

The aim of our work was to design a preclinical theranostic study with the radiolabeling of the 1C1m-Fc fusion protein antibody. We have chosen the radionuclide pair $^{64}\text{Cu}/^{177}\text{Lu}$ respectively for imaging and therapy. These two radionuclides are long-life isotopes adequate for the radiolabeling of fusion protein antibody.

For the imaging part, due to its physical properties, (β^+ , 17.4%, E_{max} 0.656 MeV; β^- , 39%, E_{max} 0.573 MeV, electron capture 44%), ^{64}Cu gives higher radiation dose and a lower images quality compared to ^{18}F (β^+ 96.7%) or ^{68}Ga (β^+ 88.9%) (179). Nevertheless, at later time points, the long half-life of ^{64}Cu gives an advantage by increasing the tumor delineation (180). The long circulating time of ^{64}Cu allows achieving good tumor to background ratios.

Several studies showed that instability of macrocyclic copper-chelates *in vivo* can lead to free radionuclide. Free ^{64}Cu can be released in the blood or be transchelated by protein such as ceruloplasmin, or superoxide dismutase and accumulates in organs such as the liver or the uterus (181, 182). On the opposite, it has been demonstrated that copper ions have a very high affinity for cancer cells. Indeed, the human copper transporter is overexpressed in malignancies (183, 184). ^{64}Cu has been presented as attractive for long term PET imaging (185) and in our study we have demonstrated that [^{64}Cu]Cu-1C1m-Fc allows to visualize TEM-1 tumors with high quality images in PET/CT modalities.

^{177}Lu is a radionuclide of choice for therapy. Indeed, this β^- and γ emitter is able to induce damages to neighboring healthy cells with a low energy emission ($E_{\beta\text{-max}}$ 0.49 MeV) and a maximal tissue penetration of 2 mm. Furthermore, the long half-life of ^{177}Lu (6.7 days) is adapted to therapeutic applications with radioimmunoconjugates. For therapy, the absorbed dose in the tumor must be higher than in the normal tissue. This criteria was reached with [^{177}Lu]Lu-1C1m-Fc conjugated either with 1 and 3 DOTA. Indeed, we observed a good tumor to normal tissue absorbed dose ratio. Another point of interest for ^{177}Lu is the capability to perform imaging after therapy to monitor the response to the treatment and perform dosimetric analysis through the emission of two photons at 113 KeV (6.4%) and 208 KeV (11%).

The biodistribution profiles of 1C1m-Fc radiolabeled with ^{64}Cu or ^{177}Lu are closed. This suggests that [^{64}Cu]Cu-1C1m-Fc could be used as a companion imaging agent for [^{177}Lu]Lu-

1C1m-Fc therapy. The comparison between the extrapolated doses based on the [^{64}Cu]Cu-1C1m-Fc biodistribution data and the experimental results obtained with the [^{177}Lu]Lu-1C1m-Fc suggests that the ^{64}Cu compound could be of interest to give a predictive indication of the toxicity in parenchymal organs after a therapy with 1C1m-Fc radiolabeled with ^{177}Lu .

Nevertheless, an overestimation has to be considered for the gastrointestinal tract (due to the natural elimination of the ^{64}Cu (186)) and for the uterus and the tumor that are TEM-1 positive tissues. Two other factors might have a role in the high uptake in the tumor and in the uterus observed with [^{64}Cu]Cu-1C1m-Fc. The first one is the transchelation of [^{64}Cu]Cu-1C1m-Fc and the second may result in the fact that ^{177}Lu effective nTAC is still not decreasing at the latest point of biodistribution (50 h).

In our work, we validated that 1C1m-Fc radiolabeled with ^{64}Cu for imaging would appear as an interesting radionuclide companion for therapeutic application with [^{177}Lu]Lu-1C1m-Fc.

1-3 Determination of the dose and of the condition of pre-saturation

An important liver uptake was observed after injection of the radiolabeled compound in our experiments. This uptake was non-specific as the absence of TEM-1 antigen was already demonstrated by quantitative polymerase chain reaction (PCR) on liver biopsies. It was described that the high level of Fc receptors in the liver of mice is associated to an important liver uptake (187, 188). However, we invalidated this hypothesis in our model as no difference in the biodistribution results was found with a pre-saturation with a commercial IgG, Kiovig®. Therefore, we chose to inject our radiolabeled compound without pre-saturation.

Saturation assays have been performed to determine the best amount of total antibody to administrate. The quantity of 50 μg per dose has been chosen for the study. Indeed, this dose gave the best tumor to tissues ratio and allowed to use a sufficient specific activity for a theranostic approach. With ^{177}Lu the specific activity with the 3 DOTA conjugate was 400 MBq/mg and for ^{64}Cu 180 MBq/mg (this activity has been defined by taking into account the variability of the specific activity of the copper source).

1-4 Impact of the conjugation

In this work we have underlined the impact of the chelation on the biodistribution, the immunoreactivity and the pharmaceutical behavior of a radiolabeled compound.

We have observed that a high number of DOTA resulted in a loss of immunoreactivity, a high liver uptake and an accelerated blood clearance.

Until now, several contrary opinions were published. Some of them have conclusions closed to ours, indicating that immunoreactivity can be affected by a high number of chelates per antibody. Indeed, the conjugation, which is non-specific, can appear on the variable chains of the antibody compromising the antigen binding and the targeting of the radiolabeled compound (176, 189). Furthermore, the hydrophilic property of the DOTA chelator has been described to be linked to a modification of the pharmacokinetic behavior with a fast blood clearance and an increase of the liver uptake (190, 191). On the other hand, other groups reported that the negative charge conferred by the DOTA chelators induces a repulsion between the phospholipid bi-layer and the radiolabeled compound, resulting in a decrease of the liver uptake (192, 193). In these studies, the negative charged conjugates presented less liver uptake than the positive ones (194-197). The differences of results compared to our observations can be explained by the methodology used. Indeed, these authors studied several chelators but the number of chelates per antibody was fixed. In our project, a new analysis was performed as we have studied the impact of a various chelate to antibody ratios but with a unique chelator, DOTA.

The understanding of this point is really important to optimize the biodistribution of a radiolabeled compound. It seems that the impact of the ligand number is specific to each antibody and chelator and have to be studied preclinically to determine the best ratio to use.

A compromise has to be done to use the lowest number of chelates per antibody to ensure the best radiochemical yield, a sufficient specific activity (that can differ between imaging or therapeutic application) and the best tumor to organ ratio.

1-5 Interest of pharmacokinetic modeling

As described in the precedent paragraph, no clear mechanism was defined in the published works to explain the role of the number of chelators grafted per fusion protein antibody. Therefore, we have used a multi-compartment model to validate the hypothesis made with our experiments. Simultaneous fit correlated with the biodistribution results. Data obtained from the model showed that a high DOTA per antibody ratio increases the liver uptake, depletes the antibody circulating in the blood and the rate of antibody in the tissues (including the tumor). We also underlined that the specific absorption in the tumor and in the uterus decreases with the loss of immunoreactivity.

This type of modeling contributes to validate the hypothesis based on the experiments and provides useful information to improve the biodistribution of the radiolabeled compound.

2 - Perspectives of this study

2-1 Optimisation of the radioimmunoconjugate

2-1-1 New fusion protein antibody

Two additional forms of dimeric 1C1m-Fc have been engineered by the LAbCore laboratory, Ludwig Institute for Cancer Research Lausanne Branch.

The 1C1m-Fc used in our work was a scFv with a variable light chain (VL) linked to the variable heavy chain (VH) [VL-link-VH] orientation, fused to a human IgG1 Fc to yield a homodimer upon expression to the extracellular media. The linker used was a flexible spacer peptide designed to allow the two VH chains to come together to form the mature Fv domain. This linker is bounded by unique restriction cloning sites to allow simple and convenient exchange of modified VH or VL domains.

An alternative homodimer similar to the initial 1C1m-Fc was generated by reversing the scFv chain orientation [VH-link-VL], and incorporating a modified inter-domain linker (minus cloning sites) that is more similar to those found in approved antibody-based drugs. It was observed that this version retains good expression and TEM-1 target recognition, and appears to have slightly improved stability over the parental 1C1m-Fc.

The second molecule is a novel experimental heterodimer lacking a Fc domain. This molecule is produced by the assembly of a two-chain humanized Fab with 1C1m scFvs fused to the C-terminus of each of the two Fab constant domains (CH1 and Ck). Production of this molecule thus requires the co-transfection of two genes. This heterodimer, in which the 1C1m scFv can be in either the VL-link-VH or VH-link-VL domain orientation is termed a TriloBiTE (198). This molecule was designed to escape glomerular filtration (similar size to 1C1m-Fc) and not to interact with Fc-receptors or undergo Neonatal Fc Receptor (FcRn) recycling (hence, a faster clearance than the Fc is expected). The heterodimerizing Fab arm in the TriloBiTE is specific for a human antigen and does not recognize the corresponding murine ortholog target.

The objective would be to test these two new forms using the knowledge we have acquired with the initial 1C1m-Fc and to evaluate if the biodistribution, the pharmacokinetic and the dosimetry are improved.

2-1-2 Site specific conjugation

In addition to the number of ligand per antibody, the site of the conjugation is a key factor. In our work, we have performed non-specific conjugations. In this case, chelators are

conjugated to the antibody through lysine or cysteine, leading to heterogeneous mixture with various conjugation sites and chelate to antibody ratios (199). Site-specific conjugation have been described to improve the consistency of the conjugation batch. Indeed it avoids the interaction between the ligand and the variable chain compromising the antigen binding or the pharmacokinetics change when the coupling occurred to FcRn domains (200).

In the past years, several groups have evaluated different site-specific approaches such as introduction of extra cysteine residues (201), enzymatic conjugation (176), sugars modification (202), genetic code expansion and click chemistry (199).

To increase the reproducibility of the 1C1m-Fc conjugation, in particular with an objective of studying our radiolabeled compound clinically, it will also be interesting for our group to standardize the process. A new antibody conjugation technology (AbYlink™) studied in Lausanne Molecular Imaging Research Laboratory could be of interest. Indeed, this technique allows a specific targeting of the Fc region and could thus be tested on ScFv-Fc forms. With this technology, the antibody keeps its affinity for the target after conjugation due to the excellent selectivity for Fc region-labelling (203).

2-1-3 Test of new bifunctional ligands

In our work we have chosen to use DOTA as BFCA. Indeed, this commercially available chelator is the most frequently used in clinic for radiolabeling with ¹⁷⁷Lu. The role of the BFCA is to stabilize the radiometal after conjugation, and to ensure a covalently link between the vector and the radionuclide. For ⁶⁴Cu, it is really important to have an inert and thermodynamically stable complex. Indeed, as mentioned previously, free copper ions can be transchelated by metalloprotein and accumulate in the liver (181). Even if DOTA is thermodynamically stable, it has been described that this chelate is not sufficiently inert in acidic or reducing conditions (186). The transchelation can increase the background noise in imaging and cause nonspecific irradiations. We have seen in our experiments that transchelation can lead to an increase of the uptake in parenchymal organs such as the liver.

To avoid this effect and evaluate the impact of the type of chelator on the biodistribution of [⁶⁴Cu]Cu-1C1m-Fc it would be interesting to compare the results obtained with DOTA to another chelating system. ⁶⁴Cu experiments have been performed in collaboration with the CRICNA, INSERM 1232 group. This group has synthesized a new copper chelator, TE1PA which is a monocolate cyclam. This new chelator has a favorable complexation kinetics and has been described to be more stable thermodynamically and more inert than DOTA (76, 204). In a previous study, hepatic uptake of TE1PA was shown to be more important at the early

times, nevertheless the complexes presented an important resistance to transchelation in the liver. Therefore, the chelator has been described of interest for later time imaging which is compatible with the use of radioimmunoconjugates (76).

2-1-4 Test of other radionuclides

We have demonstrated in our experiments that [^{64}Cu]Cu-1C1m-Fc is an interesting radiopharmaceutical for TEM-1 PET imaging. Furthermore, the estimated dosimetry based on [^{64}Cu]Cu-1C1m-Fc data appears to be an indicator to predict [^{177}Lu]Lu-1C1m-Fc toxicity. Nevertheless, some overestimations were found, in part due to the difference of half-life between ^{64}Cu and ^{177}Lu . Indeed, for ^{64}Cu the late interpretable biodistribution point is around 48 h whereas it was 6 days for ^{177}Lu . Complementary PET imaging developments with longer half-life radionuclide, such as ^{89}Zr , a positron-emitting radionuclide (half-life 78.2 h) could be of interest. As well as for ^{64}Cu , a stable chelation is required for ^{89}Zr . Indeed, free ^{89}Zr can bind to bones (205).

Another possibility was to use ^{64}Cu for the diagnosis (low dose) and the therapeutic part (high dose) as an alternative option to ^{177}Lu . Indeed, as discussed previously, this radionuclide emits low-energy positrons, β^- particles and Auger electrons, and can be used either for high resolution PET-images or for electing a therapeutic effect (206). The use of the same radionuclide allows thus to give an exact prediction of the dosimetry after therapy.

2-2 Complementary experiments necessary for human translation study

2-2-1 Preclinical therapeutic experiment

In our work, we have validated the target, the vector and the model. To go deeper in the analysis, it would be interesting to plan a dose-escalation and a therapeutic study. The hematological, kidney and liver toxicities would also have to be monitored with blood sampling.

Four arms could be defined for this preclinical evaluation: the first two with injection of the radioimmunoconjugate [^{177}Lu]Lu-1C1m-Fc (50 μg total antibody, and respectively 10 or 15 MBq of ^{177}Lu), the third one with injection of the non-radiolabeled antibody 1C1m-Fc (50 μg total antibody) and a fourth control group with injection of saline. This way, we could validate the therapeutic efficacy of [^{177}Lu]Lu-1C1m-Fc in murine model and compared the results between immunotherapy and radioimmunotherapy. The aim being to obtain a permanent cure, we expect to have a superior therapeutic efficacy of [^{177}Lu]Lu-1C1m-Fc compared to

1C1m-Fc due to ^{177}Lu -related crossfire and bystander effects that can fight against resistant cancer cells, irregular vascularization and hypoxia as described by other groups (207, 208).

It would also be of interest to validate the absence of significant effect of a pre-injection of [^{64}Cu]Cu-1C1m-Fc on the biodistribution of [^{177}Lu]Lu-1C1m-Fc.

2-2-2 Dosimetric study with human extrapolation

For clinical translation of new radiopharmaceuticals in clinical study, a human radiation dosimetry is mandatory. Usually, prior to the first-in-human-use study, the dose assessment is based on the animals preclinical studies (209). We have planned to generate dosimetry estimates using mouse biodistribution data to extrapolate the radiation absorbed dose to human with both [^{64}Cu]Cu-1C1m-Fc and [^{177}Lu]Lu-1C1m-Fc.

For this extrapolation, the tumor sink is an important aspect to take into account (173). Indeed, the size of the tumor is relatively important regarding the total mass of the animal in tumor bearing mouse. Thus, we have to consider that the availability of the fusion protein antibody for the healthy tissue would be higher if this antigenic sink was not present. Relatively, human tumors present a smaller size. A specific formula will have to be applied to consider this difference of biodistribution.

Then, it will be then interesting to compare the obtained results of this human extrapolation to those of a radioimmunoconjugate used in clinic such as [^{90}Y]Ibritumomab-tuixetan, Zevalin®. Zevalin® is the only radiolabeled antibody approved for clinical application for the treatment of recurrent or refractory non-Hodgkin's lymphomas (210).

Finally, the aim of this dosimetry extrapolation is to validate that [^{64}Cu]Cu-1C1m-Fc and [^{177}Lu]Lu-1C1m-Fc can be safely used for further evaluation in human and to determine the most appropriate dose for [^{177}Lu]Lu-1C1m-Fc therapy. The dosimetry in organs such as liver or uterus will have to be considered to determine if the absorbed dose in these tissues is a limiting point for therapeutic application.

2-3 From bench to bedside

Before performing clinical studies, preclinical drug development is required with *in vitro* and *in vivo* experiments. With the *in vivo* tests done in our project we have provided the evidence that 1C1m-Fc have a favorable tumor targeting in animals. Valuable biodistribution and pharmacokinetic data obtained in animals could be used to plan the starting dose and program a phase I study (211).

The final aim of this project would be to translate the knowledge obtained with the preclinical data to the patient, conducting a first-in-human theranostic study, using 1C1m-Fc for nuclear imaging (PET/CT) with ^{64}Cu as well as radioimmunotherapy based on ^{177}Lu . This study could be conducted in soft tissue sarcoma (STS), a disease in dire need of new therapeutic strategies, and in which TEM-1 is highly expressed.

After obtaining all preclinical data (previously discussed) three steps would be foreseen. The first one would be to obtain Swiss regulatory approval for a phase I study. The second step would focus on conducting nuclear imaging study. We would use [^{64}Cu]Cu-1C1m-Fc for PET/CT imaging in patients with known advanced STS who failed conventional chemotherapy and have a documented local or distant recurrence. A dose escalation scheme would be followed and parallel biopsies would allow us to correlate the imaging results with tissue expression of TEM-1. The last step would be to extend the phase 1 study and to add radio-immunotherapy, once PET/CT would be established as a non-invasive method of TEM-1 detection. In this case, we would use [^{177}Lu]Lu-1C1m-Fc and the same population would be enrolled following a dose escalation scheme.

This study would be innovative on several points. Indeed, it would be a first in human trial, using a new class of molecules, developing a theranostic approach and giving the opportunity to offer a new treatment for sarcoma. If successful, this study would have the potential to make a significant contribution in the treatment of sarcoma, using radioimmunotherapy. In addition, this study may have profound implications for most common carcinomas, as well as neuroblastoma, melanoma and glioblastoma, which also express TEM-1 in their vasculature and where TEM-1 targeting therapeutic antibodies are expected to have powerful vascular disrupting effects.

Conclusion

TEM-1 is an excellent therapeutic target since it is tumor-specific, it is associated with more aggressive tumor phenotypes, and its elimination leads to severe attenuation of tumor growth and metastasis without toxicity or any obvious phenotype.

Our work has illustrated the potential of a fusion protein antibody, 1C1m-Fc to target this biomarker after radiolabeling. After several optimizations to improve the antibody biodistribution and imaging contrast, we have validated that 1C1m-Fc radiolabeled either with ^{64}Cu or ^{177}Lu is a promising tool to target TEM-1 with high quality PET/CT images and to develop therapeutic applications.

The perspectives of this work will therefore be to complete the knowledge we have acquired with additional developments, in order to consider a future transfer of the preclinical data to a first in human clinical study.

References

1. Ogawa K. Development of Diagnostic and Therapeutic Probes with Controlled Pharmacokinetics for Use in Radiotheranostics. *Chem Pharm Bull (Tokyo)*. 2019;67(9):897-903.
2. Gallivanone F, Valente M, Savi A, Canevari C, Castiglioni I. Targeted radionuclide therapy: frontiers in theranostics. *Front Biosci (Landmark Ed)*. 2017;22:1750-9.
3. Jiang W, Chalich Y, Deen MJ. Sensors for Positron Emission Tomography Applications. *Sensors (Basel)*. 2019;19(22).
4. Accorsi R. Brain single-photon emission CT physics principles. *AJNR Am J Neuroradiol*. 2008;29(7):1247-56.
5. Ljungberg M, Sjogreen Gleisner K. Personalized Dosimetry for Radionuclide Therapy Using Molecular Imaging Tools. *Biomedicines*. 2016;4(4).
6. Kong FL, Ford RJ, Yang DJ. Managing lymphoma with non-FDG radiotracers: current clinical and preclinical applications. *Biomed Res Int*. 2013;2013:626910.
7. Braga LHC, Gasparini L, Grant L, Henderson RK, Massari N, Perenzoni M, et al. A Fully Digital 8 x 16 SiPM Array for PET Applications With Per-Pixel TDCs and Real-Time Energy Output. *IEEE J Solid-State Circuits*. 2014(49, 301–314).
8. Bettinardi V, Mancosu P, Danna M, Giovacchini G, Landoni C, Picchio M, et al. Two-dimensional vs three-dimensional imaging in whole body oncologic PET/CT: a Discovery-STE phantom and patient study. *Q J Nucl Med Mol Imaging*. 2007;51(3):214-23.
9. Rizzo G, Castiglioni I, Russo G, Tana MG, Dell'Acqua F, Gilardi MC, et al. Using deconvolution to improve PET spatial resolution in OSEM iterative reconstruction. *Methods Inf Med*. 2007;46(2):231-5.
10. Fraum TJ, Ludwig DR, Hope TA, Fowler KJ. PET/MRI for Gastrointestinal Imaging: Current Clinical Status and Future Prospects. *Gastroenterol Clin North Am*. 2018;47(3):691-714.
11. Prescott JW. Quantitative imaging biomarkers: the application of advanced image processing and analysis to clinical and preclinical decision making. *J Digit Imaging*. 2013;26(1):97-108.
12. Picchio M, Kirienko M, Mapelli P, Dell'Oca I, Villa E, Gallivanone F, et al. Predictive value of pre-therapy (18)F-FDG PET/CT for the outcome of (18)F-FDG PET-guided radiotherapy in patients with head and neck cancer. *Eur J Nucl Med Mol Imaging*. 2014;41(1):21-31.
13. Jadvar H, Chen X, Cai W, Mahmood U. Radiotheranostics in Cancer Diagnosis and Management. *Radiology*. 2018;286(2):388-400.
14. Kelkar SS, Reineke TM. Theranostics: combining imaging and therapy. *Bioconjug Chem*. 2011;22(10):1879-903.
15. Rampado R, Crotti S, Caliceti P, Pucciarelli S, Agostini M. Nanovectors Design for Theranostic Applications in Colorectal Cancer. *J Oncol*. 2019;2019:2740923.
16. Filippi L, Chiaravallotti A, Schillaci O, Cianni R, Bagni O. Theranostic approaches in nuclear medicine: current status and future prospects. *Expert Rev Med Devices*. 2020;17(4):331-43.
17. Turner JH. An introduction to the clinical practice of theranostics in oncology. *Br J Radiol*. 2018;91(1091):20180440.
18. Sumer B, Gao J. Theranostic nanomedicine for cancer. *Nanomedicine (Lond)*. 2008;3(2):137-40.
19. Hanahan D, Weinberg RA. Hallmarks of cancer: the next generation. *Cell*. 2011;144(5):646-74.
20. Hertz B. A tribute to Dr. Saul Hertz: The discovery of the medical uses of radioiodine. *World J Nucl Med*. 2019;18(1):8-12.
21. Fahey FH, Grant FD, Thrall JH. Saul Hertz, MD, and the birth of radionuclide therapy. *EJNMMI Phys*. 2017;4(1):15.
22. Luster M, Clarke SE, Dietlein M, Lassmann M, Lind P, Oyen WJ, et al. Guidelines for radioiodine therapy of differentiated thyroid cancer. *Eur J Nucl Med Mol Imaging*. 2008;35(10):1941-59.
23. Herrmann K, Schwaiger M, Lewis JS, Solomon SB, McNeil BJ, Baumann M, et al. Radiotheranostics: a roadmap for future development. *Lancet Oncol*. 2020;21(3):e146-e56.
24. Krenning EP, Bakker WH, Breeman WA, Koper JW, Kooij PP, Ausema L, et al. Localisation of endocrine-related tumours with radioiodinated analogue of somatostatin. *Lancet*. 1989;1(8632):242-4.
25. Baldelli R, Barnabei A, Rizza L, Isidori AM, Rota F, Di Giacinto P, et al. Somatostatin analogs therapy in gastroenteropancreatic neuroendocrine tumors: current aspects and new perspectives. *Front Endocrinol (Lausanne)*. 2014;5:7.

26. Florio T. Molecular mechanisms of the antiproliferative activity of somatostatin receptors (SSTRs) in neuroendocrine tumors. *Front Biosci.* 2008;13:822-40.
27. Grozinsky-Glasberg S, Shimon I, Korbonits M, Grossman AB. Somatostatin analogues in the control of neuroendocrine tumours: efficacy and mechanisms. *Endocr Relat Cancer.* 2008;15(3):701-20.
28. Langbein T, Weber WA, Eiber M. Future of Theranostics: An Outlook on Precision Oncology in Nuclear Medicine. *J Nucl Med.* 2019;60(Suppl 2):13S-9S.
29. Hofmann M, Maecke H, Borner R, Weckesser E, Schoffski P, Oei L, et al. Biokinetics and imaging with the somatostatin receptor PET radioligand (68)Ga-DOTATOC: preliminary data. *Eur J Nucl Med.* 2001;28(12):1751-7.
30. Buchmann I, Henze M, Engelbrecht S, Eisenhut M, Runz A, Schafer M, et al. Comparison of 68Ga-DOTATOC PET and 111In-DTPAOC (Octreoscan) SPECT in patients with neuroendocrine tumours. *Eur J Nucl Med Mol Imaging.* 2007;34(10):1617-26.
31. Schuchardt C, Kulkarni HR, Prasad V, Zachert C, Muller D, Baum RP. The Bad Berka dose protocol: comparative results of dosimetry in peptide receptor radionuclide therapy using (177)Lu-DOTATATE, (177)Lu-DOTANOC, and (177)Lu-DOTATOC. *Recent Results Cancer Res.* 2013;194:519-36.
32. Bodei L, Kidd M, Paganelli G, Grana CM, Drozdov I, Cremonesi M, et al. Long-term tolerability of PRRT in 807 patients with neuroendocrine tumours: the value and limitations of clinical factors. *Eur J Nucl Med Mol Imaging.* 2015;42(1):5-19.
33. Strosberg J, El-Haddad G, Wolin E, Hendifar A, Yao J, Chasen B, et al. Phase 3 Trial of (177)Lu-Dotatate for Midgut Neuroendocrine Tumors. *N Engl J Med.* 2017;376(2):125-35.
34. Strosberg J, Wolin E, Chasen B, Kulke M, Bushnell D, Caplin M, et al. Health-Related Quality of Life in Patients With Progressive Midgut Neuroendocrine Tumors Treated With (177)Lu-Dotatate in the Phase III NETTER-1 Trial. *J Clin Oncol.* 2018;36(25):2578-84.
35. Ballal S, Yadav MP, Bal C, Sahoo RK, Tripathi M. Broadening horizons with (225)Ac-DOTATATE targeted alpha therapy for gastroenteropancreatic neuroendocrine tumour patients stable or refractory to (177)Lu-DOTATATE PRRT: first clinical experience on the efficacy and safety. *Eur J Nucl Med Mol Imaging.* 2020;47(4):934-46.
36. Bodei L, Weber WA. Somatostatin Receptor Imaging of Neuroendocrine Tumors: From Agonists to Antagonists. *J Nucl Med.* 2018;59(6):907-8.
37. Ginj M, Zhang H, Waser B, Cescato R, Wild D, Wang X, et al. Radiolabeled somatostatin receptor antagonists are preferable to agonists for in vivo peptide receptor targeting of tumors. *Proc Natl Acad Sci U S A.* 2006;103(44):16436-41.
38. Pastorino S, Riondato M, Uccelli L, Giovacchini G, Giovannini E, Duce V, et al. Toward the Discovery and Development of PSMA Targeted Inhibitors for Nuclear Medicine Applications. *Curr Radiopharm.* 2020;13(1):63-79.
39. Haberkorn U, Eder M, Kopka K, Babich JW, Eisenhut M. New Strategies in Prostate Cancer: Prostate-Specific Membrane Antigen (PSMA) Ligands for Diagnosis and Therapy. *Clin Cancer Res.* 2016;22(1):9-15.
40. Lutje S, Heskamp S, Cornelissen AS, Poeppel TD, van den Broek SA, Rosenbaum-Krumme S, et al. PSMA Ligands for Radionuclide Imaging and Therapy of Prostate Cancer: Clinical Status. *Theranostics.* 2015;5(12):1388-401.
41. Banerjee SR, Pullambhatla M, Byun Y, Nimmagadda S, Green G, Fox JJ, et al. 68Ga-labeled inhibitors of prostate-specific membrane antigen (PSMA) for imaging prostate cancer. *J Med Chem.* 2010;53(14):5333-41.
42. Afshar-Oromieh A, Avtzi E, Giesel FL, Holland-Letz T, Linhart HG, Eder M, et al. The diagnostic value of PET/CT imaging with the (68)Ga-labelled PSMA ligand HBED-CC in the diagnosis of recurrent prostate cancer. *Eur J Nucl Med Mol Imaging.* 2015;42(2):197-209.
43. Afshar-Oromieh A, Holland-Letz T, Giesel FL, Kratochwil C, Mier W, Haufe S, et al. Diagnostic performance of (68)Ga-PSMA-11 (HBED-CC) PET/CT in patients with recurrent prostate cancer: evaluation in 1007 patients. *Eur J Nucl Med Mol Imaging.* 2017;44(8):1258-68.
44. Kratochwil C, Giesel FL, Stefanova M, Benesova M, Bronzel M, Afshar-Oromieh A, et al. PSMA-Targeted Radionuclide Therapy of Metastatic Castration-Resistant Prostate Cancer with 177Lu-Labeled PSMA-617. *J Nucl Med.* 2016;57(8):1170-6.
45. Rahbar K, Ahmadzadehfar H, Kratochwil C, Haberkorn U, Schafers M, Essler M, et al. German Multicenter Study Investigating 177Lu-PSMA-617 Radioligand Therapy in Advanced Prostate Cancer Patients. *J Nucl Med.* 2017;58(1):85-90.

46. Weineisen M, Schottelius M, Simecek J, Baum RP, Yildiz A, Beykan S, et al. 68Ga- and 177Lu-Labeled PSMA I&T: Optimization of a PSMA-Targeted Theranostic Concept and First Proof-of-Concept Human Studies. *J Nucl Med.* 2015;56(8):1169-76.
47. Morris MJ, Bono JSD, Chi KN, Fizazi K, Herrmann K, Rahbar K, et al. Phase III study of lutetium-177-PSMA-617 in patients with metastatic castration-resistant prostate cancer (VISION). 2021;39(18_suppl):LBA4-LBA.
48. DeNardo SJ, DeNardo GL, O'Grady LF, Hu E, Sytsma VM, Mills SL, et al. Treatment of B cell malignancies with 131I Lym-1 monoclonal antibodies. *Int J Cancer Suppl.* 1988;3:96-101.
49. Press OW, Eary JF, Appelbaum FR, Martin PJ, Badger CC, Nelp WB, et al. Radiolabeled-antibody therapy of B-cell lymphoma with autologous bone marrow support. *N Engl J Med.* 1993;329(17):1219-24.
50. Bodet-Milin C, Ferrer L, Pallardy A, Eugene T, Rauscher A, Alain F-C, et al. Radioimmunotherapy of B-Cell Non-Hodgkin's Lymphoma. *Front Oncol.* 2013;3:177.
51. Goldsmith SJ. Radioimmunotherapy of lymphoma: Bexxar and Zevalin. *Semin Nucl Med.* 2010;40(2):122-35.
52. Witzig TE, Gordon LI, Cabanillas F, Czuczman MS, Emmanouilides C, Joyce R, et al. Randomized controlled trial of yttrium-90-labeled ibritumomab tiuxetan radioimmunotherapy versus rituximab immunotherapy for patients with relapsed or refractory low-grade, follicular, or transformed B-cell non-Hodgkin's lymphoma. *J Clin Oncol.* 2002;20(10):2453-63.
53. Bourgeois M, Bailly C, Frindel M, Guerard F, Cherel M, Faivre-Chauvet A, et al. Radioimmunoconjugates for treating cancer: recent advances and current opportunities. *Expert Opin Biol Ther.* 2017;17(7):813-9.
54. Tagawa ST, Vallabhajosula S, Christos PJ, Jhanwar YS, Batra JS, Lam L, et al. Phase 1/2 study of fractionated dose lutetium-177-labeled anti-prostate-specific membrane antigen monoclonal antibody J591 ((177) Lu-J591) for metastatic castration-resistant prostate cancer. *Cancer.* 2019;125(15):2561-9.
55. Goldsmith SJ. Targeted Radionuclide Therapy: A Historical and Personal Review. *Semin Nucl Med.* 2020;50(1):87-97.
56. Jiang GM, Xu W, Du J, Zhang KS, Zhang QG, Wang XW, et al. The application of the fibroblast activation protein alpha-targeted immunotherapy strategy. *Oncotarget.* 2016;7(22):33472-82.
57. Giesel FL, Kratochwil C, Lindner T, Marschalek MM, Loktev A, Lehnert W, et al. (68)Ga-FAPI PET/CT: Biodistribution and Preliminary Dosimetry Estimate of 2 DOTA-Containing FAP-Targeting Agents in Patients with Various Cancers. *J Nucl Med.* 2019;60(3):386-92.
58. Chan CY, Tan KV, Cornelissen B. PARP Inhibitors in Cancer Diagnosis and Therapy. *Clin Cancer Res.* 2021;27(6):1585-94.
59. Makvandi M, Pantel A, Schwartz L, Schubert E, Xu K, Hsieh CJ, et al. A PET imaging agent for evaluating PARP-1 expression in ovarian cancer. *J Clin Invest.* 2018;128(5):2116-26.
60. Schoder H, Franca PDS, Nakajima R, Burnazi E, Roberts S, Brand C, et al. Safety and Feasibility of PARP1/2 Imaging with (18)F-PARPi in Patients with Head and Neck Cancer. *Clin Cancer Res.* 2020;26(13):3110-6.
61. Young RJ, Demetrio De Souza Franca P, Pirovano G, Piotrowski AF, Nicklin PJ, Riedl CC, et al. Preclinical and first-in-human-brain-cancer applications of [(18)F]poly (ADP-ribose) polymerase inhibitor PET/MR. *Neurooncol Adv.* 2020;2(1):vdaa119.
62. Navarro-Teulon I, Lozza C, Pelegrin A, Vives E, Pouget JP. General overview of radioimmunotherapy of solid tumors. *Immunotherapy.* 2013;5(5):467-87.
63. Mirick GR, Bradt BM, Denardo SJ, Denardo GL. A review of human anti-globulin antibody (HAGA, HAMA, HACA, HAHA) responses to monoclonal antibodies. Not four letter words. *Q J Nucl Med Mol Imaging.* 2004;48(4):251-7.
64. Laffly E, Sodoyer R. Monoclonal and recombinant antibodies, 30 years after. *Hum Antibodies.* 2005;14(1-2):33-55.
65. Scott AM, Wolchok JD, Old LJ. Antibody therapy of cancer. *Nat Rev Cancer.* 2012;12(4):278-87.
66. Holliger P, Hudson PJ. Engineered antibody fragments and the rise of single domains. *Nat Biotechnol.* 2005;23(9):1126-36.
67. Romer T, Leonhardt H, Rothbauer U. Engineering antibodies and proteins for molecular in vivo imaging. *Curr Opin Biotechnol.* 2011;22(6):882-7.
68. Nelson AL. Antibody fragments: hope and hype. *MAbs.* 2010;2(1):77-83.
69. Knowles SM, Zettlitz KA, Tavare R, Rochefort MM, Salazar FB, Stout DB, et al. Quantitative immunopET of prostate cancer xenografts with 89Zr- and 124I-labeled anti-PSCA A11 minibody. *J Nucl Med.* 2014;55(3):452-9.

70. Boswell CA, Brechbiel MW. Development of radioimmunotherapeutic and diagnostic antibodies: an inside-out view. *Nucl Med Biol.* 2007;34(7):757-78.
71. Caserta E, Chea J, Minnix M, Poku EK, Viola D, Vonderfecht S, et al. Copper 64-labeled daratumumab as a PET/CT imaging tracer for multiple myeloma. *Blood.* 2018;131(7):741-5.
72. Filippi L, Nervi C, Proietti I, Pirisino R, Potenza C, Martelli O, et al. Molecular imaging in immunoncology: current status and translational perspectives. *Expert Rev Mol Diagn.* 2020;20(12):1199-211.
73. Bhusari P, Vatsa R, Singh G, Parmar M, Bal A, Dhawan DK, et al. Development of Lu-177-trastuzumab for radioimmunotherapy of HER2 expressing breast cancer and its feasibility assessment in breast cancer patients. *Int J Cancer.* 2017;140(4):938-47.
74. Kameswaran M, Pandey U, Dhakan C, Pathak K, Gota V, Vimalnath KV, et al. Synthesis and Preclinical Evaluation of (177)Lu-CHX-A"-DTPA-Rituximab as a Radioimmunotherapeutic Agent for Non-Hodgkin's Lymphoma. *Cancer Biother Radiopharm.* 2015;30(6):240-6.
75. Haberkorn U, Giesel F, Morgenstern A, Kratochwil C. The Future of Radioligand Therapy: alpha, beta, or Both? *J Nucl Med.* 2017;58(7):1017-8.
76. Navarro AS, Le Bihan T, Le Saec P, Bris NL, Bailly C, Sai-Maurel C, et al. TE1PA as Innovating Chelator for (64)Cu Immuno-TEP Imaging: A Comparative in Vivo Study with DOTA/NOTA by Conjugation on 9E7.4 mAb in a Syngeneic Multiple Myeloma Model. *Bioconjug Chem.* 2019;30(9):2393-403.
77. Keinanen O, Brennan JM, Membreno R, Fung K, Gangangari K, Days EJ, et al. Dual Radionuclide Theranostic Pretargeting. *Mol Pharm.* 2019;16(10):4416-21.
78. Cheal SM, McDevitt MR, Santich BH, Patel M, Yang G, Fung EK, et al. Alpha radioimmunotherapy using (225)Ac-proteus-DOTA for solid tumors - safety at curative doses. *Theranostics.* 2020;10(25):11359-75.
79. Green DJ, Press OW. Whither Radioimmunotherapy: To Be or Not To Be? *Cancer Res.* 2017;77(9):2191-6.
80. Goldenberg DM, Sharkey RM, Paganelli G, Barbet J, Chatal JF. Antibody pretargeting advances cancer radioimmunodetection and radioimmunotherapy. *J Clin Oncol.* 2006;24(5):823-34.
81. Kraeber-Bodere F, Rousseau C, Bodet-Milin C, Ferrer L, Faivre-Chauvet A, Campion L, et al. Targeting, toxicity, and efficacy of 2-step, pretargeted radioimmunotherapy using a chimeric bispecific antibody and 131I-labeled bivalent hapten in a phase I optimization clinical trial. *J Nucl Med.* 2006;47(2):247-55.
82. Bodet-Milin C, Faivre-Chauvet A, Carlier T, Rauscher A, Bourgeois M, Cerato E, et al. Immuno-PET Using Anticarcinoembryonic Antigen Bispecific Antibody and 68Ga-Labeled Peptide in Metastatic Medullary Thyroid Carcinoma: Clinical Optimization of the Pretargeting Parameters in a First-in-Human Trial. *J Nucl Med.* 2016;57(10):1505-11.
83. Tennvall J, Fischer M, Bischof Delaloye A, Bombardieri E, Bodei L, Giammarile F, et al. EANM procedure guideline for radio-immunotherapy for B-cell lymphoma with 90Y-radiolabelled ibritumomab tiuxetan (Zevalin). *Eur J Nucl Med Mol Imaging.* 2007;34(4):616-22.
84. Membreno R, Keinanen OM, Cook BE, Tully KM, Fung KC, Lewis JS, et al. Toward the Optimization of Click-Mediated Pretargeted Radioimmunotherapy. *Mol Pharm.* 2019;16(5):2259-63.
85. DeNardo GL, Schlom J, Buchsbaum DJ, Meredith RF, O'Donoghue JA, Sgouros G, et al. Rationales, evidence, and design considerations for fractionated radioimmunotherapy. *Cancer.* 2002;94(4 Suppl):1332-48.
86. Teicher BA. CD248: A therapeutic target in cancer and fibrotic diseases. *Oncotarget.* 2019;10(9):993-1009.
87. Rettig WJ, Garin-Chesa P, Healey JH, Su SL, Jaffe EA, Old LJ. Identification of endosialin, a cell surface glycoprotein of vascular endothelial cells in human cancer. *Proc Natl Acad Sci U S A.* 1992;89(22):10832-6.
88. MacFadyen JR, Haworth O, Roberston D, Hardie D, Webster MT, Morris HR, et al. Endosialin (TEM1, CD248) is a marker of stromal fibroblasts and is not selectively expressed on tumour endothelium. *FEBS Lett.* 2005;579(12):2569-75.
89. Rouleau C, Curiel M, Weber W, Smale R, Kurtzberg L, Mascarello J, et al. Endosialin protein expression and therapeutic target potential in human solid tumors: sarcoma versus carcinoma. *Clin Cancer Res.* 2008;14(22):7223-36.
90. Khan KA, McMurray JL, Mohammed F, Bicknell R. C-type lectin domain group 14 proteins in vascular biology, cancer and inflammation. *FEBS J.* 2019;286(17):3299-332.

91. Opavsky R, Haviernik P, Jurkovicova D, Garin MT, Copeland NG, Gilbert DJ, et al. Molecular characterization of the mouse *Tem1*/endosialin gene regulated by cell density in vitro and expressed in normal tissues in vivo. *J Biol Chem*. 2001;276(42):38795-807.
92. Lax S, Hou TZ, Jenkinson E, Salmon M, MacFadyen JR, Isacke CM, et al. CD248/Endosialin is dynamically expressed on a subset of stromal cells during lymphoid tissue development, splenic remodeling and repair. *FEBS Lett*. 2007;581(18):3550-6.
93. MacFadyen J, Savage K, Wienke D, Isacke CM. Endosialin is expressed on stromal fibroblasts and CNS pericytes in mouse embryos and is downregulated during development. *Gene Expr Patterns*. 2007;7(3):363-9.
94. Kontsekova S, Polcicova K, Takacova M, Pastorekova S. Endosialin: molecular and functional links to tumor angiogenesis. *Neoplasma*. 2016;63(2):183-92.
95. Valdez Y, Maia M, Conway EM. CD248: reviewing its role in health and disease. *Curr Drug Targets*. 2012;13(3):432-9.
96. Christian S, Ahorn H, Novatchkova M, Garin-Chesa P, Park JE, Weber G, et al. Molecular cloning and characterization of EndoGlyx-1, an EMILIN-like multisubunit glycoprotein of vascular endothelium. *J Biol Chem*. 2001;276(51):48588-95.
97. Elashoff MR, Wingrove JA, Beineke P, Daniels SE, Tingley WG, Rosenberg S, et al. Development of a blood-based gene expression algorithm for assessment of obstructive coronary artery disease in non-diabetic patients. *BMC Med Genomics*. 2011;4:26.
98. Gonzalez-Amaro R, Sanchez-Madrid F. Cell adhesion molecules: selectins and integrins. *Crit Rev Immunol*. 1999;19(5-6):389-429.
99. Maia M, DeVriese A, Janssens T, Moons M, Lories RJ, Tavernier J, et al. CD248 facilitates tumor growth via its cytoplasmic domain. *BMC Cancer*. 2011;11:162.
100. Gardiol D. PDZ-containing proteins as targets in human pathologies. *FEBS J*. 2012;279(19):3529.
101. Bagley RG. Endosialin: from vascular target to biomarker for human sarcomas. *Biomark Med*. 2009;3(5):589-604.
102. Suzuki K, Kusumoto H, Deyashiki Y, Nishioka J, Maruyama I, Zushi M, et al. Structure and expression of human thrombomodulin, a thrombin receptor on endothelium acting as a cofactor for protein C activation. *EMBO J*. 1987;6(7):1891-7.
103. Nepomuceno RR, Henschen-Edman AH, Burgess WH, Tenner AJ. cDNA cloning and primary structure analysis of C1qR(P), the human C1q/MBL/SPA receptor that mediates enhanced phagocytosis in vitro. *Immunity*. 1997;6(2):119-29.
104. Van de Wouwer M, Conway EM. Novel functions of thrombomodulin in inflammation. *Crit Care Med*. 2004;32(5 Suppl):S254-61.
105. Lu JH, Teh BK, Wang L, Wang YN, Tan YS, Lai MC, et al. The classical and regulatory functions of C1q in immunity and autoimmunity. *Cell Mol Immunol*. 2008;5(1):9-21.
106. Liao D, Johnson RS. Hypoxia: a key regulator of angiogenesis in cancer. *Cancer Metastasis Rev*. 2007;26(2):281-90.
107. Ohradanova A, Gradin K, Barathova M, Zatovicova M, Holotnakova T, Kopacek J, et al. Hypoxia upregulates expression of human endosialin gene via hypoxia-inducible factor 2. *Br J Cancer*. 2008;99(8):1348-56.
108. Sheta EA, Trout H, Gildea JJ, Harding MA, Theodorescu D. Cell density mediated pericellular hypoxia leads to induction of HIF-1alpha via nitric oxide and Ras/MAP kinase mediated signaling pathways. *Oncogene*. 2001;20(52):7624-34.
109. Christian S, Winkler R, Helfrich I, Boos AM, Besemfelder E, Schadendorf D, et al. Endosialin (*Tem1*) is a marker of tumor-associated myofibroblasts and tumor vessel-associated mural cells. *Am J Pathol*. 2008;172(2):486-94.
110. Tomkowicz B, Rybinski K, Foley B, Ebel W, Kline B, Routhier E, et al. Interaction of endosialin/TEM1 with extracellular matrix proteins mediates cell adhesion and migration. *Proc Natl Acad Sci U S A*. 2007;104(46):17965-70.
111. Simonavicius N, Ashenden M, van Weverwijk A, Lax S, Huso DL, Buckley CD, et al. Pericytes promote selective vessel regression to regulate vascular patterning. *Blood*. 2012;120(7):1516-27.
112. Becker R, Lenter MC, Vollkommer T, Boos AM, Pfaff D, Augustin HG, et al. Tumor stroma marker endosialin (*Tem1*) is a binding partner of metastasis-related protein Mac-2 BP/90K. *FASEB J*. 2008;22(8):3059-67.
113. Marchetti A, Tinari N, Buttitta F, Chella A, Angeletti CA, Sacco R, et al. Expression of 90K (Mac-2 BP) correlates with distant metastasis and predicts survival in stage I non-small cell lung cancer patients. *Cancer Res*. 2002;62(9):2535-9.

114. Maia M, de Vriese A, Janssens T, Moons M, van Landuyt K, Tavernier J, et al. CD248 and its cytoplasmic domain: a therapeutic target for arthritis. *Arthritis Rheum.* 2010;62(12):3595-606.
115. Bagley RG, Weber W, Rouleau C, Yao M, Honma N, Kataoka S, et al. Human mesenchymal stem cells from bone marrow express tumor endothelial and stromal markers. *Int J Oncol.* 2009;34(3):619-27.
116. Spaeth EL, Dembinski JL, Sasser AK, Watson K, Klopp A, Hall B, et al. Mesenchymal stem cell transition to tumor-associated fibroblasts contributes to fibrovascular network expansion and tumor progression. *PLoS One.* 2009;4(4):e4992.
117. Carson-Walter EB, Winans BN, Whiteman MC, Liu Y, Jarvela S, Haapasalo H, et al. Characterization of TEM1/Endosialin in human and murine brain tumors. *BMC Cancer.* 2009;9:417.
118. Huang HP, Hong CL, Kao CY, Lin SW, Lin SR, Wu HL, et al. Gene targeting and expression analysis of mouse Tem1/endosialin using a lacZ reporter. *Gene Expr Patterns.* 2011;11(5-6):316-26.
119. Dolznig H, Schweifer N, Puri C, Kraut N, Rettig WJ, Kerjaschki D, et al. Characterization of cancer stroma markers: in silico analysis of an mRNA expression database for fibroblast activation protein and endosialin. *Cancer Immun.* 2005;5:10.
120. Hardie DL, Baldwin MJ, Naylor A, Haworth OJ, Hou TZ, Lax S, et al. The stromal cell antigen CD248 (endosialin) is expressed on naive CD8+ human T cells and regulates proliferation. *Immunology.* 2011;133(3):288-95.
121. Nanda A, Karim B, Peng Z, Liu G, Qiu W, Gan C, et al. Tumor endothelial marker 1 (Tem1) functions in the growth and progression of abdominal tumors. *Proc Natl Acad Sci U S A.* 2006;103(9):3351-6.
122. Croft AP, Naylor AJ, Marshall JL, Hardie DL, Zimmermann B, Turner J, et al. Rheumatoid synovial fibroblasts differentiate into distinct subsets in the presence of cytokines and cartilage. *Arthritis Res Ther.* 2016;18(1):270.
123. Naylor AJ, Azzam E, Smith S, Croft A, Poyser C, Duffield JS, et al. The mesenchymal stem cell marker CD248 (endosialin) is a negative regulator of bone formation in mice. *Arthritis Rheum.* 2012;64(10):3334-43.
124. Smith SW, Eardley KS, Croft AP, Nwosu J, Howie AJ, Cockwell P, et al. CD248+ stromal cells are associated with progressive chronic kidney disease. *Kidney Int.* 2011;80(2):199-207.
125. Smith SW, Croft AP, Morris HL, Naylor AJ, Huso DL, Isacke CM, et al. Genetic Deletion of the Stromal Cell Marker CD248 (Endosialin) Protects against the Development of Renal Fibrosis. *Nephron.* 2015;131(4):265-77.
126. Chang-Panesso M, Humphreys BD. CD248/Endosialin: A Novel Pericyte Target in Renal Fibrosis. *Nephron.* 2015;131(4):262-4.
127. Wilhelm A, Aldridge V, Haldar D, Naylor AJ, Weston CJ, Hedegaard D, et al. CD248/endosialin critically regulates hepatic stellate cell proliferation during chronic liver injury via a PDGF-regulated mechanism. *Gut.* 2016;65(7):1175-85.
128. Bartis D, Crowley LE, D'Souza VK, Borthwick L, Fisher AJ, Croft AP, et al. Role of CD248 as a potential severity marker in idiopathic pulmonary fibrosis. *BMC Pulm Med.* 2016;16(1):51.
129. Hasanov Z, Ruckdeschel T, Konig C, Mogler C, Kapel SS, Korn C, et al. Endosialin Promotes Atherosclerosis Through Phenotypic Remodeling of Vascular Smooth Muscle Cells. *Arterioscler Thromb Vasc Biol.* 2017;37(3):495-505.
130. Huber MA, Kraut N, Schweifer N, Dolznig H, Peter RU, Schubert RD, et al. Expression of stromal cell markers in distinct compartments of human skin cancers. *J Cutan Pathol.* 2006;33(2):145-55.
131. Brady J, Neal J, Sadakar N, Gasque P. Human endosialin (tumor endothelial marker 1) is abundantly expressed in highly malignant and invasive brain tumors. *J Neuropathol Exp Neurol.* 2004;63(12):1274-83.
132. Bagley RG, Honma N, Weber W, Boutin P, Rouleau C, Shankara S, et al. Endosialin/TEM 1/CD248 is a pericyte marker of embryonic and tumor neovascularization. *Microvasc Res.* 2008;76(3):180-8.
133. Tomkowicz B, Rybinski K, Sebeck D, Sass P, Nicolaidis NC, Grasso L, et al. Endosialin/TEM-1/CD248 regulates pericyte proliferation through PDGF receptor signaling. *Cancer Biol Ther.* 2010;9(11):908-15.
134. Guo Y, Hu J, Wang Y, Peng X, Min J, Wang J, et al. Tumour endothelial marker 1/endosialin-mediated targeting of human sarcoma. *Eur J Cancer.* 2018;90:111-21.
135. Simonavicius N, Robertson D, Bax DA, Jones C, Huijbers IJ, Isacke CM. Endosialin (CD248) is a marker of tumor-associated pericytes in high-grade glioma. *Mod Pathol.* 2008;21(3):308-15.
136. Viski C, Konig C, Kijewska M, Mogler C, Isacke CM, Augustin HG. Endosialin-Expressing Pericytes Promote Metastatic Dissemination. *Cancer Res.* 2016;76(18):5313-25.

137. Davies G, Cunnick GH, Mansel RE, Mason MD, Jiang WG. Levels of expression of endothelial markers specific to tumour-associated endothelial cells and their correlation with prognosis in patients with breast cancer. *Clin Exp Metastasis*. 2004;21(1):31-7.
138. Rmali KA, Puntis MC, Jiang WG. Prognostic values of tumor endothelial markers in patients with colorectal cancer. *World J Gastroenterol*. 2005;11(9):1283-6.
139. O'Shannessy DJ, Somers EB, Chandrasekaran LK, Nicolaides NC, Bordeaux J, Gustavson MD. Influence of tumor microenvironment on prognosis in colorectal cancer: Tissue architecture-dependent signature of endosialin (TEM-1) and associated proteins. *Oncotarget*. 2014;5(12):3983-95.
140. Johnsen JJ, Kogner P, Albiñá A, Henriksson MA. Embryonal neural tumours and cell death. *Apoptosis*. 2009;14(4):424-38.
141. Maris JM, Hogarty MD, Bagatell R, Cohn SL. Neuroblastoma. *Lancet*. 2007;369(9579):2106-20.
142. Rouleau C, Smale R, Sancho J, Fu YS, Kurtzberg L, Weber W, et al. Endosialin: a novel malignant cell therapeutic target for neuroblastoma. *Int J Oncol*. 2011;39(4):841-51.
143. Li C, Chacko AM, Hu J, Hasegawa K, Swails J, Grasso L, et al. Antibody-based tumor vascular theranostics targeting endosialin/TEM1 in a new mouse tumor vascular model. *Cancer Biol Ther*. 2014;15(4):443-51.
144. Diaz LA, Jr., Coughlin CM, Weil SC, Fishel J, Gounder MM, Lawrence S, et al. A first-in-human phase I study of MORAb-004, a monoclonal antibody to endosialin in patients with advanced solid tumors. *Clin Cancer Res*. 2015;21(6):1281-8.
145. Kiyohara E, Donovan N, Takeshima L, Huang S, Wilmott JS, Scolyer RA, et al. Endosialin Expression in Metastatic Melanoma Tumor Microenvironment Vasculature: Potential Therapeutic Implications. *Cancer Microenviron*. 2015;8(2):111-8.
146. Grothey A, Strosberg JR, Renfro LA, Hurwitz HI, Marshall JL, Safran H, et al. A Randomized, Double-Blind, Placebo-Controlled Phase II Study of the Efficacy and Safety of Monotherapy Ontuxizumab (MORAb-004) Plus Best Supportive Care in Patients with Chemorefractory Metastatic Colorectal Cancer. *Clin Cancer Res*. 2018;24(2):316-25.
147. D'Angelo SP, Hamid OA, Tarhini A, Schadendorf D, Chmielowski B, Collichio FA, et al. A phase 2 study of ontuxizumab, a monoclonal antibody targeting endosialin, in metastatic melanoma. *Invest New Drugs*. 2018;36(1):103-13.
148. Norris RE, Fox E, Reid JM, Ralya A, Liu XW, Minard C, et al. Phase 1 trial of ontuxizumab (MORAb-004) in children with relapsed or refractory solid tumors: A report from the Children's Oncology Group Phase 1 Pilot Consortium (ADVL1213). *Pediatr Blood Cancer*. 2018;65(5):e26944.
149. Jones RL, Chawla SP, Attia S, Schoffski P, Gelderblom H, Chmielowski B, et al. A phase 1 and randomized controlled phase 2 trial of the safety and efficacy of the combination of gemcitabine and docetaxel with ontuxizumab (MORAb-004) in metastatic soft-tissue sarcomas. *Cancer*. 2019;125(14):2445-54.
150. Thomas A, Teicher BA, Hassan R. Antibody-drug conjugates for cancer therapy. *Lancet Oncol*. 2016;17(6):e254-e62.
151. Kellogg BA, Garrett L, Kovtun Y, Lai KC, Leece B, Miller M, et al. Disulfide-linked antibody-maytansinoid conjugates: optimization of in vivo activity by varying the steric hindrance at carbon atoms adjacent to the disulfide linkage. *Bioconjug Chem*. 2011;22(4):717-27.
152. Polson AG, Ho WY, Ramakrishnan V. Investigational antibody-drug conjugates for hematological malignancies. *Expert Opin Investig Drugs*. 2011;20(1):75-85.
153. Rouleau C, Gianolio DA, Smale R, Roth SD, Krumbholz R, Harper J, et al. Anti-Endosialin Antibody-Drug Conjugate: Potential in Sarcoma and Other Malignancies. *Mol Cancer Ther*. 2015;14(9):2081-9.
154. Swann PG, Tolnay M, Muthukkumar S, Shapiro MA, Rellahan BL, Clouse KA. Considerations for the development of therapeutic monoclonal antibodies. *Curr Opin Immunol*. 2008;20(4):493-9.
155. Hoofring SA, Lopez R, Hock MB, Kaliyaperumal A, Patel SK, Swanson SJ, et al. Immunogenicity testing strategy and bioanalytical assays for antibody-drug conjugates. *Bioanalysis*. 2013;5(9):1041-55.
156. Capone E, Piccolo E, Fichera I, Ciufici P, Barcaroli D, Sala A, et al. Generation of a novel Antibody-Drug Conjugate targeting endosialin: potent and durable antitumor response in sarcoma. *Oncotarget*. 2017;8(36):60368-77.
157. Facciponte JG, Ugel S, De Sanctis F, Li C, Wang L, Nair G, et al. Tumor endothelial marker 1-specific DNA vaccination targets tumor vasculature. *J Clin Invest*. 2014;124(4):1497-511.
158. Rice J, Ottensmeier CH, Stevenson FK. DNA vaccines: precision tools for activating effective immunity against cancer. *Nat Rev Cancer*. 2008;8(2):108-20.

159. Panina-Bordignon P, Tan A, Termijtelen A, Demotz S, Corradin G, Lanzavecchia A. Universally immunogenic T cell epitopes: promiscuous binding to human MHC class II and promiscuous recognition by T cells. *Eur J Immunol*. 1989;19(12):2237-42.
160. Ugel S, Faccioponte JG, De Sanctis F, Facciabene A. Targeting tumor vasculature: expanding the potential of DNA cancer vaccines. *Cancer Immunol Immunother*. 2015;64(10):1339-48.
161. Vanderlugt CL, Miller SD. Epitope spreading in immune-mediated diseases: implications for immunotherapy. *Nat Rev Immunol*. 2002;2(2):85-95.
162. Petrou P, Georgalas I, Giavaras G, Anastasiou E, Ntana Z, Petrou C. Early loss of pregnancy after intravitreal bevacizumab injection. *Acta Ophthalmol*. 2010;88(4):e136.
163. Scappaticci FA, Fehrenbacher L, Cartwright T, Hainsworth JD, Heim W, Berlin J, et al. Surgical wound healing complications in metastatic colorectal cancer patients treated with bevacizumab. *J Surg Oncol*. 2005;91(3):173-80.
164. Lange SE, Zheleznyak A, Studer M, O'Shannessy DJ, Lapi SE, Van Tine BA. Development of 89Zr-Ontuxizumab for in vivo TEM-1/endothelialin PET applications. *Oncotarget*. 2016;7(11):13082-92.
165. Chacko AM, Li C, Nayak M, Mikitsh JL, Hu J, Hou C, et al. Development of 124I immuno-PET targeting tumor vascular TEM1/endothelialin. *J Nucl Med*. 2014;55(3):500-7.
166. Stillebroer AB, Franssen GM, Mulders PF, Oyen WJ, van Dongen GA, Laverman P, et al. ImmunoPET imaging of renal cell carcinoma with (124)I- and (89)Zr-labeled anti-CAIX monoclonal antibody cG250 in mice. *Cancer Biother Radiopharm*. 2013;28(7):510-5.
167. Rybinski K, Imtiyaz HZ, Mittica B, Drozdowski B, Fulmer J, Furuuchi K, et al. Targeting endothelialin/CD248 through antibody-mediated internalization results in impaired pericyte maturation and dysfunctional tumor microvasculature. *Oncotarget*. 2015;6(28):25429-40.
168. Zhao A, Nunez-Cruz S, Li C, Coukos G, Siegel DL, Scholler N. Rapid isolation of high-affinity human antibodies against the tumor vascular marker Endothelialin/TEM1, using a paired yeast-display/secretory scFv library platform. *J Immunol Methods*. 2011;363(2):221-32.
169. Yuan X, Yang M, Chen X, Zhang X, Sukhadia S, Musolino N, et al. Correction to: Characterization of the first fully human anti-TEM1 scFv in models of solid tumor imaging and immunotoxin-based therapy. *Cancer Immunol Immunother*. 2018;67(2):329-39.
170. Li C, Wang J, Hu J, Feng Y, Hasegawa K, Peng X, et al. Development, optimization, and validation of novel anti-TEM1/CD248 affinity agent for optical imaging in cancer. *Oncotarget*. 2014;5(16):6994-7012.
171. Carson-Walter EB, Watkins DN, Nanda A, Vogelstein B, Kinzler KW, St Croix B. Cell surface tumor endothelial markers are conserved in mice and humans. *Cancer Res*. 2001;61(18):6649-55.
172. Ogawa M, Kosaka N, Choyke PL, Kobayashi H. In vivo molecular imaging of cancer with a quenching near-infrared fluorescent probe using conjugates of monoclonal antibodies and indocyanine green. *Cancer Res*. 2009;69(4):1268-72.
173. Cicone F, Denoel T, Gnesin S, Riggi N, Irving M, Jakka G, et al. Preclinical Evaluation and Dosimetry of [(111)In]CHX-DTPA-scFv78-Fc Targeting Endothelialin/Tumor Endothelial Marker 1 (TEM1). *Mol Imaging Biol*. 2020;22(4):979-91.
174. Delage JA, Faivre-Chauvet A, Fierle JK, Gnesin S, Schaefer N, Coukos G, et al. (177)Lu radiolabeling and preclinical theranostic study of 1C1m-Fc: an anti-TEM-1 scFv-Fc fusion protein in soft tissue sarcoma. *EJNMMI Res*. 2020;10(1):98.
175. Delage JA, Faivre-Chauvet A, Barbet J, Fierle JK, Schaefer N, Coukos G, et al. Impact of DOTA Conjugation on Pharmacokinetics and Immunoreactivity of [(177)Lu]Lu-1C1m-Fc, an Anti TEM-1 Fusion Protein Antibody in a TEM-1 Positive Tumor Mouse Model. *Pharmaceutics*. 2021;13(1).
176. Grunberg J, Jeger S, Sarko D, Dennler P, Zimmermann K, Mier W, et al. DOTA-functionalized polylysine: a high number of DOTA chelates positively influences the biodistribution of enzymatic conjugated anti-tumor antibody chCE7agl. *PLoS One*. 2013;8(4):e60350.
177. Capasso E, Durzu S, Piras S, Zandieh S, Knoll P, Haug A, et al. Role of (64)CuCl 2 PET/CT in staging of prostate cancer. *Ann Nucl Med*. 2015;29(6):482-8.
178. Wittel UA, Jain M, Goel A, Chauhan SC, Colcher D, Batra SK. The in vivo characteristics of genetically engineered divalent and tetravalent single-chain antibody constructs. *Nucl Med Biol*. 2005;32(2):157-64.
179. Notni J, Wester HJ. Re-thinking the role of radiometal isotopes: Towards a future concept for theranostic radiopharmaceuticals. *J Labelled Comp Radiopharm*. 2018;61(3):141-53.
180. Lewis MR, Wang M, Axworthy DB, Theodore LJ, Mallet RW, Fritzberg AR, et al. In vivo evaluation of pretargeted 64Cu for tumor imaging and therapy. *J Nucl Med*. 2003;44(8):1284-92.
181. Bass LA, Wang M, Welch MJ, Anderson CJ. In vivo transchelation of copper-64 from TETA-octreotide to superoxide dismutase in rat liver. *Bioconjug Chem*. 2000;11(4):527-32.

182. Perez-Deben S, Gonzalez-Martin R, Palomar A, Quinonero A, Salsano S, Dominguez F. Copper and lead exposures disturb reproductive features of primary endometrial stromal and epithelial cells. *Reprod Toxicol.* 2020;93:106-17.
183. Peng F, Liu J, Wu JS, Lu X, Muzik O. Mouse extrahepatic hepatoma detected on MicroPET using copper (II)-64 chloride uptake mediated by endogenous mouse copper transporter 1. *Mol Imaging Biol.* 2005;7(5):325-9.
184. Cantiello F, Gangemi V, Cascini GL, Calabria F, Moschini M, Ferro M, et al. Diagnostic Accuracy of (64)Copper Prostate-specific Membrane Antigen Positron Emission Tomography/Computed Tomography for Primary Lymph Node Staging of Intermediate- to High-risk Prostate Cancer: Our Preliminary Experience. *Urology.* 2017;106:139-45.
185. Carlos Dos Santos J, Beijer B, Bauder-Wust U, Schafer M, Leotta K, Eder M, et al. Development of Novel PSMA Ligands for Imaging and Therapy with Copper Isotopes. *J Nucl Med.* 2020;61(1):70-9.
186. Cai Z, Anderson CJ. Chelators for copper radionuclides in positron emission tomography radiopharmaceuticals. *J Labelled Comp Radiopharm.* 2014;57(4):224-30.
187. Vivier D, Sharma SK, Adumeau P, Rodriguez C, Fung K, Zeglis BM. The Impact of FcγRI Binding on Immuno-PET. *J Nucl Med.* 2019;60(8):1174-82.
188. Rabasa Capote A, Gonzalez JE, Rodriguez-Vera L, Lopez A, Sanchez Ramirez B, Garrido Hidalgo G. Pharmacokinetics and Biodistribution Study of 7A7 Anti-Mouse Epidermal Growth Factor Receptor Monoclonal Antibody and Its F(ab')₂ Fragment in an Immunocompetent Mouse Model. *ISRN Pharmacol.* 2012;2012:417515.
189. Garnett MC. Targeted drug conjugates: principles and progress. *Adv Drug Deliv Rev.* 2001;53(2):171-216.
190. Knogler K, Grunberg J, Novak-Hofer I, Zimmermann K, Schubiger PA. Evaluation of ¹⁷⁷Lu-DOTA-labeled aglycosylated monoclonal anti-L1-CAM antibody chCE7: influence of the number of chelators on the in vitro and in vivo properties. *Nucl Med Biol.* 2006;33(7):883-9.
191. van Gog FB, Visser GW, Klok R, van der Schors R, Snow GB, van Dongen GA. Monoclonal antibodies labeled with rhenium-186 using the MAG3 chelate: relationship between the number of chelated groups and biodistribution characteristics. *J Nucl Med.* 1996;37(2):352-62.
192. Rinne SS, Dahlsson Leitao C, Gentry J, Mitran B, Abouzayed A, Tolmachev V, et al. Increase in negative charge of (68)Ga/chelator complex reduces unspecific hepatic uptake but does not improve imaging properties of HER3-targeting affibody molecules. *Sci Rep.* 2019;9(1):17710.
193. Tolmachev V, Orlova A. Influence of labelling methods on biodistribution and imaging properties of radiolabelled peptides for visualisation of molecular therapeutic targets. *Curr Med Chem.* 2010;17(24):2636-55.
194. Al-Ejeh F, Darby JM, Thierry B, Brown MP. A simplified suite of methods to evaluate chelator conjugation of antibodies: effects on hydrodynamic radius and biodistribution. *Nucl Med Biol.* 2009;36(4):395-402.
195. Baranski AC, Schafer M, Bauder-Wust U, Wacker A, Schmidt J, Liolios C, et al. Improving the Imaging Contrast of (68)Ga-PSMA-11 by Targeted Linker Design: Charged Spacer Moieties Enhance the Pharmacokinetic Properties. *Bioconjug Chem.* 2017;28(9):2485-92.
196. Darling JL, Paterson BM, Akurathi V, Betanzos-Lara S, Treves ST, Voss SD, et al. The ionic charge of copper-64 complexes conjugated to an engineered antibody affects biodistribution. *Bioconjug Chem.* 2015;26(4):707-17.
197. Dahlsson Leitao C, Rinne SS, Mitran B, Vorobyeva A, Andersson KG, Tolmachev V, et al. Molecular Design of HER3-Targeting Affibody Molecules: Influence of Chelator and Presence of HEHEHE-Tag on Biodistribution of (68)Ga-Labeled Tracers. *Int J Mol Sci.* 2019;20(5).
198. Julie K, Fierle MB, Mariastella de Tiani, Laureline Wetterwald, Vasileios Atsaves, Johan Abram-Saliba, Tatiana V. Petrova, George Coukos, Steven M. Dunn. Soluble trivalent engagers redirect cytolytic T cell activity toward tumor endothelial marker 1. *Cell Reports Medicine.* 2021.
199. Wu Y, Zhu H, Zhang B, Liu F, Chen J, Wang Y, et al. Synthesis of Site-Specific Radiolabeled Antibodies for Radioimmunotherapy via Genetic Code Expansion. *Bioconjug Chem.* 2016;27(10):2460-8.
200. Tavare R, Wu WH, Zettlitz KA, Salazar FB, McCabe KE, Marks JD, et al. Enhanced immunoPET of ALCAM-positive colorectal carcinoma using site-specific (64)Cu-DOTA conjugation. *Protein Eng Des Sel.* 2014;27(10):317-24.
201. Shinmi D, Taguchi E, Iwano J, Yamaguchi T, Masuda K, Enokizono J, et al. One-Step Conjugation Method for Site-Specific Antibody-Drug Conjugates through Reactive Cysteine-Engineered Antibodies. *Bioconjug Chem.* 2016;27(5):1324-31.

202. Agarwal P, Bertozzi CR. Site-specific antibody-drug conjugates: the nexus of bioorthogonal chemistry, protein engineering, and drug development. *Bioconjug Chem*. 2015;26(2):176-92.
203. AbYlink™, Debiopharm [Available from: <https://www.debiopharm.com/manufacturing-science/technology-pipeline/abylink/>].
204. Frindel M, Camus N, Rauscher A, Bourgeois M, Alliot C, Barre L, et al. Radiolabeling of HTE1PA: A new monopicolinate cyclam derivative for Cu-64 phenotypic imaging. In vitro and in vivo stability studies in mice. *Nucl Med Biol*. 2014;41 Suppl:e49-57.
205. Bhatt NB, Pandya DN, Wadas TJ. Recent Advances in Zirconium-89 Chelator Development. *Molecules*. 2018;23(3).
206. Gutfilen B, Souza SA, Valentini G. Copper-64: a real theranostic agent. *Drug Des Devel Ther*. 2018;12:3235-45.
207. Ullrich M, Bergmann R, Peitzsch M, Zenker EF, Cartellieri M, Bachmann M, et al. Multimodal Somatostatin Receptor Theranostics Using [(64)Cu]Cu-/[177Lu]Lu-DOTA-(Tyr(3))octreotate and AN-238 in a Mouse Pheochromocytoma Model. *Theranostics*. 2016;6(5):650-65.
208. Gulenchyn KY, Yao X, Asa SL, Singh S, Law C. Radionuclide therapy in neuroendocrine tumours: a systematic review. *Clin Oncol (R Coll Radiol)*. 2012;24(4):294-308.
209. Kranz M, Sattler B, Tiepolt S, Wilke S, Deuther-Conrad W, Donat CK, et al. Radiation dosimetry of the alpha4beta2 nicotinic receptor ligand (+)-[(18)F]flubatine, comparing preclinical PET/MRI and PET/CT to first-in-human PET/CT results. *EJNMMI Phys*. 2016;3(1):25.
210. Puvvada SD, Guillen-Rodriguez JM, Yan J, Inclan L, Heard K, Rivera XI, et al. Yttrium-90-Ibritumomab Tiuxetan (Zevalin (R)) Radioimmunotherapy after Cytoreduction with ESHAP Chemotherapy in Patients with Relapsed Follicular Non-Hodgkin Lymphoma: Final Results of a Phase II Study. *Oncology-Basel*. 2018;94(5):274-80.
211. Goodwin R, Giaccone G, Calvert H, Lobbezoo M, Eisenhauer EA. Targeted agents: how to select the winners in preclinical and early clinical studies? *Eur J Cancer*. 2012;48(2):170-8.

Appendix : Articles

Article 1 : Delage, J. A., et al. "¹⁷⁷Lu radiolabeling and preclinical theranostic study of 1C1m-Fc: an anti-TEM-1 scFv-Fc fusion protein in soft tissue sarcoma." [EJNMMI Res 2020](#)

ORIGINAL RESEARCH

Open Access



^{177}Lu radiolabeling and preclinical theranostic study of 1C1m-Fc: an anti-TEM-1 scFv-Fc fusion protein in soft tissue sarcoma

J. A. Delage¹, A. Faivre-Chauvet², J. K. Fierle³, S. Gnesin⁴, N. Schaefer⁵, G. Coukos⁶, S. M. Dunn³, D. Viertl⁵ and J. O. Prior^{5*}

Abstract

Purpose: TEM-1 (tumor endothelial marker-1) is a single-pass transmembrane cell surface glycoprotein expressed at high levels by tumor vasculature and malignant cells. We aimed to perform a preclinical investigation of a novel anti-TEM-1 scFv-Fc fusion antibody, 1C1m-Fc, which was radiolabeled with ^{177}Lu for use in soft tissue sarcomas models.

Methods: 1C1m-Fc was first conjugated to p-SCN-Bn-DOTA using different excess molar ratios and labeled with ^{177}Lu . To determine radiolabeled antibody immunoreactivity, Lindmo assays were performed.

The in vivo behavior of [^{177}Lu]Lu-1C1m-Fc was characterized in mice bearing TEM-1 positive (SK-N-AS) and negative (HT-1080) tumors by biodistribution and single-photon emission SPECT/CT imaging studies. Estimated organ absorbed doses were obtained based on biodistribution results.

Results: The DOTA conjugation and the labeling with ^{177}Lu were successful with a radiochemical purity of up to 95%. Immunoreactivity after radiolabeling was $86\% \pm 4\%$. Biodistribution showed a specific uptake in TEM-1 positive tumor versus liver as critical non-specific healthy organ, and this specificity is correlated to the number of chelates per antibody. A 1.9-fold higher signal at 72 h was observed in SPECT/CT imaging in TEM-1 positive tumors versus control tumors.

Conclusion: TEM-1 is a promising target that could allow a theranostic approach to soft-tissue sarcoma, and 1C1m-Fc appears to be a suitable targeting candidate. In this study, we observed the influence of the ratio DOTA/antibody on the biodistribution. The next step will be to investigate the best conjugation to achieve an optimal tumor-to-organ radioactivity ratio and to perform therapy in murine xenograft models as a prelude to future translation in patients.

Keywords: TEM-1, CD-248, Soft-tissue sarcoma, Theranostic, 1C1m-Fc, DOTA conjugation

* Correspondence: John.Prior@chuv.ch

⁵Department of Nuclear Medicine and Molecular Imaging, Lausanne University Hospital and University of Lausanne, Rue du Bugnon 46, CH-1011 Lausanne, Switzerland
Full list of author information is available at the end of the article



© The Author(s). 2020 **Open Access** This article is licensed under a Creative Commons Attribution 4.0 International License, which permits use, sharing, adaptation, distribution and reproduction in any medium or format, as long as you give appropriate credit to the original author(s) and the source, provide a link to the Creative Commons licence, and indicate if changes were made. The images or other third party material in this article are included in the article's Creative Commons licence, unless indicated otherwise in a credit line to the material. If material is not included in the article's Creative Commons licence and your intended use is not permitted by statutory regulation or exceeds the permitted use, you will need to obtain permission directly from the copyright holder. To view a copy of this licence, visit <http://creativecommons.org/licenses/by/4.0/>.

Background

The tumor endothelial marker 1 (TEM-1) also known as endosialin or CD248 is a type I single-pass transmembrane cell surface glycoprotein of 757 amino acids (80.9 kD) belonging to the C-lectin receptor superfamily. TEM-1 is composed of a signal leader peptide, five extracellular domains (including three EGF repeats), a mucin-like region, a transmembrane region, and a short cytoplasmic tail [1–3].

TEM-1 is expressed on mesenchymal lineage cells including pericytes and fibroblasts during tissue development, tumor neovascularization, and inflammation [4, 5].

Initially identified as the target antigen of an antibody (named FB5) raised in mice inoculated with human fetal fibroblasts, endosialin was found to be associated with the tumor vascular endothelium. TEM-1 expression has been localized to tumor vasculature, mainly in pericytes and stromal fibroblasts and in some cases to malignant cells [6, 7]. TEM-1 is implicated in tumor cell adhesion and migration, development, neoangiogenesis, and tumor progression [8, 9]. It has also been associated with tumor aggressiveness and poor patient prognosis [10, 11].

Studies with TEM-1 knockout mouse models were unaffected with regard to phenotype and wound healing responses, but showed an important reduction in tumor growth, invasiveness, and metastasis [12].

In human adults, TEM-1 expression is limited to endometrial stroma and occasionally fibroblasts, and has been shown to be upregulated in certain pathologies (including tumor progression and metastasis) [13].

TEM-1 has been described as an excellent therapeutic target since it is tumor specific, is associated with more aggressive tumor phenotypes, and its elimination (genetic or immune-mediated) leads to severe attenuation of tumor growth and metastasis without toxicity or any obvious phenotypic alterations [12, 14].

Soft-tissue sarcomas (STS) are a group of 50 different tumor entities arising from mesenchymal cells that exhibit great differences in terms of genetic alterations, pathogenesis, and clinical behavior [15]. Current treatment, besides surgery for local disease, comprises radiotherapy and chemotherapy.

Only a few patients may benefit from curative resection, however, and prognosis of metastasized or otherwise unresectable tumors is poor. For advanced stages, survival is less than 50% at 5 years [16]. The treatment for these advanced-disease patients is currently palliative.

Rouleau et al. analyzed 94 clinical sarcoma specimens and showed TEM-1 staining in 84% [17]. More recently, expression of TEM-1 was assessed in a group of 203 clinical sarcoma specimens and 96% of expression was reported [18]. Among many tumor types, sarcomas appear quite attractive for TEM-1 targeted therapy due to simultaneous expression of TEM-1 in the vasculature, stroma, and tumor cells [19].

Several endosialin targeting antibodies have already been developed for oncological applications. An anti-TEM-1, the MORAb-004 antibody, which is a humanized FB5 antibody has completed a phase-I clinical trial and is currently in phase II [20]. A few research groups have developed antibody-drug conjugates (ADCs) [21, 22] and a human antibody ScFv-Fc fragment has already been used for optical imaging and immunotoxin-based therapy [18, 23].

In this study, a fully human single-chain variable fragment (scFv) Fc-fusion, 1C1m-Fc, that cross-reacts with both mouse and human TEM-1 was used. 1C1m-Fc was conjugated to DOTA and labeled with ^{177}Lu , a γ and β^- emitting radionuclide that can be used at low activity for diagnostic applications in single-photon emission computed tomography (SPECT), and high activity for therapeutic applications (Fig. 1). ^{177}Lu is a favorable isotope for theranostic application with a half-life of 6.7 days, a maximal tissue penetration of 2 mm, and a low energy emission ($E_{\beta\text{-max}}$ 0.49) that causes damage to neighboring healthy cells. ^{177}Lu emits 2 photons at 113 KeV (6.4%) and 208 KeV (11%) which allows both imaging for monitoring and dosimetry of the same compound [24].

As anti-TEM-1 imaging could both detect tumors and monitor responses, and could help identify patients suitable for targeted therapy, we decided to perform in vitro and in vivo preclinical evaluations of this novel fusion protein antibody.

Materials and methods

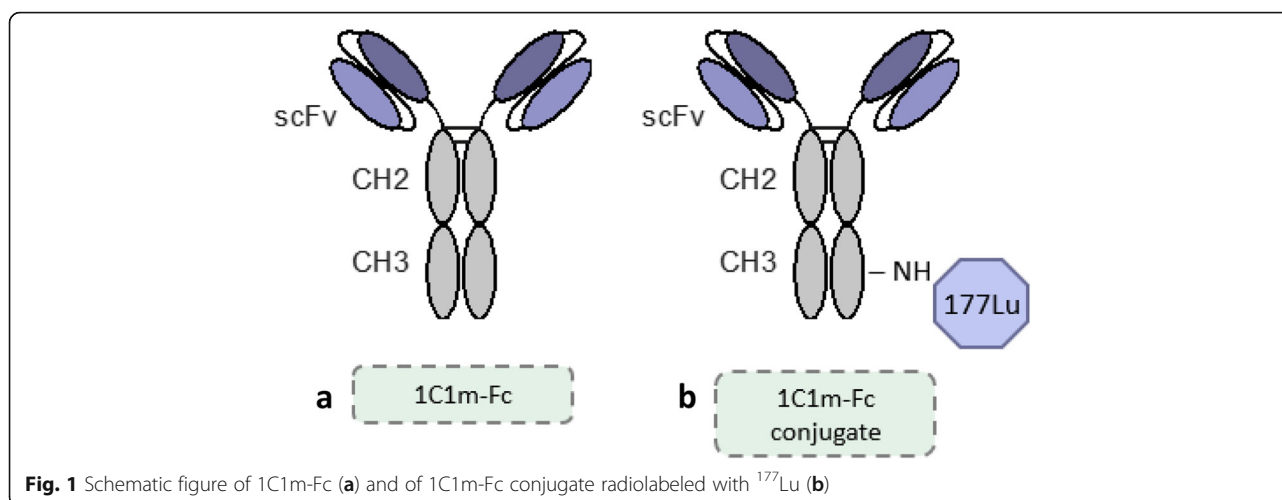
Fusion protein antibody

1C1m-Fc, also named HS06 mut (molecular weight 106196.8 Da, molar extinction coefficient $162830\text{ M}^{-1}\text{ cm}^{-1}$ at 280 nm) was isolated by phage display from a naïve human antibody phage display library at the Lab-Core immunoglobulin discovery and engineering facility, Ludwig Institute for Cancer Research, Lausanne. The scFv was made bivalent by fusion to a human Fc domain (IgG1). The fusion protein was expressed and secreted from HEK293-6E cells, purified by Protein A affinity chromatography, and buffer exchanged into PBS. Affinity to human and murine TEM-1 was respectively 1 and 6 nM [25].

Cell lines

The murine endothelial 2H-11 (TEM-1 positive), human neuroblastoma SK-N-AS (TEM-1 positive), and human fibrosarcoma HT-1080 (TEM-1 negative) cell lines were purchased from the American Type Culture Collection (ATCC, Manassas, VA, USA).

All cell lines were cultured in DMEM (Thermo Fisher Scientific, Waltham, MA, USA) supplemented with 10% fetal bovine serum (FBS, Thermo Fisher Scientific, Waltham, MA, USA) and 1% penicillin/streptomycin



(Thermo Fisher Scientific, Waltham, MA, USA). Cells were incubated in a flask at 37 °C in a humidified atmosphere at 5% CO_2 .

Conjugation

Absorbance at 280 nm of the fusion protein antibodies was measured using a spectrophotometer (NanoDrop Lite, Thermo Fisher Scientific, Waltham, MA, USA), and the molar concentrations were obtained from the absorbance and the respective molar extinction coefficients ($\text{M}^{-1}\cdot\text{cm}^{-1}$).

1C1m-Fc was conjugated with increasing ratios from 10 to 40 equivalents of p-SCN-Bn-DOTA (Macrocyclics, Plano, TX, USA) using the following procedure: after conditioning a concentration of 5 mg/ml of 1C1m-Fc in carbonate buffer 0.2 M pH 9.0 by three ultrafiltrations on 50 kD membrane (Amicon Ultra, 0.5 mL, 50 kD, Merck, Darmstadt, Germany), a calculated volume of a solution of p-SCN-Bn-DOTA at 1 equivalent per μl in a mixture of 50 μl of dimethyl sulfoxide (DMSO) and 450 μl of carbonate was added to the buffered 1C1m-Fc solution. Mixtures were incubated for 1 h at 37 °C, and the conjugated antibodies were washed by four ultrafiltrations using PBS pH 7.4 before performing high-pressure liquid chromatography (HPLC) to assess integrity of the conjugates. Material was subsequently stored between 2–8 °C.

Mass spectrometry analysis

The mass spectrometry (MS) analysis was performed using a Q Exactive™ HF Orbitrap with BioPharma option (Thermo Fisher Scientific, Waltham, MA, USA) operating in the high mass range. The mass spectrometry spectra were deconvoluted using the Protein Deconvolution Software (Thermo Fisher Scientific, Waltham, MA, USA). UPLC was also performed on the samples. The separation was done using the MAbPAC SEC-1 column,

5 μm , 300 Å, 4 × 150 mm (Thermo Fisher Scientific, Waltham, MA, USA), and ammonium acetate 50 mM pH 7.0 at 0.3 mL/min as mobile phase. By knowing the average mass of the antibody and the center of the conjugated antibody average mass distribution (broader peak in MS spectrum than the unconjugated form), an average number of chelators linked to the antibody was calculated.

Radiolabeling

The radiolabeling was optimized with 500 pmoles of DOTA-conjugated 1C1m-Fc and 20 MBq of ^{177}Lu (without carrier, EndoleucineBeta 40 GBq/ml, ITM, in aqueous 0.04 M HCl solution) in acetate buffer 0.4 M pH 5.6. After 1 h incubation time at 37 °C, the radiochemical purity was determined by instant thin layer chromatography (ITLC) and by HPLC.

Purity and stability

The 1C1m-Fc candidate was tested for chemical purity by reducing and non-reducing SDS-PAGE using NuPAGE Bis-Tris gradient gels. The purity and the stability of the native and conjugated fusion protein antibody were also evaluated at 3, 6 months, and 1 year by HPLC. The profiles at the given timepoints were compared to the initial chromatogram.

The stability of [^{177}Lu]Lu-1C1m-Fc in human serum was also assessed at 24 and 48 h by iTLC.

HPLC

HPLC analyses were performed using an Ultimate 3000 SD System (Thermo Fisher Scientific, Waltham, MA, USA) coupled to a GabiStar detector (Raytest, Straubenhard, Germany). Compound were separated with a size exclusion column, XBridge protein BEH 200 Å SEC 3.5 μm , dimension 7.8 × 300 mm (Waters, Baden-Dättwil, Switzerland). Elution was performed using

phosphate buffer pH 6.8 (1 mL/min) as mobile phase and was monitored via absorbance at 220/280 nm or γ detection.

iTLC

iTLC analysis were performed using dried iTLC-SG Glass microfiber chromatography paper impregnated with silica gel (Agilent Technologies, Folsom, CA 95630).

Detection of the radioactivity were obtained on a mini-GITA scanning device (Raytest, Straubenhard, Germany) using the Gina star software after manual integration of the peaks. In this system, the $[^{177}\text{Lu}]\text{Lu-1C1m-Fc}$ remain at $R_f = 0$ while the unbound ^{177}Lu migrate to the solvent front.

In vitro characterization

Flow cytometry

1C1m-Fc and its conjugates were tested for binding to TEM-1 using FACS analysis. Either human cell lines (SK-N-AS or HT-1080) or murine cell lines (2H-11) were distributed in a 96 well plate (100 μL at 0.5×10^6 per mL). After spinning down, the wells were washed once with 100 μL of flow cytometry staining buffer (PBS containing 2% FBS) and the cells were incubated with this FACS buffer (10–30 min) to block any unspecific binding. 1C1m-Fc or its conjugates (from 0.2 $\mu\text{g}/\text{mL}$ to 2 $\mu\text{g}/\text{mL}$) were then added and incubated at 4 °C for 45 min. After washing, 50 μL of the secondary antibody (anti-human Fc, Alexa Fluor 647, Thermo Fisher Scientific, Waltham, MA, USA) was added with incubation in the dark for 30 min at 4 °C. Cells were washed and resuspended in FACS buffer before being analyzed using a BD LSR-II (BD Biosciences) flow cytometer. The secondary antibody and unstained cells were used as negative controls. Median fluorescence intensity (MFI) was studied for 1C1m-Fc and its conjugates.

Radio-immunoreactivity

The immunoreactive fraction was assessed using Lindmo assay [26]. A fixed concentration of radiolabeled 1C1m-Fc (0.07 $\mu\text{g}/\text{mL}$) was incubated with increasing numbers (0.25 – 8×10^6) of SK-N-AS cells in PBS containing 0.5% BSA (PBS/BSA) for 3 h at 37 °C on a shaking platform. Non-specific binding was evaluated by the addition of an excess of native non-radiolabeled 1C1m-Fc (> 100-fold excess).

Unbound activity was washed away twice with PBS/BSA after centrifugation for 5 min at 300 g. The cell-bound activity was measured with a gamma counter (AMG Automatic Gamma Counter, Hidex, Turku, Finland).

All conditions were tested in triplicate. The binding curve was extrapolated to an infinite number of cells using nonlinear regression from the Graphpad Prism 8.0 software (GraphPad Software, San Diego, CA, USA).

In vivo characterization

Murine xenograft model

All animal experiments were conducted in compliance with the cantonal authorization VD-2993 and the guidelines of the Institution.

Tumors expressing huTEM-1 were established by subcutaneous injection of 3×10^6 SK-N-AS cells in mouse flank of 6–10-week-old female Balb/c nude mice (Charles River Laboratories, Wilmington, MA, USA). A negative control was also obtained with injection of 3×10^6 HT-1080 cells (TEM-1 negative).

Tumors were allowed to grow to 5–10 mm (largest diameter) before initiating studies. For SPECT imaging, some mice were injected with both TEM-1 positive and negative tumors. In this case, and due to differences in tumor cell growth rate, injection of HT1080 cells (3×10^6) was delayed by 10 days.

Saturation assay

To assess the non-specific targeting and to optimize the dose to inject for the biodistribution studies, a blocking experiment was performed. Mice bearing SK-N-AS tumors were injected in the lateral tail vein without anesthesia with 100 μL of a saline solution containing 2.5 μg of $[^{177}\text{Lu}]\text{Lu-1C1m-Fc}$ conjugated with 3 DOTA and an increasing amount of unlabeled native 1C1m-Fc (respectively 2.5, 50, 100, 200, and 500 μg).

In each group, three animals were euthanized by CO_2 inhalation and exsanguinated at 24 h after injection of the radiolabeled product. Blood was collected, organs and tumors were removed, weighed, and counted with a gamma counter (AMG Automatic Gamma Counter, Hidex, Turku, Finland).

Biodistribution studies

$[^{177}\text{Lu}]\text{Lu-1C1m-Fc}$ conjugated with 3 DOTA was injected into the lateral tail vein of the mice without anesthesia and sterile filtration. Animals were divided into 2 groups, the average weight of animals was 20.18 ± 1.7 g. Group 1 received an injection of 200 μg of a non-specific unlabeled human immunoglobulin Kiovig™ (Shire, Switzerland GmbH) on the first day (D0) and a mixture of 2.5 μg (1 MBq) of 3 DOTA's $[^{177}\text{Lu}]\text{Lu-1C1m-Fc}$ and 47.5 μg of unlabeled 1C1m-Fc the day after (D1). Group 2 received a mix of 2.5 μg (1 MBq) of 3 DOTA's $[^{177}\text{Lu}]\text{Lu-1C1m-Fc}$ and 47.5 μg of unlabeled 1C1m-Fc at D1, without Kiovig™ injection at D0. The volumes for all the injection were 100 μL , sodium chloride was used to perform the dilution.

In each group, three animals per time point were euthanized by CO_2 inhalation and exsanguinated at 4, 24, 48, 72 h, and 6 days after injection of the radiolabeled product. Blood was collected, organs and tumors were removed, weighed, and counted with a gamma counter

(AMG Automatic Gamma Counter, Hidex, Turku, Finland).

A second experiment was performed with the same conditions as for group 2, but with [^{177}Lu]Lu-1C1m-Fc conjugated with 6 DOTA.

Results were expressed as the percentage of injected activity (IA) per gram of tissue (%IA/g).

Animal imaging study

Three hours static images were acquired with a small-animal PET/SPECT/CT (Albira, Bruker Biospin Corporation, Woodbridge, CT, USA). Mice of two groups (with or without Kiovig[™] at D0) were injected with 50 μg corresponding to 18.5 ± 1.8 MBq of [^{177}Lu]Lu-1C1m-Fc via tail vein injection. Mice were anesthetized for the duration of the imaging sequence by inhalation of 1.5% isoflurane/O₂ and placed on a heated bed. SPECT/CT images were acquired at 24, 48, and 72 h after injection of the radiolabeled antibody for mice with either TEM-1 positive tumors, TEM-1 negative tumors, or both. The acquisition parameters were for SPECT: 80 mm transversal field-of-view, with a single pinhole collimator and for CT: 400 μA intensity and 35 kV voltage. Six animals were imaged: four belonging to group 1 with Kiovig[™] saturation (respectively, one with a TEM-1 negative tumor, one with a TEM-1 positive tumor, and two with both TEM-1 positive and negative tumors), and two belonging to group 2 without Kiovig[™] saturation (one with a TEM-1 positive tumor and one bearing both TEM-1 positive and negative tumors). For two animals belonging to group 2, imaging at 72 h was performed and then the mice were sacrificed to allow a biodistribution study. The image reconstruction methods were for SPECT: ordered subset expectation-maximization algorithm, 2 iterations and with scatter correction, and for CT: filtered back-projection algorithm with de-ringing correction. The tumor volumes of interest (VOI) were obtained by manual segmentation on axial CT slices using the PMOD software (PMOD technologies, version 3.709, Zurich, Switzerland).

Mouse dosimetry

Estimated absorbed doses to organs were based on the biodistribution results on SK-N-AS bearing mice of group 2. Considered source organs for the biodistribution study were the liver, the kidneys, the lungs, the spleen, the heart, the stomach, the small intestine, the colon, the urinary bladder, and the total body. We obtained the remainder by subtraction of the signal measured in source organs from the total body. For each mouse at each time point, the activity in each source organ and the remainder was normalized by the total injected activity to obtain the normalized injected

activity (nA). For each source organ at each time point, an average nA value was obtained \pm SD.

We fitted the source organs normalized time-activity curves (nTACs) with bi-exponential functions using the kinetic module of OLINDA/EXM 2.1 (HERMES Medical Solution AB, Stockholm, Sweden). We derived time-integrated activity coefficients (TIACs) by analytical time-integration of fitted source organ nTACs obtained with the average nA, nA + SD and the nA–SD values, respectively.

A specific absorbed dose estimated was obtained for the uterus, this organ, in fact, exhibited an important specific tracer uptake, but was not among the source/target organs available in the murine model of the OLINDA/EXM 2.1 software.

In the liver, the stomach, the bladder, the uterus, and in the TEM-1 positive tumor, the radioactivity was still in the uptake phase 48 h post-injection. For these tissues, the TIAC was obtained by trapezoidal integration using the Matlab software (release 2017a, The MathWorks, Inc., Natick, Massachusetts, USA), between $t = 0$ and $t = 6$ days, whereas a mono-exponential analytical integration to infinity was calculated after the last measure ($t > 6$ days) considering the ^{177}Lu physical decay constant.

Finally, the TIACs were entered into the OLINDA/EXM[®] 2.1 software kinetic module for organ absorbed dose estimates considering the 25 g murine model where the phantom source organ masses were adjusted to the average organ masses obtained from the mice population used in our experiment. In this process, the TIAC of the uterus was part of the remainder of the body.

A specific absorbed dose estimate for the uterus was obtained using the sphere model of OLINDA/EXM 2.1 where the average organ TIAC and the average organ mass were applied.

Statistics

The data are expressed as mean \pm SD. Significant differences between means were analyzed by an unpaired, 2-tailed Student t test with a correction for multiple comparison using the Holm-Sidak method ($\alpha = 0.05$). Curve-fitting and statistical analyses were conducted using Prism 8.0 (GraphPad Software, San Diego, CA, USA).

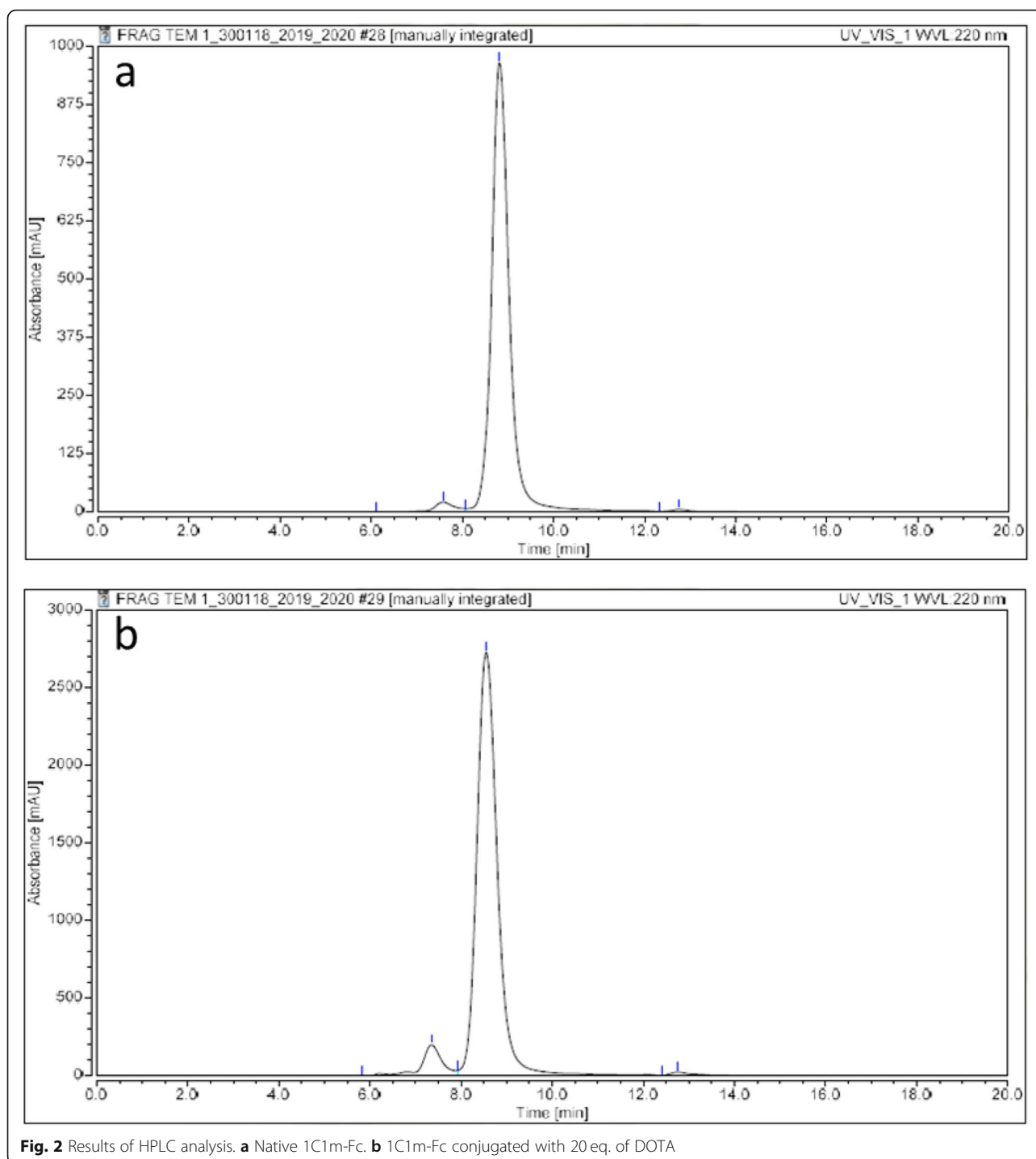
Results

Conjugation, radiolabeling, and stability tests

SDS-page of native 1C1-m and of 1C1m-Fc conjugated with 3 and 6 DOTA was performed (Fig. 1, [supplementary data](#)).

1C1m-Fc and its conjugates were analyzed by HPLC (Fig. 2).

For native 1C1m-Fc, the main peak was observed at 8.8 min. An aggregate peak at 7.5 min and another peak at 12.7 min were also observed. This profile served as a



reference antibody retention time. The area under curve (AUC) of the aggregates increase after conjugation (Table 1).

Mass spectrometry analysis gave a DOTA conjugation number of two, three, and six respectively for 10, 20, and 40 equivalents of DOTA added (Fig. 2 and Table 1, supplementary data).

1C1m-DOTA was successfully radiolabeled with ^{177}Lu . The best radiochemical purity, evaluated by radio thin layer chromatography (TLC), was obtained with 20 equivalents of DOTA and the release criteria was 95%. HPLC profile of $[^{177}\text{Lu}]\text{Lu}$ -1C1m-Fc was assessed by HPLC (Fig. 3, supplementary data). We decided to use this antibody/DOTA ratio for the study. The maximal

Table 1 HPLC analysis results of the native and conjugated 1C1m-Fc

	Native 1C1m-Fc	1C1m-Fc + 10 equivalents DOTA	1C1m-Fc + 20 equivalents DOTA	1C1m-Fc + 40 equivalents DOTA
% of the main peak	97.4	94.5	92.4	94.9
% of aggregates	2.12	5.3	6.7	4.6
% of other impurities	0.5	0.17	0.75	0.5

specific activity was 400 MBq/mg. Stability in serum was also assessed by iTLC and was up to 93% 48 h after labeling ($n = 1$) (Fig. 3).

HPLC showed that the native antibodies (stored at -80°C) and the conjugates (stored at $2-8^{\circ}\text{C}$) were stable for up to 1 year without any additional formulation.

Results: In vitro binding

In flow cytometry analysis, native 1C1m-Fc bound to both human (MFI respectively 8959 and 7714 at 2 and $0.2\ \mu\text{g/ml}$) and murine TEM-1 positive cells.

For conjugates, the binding to TEM-1 positive cells was respectively 8654, 8095, 8321 at $2\ \mu\text{g/ml}$ for 10, 20, and 40 equivalents of DOTA; 7714, 7679, 7454 at $0.2\ \mu\text{g/ml}$ for 10, 20, and 40 equivalents of DOTA and 58.6 for the isotype control (Fig. 4).

A ratio of 20 DOTA per antibody has been selected for this study to optimize the specific activity of the radiolabeling.

The immunoreactivity following the radiolabeling was determined by Lindmo assay and was $86.2\% \pm 3.9\%$ for $[^{177}\text{Lu}]\text{Lu-1C1m-Fc}$ ($n = 2$) (Fig. 5).

Results: In vivo characterization

Saturation assay

The biodistribution results of the 1C1m-Fc dose-escalation study are shown in Fig. 4, [supplementary data](#).

The total 1C1m-Fc dose of $50\ \mu\text{g}$ provided the best biodistribution in the tumor and a sufficient specific activity for a theranostic approach. This amount was chosen for the biodistribution experiments.

Biodistribution study

A biodistribution study of $[^{177}\text{Lu}]\text{Lu-1C1m-Fc}$ conjugated with 3 DOTA was performed with and without saturation with Kiovig[™] (respectively, groups 1 and 2) (Fig. 6).

For group 1 with Kiovig[™] saturation, uptake in TEM-1 negative tumor was significantly lower than TEM-1 positive tumor with uptake clearing over time from $8.4 \pm 0.97\% \text{ IA/g}$ at 24 h ($p = 0.0006$) and $4.4 \pm 1.9\% \text{ IA/g}$ on day 6 ($p = 0.02$). Pre-injection with Kiovig[™] had no influence on biodistribution ($p > 0.05$, t test). For group 1 and 2, uptake in TEM-1 positive tumor was $10.8\% \pm 1.55 \text{ IA/g}$ 4 h after injection and remained consistently high even 3 days after injection ($15.8\% \pm 1.9 \text{ IA/g}$), demonstrating retention of TEM-1 targeted antibody. Uptake

in TEM-1 positive tumor decreased to $7.6 \pm 1.8\% \text{ IA/g}$ 6 days after injection.

A second experiment was done with the same conditions as for group 2, without Kiovig[™] saturation, but with $[^{177}\text{Lu}]\text{Lu-1C1m-Fc}$ conjugated with 6 DOTA. The uptake in the liver and in the spleen was $79\% \pm 12.5 \text{ IA/g}$ and $82\% \pm 40 \text{ IA/g}$, respectively, at 24 h (Table 2).

SPECT/CT study

The SPECT/CT imaging showed a specific uptake in TEM-1 positive tumor (Fig. 7) and liver uptake. The uptake ratio between TEM-1 positive tumor and TEM-1 negative tumor was determined at 24, 48, and 72 h (Table 3). A 1.9-fold higher signal at 72 h was observed in SPECT/CT imaging in TEM-1 positive tumors versus control tumors.

The signal ratio TEM-1 positive to TEM-1 negative tumor obtained with the SPECT/CT at 72 h was similar to the one obtained in biodistribution (with a factor of 2.2 and 1.9, respectively).

Dosimetry

Extrapolated organ absorbed doses for mice derived from the injection of $[^{177}\text{Lu}]\text{Lu-1C1m-Fc}$ are reported in Table 4.

The organ receiving the highest absorbed dose was determined to be the liver (2.23 Gy/MBq), followed by the uterus (1.5 Gy/MBq), the spleen (1.2 Gy/MBq) and the stomach (1.15 Gy/MBq). The total body dose was 0.4 Gy/MBq and the tumor dose was 1.82 Gy/MBq .

Discussion

Two major challenges in the field of theranostics must be considered: firstly, the identification of suitable tumor-specific targets and secondly, the development of high-affinity antibodies. Ideal targets should present the following criteria: high and exclusive expression in tumors and a broad expression across a variety of tumor types, affording opportunities for universal cancer therapies.

TEM-1 is a robust target overexpressed specifically in the tumor vasculature of a large number of adenocarcinomas. Tumor vasculature cells provide critical support for tumor survival, growth, and invasion and act as physical and molecular barriers that protect tumor cells from the host immune system [27, 28]. In addition, endothelial cells are accessible directly via the bloodstream.

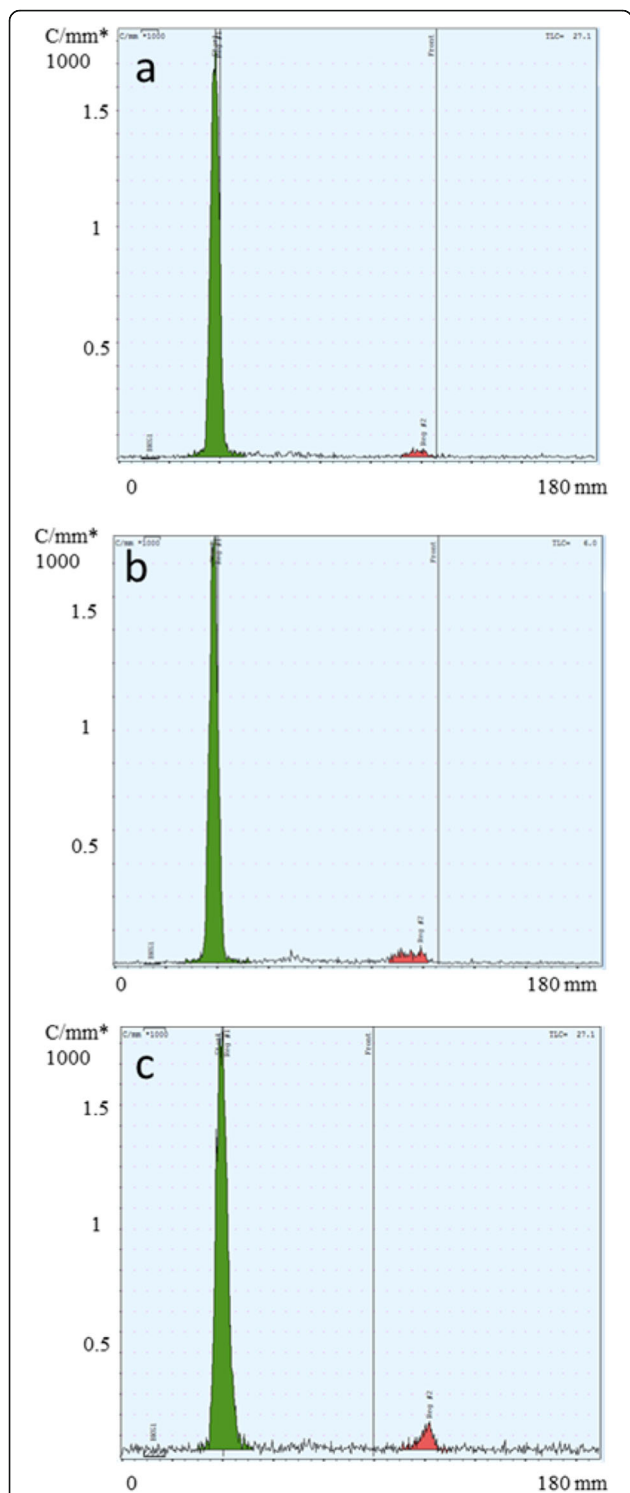


Fig. 3 Radio-TLC analysis of [177Lu]Lu-1C1m-Fc (20 MBq of ¹⁷⁷Lu). **a** After labeling RCP = 97.4%. **b** 24 h after labeling in serum RCP = 95.3%. **c** 48 h after labeling in serum RCP = 93.9%

Sarcoma is a heterogeneous group of tumors with a high unmet medical need. The literature consistently reports a strong expression of TEM-1 in sarcomas, which

is localized in malignant cells and perivascular and stromal cells, allowing simultaneous targeting of tumor cells and the tumor vasculature [17–19].

Given the very short half-life and the relative in vivo instability of monovalent scFv antibody fragments, a bivalent Fc-fusion protein based on a novel single-chain antibody, 1C1m-Fc, was chosen for evaluation in this study. The fusion of scFvs to the IgG Fc constant domains adds significant size, avidity, and stability to the targeting moiety and would be expected to lead to improved blood pharmacokinetics. In contrast to the previously described anti-TEM-1 MORAb-004 antibody, the cross-reactivity of 1C1m toward both human and murine TEM-1 allows the evaluation of anti-TEM-1 therapeutic approaches in the mouse.

1C1m-Fc was conjugated and radiolabeled with ¹⁷⁷Lu to allow its use both for SPECT imaging and for the potential delivery of a therapeutic payload. We have therefore performed a preliminary preclinical evaluation of this fusion protein. The conjugation and the radiolabeling process were optimized to obtain a radiochemical purity up to 95%.

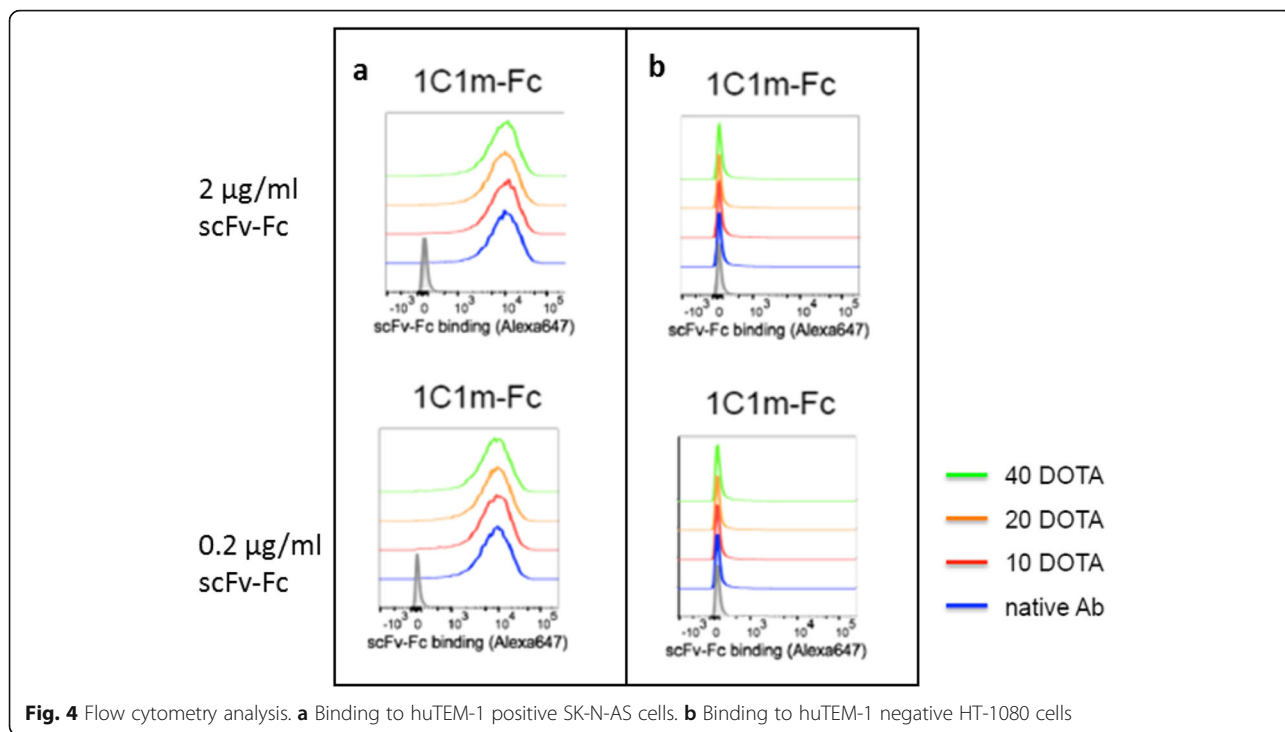
For the in vitro characterization, 1C1m-Fc and its conjugates were tested for binding to TEM-1 using flow cytometry analysis. A high percentage of binding was observed for 1C1m-Fc at each concentration tested and for each ratio used in the coupling reaction. A concentration of 20 equivalents of DOTA has been chosen as suitable for achieving an optimal specific activity of radiolabeling.

The results of the Lindmo analysis demonstrated that the radiolabeling did not affect the immunoreactivity.

A first biodistribution study using [177Lu]Lu-1C1m-Fc with co-injection of Kiovig™ was performed. The aim was to examine the influence of Fc receptor blocking on biodistribution and uptake, as mouse Fc receptors are highly abundant in mouse spleen and liver and are known to show appreciable binding to human Fc [29]. Kiovig™ is a readily available commercial IgG that does not bind or mask TEM-1 on SK-N-AS cells.

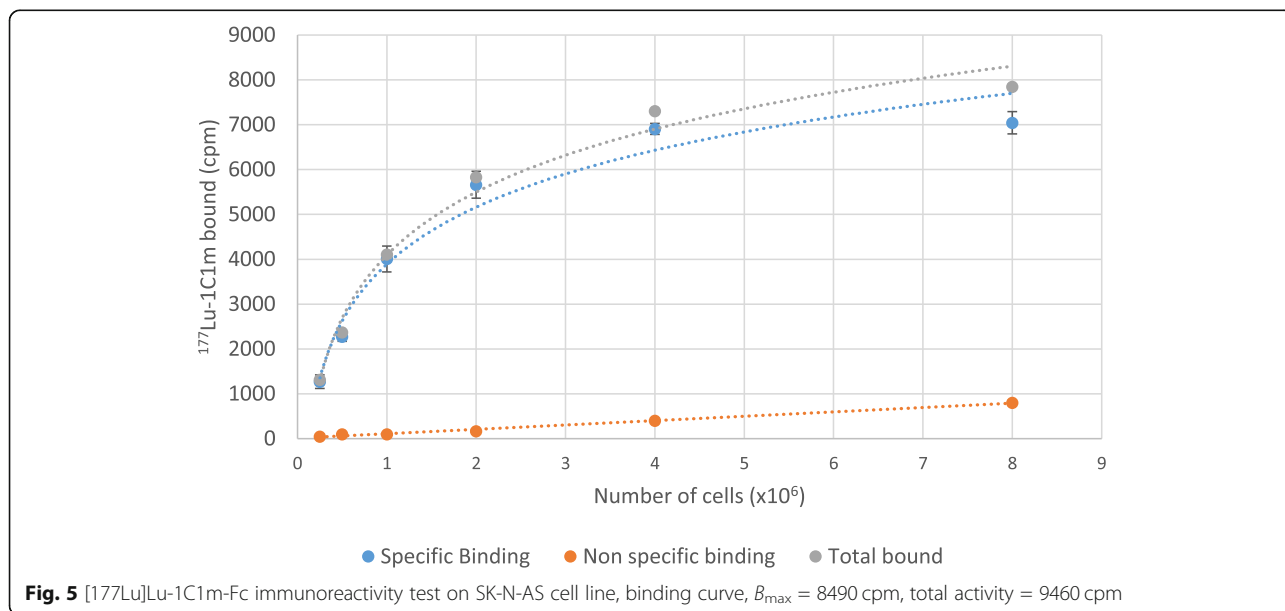
The results of this biodistribution experiment were compared with a second study arm performed without Kiovig™ co-injection. This experiment revealed specific tumor targeting in the two mouse xenograft models with no impact of the Kiovig™ co-injection on biodistribution. The [177Lu]Lu-1C1m-Fc was found to enrich mainly in the liver and the spleen, as has been observed for many antibodies [28, 30, 31]. Quantitative PCR, performed by other groups on biopsies taken from mice upon sacrifice has shown an absence of detectable TEM-1 in the liver, confirming this uptake to be non-specific in nature.

As no difference was shown with or without saturation, we asked whether the liver and the spleen uptake could be explained by the number of conjugated DOTA



moieties on the fusion protein. Indeed, the number of DOTA attached per antibody can vary depending on the molar ratios of both the antibody and DOTA used for the conjugation. To achieve a high radiolabeling efficiency and probe sensitivity it is often desirable to conjugate a higher number of chelators per antibody. However, the hydrophilic character of DOTA can significantly perturb the lipophilicity/hydrophilicity properties of the acceptor antibody with unpredictable consequences for pharmacokinetics.

Regarding the DOTA conjugate, antibody ratio, other authors have reported that a reduction of non-specific hepatic uptake is correlated with an increased number of DOTA per antibody. Indeed, it has been suggested that the negative charge conferred to the antibody by DOTA conjugation results in a reduced isoelectric point (pI), causing a net repulsion between the molecule and the phospholipid bi-layer [32, 33]. However, Rinne et al. working with gallium-68 and indium-111 did not observe a clear relationship between the extent of negative



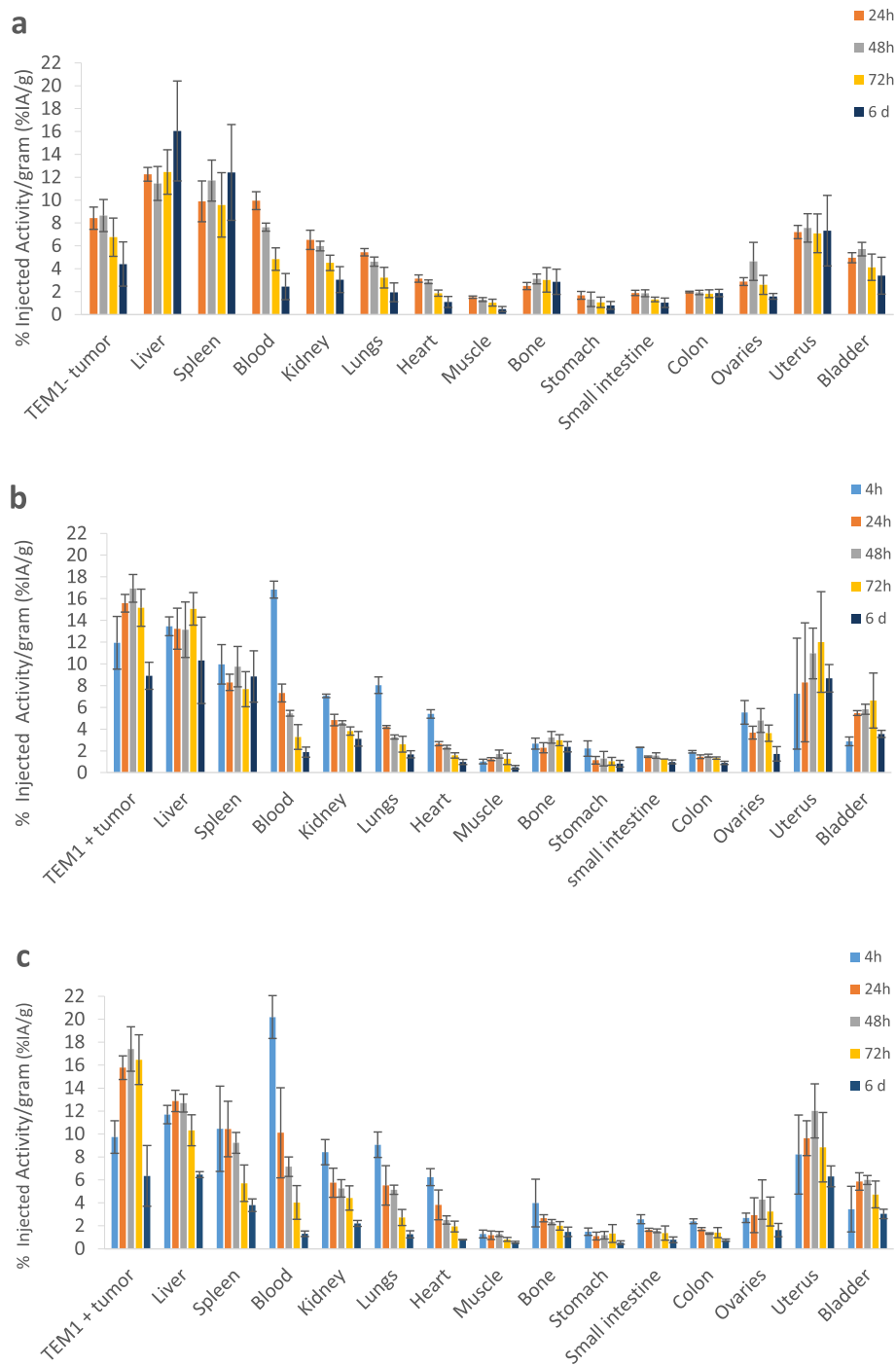
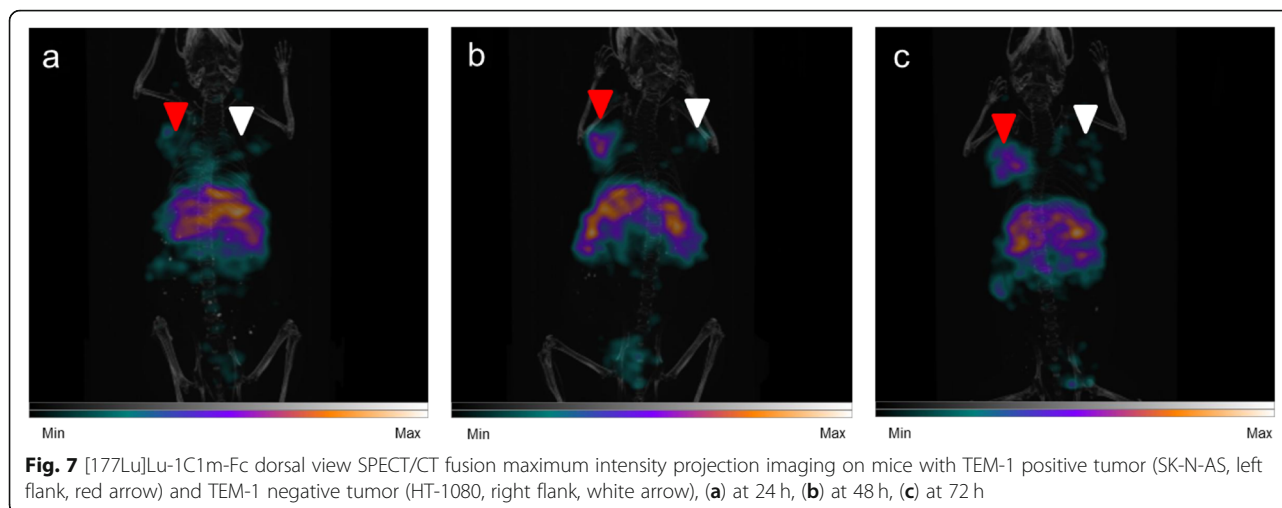


Fig. 6 Biodistribution of [177Lu]Lu-1C1m-Fc in Balb/c nu mice. **a** TEM-1 negative tumor (HT-1080)-bearing mice with Kiovig™ preinjection, group 1. **b** TEM-1 positive tumor (SK-N-AS)-bearing mice with Kiovig™ preinjection, group1. **c** TEM-1 positive tumor (SK-N-AS)-bearing mice without Kiovig™ preinjection, group 2. Data are shown as mean ± SD. There were significant differences between uptake in TEM-1 positive tumors compared with TEM-1 negative tumors ($p = 0.0006$ at 24 h). There was no difference on the biodistribution with or without Kiovig™ preinjection (all $p > 0.059$)

Table 2 Liver and tumor uptake regarding the estimated number of DOTA fixed on 1C1m-Fc

Estimated number of DOTA	Liver uptake (%IA/g) ($T = 24$ h)	Tumor TEM-1 positive uptake (%IA/g) ($T = 24$ h)
6	79 ± 12	11.6 ± 0.3
3	12.8 ± 0.9	15.8 ± 1



charge and uptake [32]. As isotopes differ in charge, coordination number, and chelation geometry, the biodistribution of any conjugate is likely to be significantly influenced by not only the choice of targeting antibody but also by the combination of chelator and radioisotope, in addition to the conjugation ratio. Hence, each conjugate should be optimized accordingly [32, 34].

In our study, the 1C1m-Fc fusion protein was conjugated with DOTA and radiolabeled with ^{177}Lu . The number of DOTA per antibody was evaluated by mass spectrometry and the uptake and retention in the liver was found to increase with the number of DOTA fixed on 1C1m-Fc. Our results are in accordance with reports showing that a high number of chelators coupled to an antibody can result in accelerated blood clearance and high liver uptake [34, 35]. Moreover, at high DOTA conjugation ratios, the possibility of DOTA attachment to important residues in the antigen-targeting variable domains of the antibody increases, potentially compromising the immunoreactivity of the molecule [36]. Additionally, high chelator conjugation ratios could cause conformational changes to an antibody that can result in rapid sequestration of the radio conjugate into the liver and spleen, as well as accelerated uptake by the reticuloendothelial system, resulting in unfavorable pharmacokinetic properties [37]. Elevated uptake in the liver can also indicate a lower stability of the radiolabeling such as trans-chelation to transferrin [38].

We observed that an optimization of the tumor/liver ratio could be achieved by reducing the number of

DOTA coupled to 1C1m-Fc. We have performed a conventional conjugation, which can produce heterogeneous mixtures with respect to conjugate ratio and sites of conjugation. In this case, site-specific conjugation could be a technique to be evaluated for the improvement of batch to batch consistency of the conjugates and to avoid the potential risks of non-specific conjugation [39, 40].

Although the binding of 1C1m has been shown to be TEM-1 specific, we have observed significant retention of the conjugates in TEM-1 negative tumors. This uptake could be explained by possible TEM-1 expression by the neo-vessels that form in these tumors. In this case, the antibodies are probably distributed only in the neo-vessels and not retained by any binding to tumor cells. As the appearance of the tumors was highly vascularized, this stasis in the neovessels could be due to the EPR effect in the neovessels. These hypotheses will be tested in future experiments using fluorescence microscopy.

Biodistribution data were used for dosimetry calculations. The organ receiving the highest absorbed dose would be the liver (2.23 Gy/MBq) followed by the uterus (1.5 Gy/MBq), the spleen (1.2 Gy/MBq), and the stomach (1.15 Gy/MBq). The total body dose would be (0.4 Gy/MBq) and the tumor dose 1.82 Gy/MBq. In particular, a specific dose estimate was performed for the uterus using the spherical model available in the OLINDA/EXM 2.1 software. This approach does not consider the specific morphology of the organ but it is at present the best approximation we can provide without applying

Table 3 SPECT imaging of tumor uptake at 24, 48, 72 h

Time post-injection	SK-N-AS (Cps/tumor volume)	HT-1080 (Cps/tumor volume)	Ratio SK-N-AS/HT-1080
24 h	2.17E+07	1.61E+07	1.3
48 h	3.17E+07	1.85E+07	1.7
72 h	3.03E+07	1.60E+07	1.9

Table 4 Mouse dosimetry of [¹⁷⁷Lu]Lu-1C1m-Fc. These estimates come from mouse TIACs calculated from source organ time-activity curves

Source organ	Mouse average organ mass (g)	Average TIAC (MBq·h/MBq)	Absorbed dose (mGy/MBq)
Tumor SK-N-AS	0.16	3.91	1.82E+03
Liver	1.28	30.42	2.23E+03
Kidneys	0.33	2.04	7.05E+02
Lung	0.15	0.71	5.39E+02
Spleen	0.09	1.12	1.20E+03
Heart	0.20	0.33	3.63E+02
Stomach	0.10	0.55	1.15E+03
Small intestine	1.38	2.73	4.38E+02
Colon	0.87	1.74	3.28E+02
Bladder	0.10	0.13	3.16E+02
Uterus*	0.08	1.66	1.5 E+03
Total body	20.19	98.78	4.25E+02

*The uterus is not part of the source/target organ in the murine model of the OLINDA/EXM 2.1 software. Specific dosimetry was obtained with the sphere model of the OLINDA/EXM 2.1 where the organ-specific average mass and TIAC were applied

specific Monte Carlo dose calculations which are beyond the scope of this study.

To evaluate the organ radiotoxicity after therapy administration in humans it would be necessary to extrapolate the human dosimetry to from the pre-clinical model. This study will be the subject of a forthcoming analysis in which the extrapolation will be performed for the optimized radiolabeled compound.

We have performed SPECT/CT imaging experiments on an scFv-Fc antibody that binds both human and mouse TEM-1, and generated data showing that TEM-1 was either absent or present at negligible levels in normal mouse organs and that [¹⁷⁷Lu]Lu-1C1m-Fc was able to efficiently target a TEM-1 positive tumor in vivo. The imaging at the 72 h timepoint compared with the biodistribution data for the same mouse showed that the results of the two techniques can be complementary.

Hence, SPECT molecular imaging of sarcoma or other solid tumors could contribute in radiologic staging and in applications such as the preoperative evaluation of patients to assess tumor resectability or radio-guided surgery of metastases.

Conclusion

The highly specific expression of TEM-1 in several types of solids tumors suggests that [¹⁷⁷Lu]Lu-1C1m-Fc could prove a potentially useful and safe tool for molecular imaging and theranostic applications.

The number of DOTA molecules attached per antibody moiety plays a significant role in determining the success of tumor targeting employing radiolabeled antibodies [36]. Further experiments could be done to find the best ratio of DOTA per antibody to maintain a balance between radiochemical yield, immunoreactivity, and pharmacokinetic behavior to develop an optimal radiolabeled 1C1m-Fc suitable for theranostic application.

Supplementary information

Supplementary information accompanies this paper at <https://doi.org/10.1186/s13550-020-00685-3>.

Additional file 1: Supplementary data. **Figure S1.** SDS-page in non-reducing (**b, c, d**) and reducing conditions (**e, f, g**) using NuPAGE Bis-Tris gradient gels. (**a**) marker; (**b, e**) native 1C1m-Fc; (**c, f**) 1C1m-Fc conjugated with 3 DOTA; (**d, g**) 1C1m-Fc conjugated with 6 DOTA. **Figure S2.** Mass spectrometry analysis of native 1C1m-Fc (**a**) and of 1C1m-Fc conjugated with 3 DOTA (**b**). **Figure S3.** HPLC profile of [¹⁷⁷Lu]Lu-1C1m-Fc conjugated with 3 DOTA. **Figure S4.** Saturation assay in Balb/c nu mice. 2.5 µg of [¹⁷⁷Lu]Lu-1C1m-Fc conjugated with 3 DOTA was co-injected with an increasing amount of unlabeled native 1C1m-Fc (respectively 2.5, 50, 100, 200 and 500 µg). The %IA/g was evaluated at 24 hours. **Table S1.** Estimated number of DOTA per 1C1m-Fc based on mass spectrometry analysis

Acknowledgements

Not applicable.

Authors' contributions

JD performed the experiments and drafted the manuscript. JOP and AFC participated in the study design and coordination and helped to draft the manuscript. JKF and SMD produced the 1C1m-Fc fusion protein antibody. SG helped to perform dosimetry analysis. DV, NS, and GC helped to draft the manuscript. All authors read and approved the final manuscript.

Funding

This research was funded with the help of the Alfred and Annemarie von Sick Grant (Zurich, Switzerland) and the Department of Nuclear Medicine and Molecular Imaging, Lausanne University Hospital (Lausanne, Switzerland).

Availability of data and materials

The datasets used and/or analyzed during the current study are available from the corresponding author on reasonable request.

Ethics approval and consent to participate

All applicable institutional and/or national guidelines for the care and use of animals were followed. In particular, all animal experiments in the present study were conducted according to the Swiss federal law on animal experimentation under the cantonal authorization number VD-2993.

Consent for publication

Not applicable.

Competing interests

George Coukos has received grants, research support, or is coinvestigator in clinical trials by BMS, Celgene, Boehringer Ingelheim, Roche, Iovance, and Kite. Prof. Coukos has received honoraria for consultations or presentations by Roche, Genentech, BMS, AstraZeneca, Sanofi-Aventis, Nextcure, and GenosTx. Prof. Coukos has patents in the domain of antibodies and vaccines targeting the tumor vasculature as well as technologies related to T cell expansion and engineering for T cell therapy. George Coukos holds patents around TEM1 antibodies and receives royalties from the University of Pennsylvania regarding technology licensed to Novartis. Julie K. Fierle and Steven M. Dunn hold patents in the domain of antibodies and in particular on the 1C1m antibody used in this study. All other authors declare that they have no conflict of interest.

Author details

¹Radiopharmacy Unit, Department of Pharmacy, Lausanne University Hospital and University of Lausanne, Lausanne, Switzerland. ²CRCINA, INSERM, CNRS, Université d'Angers, Université de Nantes, Nantes, France. ³LabCore, Ludwig Institute for Cancer Research, Lausanne University Hospital and University of Lausanne, Lausanne, Switzerland. ⁴Institute of Radiation Physics, Lausanne University Hospital and University of Lausanne, Lausanne, Switzerland. ⁵Department of Nuclear Medicine and Molecular Imaging, Lausanne University Hospital and University of Lausanne, Rue du Bugnon 46, CH-1011 Lausanne, Switzerland. ⁶Ludwig Institute for Cancer Research and Department of Oncology, Lausanne University Hospital and University of Lausanne, Lausanne, Switzerland.

Received: 11 May 2020 Accepted: 6 August 2020

Published online: 17 August 2020

References

- Elashoff MR, Wingrove JA, Beineke P, Daniels SE, Tingley WG, Rosenberg S, et al. Development of a blood-based gene expression algorithm for assessment of obstructive coronary artery disease in non-diabetic patients. *BMC Med Genet*. 2011;4:26.
- Teicher BA. CD248: A therapeutic target in cancer and fibrotic diseases. *Oncotarget*. 2019;10(9):993–1009.
- Christian S, Ahorn H, Novatchkova M, Garin-Chesa P, Park JE, Weber G, et al. Molecular cloning and characterization of EndoGlyx-1, an EMILIN-like multisubunit glycoprotein of vascular endothelium. *J Biol Chem*. 2001; 276(51):48588–95.
- Lax S, Hou TZ, Jenkinson E, Salmon M, MacFadyen JR, Isacke CM, et al. CD248/Endosialin is dynamically expressed on a subset of stromal cells during lymphoid tissue development, splenic remodeling and repair. *FEBS Lett*. 2007;581(18):3550–6.
- MacFadyen JR, Haworth O, Roberston D, Hardie D, Webster MT, Morris HR, et al. Endosialin (TEM1, CD248) is a marker of stromal fibroblasts and is not selectively expressed on tumour endothelium. *FEBS Lett*. 2005;579(12):2569–75.
- Bagley RG. Endosialin: from vascular target to biomarker for human sarcomas. *Biomark Med*. 2009;3(5):589–604.
- Rettig WJ, Garin-Chesa P, Healey JH, Su SL, Jaffe EA, Old LJ. Identification of endosialin, a cell surface glycoprotein of vascular endothelial cells in human cancer. *Proc Natl Acad Sci U S A*. 1992;89(22):10832–6.
- Tomkowicz B, Rybinski K, Foley B, Ebel W, Kline B, Routhier E, et al. Interaction of endosialin/TEM1 with extracellular matrix proteins mediates cell adhesion and migration. *Proc Natl Acad Sci U S A*. 2007;104(46):17965–70.
- Maia M, DeVriese A, Janssens T, Moons M, Lories RJ, Tavernier J, et al. CD248 facilitates tumor growth via its cytoplasmic domain. *BMC Cancer*. 2011;11:162.
- Fujii S, Fujihara A, Natori K, Abe A, Kuboki Y, Higuchi Y, et al. TEM1 expression in cancer-associated fibroblasts is correlated with a poor prognosis in patients with gastric cancer. *Cancer Med*. 2015;4(11):1667–78.
- Davies G, Cunnick GH, Mansel RE, Mason MD, Jiang WG. Levels of expression of endothelial markers specific to tumour-associated endothelial cells and their correlation with prognosis in patients with breast cancer. *Clin Exp Metastasis*. 2004;21(1):31–7.
- Nanda A, Karim B, Peng Z, Liu G, Qiu W, Gan C, et al. Tumor endothelial marker 1 (Tem1) functions in the growth and progression of abdominal tumors. *Proc Natl Acad Sci U S A*. 2006;103(9):3351–6.
- Opavsky R, Haviernik P, Jurkovicova D, Garin MT, Copeland NG, Gilbert DJ, et al. Molecular characterization of the mouse Tem1/endosialin gene regulated by cell density in vitro and expressed in normal tissues in vivo. *J Biol Chem*. 2001;276(42):38795–807.
- Simonavicius N, Robertson D, Bax DA, Jones C, Huijbers IJ, Isacke CM. Endosialin (CD248) is a marker of tumor-associated pericytes in high-grade glioma. *Mod Pathol*. 2008;21(3):308–15.
- Fletcher CD. The evolving classification of soft tissue tumours - an update based on the new 2013 WHO classification. *Histopathology*. 2014;64(1):2–11.
- Edge SB, Compton CC. The American Joint Committee on Cancer: The 7th edition of the AJCC cancer staging manual and the future of TNM. *Ann Surg Oncol*. 2010;17(6):1471–4.
- Rouleau C, Curiel M, Weber W, Smale R, Kurtzberg L, Mascarello J, et al. Endosialin protein expression and therapeutic target potential in human solid tumors: sarcoma versus carcinoma. *Clin Cancer Res*. 2008;14(22):7223–36.
- Guo Y, Hu J, Wang Y, Peng X, Min J, Wang J, et al. Tumour endothelial marker 1/endosialin-mediated targeting of human sarcoma. *Eur J Cancer*. 2018;90:111–21.
- Thway K, Robertson D, Jones RL, Selfe J, Shipley J, Fisher C, et al. Endosialin expression in soft tissue sarcoma as a potential marker of undifferentiated mesenchymal cells. *Br J Cancer*. 2016;115(4):473–9.
- Chacko AM, Li C, Nayak M, Mikitsh JL, Hu J, Hou C, et al. Development of 124I immuno-PET targeting tumor vascular TEM1/endosialin. *J Nucl Med*. 2014;55(3):500–7.
- Capone E, Piccolo E, Fichera I, Ciufici P, Barcaroli D, Sala A, et al. Generation of a novel antibody-drug conjugate targeting endosialin: potent and durable antitumor response in sarcoma. *Oncotarget*. 2017;8(36):60368–77.
- Rouleau C, Gianolio DA, Smale R, Roth SD, Krumbholz R, Harper J, et al. Anti-endosialin antibody-drug conjugate: potential in sarcoma and other malignancies. *Mol Cancer Ther*. 2015;14(9):2081–9.
- Li C, Chacko AM, Hu J, Hasegawa K, Swails J, Grasso L, et al. Antibody-based tumor vascular theranostics targeting endosialin/TEM1 in a new mouse tumor vascular model. *Cancer Biol Ther*. 2014;15(4):443–51.
- Kim K, Kim SJ. Lu-177-based peptide receptor radionuclide therapy for advanced neuroendocrine tumors. *Nucl Med Mol Imaging*. 2018;52(3):208–15.
- Fierle JK, Abram-Saliba J, Brioschi M, de Tiani M, Coukos G, Dunn SM. Integrating SpyCatcher/SpyTag covalent fusion technology into phase display workflows for rapid antibody discovery. *Sci Rep*. 2019;9(1):12815.
- Lindmo T, Boven E, Cuttitta F, Fedorko J, Bunn PA Jr. Determination of the immunoreactive fraction of radiolabeled monoclonal antibodies by linear extrapolation to binding at infinite antigen excess. *J Immunol Methods*. 1984;72(1):77–89.
- Motz GT, Coukos G. The parallel lives of angiogenesis and immunosuppression: cancer and other tales. *Nat Rev Immunol*. 2011;11(10):702–11.
- Yuan X, Yang M, Chen X, Zhang X, Sukhadia S, Musolino N, et al. Correction to: characterization of the first fully human anti-TEM1 scFv in models of solid tumor imaging and immunotoxin-based therapy. *Cancer Immunol Immunother*. 2018;67(2):329–39.
- Vivier D, Sharma SK, Adumeau P, Rodriguez C, Fung K, Zeglis BM. The impact of FcγRIIIb binding on immuno-PET. *J Nucl Med*. 2019;60(8):1174–82.
- Crombet T, Torres L, Neningen E, Catala M, Solano ME, Perera A, et al. Pharmacological evaluation of humanized anti-epidermal growth factor receptor, monoclonal antibody h-R3, in patients with advanced epithelial-derived cancer. *J Immunother*. 2003;26(2):139–48.
- Rabasa Capote A, Gonzalez JE, Rodriguez-Vera L, Lopez A, Sanchez Ramirez B, Garrido HG. Pharmacokinetics and biodistribution study of 7A7 anti-mouse epidermal growth factor receptor monoclonal antibody and its F(ab')₂ fragment in an immunocompetent mouse model. *ISRN Pharmacol*. 2012;2012:417515.
- Rinne SS, Dahlsson Leitao C, Gentry J, Mitran B, Abouzayed A, Tolmachev V, et al. Increase in negative charge of (68)Ga/chelator complex reduces unspecific hepatic uptake but does not improve imaging properties of HER3-targeting affibody molecules. *Sci Rep*. 2019;9(1):17710.
- Tolmachev V, Orlova A. Influence of labelling methods on biodistribution and imaging properties of radiolabelled peptides for visualisation of molecular therapeutic targets. *Curr Med Chem*. 2010;17(24):2636–55.
- Knogler K, Grunberg J, Novak-Hofer I, Zimmermann K, Schubiger PA. Evaluation of 177Lu-DOTA-labeled aglycosylated monoclonal anti-L1-CAM antibody chCE7: influence of the number of chelators on the in vitro and in vivo properties. *Nucl Med Biol*. 2006;33(7):883–9.
- Al-Ejeh F, Darby JM, Thierry B, Brown MP. A simplified suite of methods to evaluate chelator conjugation of antibodies: effects on hydrodynamic radius and biodistribution. *Nucl Med Biol*. 2009;36(4):395–402.
- Guleria M, Das T, Kumar C, Sharma R, Amirhanayagam J, Sarma HD, et al. Effect of number of bifunctional chelating agents on the pharmacokinetics and immunoreactivity of 177Lu-labeled rituximab: a systemic study. *Anti Cancer Agents Med Chem*. 2018;18(1):146–53.
- Shin IS, Lee SM, Kim HS, Yao Z, Regino C, Sato N, et al. Effect of chelator conjugation level and injection dose on tumor and organ uptake of 111In-labeled MORAb-009, an anti-mesothelin antibody. *Nucl Med Biol*. 2011;38(8):1119–27.

38. Hosseinimehr SJ, Tolmachev V, Orlova A. Liver uptake of radiolabeled targeting proteins and peptides: considerations for targeting peptide conjugate design. *Drug Discov Today*. 2012;17(21-22):1224–32.
39. Wu Y, Zhu H, Zhang B, Liu F, Chen J, Wang Y, et al. Synthesis of site-specific radiolabeled antibodies for radioimmunotherapy via genetic code expansion. *Bioconjug Chem*. 2016;27(10):2460–8.
40. Tavare R, Wu WH, Zettlitz KA, Salazar FB, McCabe KE, Marks JD, et al. Enhanced immunoPET of ALCAM-positive colorectal carcinoma using site-specific (6)(4)Cu-DOTA conjugation. *Protein Eng Des Sel*. 2014;27(10):317–24.

Publisher's Note

Springer Nature remains neutral with regard to jurisdictional claims in published maps and institutional affiliations.

Submit your manuscript to a SpringerOpen[®] journal and benefit from:




- ▶ Convenient online submission
- ▶ Rigorous peer review
- ▶ Open access: articles freely available online
- ▶ High visibility within the field
- ▶ Retaining the copyright to your article

Submit your next manuscript at ▶ [springeropen.com](https://www.springeropen.com)

Article 2: Delage, J. A., et al. "Impact of DOTA Conjugation on Pharmacokinetics and Immunoreactivity of [(177)Lu]Lu-1C1m-Fc, an Anti TEM-1 Fusion Protein Antibody in a TEM-1 Positive Tumor Mouse Model." [Pharmaceutics 2021](#)

Article

Impact of DOTA Conjugation on Pharmacokinetics and Immunoreactivity of [¹⁷⁷Lu]Lu-1C1m-Fc, an Anti TEM-1 Fusion Protein Antibody in a TEM-1 Positive Tumor Mouse Model

Judith Anna Delage^{1,*}, Alain Faivre-Chauvet², Jacques Barbet³ , Julie Katrin Fierle⁴, Niklaus Schaefer⁵, George Coukos⁶, David Viertl⁵, Steven Mark Dunn⁴, Silvano Gnesin⁷  and John O. Prior^{5,*} 

- ¹ Radiopharmacy Unit, Department of Pharmacy, Lausanne University Hospital and University of Lausanne, CH-1011 Lausanne, Switzerland
 - ² CRCINA, INSERM 1232-CNRS ERL 6001, University of Angers, University of Nantes, 44000 Nantes, France; alain.favier-chauvet@univ-nantes.fr
 - ³ Groupement d'Intérêt Public Arronax, F-44800 Saint-Herblain, France; jacques.barbet@univ-nantes.fr
 - ⁴ LAbCore, Ludwig Institute for Cancer Research, Lausanne University Hospital and University of Lausanne, CH-1066 Epalinges, Switzerland; julie.fierle@unil.ch (J.K.F.); steven.dunn@chuv.ch (S.M.D.)
 - ⁵ Department of Nuclear Medicine and Molecular Imaging, Lausanne University Hospital and University of Lausanne, CH-1011 Lausanne, Switzerland; niklaus.schaefer@chuv.ch (N.S.); david.viertl@chuv.ch (D.V.)
 - ⁶ Ludwig Institute for Cancer Research and Department of Oncology, Lausanne University Hospital and University of Lausanne, CH-1011 Lausanne, Switzerland; george.coukos@chuv.ch
 - ⁷ Institute of Radiation Physics, Lausanne University Hospital and University of Lausanne, CH-1011 Lausanne, Switzerland; silvano.gnesin@chuv.ch
- * Correspondence: judith.delage@chuv.ch (J.A.D.); john.prior@chuv.ch (J.O.P.);
Tel.: +41-21-314-43-53 (J.A.D.); +41-21-314-43-47 (J.O.P.)



Citation: Delage, J.A.; Faivre-Chauvet, A.; Barbet, J.; Fierle, J.K.; Schaefer, N.; Coukos, G.; Viertl, D.; Dunn, S.M.; Gnesin, S.; Prior, J.O. Impact of DOTA Conjugation on Pharmacokinetics and Immunoreactivity of [¹⁷⁷Lu]Lu-1C1m-Fc, an Anti TEM-1 Fusion Protein Antibody in a TEM-1 Positive Tumor Mouse Model. *Pharmaceutics* **2021**, *13*, 96. <https://doi.org/10.3390/pharmaceutics13010096>

Received: 4 December 2020
Accepted: 6 January 2021
Published: 13 January 2021

Publisher's Note: MDPI stays neutral with regard to jurisdictional claims in published maps and institutional affiliations.



Copyright: © 2021 by the authors. Licensee MDPI, Basel, Switzerland. This article is an open access article distributed under the terms and conditions of the Creative Commons Attribution (CC BY) license (<https://creativecommons.org/licenses/by/4.0/>).

Abstract: 1C1m-Fc, an anti-tumor endothelial marker 1 (TEM-1) scFv-Fc fusion protein antibody, was previously successfully radiolabeled with ¹⁷⁷Lu. TEM-1 specific tumor uptake was observed together with a non-saturation dependent liver uptake that could be related to the number of dodecane tetraacetic acid (DOTA) chelator per 1C1m-Fc. The objective of this study was to verify this hypothesis and to find the best DOTA per 1C1m-Fc ratio for theranostic applications. 1C1m-Fc was conjugated with six concentrations of DOTA. High-pressure liquid chromatography, mass spectrometry, immunoreactivity assessment, and biodistribution studies in mice bearing TEM-1 positive tumors were performed. A multi-compartment pharmacokinetic model was used to fit the data and a global pharmacokinetic model was developed to illustrate the effect of liver capture and immunoreactivity loss. Organ absorbed doses in mice were calculated from biodistribution results. A loss of immunoreactivity was observed with the highest DOTA per 1C1m-Fc ratio. Except for the spleen and bone, an increase of DOTA per 1C1m-Fc ratio resulted in an increase of liver uptake and absorbed dose and a decrease of uptake in tumor and other tissues. Pharmacokinetic models correlated these results. The number of DOTA per antibody played a determining role in tumor targeting. One DOTA per 1C1m-Fc gave the best pharmacokinetic behavior for a future translation of [¹⁷⁷Lu]Lu-1C1m-Fc in patients.

Keywords: TEM-1; fusion protein antibody; DOTA conjugation; ¹⁷⁷Lu radiolabeling; biodistribution; tumor/liver ratio; theranostic

1. Introduction

Radiolabeled monoclonal antibodies (mAbs) have been actively investigated for theranostic applications [1]. The radiolabeling of a mAb with a metallic radionuclide, generally involves the use of suitable bifunctional chelating agents (BFCAs) with high metal-chelate stability constants. BFCAs are designed to stably coordinate the radionuclide and to allow a covalent attachment to protein functional groups [2,3]. Most protocols used to conjugate

antibodies with BFCAs are not site-specific and result in a variable number of BFCAs per antibody, depending on experimental conditions and antibodies themselves. With non-site-specific processes, the average number of BFCA attached per antibody depends upon the molar ratios of antibody and BFCA used for the conjugation as well as on the reaction conditions employed for the conjugation [4].

Dodecane tetraacetic acid (DOTA) derivatives, which are hydrophilic macrocyclic ligands, have been used as the most popular BFCAs for the development of radio-lanthanide-labeled mAbs [5].

An increasing chelator-to-antibody ratio often allows to improve the specific activity of the radiolabeled compound. Nevertheless, the hydrophilicity/lipophilicity, the charges of the conjugate, and consequently the pharmacokinetics of the antibody can be modified by the conjugation of hydrophilic DOTA chelator [4].

Authors showed that an increasing number of DOTA per antibody resulted in a decrease of the non-specific liver uptake [6,7]. The provided explanation was the reduction of the isoelectric point (pI) correlated to the increase of the negative charge given by the DOTA chelator resulting in important repulsion between the lipid bilayer and the conjugate. However, the impact of the increasing number of negative charges on the biodistribution was unclear. On the opposite, some groups observed a rapid blood clearance, a decrease of the tumor uptake and an increase of the hepatic uptake with high number of chelators conjugated to an antibody [8,9]. The conjugation with a high number of DOTA can alter the immunological properties of the antibody due to the possibility of DOTA to bind the variable domains of the antibody, involved in antigen targeting [4]. Moreover, a high number of chelators per antibody could change the tumor targeting pharmacokinetic due to the uptake of the conjugate by the reticuloendothelial system in liver and spleen [1].

The biodistribution of radiolabeled conjugated antibody is determined by the chelator to antibody ratio but also by many different parameters of the radionuclide such as the size, the chelation geometry and the coordination number. It would be necessary to optimize the conjugate regarding these criteria [6,8].

In this study, 1C1m-Fc, a scFv-Fc fusion antibody constructs which bind to murine and human tumor endothelial marker 1 (TEM-1) was conjugated to p-SCN-Bn-DOTA chelator. After conjugation 1C1m-Fc was radiolabeled with ^{177}Lu . This radionuclide, which is a γ and β^- emitter allowing theranostic approach.

TEM-1, also named endosialin/CD248, is a 80.9 kDa type I cell surface transmembrane protein of the C-lectin receptor family [10–12] implicated in development, vascular cell adhesion and migration, neoangiogenesis, and tumor progression [13,14]. TEM-1 over expression correlates with a poor patient prognosis and a tumor aggressiveness [15,16].

Its high expression on the tumor vasculature of several solid human cancers, with limited expression in normal adult tissue, makes TEM-1 an ideal target for theranostic applications [17,18].

Our previous study showed that [^{177}Lu]Lu-1C1m-Fc could prove as a potentially useful and safe tool for theranostic applications [19]. In these experiments, while the TEM-1 positive uptake was specific, we also observed an important liver uptake that was not saturation-dependent. Our hypothesis for this phenomenon was the influence of the number of DOTA on the biodistribution.

The conjugation of antibodies and antibody fragments with chelator plays a significant role in determining the success of tumor targeting employing radiolabeled antibodies [4,8]. Therefore, the goal of this study was to evaluate the effect of coupling an increasing number of DOTA per 1C1m-Fc on the pharmacokinetic behavior, immunoreactivity, and dosimetry of the radiolabeled antibody complex to develop an optimal radiolabeled 1C1m-Fc suitable for theranostic application.

2. Materials and Methods

2.1. Fusion Protein Antibody

Complete description of the single-chain variable fragment (scFv) 1C1m-Fc (Molecular Weight = 106196.8 Da) was done in Delage et al [19] and Fierle et al [20]. Briefly, this fusion protein antibody recognizes efficiently human and murine TEM-1 antigen over expressed in tumor cells and in SK-N-AS cell line that was chosen to develop the animal model.

2.2. Cell Lines

The human neuroblastoma SK-N-AS (TEM-1 positive) cell lines was purchased from American Type Culture Collection (ATCC, Manassas, VA, USA).

SK-N-AS cells were cultured in DMEM (Thermo Fisher Scientific, Waltham, MA, USA) supplemented with 0.1 mM Non-Essential Amino Acids (Thermo Fisher Scientific, Waltham, MA, USA), 10% fetal bovine serum (FBS, Thermo Fisher Scientific, Waltham, MA, USA) and 1% penicillin/streptomycin (Thermo Fisher Scientific, Waltham, MA, USA). Cells were incubated at 37 °C in a humidified atmosphere at 5% CO₂.

2.3. Conjugation

Antibody concentration was measured at 280 nm using a spectrophotometer (NanoDrop Lite, Thermo Fisher Scientific, Waltham, MA, USA). To obtain conjugates with increasing ligand-to-antibody ratios, 6 concentrations of p-SCN-Bn-DOTA (Macrocyclics, Plano, TX, USA; MW: 551.6) from 5 to 50 equivalents were used.

Prior to the coupling procedure, the 1C1m-Fc was conditioned in carbonate buffer 0.2 M pH 9.0 by ultrafiltration on a 50 kDa ultrafiltration membrane (Amicon Ultra, 0.5 mL, 50 kDa, Merck, Darmstadt, Germany). To 1 mg (9.4 nmol; 200 µL) of 1C1m-Fc was added a calculated quantity of a 25.9 mg/mL (47 µmol/mL) p-SCN-Bn-DOTA solution in an extemporaneously made mixture of 10% DMSO (*v/v*) in the same carbonate buffer. The BFCa-to-1C1m-Fc ratios used were 5, 10, 20, 30, 40, and 50.

Antibody coupling solutions were incubated for 1 h at 37 °C and the conjugated antibodies were washed by four ultrafiltrations using PBS pH 7.4 before performing high-pressure liquid chromatography (HPLC) to assess integrity of the conjugates. Conjugated fusion protein antibodies were subsequently stored between 2 and 8 °C.

2.4. Mass Spectrometry Analysis

Mass spectrometry (MS) analysis was performed using a Q Exactive HF Orbitrap (Thermo Fisher Scientific, Waltham, MA, USA) and separation was done using a MAbPAC SEC-1 column, (Thermo Fisher Scientific, Waltham, MA, USA) with a mobile phase of ammonium acetate 50 mM pH 7.0 at 0.3 mL/min as previously described [19]. After deconvolution of the mass spectrometry spectra, the drug-to-antibody ratio (DAR) is calculated using the formula:

$$\frac{\sum(n \cdot \text{Int})}{\sum(\text{Int})}$$

where *n* = number of attached molecules for this peak and Int = intensity of the peak.

2.5. Radiolabeling

The radiolabeling was optimized in acetate buffer 0.4 M pH 5.6 with respectively 500 pmol of DOTA-conjugated 1C1m-Fc and 20 MBq of ¹⁷⁷Lu without carrier in aqueous 0.04 M HCl solution (EndoleucineBeta 40 GBq/mL, ITM, Garching bei München, Germany). After 1 h incubation time at 37 °C, the radiochemical purity was determined by instant thin layer chromatography (iTLC) in citrate buffer 0.1 M pH 5.0.

The release criterion was radiochemical purity over 95%.

If necessary, the excess of ¹⁷⁷Lu was removed with one to three ultrafiltrations on 50 kDa membrane (Amicon Ultra, 0.5 mL, 50 kDa, Merck, Darmstadt, Germany) in acetate buffer 0.4 M pH 5.6.

2.6. Purity and Stability

Chemical purity of 1C1m-Fc was tested using HPLC and gel electrophoresis as described in Delage et al. [19]. Stability of the fusion protein was evaluated at 3, 6, and 12 months after its production by HPLC only. Radiochemical purity after antibody radiolabelling was assessed by TLC on iTLC-SG at 24 and 48 h.

2.6.1. HPLC

As described in Delage et al. [19], HPLC analyses were done using an Ultimate 3000 SD System (Thermo Fisher Scientific, Waltham, MA, USA) and a GabiStar radiodetector (Elysia-Raytest GmBH, Straubenhard, Germany). A size exclusion chromatography was performed using phosphate buffer pH 6.8 as solvent and a 200 kDa size exclusion column (XBridge protein BEH, Waters, Baden-Dättwil, Switzerland). Each chromatography profile was analyzed at 280 nm.

2.6.2. iTLC

TLC on iTLC-SG (Agilent Technologies, Folsom, CA, USA) was performed in citrate buffer 0.1 M pH 5.0. Using these conditions, unbound ^{177}Lu is complexed by the solvent and migrates at retention factor (R_f) = 1 while charged [^{177}Lu]Lu-1C1m-Fc remains at R_f = 0.

2.7. In Vitro Characterization of Immunoreactivity

Immunoreactive fraction assessment was done as in Delage et al. [19]. Briefly, each coupled 1C1m-Fc-DOTA and native 1C1m-Fc were evaluated by Lindmo assay [21]. An increasing number of SK-N-AS cells ($0.25\text{--}8 \times 10^6$) were incubated with a fixed concentration of radiolabeled 1C1m-Fc ($0.07 \mu\text{g}/\text{mL}$; $0.659 \text{ pmol}/\text{mL}$). A fusion protein antibody excess of 100-fold concentration was used to evaluate the non-specific binding. The immunoreactive fraction was calculated by extrapolation to an infinite cells number by fitting the curve with a non-linear regression method (Graphpad Prism 8.0, 2018 GraphPad Software, San Diego, CA, USA).

2.8. In Vivo Characterization

2.8.1. Murine Xenograft Model

All animal experiments were performed in accordance with the Swiss legislation for the care and use of laboratory animals under the license VD-2993 (09/2018) delivered after approbation by the Veterinarian Office of the canton of Vaud and the ethics committee.

Female Balb/C nude mice (Charles River Laboratories, Wilmington, MA, USA) between 8 and 10 weeks were subcutaneously grafted with 3.00×10^6 SK-N-AS cells as described in Delage et al. [19]. Mice were assigned to the experimental groups when the tumor reached 5–10 mm diameter size.

2.8.2. Biodistribution Studies

To define the impact of the conjugation on the biodistribution, a mixture of $2.5 \mu\text{g}$ (23.5 pmol) of [^{177}Lu]Lu-1C1m-Fc conjugated with respectively 1, 2.5, 3, 6, 8, and 11 DOTA per 1C1m-Fc and $47.5 \mu\text{g}$ (447.3 pmol) of native unlabeled 1C1m-Fc was injected into the lateral tail vein of the mice ($n = 3$) without anesthesia. The volume for all the injections was $100 \mu\text{L}$ and sodium chloride 0.9% (B.Braun, Sempach, Switzerland) was used to perform the dilution. The injected solution was not filtered.

The average weight of animals was $18.4 \pm 1.8 \text{ g}$. The dose of $50 \mu\text{g}$ (470 pmol) of antibody has been selected from our previous study [19].

Mice were sacrificed by CO₂ inhalation 24 h after radiolabeled antibody injection. Blood was collected by exsanguination. Organs and tumors were weighted after drying and them and counted with a gamma counter (AMG Automatic Gamma Counter, Hidex, Turku, Finland).

For the [^{177}Lu]Lu-1C1m-Fc conjugated with 1 and 3 DOTA, complementary time points have been added for the biodistribution, and animals ($n = 3$) were euthanized 4, 24, 48, 72 h, and 6 days after injection.

Results were expressed as a percentage of injected activity (IA) per gram of tissue (%IA/g).

2.8.3. Pharmacokinetic Modeling

Data were expressed as percent injected activity per gram of tissues. A multi-compartment pharmacokinetic model was used in which the injected antibody was distributed from a central compartment, representing the blood, into peripheric compartments corresponding to all investigated organs plus an additional compartment representing all uncounted tissues. Tissue contents were calculated as the content of the tissue compartment plus a fraction of blood activity. This is equivalent to consider fast and a slow distribution compartments as in similar models [22] given that the fast kinetics cannot be accounted for from data collected over 6 days. The biodistribution kinetics for all studied tissues were modelled for the 1 and 3 DOTA per 1C1m-Fc using a software package developed in Arronax Laboratory available upon request (www.arronax-nantes.fr). This software package, similar to and validated by comparison with WinSAAM [23], allows pharmacokinetic modelling directly from a Microsoft Excel worksheet. Differential equations were solved numerically using the Chu–Berman algorithm [24]. Variable parameters were estimated using the non-linear weighted least squares Levenberg–Marquardt algorithm.

It was then assumed that the rate of liver uptake was proportional to the number of DOTA per antibody and that the rates of uptake into tumor and uterus (a normal tissue expressing low amounts of antigen) increased linearly with the immunoreactivity. Conversely, the rates of spleen and bone uptake were assumed to decrease linearly with the immunoreactivity. Then all available biodistribution data, at all time-points for 1 and 3 DOTA per 1C1m-Fc, and at 24 h after injection for the other conjugates were fitted simultaneously using a single set of kinetic parameters. The model is described in Appendix A (Figures A1–A3 and Table A1.).

2.8.4. Murine Dosimetry

Estimated absorbed doses to organs were based on the biodistribution results of mice bearing TEM-1 positive tumor injected with [^{177}Lu]Lu-1C1m-Fc conjugated with 1 DOTA. Considered source organs were liver, kidneys, lungs, spleen, heart (cardiac muscle), blood pool, stomach, small intestine, colon, ovaries, uterus, urinary bladder, salivary glands, and the total body. The remainder was obtained by subtraction of the signal measured in source organs from the total body. For each mouse at each time point, the activity in each source organ and the remainder was normalized by the total injected activity to obtain the normalized injected activity (nA). For each source organ at each time point, an average nA value was obtained \pm SD.

For all source organs with the exception of stomach, uterus, salivary glands and the urinary bladder, the normalized time activity curves (nTACs) were fitted with bi-exponential functions using the kinetic module of OLINDA/EXM 2.1 (HERMES Medical Solution AB, Stockholm, Sweden). Time-integrated activity coefficients (TIACs) were derived by analytical time-integration of fitted source organ nTACs obtained with the average nA, nA + SD and the nA – SD values, respectively.

The nTACs for stomach, uterus, salivary glands, urinary bladder and the tumor were not conveniently fitted by monotonically decreasing bi-exponential functions. For these tissues, the TIAC was obtained by trapezoidal integration using Matlab software (Release 2019b, The MathWorks, Inc., Natick, MA, USA), between $t = 0$ and $t = 6$ days, whereas a mono-exponential analytical integration to infinity was calculated after the last measure ($t > 6$ days) considering the ^{177}Lu physical decay constant.

Finally, source organ TIACs were entered into the OLINDA/EXM[®] 2.1 software kinetic module for organ absorbed dose estimates considering the 25 g murine model where the

phantom source organ masses were adjusted to the average organ masses obtained from the mice population considered for the dosimetry experiment. In this process, the TIAC of the ovaries, uterus and the salivary glands was part of the remainder of the body.

A specific absorbed dose estimation was obtained for ovaries, uterus and the salivary glands. These organs, in fact, exhibit an important specific tracer uptake, but were not among the source/target organs available in the murine model of OLINDA/EXM 2.1 software. For these organs, the absorbed dose estimation was obtained using the sphere model of OLINDA/EXM 2.1 where the average organ TIAC and the average organ mass were applied.

Estimated absorbed doses to tumor and selected organs based on the biodistribution results on TEM-1 positive tumor bearing mice injected with [¹⁷⁷Lu]Lu-1C1m-Fc conjugated respectively with 1 and 3 DOTA were compared. The dosimetry with the 3 DOTA conjugation was obtained from our previous study [19]. The selected organs were the liver, the lungs, the kidney, the spleen and the uterus.

2.9. Statistics

The data are expressed as mean ± SD (standard deviation) or SEM (standard error to the mean). Significant differences between immunoreactive fractions were analyzed by ordinary one-way Anova using the Turkey's multiple comparisons method. Data from biodistribution studies were analyzed by an unpaired, 2-tailed Student t test with a correction for multiple comparison using the Holm–Sidak method ($\alpha = 0.05$). Correlation between the tumor/liver ratio and the ratio of DOTA per 1Cm-Fc were analyzed with a Spearman test. Curve-fitting and statistical analyses were conducted using Prism 8.0 (GraphPad Software, San Diego, CA, USA). Pharmacokinetics analyses were performed with Kinetics software.

3. Results

3.1. Conjugation and Radiolabeling

1C1m-Fc was conjugated with six concentrations of DOTA between 5 and 50 equivalents. The number of DOTA was estimated for each concentration (Table 1, Figure S1) and was between 1 and 11 DOTA.

Table 1. Estimated number of DOTA per 1C1m-Fc based on mass spectrometry and purity analyses of the conjugates from 5 to 50 equivalents (eq) of DOTA. The estimated DAR is calculated using the formula: $\Sigma(n \cdot \text{Int}) / \Sigma(\text{Int})$, where n = number of attached molecules for this peak, Int = intensity of the peak.

Compound	Mass Weight (Da)	Estimated Number of DOTA per 1C1m-Fc	% Purity (HPLC)
Unmodified 1C1m-Fc	108,394	NA (not applicable)	97.4%
DOTA (- HCl-H ₂ O)	551	NA	NA
1C1m-Fc 5 eq DOTA	108,395–108,985	1	95.6%
1C1m-Fc 10 eq DOTA	108,986–110,758	2.5	96.2%
1C1m-Fc 20 eq DOTA	109,496–111,746	3	95.7%
1C1m-Fc 30 eq DOTA	110,755–113,117	6	96.9%
1C1m-Fc 40 eq DOTA	111,746–114,664	8.5	96.2%
1C1m-Fc 50 eq DOTA	113,711–116,068	11	96.8%

1C1m-Fc and its conjugates were analyzed by HPLC. The purity of conjugated antibodies is reported in Table 1. The HPLC profiles, the stability of the native and conjugated fusion protein antibody, and the stability in serum of [¹⁷⁷Lu]Lu-1C1m-Fc were given in our prior publication [19].

The release criteria for the radiochemical purity (RCP) evaluated by TLC was more than 95%. To reach this criterion with antibodies modified with 1 and 2.5 DOTA, ultrafiltration on amicon membrane (Amicon Ultra, 0.5 mL, 50 kDa, Merck, Darmstadt, Germany) was used. HPLC was not used in this study to evaluate the RCP as this test was done in our previous study [19] and the results were similar to that obtained using TLC.

3.2. Immunoreactive Fraction

The immunoreactivity following the radiolabeling was assessed by Lindmo assay (Table 2; Figure S2).

Table 2. Radioimmunoreactive fraction results for [¹⁷⁷Lu]Lu-1C1m-Fc conjugated with 1 to 11 DOTA.

Number of DOTA per 1C1m-Fc	Immunoreactivity (%) ± SEM
1	85.1 ± 1.3
3	86.2 ± 2.7
6	87.5 ± 1.0
8.5	78 ± 1.4
11	24 ± 1.7

For validation tests comparative immunoreactivity assessment with incubation at 37 °C and 4 °C were carried out and the results obtained showed no difference at 3 h. Furthermore, internalization results of 1C1m-Fc radiolabeled with ¹²⁵I have been published and showed that the rate of internalization was quite slow suggesting that the antibody does not trigger the rapid migration of TEM-1 from the cell surface [25]. The immunoreactivity, that was 85.1 ± 1.3, 86.2 ± 2.7, 87.5 ± 1.0, and 78 ± 1.4% for 1, 3, 6, and 8.5 DOTA, respectively suggesting that it was not affected by the conjugation up to 8.5 DOTA (Turkey's multiple comparisons test, $p > 0.068$, $n = 17$).

On the other hand, a significative loss of immunoreactivity to 24 ± 1.7% was obtained with the highest number of BFCA (11 DOTA per fusion protein antibody) compared to the others ratios (Turkey's multiple comparisons test, $p < 0.0001$, $n = 17$).

3.3. In Vivo Characterization

3.3.1. Biodistribution Study at 24 h

The biodistribution of [¹⁷⁷Lu]Lu-1C1m-Fc conjugated with 1, 2.5, 3, 6, 8, and 11 DOTA units respectively was performed 24 h after injection.

A decrease of tumor uptake was observed with the 1C1m-Fc conjugated with more than 3 DOTA (18.8 ± 1.5% IA/g up to 3 DOTA to 5.3 ± 1.6% IA/g for 11 DOTA). In parallel, an accelerated blood clearance was observed with the increasing number of chelator and the radiotracer circulating in the blood at 24 h varied from 10.2 ± 0.6% for 1 DOTA per antibody to 2.2 ± 0.7% for 11 DOTA per antibody (Figure 1a).

An inverse correlation of the tumor/liver ratio was observed with the increasing number of DOTA per antibody, from 2 with 1 DOTA per antibody to 0.15 with 11 DOTA per antibody (Spearman test, $\rho = -0.99$, $p < 0.0001$) (Figure 1b).

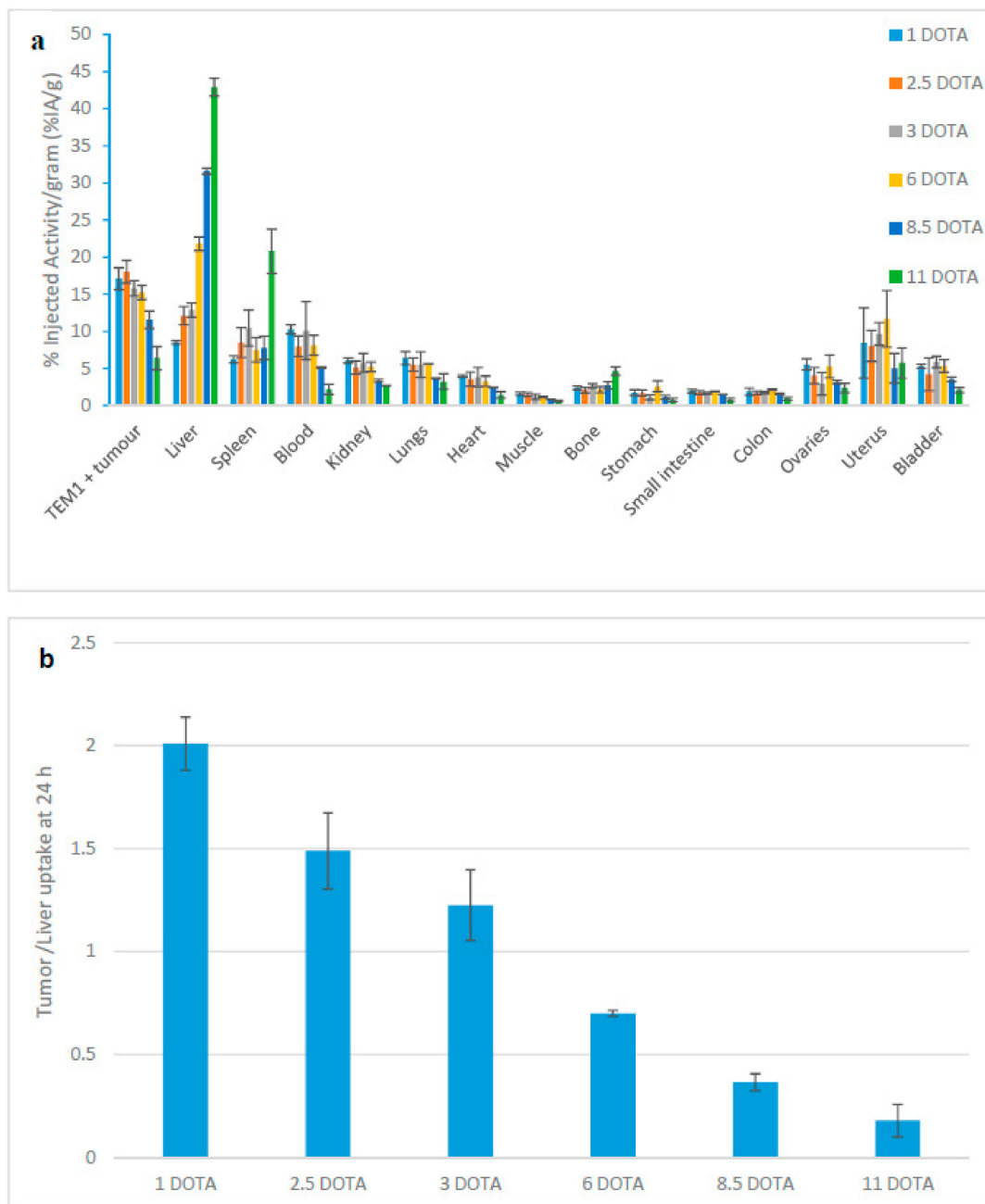


Figure 1. (a) Biodistribution at 24 h of $[^{177}\text{Lu}]\text{Lu-1C1m-Fc}$ conjugated with 1 to 11 DOTA in Balb/c nu mice bearing TEM-1 positive tumor. Data are shown as mean \pm SD. (b) Ratio between the tumor and the liver uptake at 24 h with respect to the number of DOTA per $[^{177}\text{Lu}]\text{Lu-1C1m-Fc}$ in Balb/c mice bearing TEM-1 positive tumor. Spearman test gives a rho = -0.99 , $p < 0.0001$.

3.3.2. Complementary Analyses for 1C1m-(DOTA)_1 and 1C1m-(DOTA)_3

For the $[^{177}\text{Lu}]\text{Lu-1C1m-Fc}$ conjugated with 1 and 3 DOTA, complementary time points have been added for the biodistribution and animals were euthanized at 4, 24, 48, 72 h, and six days after injection.

The uptake in TEM-1 positive tumors was unchanged between the two groups. However, in the case of $[^{177}\text{Lu}]\text{Lu-1C1m-Fc}$ conjugated with 1 DOTA, the non-specific uptake in the liver was lower than that observed with 3 DOTA conjugated at 24 and 48 h, where $p = 0.02$ and 0.01 (unpaired t-test, $n = 3$) respectively (Figure 2a,b).

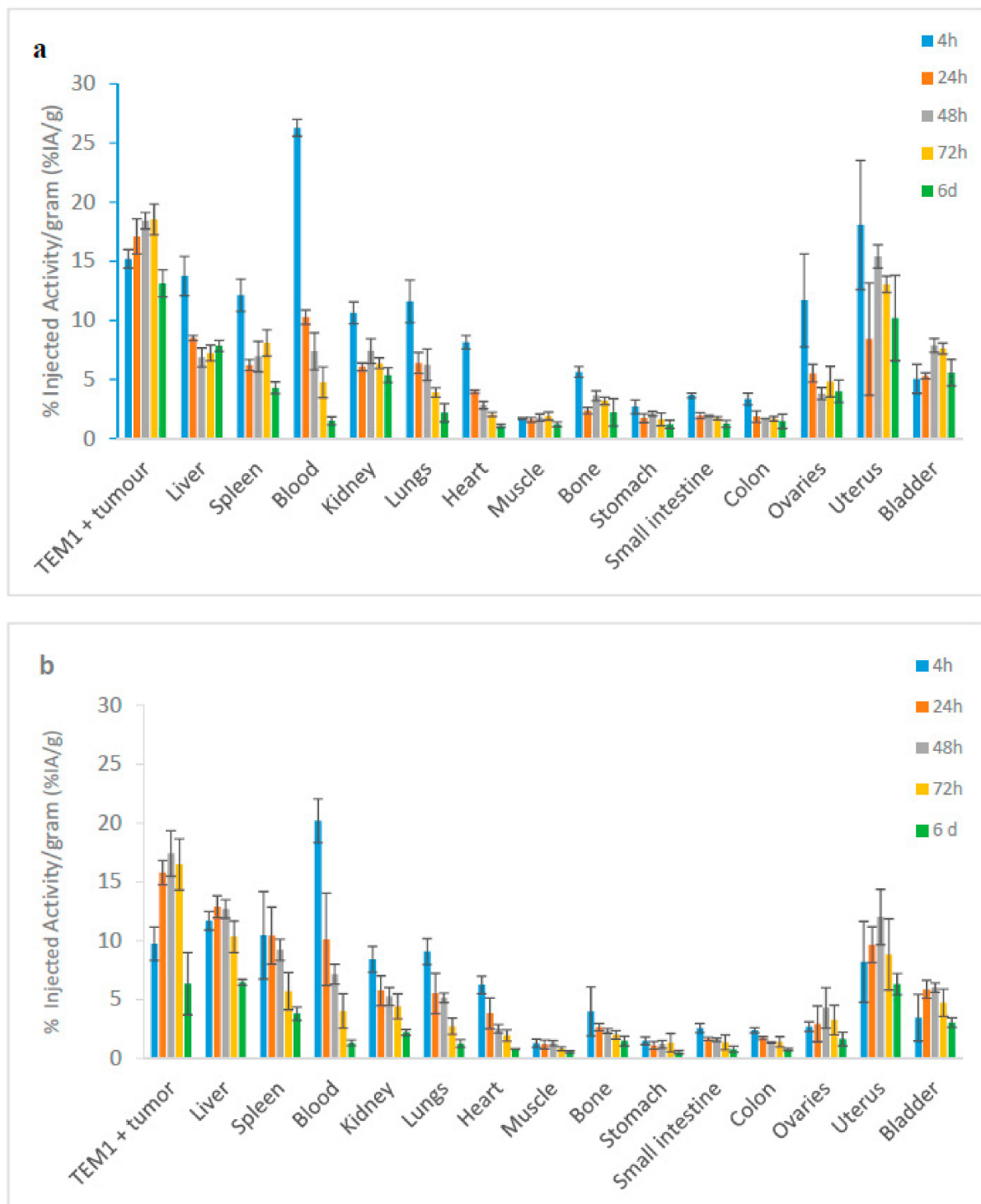


Figure 2. Biodistribution of $[^{177}\text{Lu}]\text{Lu-1C1m-Fc}$ in Balb/c nu mice bearing TEM-1 positive tumor, (a) conjugated with 1 DOTA; (b) conjugated with 3 DOTA. Data are shown as mean \pm SD, ($n = 3$).

3.3.3. Pharmacokinetic Modeling

Kinetics with 1C1m-Fc conjugated respectively with 1 and 3 DOTA were satisfactorily fitted by the model (Figure S3a,b).

Tissues showing highest uptake were the tumor and the uterus and, for 1C1m-Fc conjugated with 3 DOTA, the liver. For the liver, the estimated uptake rate constants of the 1C1m-Fc conjugated with 3 DOTA was 3.5 times that of the 1 DOTA, in line with the higher uptake. The wash-out rate was relatively fast for the 3 DOTA, but, because of a single

high value at six days, was fitted to 0 for the 1 DOTA, preventing further comparison. The differences in estimated rate constants and tissue blood contents for the other tissues were hard to interpret because of relatively high SD on measurements, particularly for uterus and bone.

As expected, the simultaneous fit (Figure S4) represented less closely the biodistribution data, but the general shape and trends were conserved.

More interestingly, the trends in 24 h biodistributions for the six different concentrations of DOTA were well replicated (Figure 3).

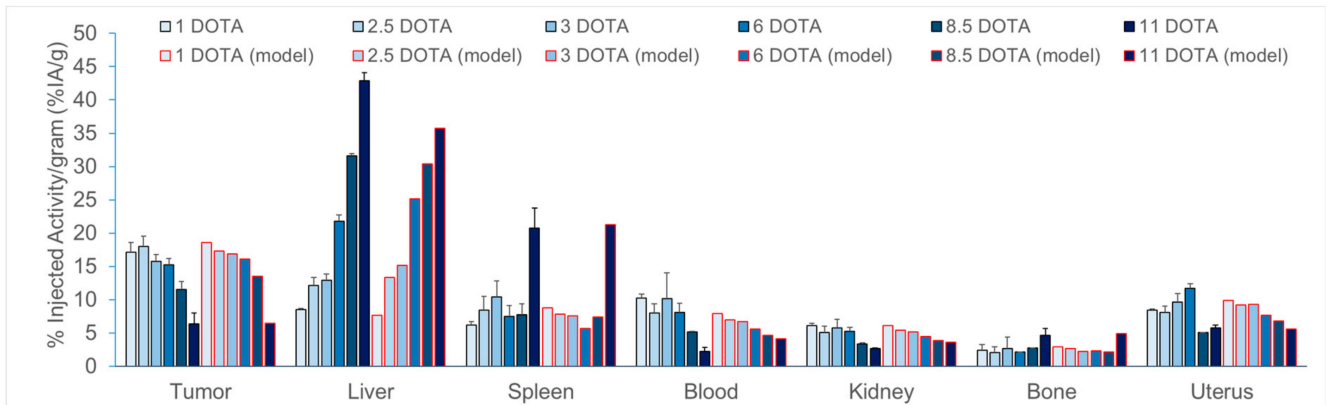


Figure 3. Comparison between the results obtained by biodistribution (in grey) and pharmacokinetic modeling (in red) at 24 h for $[^{177}\text{Lu}]\text{Lu-1C1m-Fc}$ conjugated with 1 to 11 DOTA in Balb/c nu mice bearing TEM-1 positive tumor.

The increased liver uptake at higher numbers of DOTA effectively decreases the amount of circulating $[^{177}\text{Lu}]\text{Lu-1C1m-Fc}$ and consequently the amount of $[^{177}\text{Lu}]\text{Lu-1C1m-Fc}$ in most of other organs. The loss of immunoreactivity explains the decrease of the TEM-1 specific uptake in the tumor and the uterus, especially at the two highest DOTA per antibody ratios. Finally, the increase of the spleen and bone uptake at the highest concentrations of DOTA was accounted by a higher uptake of non-immunoreactive $[^{177}\text{Lu}]\text{Lu-1C1m-Fc}$. This condition was simulated by a linear decrease of the spleen uptake rate with immunoreactivity.

3.3.4. Murine Dosimetry

Extrapolated organ absorbed doses for mice derived from the injection of $[^{177}\text{Lu}]\text{Lu-1C1m-Fc}$ conjugated with 1 DOTA are given in Table 3. The organs receiving the highest absorbed dose was the uterus (1.83 ± 0.14 Gy/MBq), followed by the liver (1.79 ± 0.13 Gy/MBq), the stomach wall (1.66 ± 0.08 Gy/MBq) and the kidneys (1.32 ± 0.05 Gy/MBq). The total body dose was 0.55 ± 0.04 Gy/MBq and the tumor dose was 2.53 ± 0.25 Gy/MBq. The tumor-to-liver absorbed dose ratio was 1.41.

The absorbed doses for tumor, liver, kidneys, lungs, uterus and bladder were compared between $[^{177}\text{Lu}]\text{Lu-1C1m-Fc}$ conjugated respectively with 1 DOTA and 3 DOTA (Table 4).

Table 3. Considered organ masses, estimated source organ TIAC and organ absorbed doses [^{177}Lu]Lu-1C1m-Fc. Organ masses of the 25g mouse model of Olinda/EXM 2.1 were used for: brain, thyroid, testes, skeleton, pancreas and the heart content, for all other organs we used the experimental mean masses.

Organ	Mean Organ Mass (g)	TIAC (MBq·h/MBq)		Abs. Dose (mGy/MBq)	
		Mean	SD	Mean	SD
Brain ^t	0.50	-	-	4.08×10^2	2.70×10^1
Large intestine ^{s,t}	0.78	1.98	0.33	7.03×10^2	8.10×10^1
Small intestine ^{s,t}	1.20	3.33	0.25	5.77×10^2	4.00×10^1
Stomach ^{s,t}	0.26	0.77	0.03	1.66×10^3	8.00×10^1
Heart ^t	0.11	0.48	0.06	1.10×10^3	1.50×10^2
Heart content ^s	0.2	1.84	0.35		
Kidneys ^{s,t}	0.31	3.37	0.13	1.32×10^3	5.00×10^1
Liver ^{s,t}	1.13	21.49	1.72	1.79×10^3	1.30×10^2
Lungs ^{s,t}	0.15	1.03	0.31	9.83×10^2	2.07×10^2
Pancreas ^t	0.30			4.41×10^2	2.80×10^1
Skeleton ^t	2.20			4.18×10^2	2.80×10^1
Spleen ^{s,t}	0.10	1.06	0.03	1.18×10^3	1.00×10^2
Ovaries ^{s,*}	0.04	0.41	0.08	7.42×10^2	9.90×10^1
Uterus ^{s,*}	0.11	2.54	0.24	1.83×10^3	1.40×10^2
Testes ^t	0.16			4.09×10^2	2.60×10^1
Thyroid ^t	0.01			4.09×10^2	2.70×10^1
Salivary glands ^{s,*}	0.11	0.75	0.02	5.41×10^2	1.70×10^1
Urinary Bladder ^{s,t}	0.02	0.17	0.01	5.34×10^2	3.70×10^1
Total Body ^{s,t}	18.44	111.08	6.54	5.49×10^2	3.80×10^1
Tumor ^{s,*}	0.21	6.81	0.71	2.53×10^3	2.50×10^2

(^s) Source organs with experimentally derived TIAC; in walled organs, the TIAC included the content. (^t) Target organs available for the 25g mouse model in OLINDA/EXM 2.1 from which mean absorbed dose was obtained; in walled organs, the absorbed dose is computed for the wall. (^{*}) Absorbed dose computed with the sphere model of OLINDA/EXM 2.1. The organ %IA/g decay corrected and the normalized time-activity curves for the considered source organs are presented in the Supplementary Materials (respectively Figures S5 and S6).

Table 4. Mouse dosimetry comparison between [^{177}Lu]Lu-1C1m-Fc conjugated with 1 or 3 DOTA. The selected organ of interested are the TEM-1 positive tumor, the liver, the kidneys, the lungs, the spleen and the uterus.

Source Organ	Absorbed Dose (mGy/MBq)	
	1 DOTA	3 DOTA
Tumor SK-N-AS	$2.53 \times 10^3 \pm 2.50 \times 10^2$	$1.82 \times 10^3 \pm 3.23 \times 10^2$
Liver	$1.79 \times 10^3 \pm 1.30 \times 10^2$	$2.23 \times 10^3 \pm 3.99 \times 10^2$
Kidneys	$1.32 \times 10^3 \pm 5.00 \times 10^1$	$7.05 \times 10^2 \pm 6.03 \times 10^1$
Lungs	$9.83 \times 10^2 \pm 2.07 \times 10^2$	$5.39 \times 10^2 \pm 1.30 \times 10^2$
Spleen	$1.18 \times 10^3 \pm 1.00 \times 10^2$	$1.20 \times 10^3 \pm 7.51 \times 10^1$
Uterus	$1.83 \times 10^3 \pm 1.40 \times 10^2$	$1.50 \times 10^3 \pm 5.15 \times 10^2$
Tumor/Liver ratio	1.4	0.8

The tumor/liver absorbed dose ratio increased from 0.8 for the [^{177}Lu]Lu-1C1m-Fc conjugated to 3 DOTA to 1.4 for the [^{177}Lu]Lu-1C1m-Fc conjugated to 1 DOTA. The non-specific uptake in the kidneys, the lungs and the specific uterus uptake was higher with the fusion protein conjugated with 1 DOTA.

4. Discussion

Because of its expression across many tumors, its low expression in normal tissues and accessibility from the vascular circulation, TEM-1 is emerging as an interesting biomarker for theranostics [26]. Several IgG antibodies targeting the lectin-like domain of TEM-1 have already been developed for oncological application [13,26].

Given the very short half-life and the relative *in vivo* instability of monovalent scFv antibody fragments, a bivalent Fc-fusion protein based on a novel single chain antibody, 1C1m-Fc, has been synthesized. The fusion of scFvs to the IgG Fc constant domains adds significant size, avidity and stability to the targeting moiety and would be expected to lead to improved blood pharmacokinetics.

Our previous study showed the relevance of this novel fusion protein antibody radiolabeled with ^{177}Lu for a theranostic approach [19]. The aim of the present work was to study the effect of the DOTA conjugation on the immunoreactivity, the pharmacokinetics and the dosimetry of [^{177}Lu]Lu-1C1m-Fc.

Six different conjugates were obtained by incubating 1C1m-Fc with several molar ratio of DOTA respectively: 5, 10, 20, 30, 40, and 50 equivalents of DOTA. All the conjugates were analyzed by mass spectrometry and the number of DOTA moieties attached per 1C1m-Fc were respectively 1, 2.5, 3, 6, 8.5, and 11. Even if the HPLC profile of these conjugates was similar, they are expected to have different pharmacokinetics behavior.

Radiolabeling was performed with ^{177}Lu to obtain formulation with a RCP of more than 95%. The immunoreactivity following the radiolabeling was assessed by Lindmo assay. The immunoreactivity was not affected by the conjugation up to 8.5 DOTA. Nevertheless, a significant loss of the immunoreactivity was observed with 11 DOTA (IR = 24%). Several studies indicated that immunoreactivities of radiolabeled antibody were getting compromised with the increase in the number of BFCA attached per antibody moieties. Indeed, conjugation of the variable chain can weaken or abrogate antigen binding which in turn decreases the efficacy of the targeting of the immunoconjugate [27,28]. Wangler et al. demonstrated that the size of the conjugated dendritic structure does not significantly influence the immunoreactivity of the antibodies over a wide molecular weight range, whereas the number of derivatization sites is the major factor that determines the binding affinity of the conjugates [29]. Grunberg et al. and Fischer et al. [28,30] showed that an enzymatic conjugation leads to immunoconjugates with a uniform and well-defined substitution only on the heavy chain. With this technique increasing numbers of DOTA moieties was accompanied by an increasing specific activity of the immunoconjugates when labeled with ^{177}Lu . The advantage of the high specific activity was not counteracted by the simultaneous decrease of immunoreactivity. A site-specific enzymatic conjugation to the constant region could be better by less altered radio-immunoreactivity [31].

A biodistribution study of [^{177}Lu]Lu-1C1m-Fc conjugated with all the DOTA conjugates was performed. A significant decrease of the tumor uptake was observed 24 h after injection with the 1C1m-Fc conjugated with more than 3 DOTA. This time point has been chosen as we have seen in our previous study that it was the most informative one [19]. This behavior could be attributed to the increased hydrophilicity of [^{177}Lu]Lu-1C1m-Fc with the number of DOTA attached to the molecule. Indeed, highest number of hydrophilic DOTA or chelator has been described to exhibit a rapid blood clearance resulted in an increasing uptake in the liver [4,8,32,33], but the mechanism was unclear. Knogler et al. proposed that it can be due to the conformational change of the backbone structure of the antibody induced by over-coupling, resulting in a rapid sequestration by the reticuloendothelial system in the liver but invalidated this hypothesis as no difference was found in CD spectra between substituted and unsubstituted antibody [1,8].

On the other hand, it has been suggested that the negative charge conferred to the antibody by DOTA conjugation results in a reduced isoelectric point (pI), causing a net repulsion between the molecule and the phospholipid bilayer, reducing the hepatobiliary excretion or the hepatic uptake [6,7]. Several publications indicate that a decrease of the liver uptake could be observed with negatively charged peptides or antibodies derivatives compared to neutral or positively charged conjugated variants [9,34–36]. General approach described to improve imaging contrast in the liver include increasing the hydrophilicity via a hydrophilic chelator or linker, modifying the positioning and composition of potential purification tags or increasing negative charge [34–36]. These observations differ to the results of our experiment. However, it is relevant to note that, in these publications,

different types of chelates grafted on same vector were compared but with the same chelate-to-vector ratio. The impact of the different chelators on biodistribution and imaging contrast was assessed. On the contrary, we have studied the effect of a same chelate, DOTA, with various antibody-to-ligands ratios. This difference in the methodology could explain the different results.

Complementary analysis has been added for 1 and 3 DOTA to ensure the consistency of the model. The biodistribution of the radiolabeled antibody was well described using a multi-compartment model that showed a clear increase in the liver uptake rate between 1 and 3 DOTA per antibody. To further rationalize this effect, all available data were fitted simultaneously using the same compartment model, assuming linear relationships between the liver uptake rate constant and the number of DOTA and between the tumor and uterus uptake rate constants and the immunoreactivity. Finally, uptake in the spleen and the bone was assumed to increase with the loss of immunoreactivity. Linear relationships were selected as first order approximations. This model was consistent with the observed data: increased liver uptake at higher DOTA-substitution ratios depletes the circulating antibody and the amount of antibody found in all tissues. In addition, the loss of immunoreactivity further decreases the specific absorption into the tumor and uterus. Assuming a faster uptake of non-immunoreactive antibody in spleen and bone accounts for the high uptake seen with the 11-DOTA antibody. While a model cannot be considered a proof, this one shows that simple hypotheses may explain the observations made in biodistribution experiments.

We decided to evaluate the extrapolated organ absorbed doses for mice derived from the injection of [^{177}Lu]Lu-1C1m-Fc conjugated with the two lowest concentrations of DOTA, namely 1 and 3 DOTA per fusion protein antibody as they gave the best specific/non-specific uptake ratio in the biodistribution study. Organ receiving the highest doses were liver and uterus. Two other anti TEM-1 antibodies, 78Fc labeled with ^{111}In and Morab-004 labeled with ^{124}I showed similar results in these organs [26,37].

The tumor/liver absorbed dose ratio increased from 0.8 for the [^{177}Lu]Lu-1C1m-Fc conjugated to 3 DOTA to 1.4 for the [^{177}Lu]Lu-1C1m-Fc conjugated to 1 DOTA. The absorbed dose ratio tumor/liver was multiplied by 1.75 with the [^{177}Lu]Lu-1C1m-Fc conjugated to 1 DOTA compared to 3 DOTA.

Even if the theoretical and experimental specific activity for 3 DOTA is higher than for 1 DOTA (experimentally 400 MBq/mg vs. 200 MBq/mg; data not shown), this difference has not been taken into account in this study considering its small influence in therapeutic applications. Indeed, regarding the professional practices in radioimmunotherapy the amount of antibody usually injected in human is comprised between 1 and 1.5 mg/kg. If we consider the lowest specific activity obtained with 1 DOTA, the quantity of antibody injected will be sufficient to reach more than 8 GBq for all patients of more than 45 kg weight. Therefore, 1C1m-Fc appeared as a very promising compound for a theranostic approach.

5. Conclusions

Antibody labeling with metal radionuclides requires the use of a bifunctional chelator to attach radioactive metal to the protein, ideally without affecting the pharmacokinetics of the antibody [34]. In our experiments, we have demonstrated that the number of chelators per fusion protein antibody plays a significant role in determining successful tumor targeting. There is thus an opportunity to further improve the biodistribution and imaging contrast. Both absolute tumor uptake and target-to-non target ratios are important for the selection of the best imaging agent [35]. In this study, [^{177}Lu]Lu-1C1m-Fc conjugated with 1 DOTA was to be the best ratio to maintain a balance between the specific activity, immunoreactivity, and pharmacokinetic behavior and appears as an interesting candidate for further theranostic development.

6. Patents

J.K.F, S.M.D. and G.C. hold patents in the domain of antibodies and in particular on the 1C1m antibody used in this study.

Supplementary Materials: The following are available online at <https://www.mdpi.com/1999-4923/13/1/96/s1>, Figure S1: Mass spectra of 1C1m-Fc conjugated with 1; 2.5; 3; 6 and 11 DOTA; Figure S2: [¹⁷⁷Lu]Lu-1C1m-Fc immunoreactivity (IR) test on SK-N-AS cell line. The IR was not affected by the conjugation until 8.5 DOTA. A loss of immunoreactivity was observed with the highest number of DOTA; Figure S3: Pharmacokinetic modeling of [¹⁷⁷Lu]Lu-1C1m-Fc in Balb/c nu mice bearing TEM-1 positive tumor. (a) conjugated with 1 DOTA; (b) conjugated with 3 DOTA. Error bars = SD; Figure S4: Simultaneous fit modeling of [¹⁷⁷Lu]Lu-1C1m-Fc in Balb/c nu mice bearing TEM-1 positive tumor obtained with the pharmacokinetic model, (a1 to a4) conjugated with 1 DOTA; (b1 to b4) 1C1m-Fc conjugated with 3 DOTA. Error bars = SD; Figure S5: Organ %IA/g decay corrected at injection time; Figure S6: Normalized time-activity curves for the considered source organs. Red lines represent bi-exponential fitting curves obtained for source organs with exclusion of the tumor, stomach, urinary bladder, uterus and the salivary glands. The coefficient of determination (R²) of the fit in respect to experimental data is also reported when applicable.

Author Contributions: Methodology, J.A.D., A.F.-C., and J.B.; software, J.B.; data curation, J.A.D.; writing—original draft preparation, J.A.D., A.F.-C., J.B., S.G., D.V., and J.O.P.; writing—review and editing J.K.F., N.S., G.C., and S.M.D.; supervision A.F.-C. and J.O.P.; project administration, J.A.D.; funding acquisition N.S., J.O.P., and G.C. All authors have read and agreed to the published version of the manuscript.

Funding: This research was funded with the help of the Alfred and Annemarie von Sick Grant (Zurich, Switzerland) and the Department of Nuclear Medicine and Molecular Imaging, Lausanne University Hospital (Lausanne, Switzerland).

Informed Consent Statement: Not applicable.

Data Availability Statement: The data presented in this study are available in article or Supplementary Materials here.

Acknowledgments: The software for the pharmacokinetics studies has been provided by provided ARRONAX GIP. We acknowledge support from ARRONAX GIP for Open Access to this software through the Labex IRON no. ANR-11-LABX-0018-01 and Equipex Arronax plus no. ANR-11-EQPX-0004.

Conflicts of Interest: G.C. has received grants, research support or is coinvestigator in clinical trials by BMS, Celgene, Boehringer Ingelheim, Roche, Iovance and Kite. G.C. has received honoraria for consultations or presentations by Roche, Genentech, BMS, AstraZeneca, Sanofi-Aventis, Nextcure and GeneosTx. G.C. has patents in the domain of antibodies and vaccines targeting the tumor vasculature as well as technologies related to T cell expansion and engineering for T cell therapy. G.C. holds patents around TEM1 antibodies and receives royalties from the University of Pennsylvania regarding technology licensed to Novartis. All other authors declare that they have no conflict of interest.

Appendix A

Model Description

The “Kinetics” software (www.aronax-nantes.fr) allows a full description of the model and data within a single Microsoft excel worksheet. Formulas are entered in worksheet cells in a nearly natural mathematical language. The model involves 16 compartments (F1 to F16) representing blood, all measured tissues and an additional compartment (F2) for the rest of the mouse body (carcass). Tissue weights (W_i), antibody immunoreactivity (IR) and number of DOTA per antibody (DOTA) are fixed parameters. In the simultaneous fit of all data, the different preparations are represented in different “Time interrupts”, a feature, present in WinSAAM and used in the “Kinetics” software package, that allows the fixed parameters to be changed.

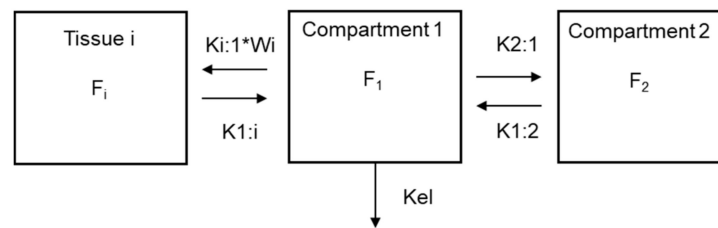


Figure A1. Multiple compartment mathematical model.

Transfers are assumed linear and defined in a matrix form as $K_{i:1} * W_i * F_1$ ($K_{i:1}$ an adjustable rate constant and W_i the weight of tissue i) for the transfer from blood to tissue i and $K_{1:i} * F_i$ for the transfer back to blood (for compartment 2, the weight is unknown and omitted). Elimination is set from the blood compartment (K_{el}). Total blood volume cannot be identified from data because the earlier time point is 4 h. It is set to 2.2 mL (WTB). Two additional fixed parameters are DOTA, the number of DOTA per antibody, and IR, the immunoreactivity of the preparations. Then the effect of DOTA is described by setting the transfer rate from blood to liver as: $K_{5:1} * DOTA * W_{Li} * F_1$ and the effect of immunoreactivity as $(K_{3:1} + A_{TIR} * IR) * W_{Tu} * F_1$ and $(K_{15:1} + A_{UIR} * IR) * W_{Ut} * F_1$ for tumor and uterus uptake respectively (increase in uptake rate for higher immunoreactivity) and as $(K_{6:1} - A_{SIR} * IR) * W_{Sp} * F_1$ and $(K_{10:1} - A_{BIR} * IR) * W_{Bo} * F_1$ for spleen and bone (increase in uptake rate for lower immunoreactivity).

Since the tissue contents is given as % of injected activity per g (%IA/g) and each measured tissue is represented by the content of a compartment plus an adjustable fraction (BTu to BBl) of blood (F_1). The injected activity is set to 100 and the tissue contents are normalized by the tissue weights (W_{Tu} to W_{Bl}).

The calculations (simulations and parameter adjustment) are triggered by the user from the Excel worksheet through a VBA macro that call advanced functions of a dynamic linked library written in Pascal. The results are returned to the same Excel worksheet. Reasonably close starting values for the 49 adjustable parameters and supervised fitting are necessary.

	Blood		Tumor	Lung	Liver	Spleen	Kidney	Heart	Muscle	Bone	Stomach	Small intestine	Colon	Ovaries	Uterus	Bladder
Equations	F1	F2	F3	F4	F5	F6	F7	F8	F9	F10	F11	F12	F13	F14	F15	F16
d(F1)/dt	-K2:1-(K3:1+ATIR*IR)*WTu-K4:1*WLu-K5:1*DOTA*WLi-(K6:1-ASIR*IR)*WSp-K7:1*WKi-K8:1*WHe-K9:1*WMu-(K10:1-ABIR*IR)*WBo-K11:1*WSt-K12:1*WSi-K13:1*WCo-K14:1*WOv-(K15:1+AUJIR*IR)*WUt-K16:1*WBI-Kel	K1:2	K1:3	K1:4	K1:5	K1:6	K1:7	K1:8	K1:9	K1:10	K1:11	K1:12	K1:13	K1:14	K1:15	K1:16
d(F2)/dt	K2:1	-K1:2														
d(F3)/dt	(K3:1+ATIR*IR)*WTu		-K1:3													
d(F4)/dt	K4:1*WLu			-K1:4												
d(F5)/dt	K5:1*DOTA*WLi				-K1:5											
d(F6)/dt	(K6:1-ASIR*IR)*WSp					-K1:6										
d(F7)/dt	K7:1*WKi						-K1:7									
d(F8)/dt	K8:1*WHe							-K1:8								
d(F9)/dt	K9:1*WMu								-K1:9							
d(F10)/dt	(K10:1-ABIR*IR)*WBo									-K1:10						
d(F11)/dt	K11:1*WSt										-K1:11					
d(F12)/dt	K12:1*WSi											-K1:12				
d(F13)/dt	K13:1*WCo												-K1:13			
d(F14)/dt	K14:1*WOv													-K1:14		
d(F15)/dt	(K15:1+AUJIR*IR)*WUt														-K1:15	
d(F16)/dt	K16:1*WBI															-K1:16

Figure A2. Excel data sheet example of a multi-tissue biodistribution (16 compartments) modeling.

Blood	Tumour	Lungs	Liver	Spleen	Kidneys	Heart	Muscle	Bone	Stomach	Small intestine	Colon	Ovaries	Uterus	Bladder
F1/WTB	(F3+BTu*F1)/WTu	(F4+BLu*F1)/WLu	(F5+BLi*F1)/WLi	(F6+BSp*F1)/WSp	(F7+BKi*F1)/WKi	(F8+BHe*F1)/WHe	(F9+BMu*F1)/WMu	(F10+BBo*F1)/WBo	(F11+BSi*F1)/WSt	(F12+BSi*F1)/WSi	(F13+BCo*F1)/WCo	(F14+BOv*F1)/WOv	(F15+BUt*F1)/WUt	(F16+BBi*F1)/WBI

Figure A3. Example of formulas used for modeling each measured tissue.

Table A1. Simultaneous fit modeling.

1 DOTA				3 DOTA			Simultaneous Fit				1 DOTA				3 DOTA			Simultaneous Fit			
Parameter	Value	±	SD	Value	±	SD	Value	±	SD	Parameter	Value	±	SD	Value	±	SD	Value	±	SD		
K2:1	1.01×10^{-1}	±	7.31×10^{-3}	2.67×10^{-1}	±	2.92×10^{-2}	1.08×10^{-1}	±	1.65×10^{-2}	BTu	3.68×10^{-2}	±	1.98×10^{-3}	1.41×10^{-2}	±	1.88×10^{-3}	4.74×10^{-3}	±	3.21×10^{-3}		
K1:2	7.65×10^{-2}	±	4.28×10^{-3}	2.76×10^{-1}	±	3.28×10^{-2}	8.11×10^{-2}	±	1.01×10^{-2}	BLu	2.75×10^{-2}	±	1.25×10^{-3}	2.75×10^{-2}	±	1.54×10^{-3}	2.38×10^{-2}	±	3.03×10^{-3}		
K3:1	1.63×10^{-2}	±	7.06×10^{-4}	2.37×10^{-2}	±	1.30×10^{-3}	9.27×10^{-3}	±	2.87×10^{-3}	BLi	2.49×10^{-1}	±	8.67×10^{-3}	2.75×10^{-1}	±	1.46×10^{-2}	1.83×10^{-1}	±	2.05×10^{-2}		
K1:3	1.07×10^{-2}	±	6.96×10^{-4}	2.31×10^{-2}	±	1.20×10^{-3}	2.33×10^{-2}	±	2.44×10^{-3}	BSp	1.65×10^{-2}	±	7.39×10^{-4}	1.68×10^{-2}	±	9.29×10^{-4}	1.51×10^{-2}	±	1.73×10^{-3}		
K4:1	3.85×10^{-3}	±	4.44×10^{-4}	3.32×10^{-3}	±	7.04×10^{-4}	7.97×10^{-3}	±	1.87×10^{-3}	BKi	4.85×10^{-2}	±	2.12×10^{-3}	5.38×10^{-2}	±	2.78×10^{-3}	4.93×10^{-2}	±	5.31×10^{-3}		
K1:4	2.06×10^{-2}	±	2.24×10^{-3}	3.03×10^{-2}	±	5.00×10^{-3}	3.98×10^{-2}	±	8.80×10^{-3}	BHe	1.43×10^{-2}	±	6.17×10^{-4}	1.54×10^{-2}	±	8.02×10^{-4}	1.36×10^{-2}	±	1.63×10^{-3}		
K5:1	3.18×10^{-3}	±	1.02×10^{-4}	9.90×10^{-3}	±	6.29×10^{-4}	7.62×10^{-3}	±	5.80×10^{-4}	BMu	2.07×10^{-3}	±	1.53×10^{-4}	2.62×10^{-3}	±	1.96×10^{-4}	2.23×10^{-3}	±	3.70×10^{-4}		
K1:5	0.00	±	NA	1.25×10^{-2}	±	9.88×10^{-4}	1.76×10^{-2}	±	1.94×10^{-3}	BBo	2.35×10^{-3}	±	1.16×10^{-4}	2.99×10^{-3}	±	1.53×10^{-4}	2.49×10^{-3}	±	2.90×10^{-4}		
K6:1	4.20×10^{-3}	±	3.06×10^{-4}	7.83×10^{-3}	±	6.85×10^{-4}	6.36×10^{-2}	±	6.77×10^{-3}	BSt	9.96×10^{-3}	±	5.69×10^{-4}	8.55×10^{-3}	±	6.54×10^{-4}	8.84×10^{-3}	±	1.34×10^{-3}		
K1:6	8.50×10^{-3}	±	9.92×10^{-4}	1.95×10^{-2}	±	1.70×10^{-3}	1.77×10^{-2}	±	2.60×10^{-3}	BSi	6.85×10^{-2}	±	3.37×10^{-3}	7.03×10^{-2}	±	4.05×10^{-3}	6.69×10^{-2}	±	8.29×10^{-3}		
K7:1	3.68×10^{-3}	±	2.50×10^{-4}	3.54×10^{-3}	±	3.78×10^{-4}	4.91×10^{-3}	±	6.68×10^{-4}	BCo	4.14×10^{-2}	±	2.00×10^{-3}	4.14×10^{-2}	±	2.41×10^{-3}	3.74×10^{-2}	±	4.94×10^{-3}		
K1:7	4.72×10^{-3}	±	8.76×10^{-4}	1.50×10^{-2}	±	1.66×10^{-3}	1.32×10^{-2}	±	2.45×10^{-3}	BOv	7.59×10^{-3}	±	2.54×10^{-4}	2.48×10^{-3}	±	2.32×10^{-4}	3.33×10^{-3}	±	5.24×10^{-4}		
K8:1	1.03×10^{-3}	±	2.24×10^{-4}	1.37×10^{-3}	±	3.52×10^{-4}	3.28×10^{-3}	±	1.09×10^{-3}	BUt	2.65×10^{-2}	±	1.14×10^{-3}	1.08×10^{-2}	±	7.19×10^{-4}	1.17×10^{-2}	±	1.57×10^{-3}		
K1:8	1.58×10^{-2}	±	3.35×10^{-3}	2.42×10^{-2}	±	4.96×10^{-3}	3.68×10^{-2}	±	1.12×10^{-2}	BBl	7.88×10^{-4}	±	5.44×10^{-5}	5.88×10^{-4}	±	6.41×10^{-5}	6.32×10^{-4}	±	1.15×10^{-4}		
K9:1	1.53×10^{-3}	±	1.00×10^{-4}	9.49×10^{-4}	±	1.01×10^{-4}	1.46×10^{-3}	±	2.07×10^{-4}	Kel	3.51×10^{-2}	±	5.48×10^{-4}	4.23×10^{-2}	±	6.64×10^{-4}	4.53×10^{-2}	±	1.54×10^{-3}		
K1:9	1.07×10^{-2}	±	1.08×10^{-3}	1.53×10^{-2}	±	1.85×10^{-3}	1.49×10^{-2}	±	2.92×10^{-3}	ATIR				2.57×10^{-2}	±		2.57×10^{-2}	±	3.74×10^{-3}		
K10:1	1.51×10^{-3}	±	1.33×10^{-4}	1.14×10^{-3}	±	1.32×10^{-4}	1.09×10^{-2}	±	1.58×10^{-3}	ASIR				6.37×10^{-2}	±		6.37×10^{-2}	±	7.45×10^{-3}		
K1:10	4.42×10^{-3}	±	1.09×10^{-3}	6.08×10^{-3}	±	1.45×10^{-3}	7.62×10^{-3}	±	2.48×10^{-3}	ABIR				1.05×10^{-2}	±		1.05×10^{-2}	±	1.75×10^{-3}		
K11:1	1.26×10^{-3}	±	1.04×10^{-4}	9.95×10^{-4}	±	1.02×10^{-4}	1.78×10^{-3}	±	2.62×10^{-4}	AUIR				1.68×10^{-3}	±		1.68×10^{-3}	±	2.31×10^{-3}		
K1:11	9.67×10^{-3}	±	1.26×10^{-3}	1.46×10^{-2}	±	1.65×10^{-3}	1.80×10^{-2}	±	3.28×10^{-3}												
K12:1	9.21×10^{-4}	±	9.60×10^{-5}	8.57×10^{-4}	±	1.10×10^{-4}	1.49×10^{-3}	±	2.57×10^{-4}												
K1:12	6.19×10^{-3}	±	1.36×10^{-3}	9.86×10^{-3}	±	1.75×10^{-3}	1.30×10^{-2}	±	3.08×10^{-3}												
K13:1	7.66×10^{-4}	±	7.69×10^{-5}	8.51×10^{-4}	±	1.06×10^{-4}	1.72×10^{-3}	±	2.76×10^{-4}												
K1:13	2.28×10^{-3}	±	1.21×10^{-3}	1.02×10^{-2}	±	1.73×10^{-3}	1.52×10^{-2}	±	3.24×10^{-3}												
K14:1	1.49×10^{-3}	±	6.42×10^{-5}	3.81×10^{-3}	±	2.60×10^{-4}	4.80×10^{-3}	±	5.90×10^{-4}												
K1:14	0.00	±	NA	1.68×10^{-2}	±	1.25×10^{-3}	1.57×10^{-2}	±	2.50×10^{-3}												
K15:1	6.36×10^{-3}	±	3.76×10^{-4}	9.85×10^{-3}	±	5.63×10^{-4}	9.90×10^{-3}	±	1.87×10^{-3}												
K1:15	2.98×10^{-3}	±	7.11×10^{-4}	1.27×10^{-2}	±	9.37×10^{-4}	1.01×10^{-2}	±	1.51×10^{-3}												
K16:1	5.86×10^{-3}	±	2.74×10^{-4}	6.82×10^{-3}	±	4.16×10^{-4}	6.38×10^{-3}	±	5.53×10^{-4}												
K1:16	8.19×10^{-3}	±	7.14×10^{-4}	1.75×10^{-2}	±	1.20×10^{-3}	1.10×10^{-2}	±	1.64×10^{-3}												

References


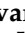



1. Shin, I.S.; Lee, S.-M.; Kim, H.S.; Yao, Z.; Regino, C.; Sato, N.; Cheng, K.T.; Hassan, R.; Campo, M.F.; Albone, E.F.; et al. Effect of chelator conjugation level and injection dose on tumor and organ uptake of ¹¹¹In-labeled MORAb-009, an anti-mesothelin antibody. *Nucl. Med. Biol.* **2011**, *38*, 1119–1127. [[CrossRef](#)]
2. Banerjee, S.; Pillai, M.R.A.; Knapp, F.F. (Russ) Lutetium-177 Therapeutic Radiopharmaceuticals: Linking Chemistry, Radiochemistry, and Practical Applications. *Chem. Rev.* **2015**, *115*, 2934–2974. [[CrossRef](#)] [[PubMed](#)]
3. Wojdowska, W.; Karczmarczyk, U.; Balog, L.; Sawicka, A.; Pöstényi, Z.; Kovács-Haász, V.; Polyák, A.; Laszuk, E.; Mikołajczak, R.; Garnuszek, P. Impact of DOTA-Chelators on the Antitumor Activity of ¹⁷⁷Lu-DOTA-Rituximab Preparations in Lymphoma Tumor-Bearing Mice. *Cancer Biother. Radiopharm.* **2020**, *35*, 558–562. [[CrossRef](#)] [[PubMed](#)]
4. Bhadwal, M.; Das, T.; Kumar, C.; Sharma, R.; Amirhdhanayagam, J.; Sarma, H.D.; Dash, A. Effect of Number of Bifunctional Chelating Agents on the Pharmacokinetics and Immunoreactivity of ¹⁷⁷Lu-labeled Rituximab: A Systemic Study. *Anti Cancer Agents Med. Chem.* **2018**, *18*, 146–153. [[CrossRef](#)]
5. Liu, S.; Edwards, D.S. Bifunctional Chelators for Therapeutic Lanthanide Radiopharmaceuticals. *Bioconjug. Chem.* **2001**, *12*, 7–34. [[CrossRef](#)] [[PubMed](#)]
6. Rinne, S.S.; Leitao, C.D.; Gentry, J.; Mitran, B.; Abouzayed, A.; Tolmachev, V.; Ståhl, S.; Löfblom, J.; Orlova, A. Increase in negative charge of ⁶⁸Ga/chelator complex reduces unspecific hepatic uptake but does not improve imaging properties of HER3-targeting affibody molecules. *Sci. Rep.* **2019**, *9*, 17710. [[CrossRef](#)] [[PubMed](#)]
7. Tolmachev, V.; Orlova, A. Influence of labelling methods on biodistribution and imaging properties of radiolabelled peptides for visualisation of molecular therapeutic targets. *Curr. Med. Chem.* **2010**, *17*, 2636–2655.
8. Knogler, K.; Grünberg, J.; Novak-Hofer, I.; Zimmermann, K.; Schubiger, P.A. Evaluation of ¹⁷⁷Lu-DOTA-labeled aglycosylated monoclonal anti-L1-CAM antibody chCE7: Influence of the number of chelators on the in vitro and in vivo properties. *Nucl. Med. Biol.* **2006**, *33*, 883–889. [[CrossRef](#)]
9. Al-Ejeh, F.; Darby, J.M.; Thierry, B.; Brown, M.P. A simplified suite of methods to evaluate chelator conjugation of antibodies: Effects on hydrodynamic radius and biodistribution. *Nucl. Med. Biol.* **2009**, *36*, 395–402. [[CrossRef](#)]
10. Elashoff, M.R.; Wingrove, J.; Beineke, P.; Daniels, S.; Tingley, W.G.; Rosenberg, S.; Voros, S.; Kraus, W.E.; Ginsburg, G.S.; Schwartz, R.S.; et al. Development of a blood-based gene expression algorithm for assessment of obstructive coronary artery disease in non-diabetic patients. *BMC Med. Genom.* **2011**, *4*, 26. [[CrossRef](#)]
11. Teicher, B.A. CD248: A therapeutic target in cancer and fibrotic diseases. *Oncotarget* **2019**, *10*, 993–1009. [[CrossRef](#)] [[PubMed](#)]
12. Christian, S.; Ahorn, H.; Novatchkova, M.; Garin-Chesa, P.; Park, J.E.; Weber, G.; Eisenhaber, F.; Rettig, W.J.; Lenter, M.C. Molecular Cloning and Characterization of EndoGlyx-1, an EMILIN-like Multisubunit Glycoprotein of Vascular Endothelium. *J. Biol. Chem.* **2001**, *276*, 48588–48595. [[CrossRef](#)] [[PubMed](#)]
13. Tomkowicz, B.; Rybinski, K.; Foley, B.; Ebel, W.; Kline, B.; Routhier, E.; Sass, P.; Nicolaides, N.C.; Grasso, L.; Zhou, Y. Interaction of endosialin/TEM1 with extracellular matrix proteins mediates cell adhesion and migration. *Proc. Natl. Acad. Sci. USA* **2007**, *104*, 17965–17970. [[CrossRef](#)] [[PubMed](#)]
14. Maia, M.; Devriese, A.; Jan, T.; Moons, M.; Lories, R.J.; Tavernier, J.; Conway, E.M. CD248 facilitates tumor growth via its cytoplasmic domain. *BMC Cancer* **2011**, *11*, 162. [[CrossRef](#)]
15. Fujii, S.; Fujihara, A.; Natori, K.; Abe, A.; Kuboki, Y.; Higuchi, Y.; Aizawa, M.; Kuwata, T.; Kinoshita, T.; Yasui, W.; et al. TEM1 expression in cancer-associated fibroblasts is correlated with a poor prognosis in patients with gastric cancer. *Cancer Med.* **2015**, *4*, 1667–1678. [[CrossRef](#)]
16. Davies, G.; Cunnick, G.H.; Mansel, R.E.; Mason, M.D.; Jiang, W.G. Levels of expression of endothelial markers specific to tumour-associated endothelial cells and their correlation with prognosis in patients with breast cancer. *Clin. Exp. Metastasis* **2004**, *21*, 31–37. [[CrossRef](#)]
17. Simonavicius, N.; Robertson, D.; Bax, D.; Jones, C.; Huijbers, I.J.; Isacke, C.M. Endosialin (CD248) is a marker of tumor-associated pericytes in high-grade glioma. *Mod. Pathol.* **2008**, *21*, 308–315. [[CrossRef](#)]
18. Nanda, A.; Karim, B.; Peng, Z.; Liu, G.; Qiu, W.; Gan, C.; Vogelstein, B.; Croix, B.S.; Kinzler, K.W.; Huso, D.L. Tumor endothelial marker 1 (Tem1) functions in the growth and progression of abdominal tumors. *Proc. Natl. Acad. Sci. USA* **2006**, *103*, 3351–3356. [[CrossRef](#)]
19. Delage, J.A.; Faivre-Chauvet, A.; Fierle, J.K.; Gnesin, S.; Schaefer, N.; Coukos, G.; Dunn, S.M.; Viertl, D.; Prior, J.O. (177)Lu radiolabeling and preclinical theranostic study of 1C1m-Fc: An anti-TEM-1 scFv-Fc fusion protein in soft tissue sarcoma. *EJNMMI Res.* **2020**, *10*, 98.
20. Fierle, J.K.; Abram-Saliba, J.; Brioschi, M.; Detiani, M.; Coukos, G.; Dunn, S.M. Integrating SpyCatcher/SpyTag covalent fusion technology into phage display workflows for rapid antibody discovery. *Sci. Rep.* **2019**, *9*, 12815. [[CrossRef](#)]
21. Lindmo, T.; Boven, E.; Cuttitta, F.; Fedorko, J.; Bunn, P.A., Jr. Determination of the immunoreactive fraction of radiolabeled monoclonal antibodies by linear extrapolation to binding at infinite antigen excess. *J. Immunol. Methods* **1984**, *72*, 77–89.
22. Watabe, H.; Channing, M.A.; Der, M.G.; Adams, H.R.; Jagoda, E.M.; Herscovitch, P.; Eckelman, W.C.; Carson, R.E. Kinetic Analysis of the 5-HT_{2A} Ligand [¹¹C]MDL 100,907. *Br. J. Pharmacol.* **2000**, *20*, 899–909. [[CrossRef](#)]

23. Novotny, J.A.; Greif, P.; Boston, R.C. WinSAAM: Application and explanation of use. In *Mathematical Modeling in Nutrition and the Health Sciences*; Springer: Boston, MA, USA, 2003; pp. 343–351. [[CrossRef](#)]
24. Chu, S.C.; Berman, M. An exponential method for the solution of systems of ordinary differential equations. *Commun. ACM* **1974**, *17*, 699–702. [[CrossRef](#)]
25. D’Onofrio, A.; Gano, L.; Melo, R.; Mendes, F.; Oliveira, M.C.; Denoël, T.; Schaefer, N.; Viertl, D.; Fierle, J.; Coukos, G.; et al. Biological evaluation of new TEM1 targeting recombinant antibodies for radioimmunotherapy: In vitro, in vivo and in silico studies. *Eur. J. Pharm. Biopharm.* **2021**, *158*, 233–244. [[CrossRef](#)]
26. Chacko, A.-M.; Li, C.; Nayak, M.; Mikitsh, J.L.; Hu, J.; Hou, C.; Grasso, L.; Nicolaides, N.C.; Muzykantov, V.R.; Divgi, C.R.; et al. Development of ¹²⁴I Immuno-PET Targeting Tumor Vascular TEM1/Endosialin. *J. Nucl. Med.* **2014**, *55*, 500–507. [[CrossRef](#)]
27. Garnett, M.C. Targeted drug conjugates: Principles and progress. *Adv. Drug Deliv. Rev.* **2001**, *53*, 171–216. [[CrossRef](#)]
28. Grunberg, J.; Jeger, S.; Sarko, D.; Dennler, P.; Zimmermann, K.; Mier, W.; Schibli, R. DOTA-Functionalized Polylysine: A High Number of DOTA Chelates Positively Influences the Biodistribution of Enzymatic Conjugated Anti-Tumor Antibody chCE7ag. *PLoS ONE* **2013**, *8*, e60350. [[CrossRef](#)]
29. Wangler, C.; Moldenhauer, G.; Eisenhut, M.; Haberkorn, U.; Mier, W. Antibody–Dendrimer Conjugates: The Number, Not the Size of the Dendrimers, Determines the Immunoreactivity. *Bioconjug. Chem.* **2008**, *19*, 813–820. [[CrossRef](#)]
30. Fischer, E.; Grünberg, J.; Cohrs, S.; Hohn, A.; Waldner-Knogler, K.; Jeger, S.; Zimmermann, K.; Novak-Hofer, I.; Schibli, R. L1-CAM-targeted antibody therapy and ¹⁷⁷Lu-radioimmunotherapy of disseminated ovarian cancer. *Int. J. Cancer* **2011**, *130*, 2715–2721. [[CrossRef](#)]
31. Mindt, T.L.; Jungi, V.; Wyss, S.; Friedli, A.; Pla, G.; Novak-Hofer, I.; Grünberg, J.; Schibli, R. Modification of Different IgG1 Antibodies via Glutamine and Lysine using Bacterial and Human Tissue Transglutaminase. *Bioconjug. Chem.* **2008**, *19*, 271–278. [[CrossRef](#)]
32. Grunberg, J.; Novak-Hofer, I.; Honer, M.; Zimmermann, K.; Knogler, K.; Blauenstein, P.; Ametamey, S.; Maecke, H.R.; Schubiger, P.A. In vivo evaluation of ¹⁷⁷Lu- and ^{67/64}Cu-labeled recombinant fragments of antibody chCE7 for radioimmunotherapy and PET imaging of L1-CAM-positive tumors. *Clin. Cancer Res.* **2005**, *11*, 5112–5120. [[CrossRef](#)] [[PubMed](#)]
33. Van Gog, F.B.; Visser, G.W.; Klok, R.; van der Schors, R.; Snow, G.B.; van Dongen, G.A. Monoclonal antibodies labeled with rhenium-186 using the MAG3 chelate: Relationship between the number of chelated groups and biodistribution characteristics. *J. Nucl. Med.* **1996**, *37*, 352–362. [[PubMed](#)]
34. Dearling, J.L.; Paterson, B.M.; Akurathi, V.; Betanzos-Lara, S.; Treves, S.T.; Voss, S.D.; White, J.M.; Huston, J.S.; Smith, S.V.; Donnelly, P.S.; et al. The Ionic Charge of Copper-64 Complexes Conjugated to an Engineered Antibody Affects Biodistribution. *Bioconjug. Chem.* **2015**, *26*, 707–717. [[CrossRef](#)] [[PubMed](#)]
35. Dahlsson Leitao, C.; Rinne, S.S.; Mitran, B.; Vorobyeva, A.; Andersson, K.G.; Tolmachev, V.; Ståhl, S.; Löfblom, J.; Orlova, A. Molecular Design of HER3-Targeting Affibody Molecules: Influence of Chelator and Presence of HEHEHE-Tag on Biodistribution of (⁶⁸Ga)-Labeled Tracers. *Int. J. Mol. Sci.* **2019**, *20*, 1080. [[CrossRef](#)] [[PubMed](#)]
36. Baranski, A.-C.; Schäfer, M.; Bauder-Wüst, U.; Wacker, A.; Schmidt, J.; Liolios, C.; Mier, W.; Haberkorn, U.; Eisenhut, M.; Kopka, K.; et al. Improving the Imaging Contrast of ⁶⁸Ga-PSMA-11 by Targeted Linker Design: Charged Spacer Moieties Enhance the Pharmacokinetic Properties. *Bioconjug. Chem.* **2017**, *28*, 2485–2492. [[CrossRef](#)] [[PubMed](#)]
37. Cicone, F.; Denoel, T.; Gnesin, S.; Riggi, N.; Irving, M.; Jakka, G.; Schaefer, N.; Viertl, D.; Coukos, G.; Prior, J.O. Preclinical Evaluation and Dosimetry of [(111)In]CHX-DTPA-scFv78-Fc Targeting Endosialin/Tumor Endothelial Marker 1 (TEM1). *Mol. Imaging Biol.* **2020**, *22*, 979–991. [[CrossRef](#)]

Article 3: Delage, J. A., et al. "Copper-64-labeled 1C1m-Fc, a new tool for TEM-1 PET imaging and prediction of Lutetium-177-labeled 1C1m-Fc therapy efficacy and safety." [Cancers 2021](#).

Article

Copper-64-Labeled 1C1m-Fc, a New Tool for TEM-1 PET Imaging and Prediction of Lutetium-177-Labeled 1C1m-Fc Therapy Efficacy and Safety

Judith Anna Delage ^{1,*}, Silvano Gnesin ², John O. Prior ^{3,*}, Jacques Barbet ⁴, Patricia Le Saëc ⁵, Séverine Marionneau-Lambot ⁵, Sébastien Gouard ⁵, Michel Chérel ⁵, Mickael Bourgeois ⁴, Niklaus Schaefer ³, David Viertl ^{6,7}, Julie Katrin Fierle ⁸, Steven Mark Dunn ⁸ and Alain Faivre-Chauvet ⁵

- Citation:** Delage, J.A.; Gnesin, S.; Prior, J.O.; Barbet, J.; Saëc, P.L.; Marionneau-Lambot, S.; Gouard, S.; Chérel, M.; Bourgeois, M.; Schaefer, N.; et al. Copper-64-Labeled 1C1m-Fc, a New Tool for TEM-1 PET Imaging and Prediction of Lutetium-177-Labeled 1C1m-Fc Therapy Efficacy and Safety. *Cancers* **2021**, *13*, 5936. <https://doi.org/10.3390/cancers13235936>
- Academic Editors:** Markus Luster, Behrooz H. Yousefi, Janina Baranowska-Kortylewicz and Stefano Fanti
- Received: 24 September 2021
Accepted: 19 November 2021
Published: 25 November 2021
- Publisher's Note:** MDPI stays neutral with regard to jurisdictional claims in published maps and institutional affiliations.
- Check for updates**
- ¹ Radiopharmacy Unit, Department of Pharmacy, Lausanne University Hospital and University of Lausanne, CH-1011 Lausanne, Switzerland
 - ² Institute of Radiation Physics, Lausanne University Hospital and University of Lausanne, CH-1011 Lausanne, Switzerland; silvano.gnesin@chuv.ch
 - ³ Department of Nuclear Medicine and Molecular Imaging, Lausanne University Hospital and University of Lausanne, CH-1011 Lausanne, Switzerland; niklaus.schaefer@chuv.ch
 - ⁴ GIP Arronax, F-44800 Saint-Herblain, France; jacques.barbet@univ-nantes.fr (J.B.); mickael.bourgeois@univ-nantes.fr (M.B.)
 - ⁵ CRCINA, Inserm, CNRS, CHU Nantes, University of Nantes, F-44000 Nantes, France; patricia.lesaec@univ-nantes.fr (P.L.S.); severine.marionneau-lambot@univ-nantes.fr (S.M.-L.); sebastien.gouard@univ-nantes.fr (S.G.); michel.cherel@univ-nantes.fr (M.C.); alain.favre-chauvet@univ-nantes.fr (A.F.-C.)
 - ⁶ Translational Radiopharmaceutical Sciences, Department of Nuclear Medicine and Molecular Imaging, Lausanne University Hospital and University of Lausanne, CH-1011 Lausanne, Switzerland; david.viertl@chuv.ch
 - ⁷ In Vivo Imaging Facility, Department of Research and Training, University of Lausanne, CH-1005 Lausanne, Switzerland
 - ⁸ LAbCore, Ludwig Institute for Cancer Research, Lausanne University Hospital and University of Lausanne, CH-1066 Epalinges, Switzerland; julie.fierle@unil.ch (J.K.F.); steven.dunn@chuv.ch (S.M.D.)
- * Correspondence: judith.delage@chuv.ch (J.A.D.); john.prior@chuv.ch (J.O.P.); Tel.: +41-21-314-43-53 (J.A.D.); +41-21-314-43-47 (J.O.P.)

Simple Summary: The prevalence of TEM-1 in the vasculature and the stroma of solid tumors and in malignant cells of sarcomas suggests that targeting TEM-1 could have therapeutic benefit. In this context, an anti-TEM-1 companion diagnostic may assist in the personalized medicine approach, whereby TEM-1 expression is exploited as a biomarker to select patients that would most benefit from a treatment directed toward the TEM-1 antigen. In our previous works, we have selected 1C1m-Fc, a fusion protein antibody, radiolabeled it with ¹⁷⁷Lu and demonstrated that [¹⁷⁷Lu]Lu-1C1m-Fc has interesting therapeutic performance. To define a suitable radiopharmaceutical companion for theranostic applications, ⁶⁴Cu was chosen to radiolabel the fusion protein antibody. The aim of this work was thus to determine if [⁶⁴Cu]Cu-1C1m-Fc can be considered for TEM-1 PET imaging and to predict the dosimetry of the [¹⁷⁷Lu]Lu-1C1m-Fc companion therapy.

Abstract: 1C1m-Fc, a promising anti-TEM-1 DOTA conjugate, was labeled with ⁶⁴Cu to target cancer cells for PET imaging and predicting the efficacy and safety of a previously studied [¹⁷⁷Lu]Lu-1C1m-Fc companion therapy. DOTA-conjugated 1C1m-Fc was characterized by mass spectrometry, thin layer chromatography and immunoreactivity assessment. PET/CT and biodistribution studies were performed in human neuroblastoma xenografted mice. Absorbed doses were assessed from biodistribution results and extrapolated to ¹⁷⁷Lu based on the [⁶⁴Cu]Cu-1C1m-Fc data. The immunoreactivity was $\geq 70\%$ after 48 h of incubation in serum, and the specificity of [⁶⁴Cu]Cu-1C1m-Fc for the target was validated. High-resolution PET/CT images were obtained, with the best tumor-to-organ ratios reached at 24 or 48 h and correlated with results of the biodistribution study. Healthy organs receiving the highest doses were the liver, the kidneys and the uterus. [⁶⁴Cu]Cu-1C1m-Fc could be of interest to give an indication of ¹⁷⁷Lu dosimetry for parenchymal organs. In the uterus and the tumor, characterized by specific TEM-1 expression, the ¹⁷⁷Lu-extrapolated absorbed doses are overestimated



Copyright: © 2021 by the authors. Licensee MDPI, Basel, Switzerland. This article is an open access article distributed under the terms and conditions of the Creative Commons Attribution (CC BY) license (<https://creativecommons.org/licenses/by/4.0/>).

because of the lack of later measurement time points. Nevertheless, ^{64}Cu -1C1m-Fc radiolabeled with ^{64}Cu for imaging would appear as an interesting radionuclide companion for therapeutic application with ^{177}Lu -1C1m-Fc.

Keywords: theranostic; tumor endothelial marker 1; DOTA conjugation; copper-64; PET imaging; Lutetium-177; dosimetry

1. Introduction

Theranostics is an emerging strategy combining diagnosis and therapy to achieve personalized treatments. Currently, this approach involves a number of scientific disciplines but is particularly linked to nuclear medicine [1]. Indeed, radionuclide imaging offers the opportunity to select patients, monitor therapy, and optimize the dosimetry to increase the efficacy and safety of targeted radionuclide therapy [2]. This approach is made possible by the discovery of biomarkers overexpressed in oncologic diseases that can be used as molecular targets [3] and by the development of vectors specifically binding these targets.

In clinical practice, the same vector may be radiolabeled with two different radionuclides, one for single photon emission computed tomography (SPECT) or positron emission tomography (PET) (respectively gamma or positron emitters) and one for therapy (electron or alpha particle emitter). Currently, PET is considered as having a higher sensitivity and a better spatial resolution than SPECT and a true potential for accurate quantitative imaging [4]. While electron emitters have been used in the vast majority of clinical applications, the use of radionuclides emitting alpha particle is also emerging. Small molecules, peptides or antibodies can be chosen as vectors [5].

Tumor endothelial marker 1 (TEM-1), also referred as CD248 or endosialin, is a cell surface transmembrane protein belonging to the C-lectin receptor superfamily. TEM-1 is expressed on pericytes and fibroblasts during tissue development, tumor neovascularization and inflammation [6–8]. TEM-1 has been described as an interesting target, as it is expressed by tumor stroma and tumor vessels in several oncological disease but has no or limited expression in normal adult tissues [9,10]. Furthermore, a high level of TEM-1 expression is associated with a poor prognosis and correlates with the aggressiveness of the tumor [11,12]. TEM-1 was thus considered by the research community as a potential therapeutic target, and several anti-TEM-1 antibodies have been developed [13]. Antibody drug conjugates [14,15], ScFv-Fc fragments for optical imaging and radionuclide imaging [16–18] and a radiolabeled humanized anti-TEM-1 monoclonal antibody MORAb-004 [19,20] have been tested preclinically. Currently, no clinical trial has been conducted with radiopharmaceuticals targeting TEM-1. Nevertheless, the naked MORAb-004 antibody has been evaluated in clinical immunotherapy trials [21–23]. Based upon a Phase I study conducted in sarcoma patients, this compound received FDA orphan drug designation for sarcoma [6].

Even though radioimmunoconjugates have been studied for more than 30 years, both for hematological disorders and solid tumors [24], only one of them, ^{90}Y ibritumomab-tiuxetan, Zevalin[®], has been approved for the treatment of recurrent or refractory non-Hodgkin's lymphomas [25]. Several strategies are currently used to improve radioimmunotherapy success such as antibody engineering, development of new bifunctional chelating agent (BFCA) or a choice of the most appropriate radionuclide. Radionuclide physical properties, and particularly their radioactive decay half-life, must be compatible with the radioimmunoconjugate targeting, disposition kinetics [26] and intended use.

In our previous works, 1C1m-Fc, a novel anti-TEM-1 ScFv-Fc construct, which binds both murine and human TEM-1, has been conjugated to a BFCA, p-SCN-Bn-DOTA, radiolabeled with ^{177}Lu and evaluated in a TEM-1-positive tumor model in mice. The results of the first experiments were promising, as a specific uptake of ^{177}Lu -1C1m-Fc in TEM-1-positive tumor was observed [27]. The impact of DOTA conjugation was evaluated. Using a pharmacokinetic model, the number of DOTA per fusion protein antibody

was demonstrated to have an impact on the pharmacokinetics and immunoreactivity of [^{177}Lu]Lu-1C1m-Fc [28]. The biodistribution and imaging contrast was improved by decreasing the number of chelating agents per 1C1m-Fc molecule: one DOTA per 1C1m-Fc gave the best tumor-to-liver ratio, but the specific activity was only 200 MBq/mg. Three to four DOTA per 1C1m-Fc was also adequate and provided a higher specific activity of 400 MBq/mg.

The aim of the present work is to pursue the evaluation of this new fusion protein antibody, 1C1m-Fc, in a theranostic strategy using ^{64}Cu for pretherapeutic PET imaging and dosimetry assessment and ^{177}Lu for targeted radionuclide therapy. ^{64}Cu presents a particular interest [29]. Indeed, this radionuclide is produced by cyclotrons, has a half-life of 12.7 h that allows PET immunoimaging and decays by emitting both low energy positrons and electrons. Promising results have already been obtained in preclinical and clinical trials using ^{64}Cu as a theranostic imaging agent [30].

In this study, although the vector 1C1m-Fc is kept constant, ^{64}Cu and ^{177}Lu differ by their half-life, their stability in DOTA complexes and possibly by their biodistribution. We have thus studied preclinically the [^{64}Cu]Cu-1C1m-Fc compound to determine if it can be considered as a new tool for TEM-1 PET imaging and to predict the dosimetry of the [^{177}Lu]Lu-1C1m-Fc companion therapy.

2. Materials and Methods

2.1. Cell Lines

The human fibrosarcoma HT-1080 (TEM-1-negative) and human neuroblastoma SK-N-AS (TEM-1-positive) were acquired from American Type Culture Collection (ATCC, Manassas, VA, USA).

The two cell lines were cultured in DMEM media (Thermo Fisher Scientific, Waltham, MA, USA) supplemented with 10% fetal bovine serum (FBS, Thermo Fisher Scientific, Waltham, MA, USA), 1% penicillin/streptomycin (Thermo Fisher Scientific, Waltham, MA, USA), 0.1 mM of nonessential amino acids (Thermo Fisher Scientific, Waltham, MA, USA) were also added for SK-N-AS culture. Cells were incubated in a flask at 37 °C in a humidified atmosphere at 5% CO_2 .

2.2. Fusion Protein Antibody

A complete description of the 1C1m-Fc fusion protein antibody may be found in Fierle et al. [31] and in Delage et al. [27]. Briefly, this single-chain variable fragment (scFv) fused to a human Fc domain (Ig G) binds both human and murine TEM-1 with an affinity of 1 and 6 nM, respectively.

2.3. Conjugation

Antibody concentrations were measured at 280 nm using a spectrophotometer (NanoDrop Lite, Thermo Fisher Scientific, Waltham, MA, USA). 1C1m-Fc was conjugated with p-SCN-Bn-DOTA (Macrocyclics, Plano, TX, USA). A calculated volume of p-SCN-Bn-DOTA (25.9 mg/mL, 47 $\mu\text{mol}/\text{mL}$, in DMSO 10% *v/v*) was added to 1C1m-Fc (1 mg, 9.4 nmol) in 0.2 M carbonate buffer pH 9.0. The solution was maintained at 37 °C for 1 h. The number of DOTA conjugated per fusion protein antibody ratio was 3 to 4 DOTA. Conjugated antibodies were washed by four rounds of ultrafiltration in 0.1 M sodium acetate buffer pH 5.0 (Alfa Aesar, Haverhill, MA, USA). High pressure liquid chromatography (HPLC) was performed to assess the integrity of the conjugates. DOTA-conjugated 1C1m-Fc was subsequently stored between 2 and 8 °C. The purity and the stability of the conjugate were evaluated by HPLC, as described in Delage et al. [27].

2.4. Characterization of the Immunoconjugates: Mass Spectrometry Analysis

The number of chelate per antibody was determined by mass spectrometry (MS) analysis using a Q Exactive HF Orbitrap (Thermo Fisher Scientific, Waltham, MA, USA), as previously described in Delage et al. [27,28].

After analysis, the mass spectrometry spectra were deconvoluted, and the drug-to-antibody ratio (DAR) was obtained using the formula: $\Sigma(n \times \text{Int})/\Sigma(\text{Int})$, where n is the number of attached molecules for each peak, and Int the intensity of the peak.

2.5. Radiolabeling

^{64}Cu dichloride ($^{64}\text{CuCl}_2$) in 0.1 N HCl solution was produced by the ARRONAX cyclotron (Saint Herblain, France). A calculated volume of sodium acetate 2.5 M metal-free (Alfa Aesar, Haverhill, MA, USA) was first added to the $^{64}\text{CuCl}_2$ solution, followed by a calculated volume of 5 mg/mL DOTA-conjugated 1C1m-Fc in acetate buffer 0.1 M. After 30 min incubation at 42 °C, 1 mM EDTA pH 7.0 (Sigma–Aldrich, St. Quentin Fallavier, France) was added to obtain a final concentration of 0.01 mM to complex free $^{64}\text{Cu}(\text{II})$.

The radiochemical purity of [^{64}Cu]Cu-1C1m-Fc was determined by instant thin layer chromatography (iTLC). The release criterium was $\geq 95\%$. iTLC analyses were performed using dried iTLC-SG glass microfiber chromatography paper impregnated with silica gel (Agilent Technologies, Folsom, CA 95630). Citrate buffer (0.1 M, pH 4.5) was used as eluent. In this system, [^{64}Cu]Cu-1C1m-Fc remains at $R_f = 0$, while unbound [^{64}Cu]Cu-EDTA migrates to the solvent front ($R_f = 1$).

The radiochemical purity after antibody radiolabeling was assessed by iTLC-SG just after radiolabeling and 24 h after.

2.6. In Vitro Studies: Radio-Immunoreactivity

Immunoreactivity of [^{64}Cu]Cu-1C1m-Fc was assessed using Pierce™ Streptavidin Magnetic Beads (Thermo Fischer Scientific, Waltham, MA, USA). Streptavidin is covalently coupled to the surface of the magnetic beads. For each streptavidin molecule on the bead, around 3 biotin-binding sites are available. The Streptavidin beads (250 μL , 10 mg/mL) were first coupled to biotin-conjugated TEM-1 antigen (50 μL , 0.33 mg/mL) obtained from the LAbCore immunoglobulin discovery and engineering facility, Ludwig Institute for Cancer Research, Lausanne, (following the instructions given by Thermo Fischer Scientific). The biotinylated fragment comprises the 353 N-terminal amino acids of the mature human TEM-1 protein. The TEM-1-coated beads (10 μL at 10 mg/mL) were mixed to 0.016 pmol of radiolabeled antibody in human serum, and PBS/BSA 0.1% was added to obtain a final volume of 100 μL . The mixture was incubated at 37°C in human serum for 48 h. The time points were chosen to correlate with those of the biodistribution study (until 24 h for the [^{64}Cu]Cu-3DOTA-1C1m-Fc and 48 h for the [^{64}Cu]Cu-4DOTA-1C1m-Fc).

The radioactivity bound to the beads, collected with a magnetic stand and, remaining in the supernatant, was measured with a gamma counter (AMG Automatic Gamma Counter, Hidex, Turku, Finland). Each test was run in duplicate. The immunoreactivity was calculated as the ratio between the activity of the beads to the total activity. Nonspecific uptake on the tube was also measured and accounted for.

2.7. In Vivo Characterization Studies

2.7.1. Animal Model

The in vivo studies were carried out in female BALB/c nude mice from 7 to 9 weeks old (Janvier Labs, Le Genest-Saint-Isle, France or Charles River Laboratories, Wilmington, MA, USA). A group of mice was xenografted subcutaneously in the left flank with 3×10^6 SK-N-AS (TEM-1-positive) cells suspended in a solution of 100 μL of medium (group 1, $n = 14$). As a negative control, a second group (group 2, $n = 3$), was grafted in the right flank with 3×10^6 SK-N-AS cells and with 3×10^6 HT-1080 (TEM-1-negative) cells suspended in 100 μL of a solution containing 1:1 mixture of Matrigel and medium in the left flank.

2.7.2. PET Imaging Study

All mice were anesthetized for the duration of the imaging sequence by inhalation of isoflurane 2%/O₂ and warmed on a heating pad during the scan.

For two SK-N-AS tumor-bearing mice of group 1, 10-, 20- or 30-min images (energy window 358–664 keV) were acquired on a small-animal PET/SPECT/CT device (Albira, Bruker BioSpin MRI GmbH, Ettlingen, Germany) at three time-points (respectively, 4, 24, and 48 h) after intravenous injection of 6.0 ± 0.3 MBq [^{64}Cu]Cu-1C1m-Fc (50 μg of total antibody per mouse). Images were reconstructed using a three-dimensional maximum likelihood expectation maximization algorithm with 12 iterations, without postreconstruction smoothing. The PET in-plane FOV size was 80 mm with axial extension of 149 mm; reconstructed image voxel size was 0.5 mm isotropic in space. Dead-time, scatter and random corrections were applied. Coregistered CT (0.4 mA, 35 kV, 600 projections, 125 μm voxel size) was used for anatomical localization of uptake. PET and CT images were visualized and analyzed using PMOD (PMOD Technologies, version 3.7, Zurich, Switzerland).

For group 2, ten-minute images (energy window 250–750 KeV, FOV size 90 mm) of mice ($n = 3$) bearing both SK-N-AS and HT 1080 tumors were recorded 24 h after injection of 7.7 ± 0.2 MBq of [^{64}Cu]Cu-1C1m-Fc (50 μg of total antibody per mouse) with an IRIS PET/CT, (Inviscan SAS, Strasbourg, France). The CT acquisition parameters were 20 s, 0.9 mA, 80 KV, 576 projections, 160 μm voxel size. PET images were reconstructed with 3D-OSEM-MC, eight subsets, eight iterations with decay, random and dead-time corrections. For CT, filtered back-projection algorithm with beam hardening and ring artefact correction was used.

2.7.3. Biodistribution Study

[^{64}Cu]Cu-1C1m-Fc was injected in the lateral tail vein of the mice. Animals received [^{64}Cu]Cu-4DOTA-1C1m-Fc (group 1) or [^{64}Cu]Cu-3DOTA-1C1m-Fc (group 2) and unlabeled 1C1m-Fc corresponding to a total antibody dose of 50 μg per mice, in a total volume of 100 μL . The average weight of animals was 17.79 ± 0.66 mg for group 1 and 17.93 ± 2.57 mg for group 2. The dose of 50 μg (470 pmol) of antibody has been selected from our previous study [27].

In group 1, animals were euthanized and exsanguinated at 4, 24, 48 h (corresponding precisely to 4.3, 26.0 and 50.2 h), after injection of the radiolabeled product and 24 h after injection for group 2. Blood was collected, and organs and tumors were removed, weighed, and counted with a gamma counter (AMG Automatic Gamma Counter, Hidex, Turku, Finland). Results were expressed as the percentage of injected activity (IA) per gram of tissue (%IA/g).

2.7.4. Murine Dosimetry

Estimated absorbed doses to organs were based on the biodistribution results on SK-N-AS-bearing mice. Considered source organs for the dosimetry study were the liver, the kidneys, the lungs, the spleen, the heart content, the stomach, the small intestine, the colon, the uterus and ovaries, the tumor and the remainder of the body.

The biodistribution for the remainder tissues was obtained by multiplying the rest-of-body mass (17.8 g average mouse mass—sum of the masses of all other considered source organs) by the normalized mass-activity concentration (g^{-1}) measured in the muscle, which was taken as representative of the background body uptake.

For each mouse at each time point (4.3, 26.0 and 50.2 h), the activity in each source organ and the remainder was normalized by the total injected activity to obtain the normalized injected activity (nA). For each source organ at each time point, an average nA value was obtained \pm SD. The source organs' normalized time-activity curves (nTACs) were fitted with monoexponential functions using the kinetic module of OLINDA/EXM 2.1 (HERMES Medical Solution AB, Stockholm, Sweden). For source organs having an effective decay constant (λ_{eff}) larger than the physical decay constant of ^{64}Cu ($\lambda_{\text{p,Cu64}}$), time-integrated activity coefficients (TIACs) were derived by monoexponential analytical time integration (extended to infinite) of fitted source organ nTACs obtained with the average nA, nA + SD and the nA–SD values, respectively. To avoid unrealistic TIACs overestimates, when the source organ λ_{eff} was smaller than the $\lambda_{\text{p,Cu-64}}$, monoexponential time integration

with λ_{eff} was applied only from time zero until the time of the last biokinetic measurement (50.2 h), and a monoexponential analytic integration using $\lambda_{p,\text{Cu}64}$ was applied beyond ($t > 50.2$ h). Finally, the source organ TIACs were entered into the OLINDA/EXM 2.1 software kinetic module for organ absorbed dose estimates, where the 25 g murine model was adjusted to match the source organ average masses obtained from the mice population used in our experiment. In this process, the TIAC of the uterus and the ovaries were part of the remainder of the body. A specific absorbed dose estimate was performed for the uterus, the ovaries and the tumor. These tissues exhibited an important specific tracer uptake but were not among the source/target organs available in the murine model of the OLINDA/EXM 2.1 software. Absorbed dose estimates were thus obtained using the sphere model of OLINDA/EXM 2.1, where the average organ TIACs and the average organ masses for these reproductive organs and the tumor were applied.

2.7.5. Dose Extrapolation to the ^{177}Lu Compound

To allow the comparison with previously published data for similar molecules labeled with ^{177}Lu , we extrapolated the organ absorbed doses for the ^{177}Lu radiolabeled compound from experimental data obtained for the ^{64}Cu murine biodistribution data. nA values for ^{177}Lu were extrapolated from ^{64}Cu measured data points by the application of a scale factor (SF):

$$SF(t_m) = \exp(-\lambda_{p,\text{Lu}-177} \times t_m) / \exp(-\lambda_{p,\text{Cu}-64} \times t_m)$$

where t_m indicates the measured time points (4.3, 26 and 50.2 h postinjection, respectively); therefore, $n\text{ALu}-177(t_m) = n\text{ACu}-64(t_m) \times \text{SF}(t_m)$. The rescaling procedure compensates for the different physical half-life of the two radioisotopes, assuming the same biological half-life. To perform ^{177}Lu nTACs' time integration and absorbed dose estimates, we applied the methodology previously described above for the ^{64}Cu .

2.8. Statistical Analysis

The data are expressed as mean \pm SD (standard deviation). Significant differences between means were analyzed by an unpaired, 2-tailed Student *t*-test with a correction for multiple comparison using the Holm–Sidak method ($\alpha = 0.05$). Statistical analyses were conducted using Prism 8.0 (GraphPad Software, San Diego, CA, USA).

3. Results

3.1. Conjugation

1C1m-Fc conjugated with DOTA was analyzed by mass spectrometry, and the mass obtained for the native antibody was 108 394. The samples used for radiolabeling were conjugated with 3 (Figure S1a) to 4 DOTA (Figure S1b).

The conjugates were evaluated by HPLC, and the purity was, respectively, of 96.2% for 3DOTA-1C1m-Fc and 95.0% for 4DOTA-1C1m-Fc.

3.2. Radiolabeling

The release criterium for the radiochemical purity (RCP) evaluated by iTLC was more than 95% (Figure 1).

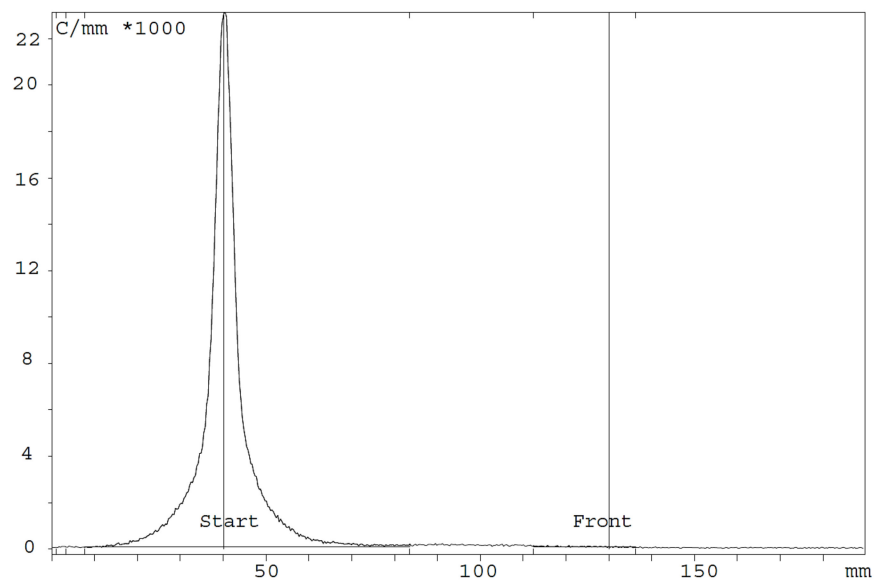


Figure 1. Radio-TLC example of $[^{64}\text{Cu}]\text{Cu-1C1m-Fc}$. The radiochemical purity (RCP) is 99.85%. $[^{64}\text{Cu}]\text{Cu-1C1m-Fc}$ remains at $R_f = 0$, and the unbound $[^{64}\text{Cu}]\text{Cu-EDTA}$ migrates to the solvent front. With the used radiolabeling process, the average radiochemical purity was $99.5 \pm 0.6\%$ immediately after radiolabeling ($n = 5$) and $98.3 \pm 2.1\%$ ($n = 3$) after 24 h. The specific activity was comprised between 156 and 200 MBq/mg.

3.3. In Vitro Studies: Radio-Immunoreactivity

The results of the immunoreactivity assessment of $[^{64}\text{Cu}]\text{Cu-1C1m-Fc}$ in serum media are reported in Table 1.

Table 1. Immunoreactivity assessment of $[^{64}\text{Cu}]\text{Cu-1C1m-Fc}$ after incubation in serum. The results are expressed as mean \pm SD.

Immunoreactivity (%) \pm SD	4 h	24 h	48 h
$[^{64}\text{Cu}]\text{Cu-3DOTA-1C1m-Fc}$	76 ± 1.4 ($n = 2$)	70 ($n = 1$)	NA
$[^{64}\text{Cu}]\text{Cu-4DOTA-1C1m-Fc}$	75 ± 15 ($n = 3$)	77 ± 14 ($n = 3$)	72 ± 13 ($n = 3$)

3.4. Imaging Study

High-quality PET/CT images were obtained at 4 h, 24 h and 48 h in mice bearing TEM-1-positive tumor. At 4 h, the activity was found predominantly in blood; the heart and carotid arteries were visible, as well as the liver, but the tumor was also already clearly visible. The circulating and liver activities decreased thereafter, and tumor-to-liver ratios determined by imaging were, respectively, 0.8, 1.8 and 1.7 at 4 h, 24 h and 48 h (Figure 2).

The PET/CT performed at 24 h in mice ($n = 3$) bearing both TEM-1-positive and negative tumors confirmed the specificity of the uptake in TEM-1-positive tumor (higher uptake) as opposed to control tumor (lower uptake) (Figure 3).

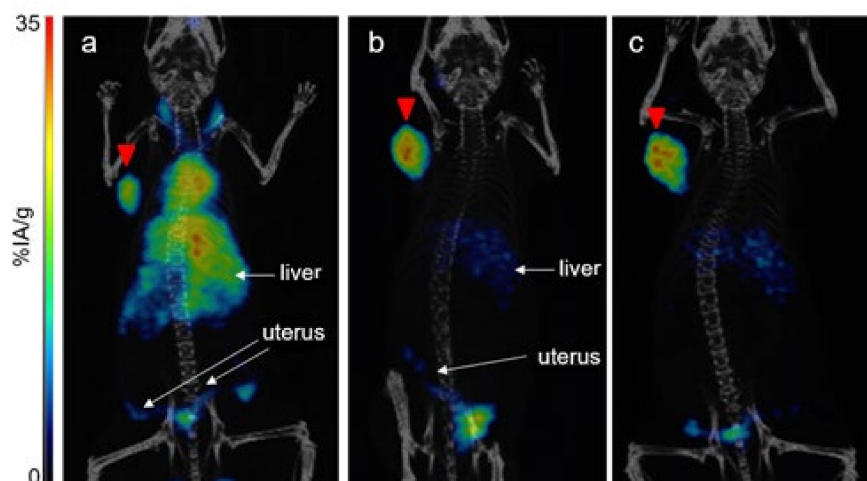


Figure 2. [^{64}Cu]Cu-1C1m-Fc dorsal view PET/CT fusion maximum intensity projection in mouse bearing TEM-1-positive tumors (SK-N-AS, left flank, red arrow), (a) at 4 h, (b) at 24 h, (c) at 48 h.

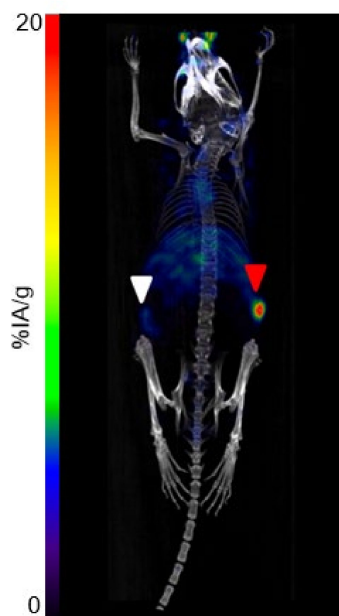


Figure 3. [^{64}Cu]Cu-1C1m-Fc dorsal view PET/CT fusion maximum intensity projection at 24 h on mouse bearing TEM-1-negative tumor (HT-1080; left flank; white arrow) and TEM-1-positive tumor (SK-N-AS; right flank; red arrow).

3.5. Biodistribution Study

A biodistribution study of [^{64}Cu]Cu-1C1m-Fc was performed in mice bearing TEM-1-positive tumors (group 1) and in mice bearing both TEM-1-positive and negative tumors as control (group 2).

For group 1 (Figure 4a), the uptake in the tumor was maximum at 24 h ($24.5 \pm 1.5\%$ IA/g). The uptake in the liver decreased between 4 h ($16.3 \pm 0.6\%$ IA/g) and 24 h ($12.7 \pm 1.4\%$ IA/g) and remained stable until 48 h ($12.8 \pm 2.8\%$ IA/g). A rapid blood clearance was observed as the amount of radiotracer in the blood decreased from $29.0 \pm 2.4\%$ IA/g at 4 h to $6.2 \pm 1.1\%$ IA/g at 48 h. The uptake in the uterus was $15.3 \pm 2.9\%$ IA/g at 4 h, and no significant difference was observed at 24 and 48 h ($p = 0.87$, unpaired Student's *t*-test). The best tumor-to-liver ratio was observed at 24 h (1.9), and the best tumor-to-blood ratio, at 48 h (3.6) (Table 2).

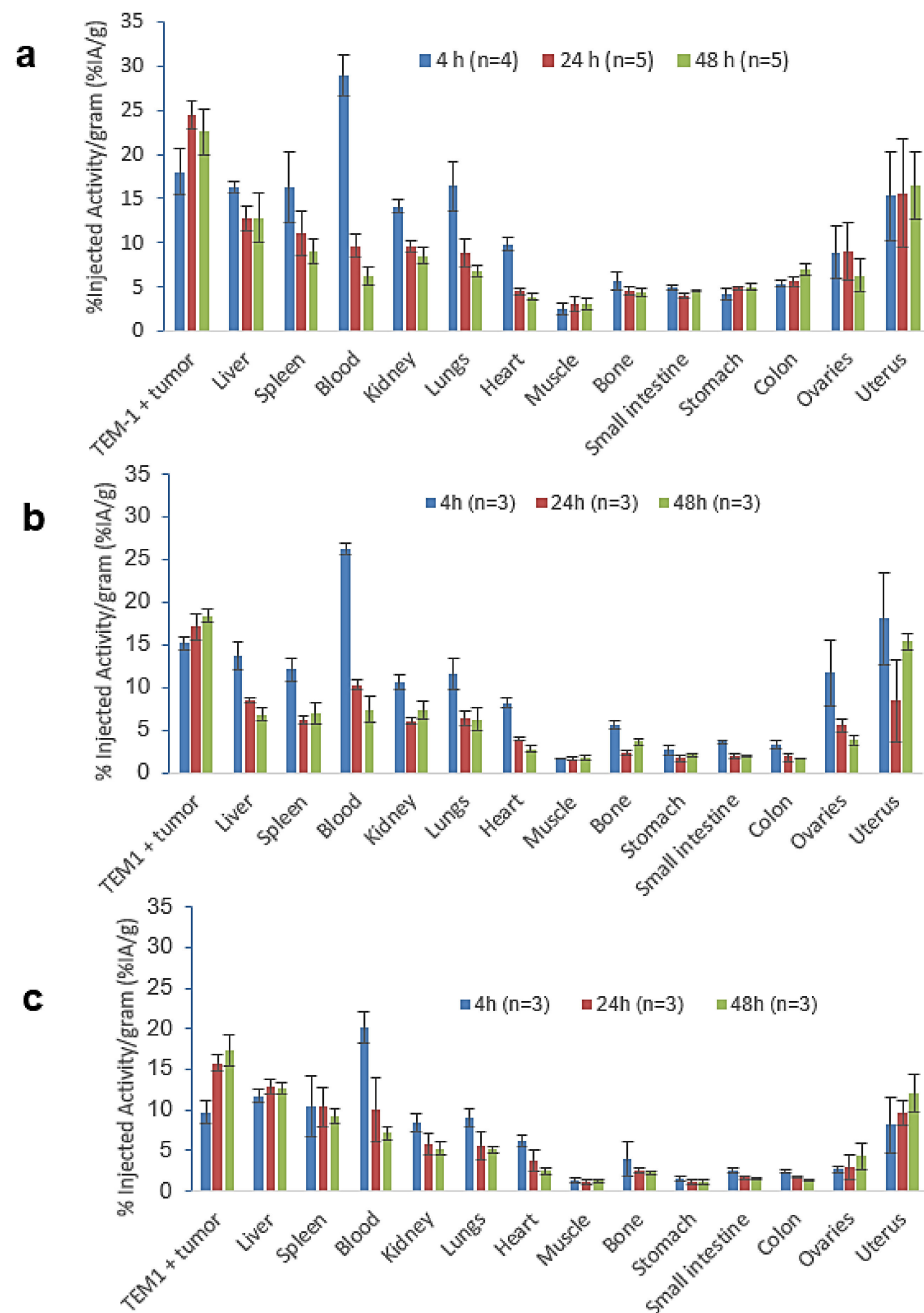


Figure 4. Biodistribution in BALB/c nude mice bearing TEM-1-positive tumor of (a) [^{64}Cu]Cu-4DOTA-1C1m-Fc, group 1; (b) [^{177}Lu]Lu-1DOTA-1C1m-Fc (data from Delage et al. [28]); (c) [^{177}Lu]Lu-3DOTA-1C1m-Fc (data from Delage et al. [27]). The total antibody dose used for this biodistribution was 50 μg . Data are shown as mean \pm SD.

No significant difference was observed between groups 1 and 2 regarding the uptake in the TEM-1-positive tumor, the liver, the spleen or the blood ($p = 0.93$, unpaired t -test). For group 2, at 24 h, the uptake in TEM-1-positive tumor ($21.5 \pm 7.5\%$ IA/g) was 2.4-fold higher than the one in TEM-1-negative tumor ($9.0 \pm 4.1\%$ IA/g), showing the specificity of the antibody for TEM-1 (Figure S2).

The biodistribution profile of [^{64}Cu]Cu-4DOTA-1C1m-Fc (Figure 4a) was very similar to the one of [^{177}Lu]Lu-1DOTA-1C1m-Fc (Figure 4b, data already published in [28]) or [^{177}Lu]Lu-3DOTA-1C1m-Fc (Figure 4c, data already published in [27]). The blood uptake at 4 h of [^{64}Cu]Cu-4DOTA-1C1m-Fc was closer to that of [^{177}Lu]Lu-1DOTA-1C1m-Fc. A hepatic accumulation was observed with the [^{64}Cu]Cu-4DOTA-1C1m-Fc or [^{177}Lu]Lu-

3DOTA-1C1m-Fc antibody. The main difference seen was the uptake in the gastrointestinal tract; the stomach, small intestine and colon uptakes were higher with [⁶⁴Cu]Cu-1C1m-Fc than with [¹⁷⁷Lu]Lu-1C1m-Fc ($p = 0.000012$, 0.00026 and 0.00026 , respectively, at 24 h, and $p = 0.000114$, 0.000002 and 0.000041 at 48 h) (unpaired Student's *t*-test).

Table 2. Tumor-to-organ ratio of [⁶⁴Cu]Cu-1C1m-Fc determined by biodistribution of group 1 at 4 h, 24 h and 48 h.

Ratio	4 h	24 h	48 h
Tumor/Liver	1.1	1.9	1.8
Tumor/Spleen	1.1	2.2	2.5
Tumor/Blood	0.6	2.5	3.6
Tumor/Kidney	1.3	2.5	2.6
Tumor/Lungs	1.1	2.8	3.3
Tumor/Heart	1.8	5.4	5.8
Tumor/Muscle	7.2	8.0	7.3
Tumor/Bone	3.2	5.3	5.1
Tumor/Small Intestine	3.6	6.0	4.9
Tumor/Stomach	4.3	5.0	4.5
Tumor/Colon	3.3	4.3	3.2
Tumor/Ovaries	2.0	2.7	3.6
Tumor/Uterus	1.2	1.6	1.4

3.6. Murine Dosimetry

The organ-absorbed doses for target tissues obtained using the mouse model of the OLINDA/EXM 2.1 software are summarized in Table 3. The healthy organs receiving the most important irradiation were the liver, the uterus, the heart, the kidneys and the lungs. The estimated tumor-absorbed dose exceeded by a factor of 1.2 that of the liver.

Table 3. Measured average organ masses and TIAC (only for source organs) and estimated organ doses obtained with the OLINDA/EXM 2.1 software for [⁶⁴Cu]Cu-1C1m-Fc. Source organs are indicated with *. Absorbed dose estimates using the sphere model of the OLINDA/EXM 2.1 software are labeled with ^s. The normalized time–activity curves for the considered source organs are presented in the Supplementary Materials (Figure S3).

Organ	Mean Organ Mass (g)	TIAC (MBq.h/MBq)			Absorbed Dose (mGy/MBq)		
		Mean	Mean – SD	Mean + SD	Mean	Mean – SD	Mean + SD
Brain					30	20.7	39.3
Large Intestine *	0.25	0.264	0.199	0.321	110	81.1	137
Small Intestine *	0.58	0.422	0.263	0.565	87.4	57.3	115
Stomach Wall *	0.11	0.093	0.078	0.108	98.3	78.2	118
Heart *	0.14	0.182	0.169	0.194	137	118	155
Kidneys *	0.27	0.569	0.535	0.601	167	149	184
Liver *	1.01	2.613	2.242	2.932	184	152	212
Lungs *	0.14	0.328	0.248	0.407	159	119	198
Pancreas					38.2	27.8	48.4
Skeleton					33.2	23.2	43
Spleen *	0.08	0.189	0.174	0.204	169	149	189

Table 3. Cont.

Organ	Mean Organ Mass (g)	TIAC (MBq.h/MBq)			Absorbed Dose (mGy/MBq)		
		Mean	Mean – SD	Mean + SD	Mean	Mean – SD	Mean + SD
Testes					30.1	20.7	39.4
Thyroid					30.8	21.2	40.3
Urinary Bladder					30.6	21.1	40
Total Body	17.8	13.349	10.311	16.631	46.1	34.5	57.3
Rest of the body *	15.2	7.06	4.857	9.25			
Uterus ^{*,s}	0.09	0.246	0.108	0.363	178	78.4	263
Ovaries ^{*,s}	0.04	0.054	0.034	0.073	85.1	53.6	115
Tumor ^{*,s}	0.11	0.377	0.141	0.613	225	84.2	366

[¹⁷⁷Lu]Lu-1C1m-Fc-absorbed dose data were extrapolated from [⁶⁴Cu]Cu-1C1m-Fc biodistribution data and compared to the experimental absorbed doses previously published in [27,28] (Table 4). Extrapolated absorbed doses for parenchymal organs (such as: liver, lung, spleen and kidneys) showed a 20% difference when compared with [¹⁷⁷Lu]Lu-1DOTA-1C1m-Fc. The difference was higher with [¹⁷⁷Lu]Lu-3DOTA-1C1m-Fc. In both cases, the major discrepancies were found in the gastrointestinal tract, the uterus and the tumor (extrapolated absorbed doses were overestimated).

Table 4. 1: TIAC (only for source organs) and organ-absorbed doses for [¹⁷⁷Lu]Lu-1C1m-Fc extrapolated from experimental murine biodistribution data of [⁶⁴Cu]Cu-1C1m-Fc. Source organs are indicated with *. Absorbed dose estimates using the sphere model of the OLINDA/EXM 2.1 software are labeled with ^s. 2: Absorbed doses of [¹⁷⁷Lu]Lu-1DOTA-1C1m-Fc from experimental data obtained in our previous study [28]. 3: Difference ratio between the estimated absorbed dose and the absorbed dose obtained from biodistribution data of [¹⁷⁷Lu]Lu-1DOTA-1C1m-Fc. 4: Absorbed doses of [¹⁷⁷Lu]Lu-3DOTA-1C1m-Fc from experimental data obtained in our previous study [27]. 5: Difference ratio between the estimated absorbed dose and the absorbed dose obtained from biodistribution data of [¹⁷⁷Lu]Lu-3DOTA-1C1m-Fc.

Target Organs	1: [¹⁷⁷ Lu]Lu-1C1m-Fc TIAC and Absorbed Dose Extrapolation from [⁶⁴ Cu]Cu-1C1m-Fc Biodistribution Data		2: [¹⁷⁷ Lu]Lu-1DOTA-1C1m-Fc Absorbed Dose (mGy/MBq) AD2 Data from [28]	3: Difference Ratio between AD1 and AD2 (%)	4: [¹⁷⁷ Lu]Lu-3DOTA-1C1m-Fc Absorbed Dose (mGy/MBq) AD3 Data from [27]	5: Difference Ratio between AD1 and AD3 (%)
	TIAC (MBq-h/MBq)	Absorbed Dose (mGy/MBq) AD1				
Brain		485	408	19		
Large Intestine *	2.921	1490	703	112	328	354
Small Intestine *	5.844	1350	577	134	438	208
Stomach Wall *	0.803	1130	1660	–32	1150	–2
Heart *	0.45	904	1110	–19	363	159
Kidneys *	1.99	1070	1320	–19	705	52
Liver *	16.559	1630	1790	–9	2230	–27
Lungs *	0.864	976	983	–1	539	81
Pancreas		512	441	16		
Skeleton		492	418	18		
Spleen *	0.672	1090	1180	–8	1200	–9
Testes		485	409	19		
Thyroid		486	409	19		

Table 4. Cont.

Target Organs	1: [¹⁷⁷ Lu]Lu-1C1m-Fc TIAC and Absorbed Dose Extrapolation from [⁶⁴ Cu]Cu-1C1m-Fc Biodistribution Data		2: [¹⁷⁷ Lu]Lu-1DOTA-1C1m-Fc Absorbed Dose (mGy/MBq) AD2 Data from [28]	3: Difference Ratio between AD1 and AD2 (%)	4: [¹⁷⁷ Lu]Lu-3DOTA-1C1m-Fc Absorbed Dose (mGy/MBq) AD3 Data from [27]	5: Difference Ratio between AD1 and AD3 (%)
	TIAC (MBq-h/MBq)	Absorbed Dose (mGy/MBq) AD1				
Urinary Bladder		486	534	−9		
Total Body	130.205	590	549	7		
Rest of the body *	100.102					
Uterus * ^s	3.31	2890	1830	58	1500	93
Ovaries * ^s	0.272	570	742	−23		
Tumor * ^s	5.294	3850	2530	52	1820	111

4. Discussion

In the last ten years, theranostic approaches have emerged as valuable tools in oncology to identify therapeutic targets, to select the patients that would most benefit from therapeutics and to monitor the response to treatments [2,32]. Among the potential biomarkers, TEM-1 appears as an emerging target, as it is expressed in tumor vessels and in the stroma of various cancers but has no or little expression in normal adult tissues (expression is limited to endometrial stroma and occasionally fibroblast) [33,34]. Currently, the expression of TEM-1 in patients is assessed by invasive techniques such as immunohistochemistry of biopsies. In addition, these techniques do not identify the total TEM-1-positive tumor burden in a patient [20]. Consequently, immunoPET may play an important role in determining the clinical expression of tumor biomarkers.

In our previous works, we have validated the relevance of a bivalent Fc-fusion protein based on a novel single chain antibody, 1C1m-Fc, radiolabeled with ¹⁷⁷Lu for a therapeutic approach [27,28]. In the present study, we studied the detection of TEM-1 in tumors using 1C1m-Fc radiolabeled with ⁶⁴Cu for PET imaging. Another objective was to determine if [⁶⁴Cu]Cu-1C1m-Fc can predict the dosimetry of the [¹⁷⁷Lu]Lu-1C1m-Fc companion therapy.

1C1m-Fc was first conjugated to p-SCN-Bn-DOTA, as in the previous studies, with [¹⁷⁷Lu]Lu-1C1m-Fc [27,28]. In a theranostic approach, the same agent, antibody and chelator must be used for imaging and therapy. The intermediate half-life of ⁶⁴Cu (12.7 h) makes it compatible with the use of slow kinetic vectors such as antibodies. This radionuclide that emits both positrons and electrons is suitable for theranostic applications, and promising results have been obtained in recent preclinical and clinical trials [30,35–38]. DOTA-conjugated 1C1m-Fc was thus labeled with ⁶⁴Cu, and good radiochemical purity was achieved (RCP > 95%). Cu²⁺ ions are efficiently coordinated to the DOTA ligand through four nitrogen atoms and two oxygen atoms of the pendant carboxylic groups [39,40]. The number of DOTA conjugated, determined by mass spectrometry analysis, has been shown to have an impact of the antibody biodistribution. Thus, a DOTA-to-antibody ratio between 3 and 4 was used. This ratio was selected as the lowest that allows radiolabeling of the fusion protein antibody without final purification, taking into account the variability of the copper source specific activity, while not significantly altering the biodistribution, immunoreactivity and pharmacokinetic behavior of the radioimmunoconjugates [28]. In addition, the immunoreactivity of [⁶⁴Cu]Cu-1C1m-Fc was assessed using streptavidin-coated magnetic beads after incubation of the radiolabeled compound in serum to mimic the in vivo conditions. The immunoreactivity of [⁶⁴Cu]Cu-1C1m-Fc evaluated in serum remained stable and ≥70% from 4 to 48 h after radiolabeling, meaning that the conjugation and the radiolabeling process do not affect the binding properties.

High-quality PET/CT images were obtained after injection of [⁶⁴Cu]Cu-1C1m-Fc. The low energy positrons of ⁶⁴Cu result in a good spatial resolution and a high detection rate of positive lesions [39]. Furthermore, at later time points (24 and 48 h), the relatively

long half-life of ^{64}Cu enables tumor assessments when higher tumor-to-background ratios are reached. The presented results motivate the use of PET/CT imaging with [^{64}Cu]Cu-1C1m-Fc for the specific detection of TEM-1-positive tumors. A low but non-negligible uptake is also observed in the TEM-1-negative tumor. This may be explained by the known expression of TEM-1 in tumor neovessels and tumor stroma and by the cross-reactivity of the antibody with murine TEM-1 [41]. This visualization is allowed by the use of a fusion protein antibody that cross-reacts with both human and murine TEM-1. In this case, contrary to TEM-1-positive tumor, the antibody may not be retained by the tumor cells.

Biodistribution confirmed the imaging studies. Tumor uptake was maximum at 24 h ($24.5 \pm 1.5\%$ IA/g). A specific uptake was also found in the uterus, as this endometrial stroma expresses low levels TEM-1 antigen [42]. A rapid blood clearance was observed, and the tumor-to-organ ratios were high at 24 h. The uptake in the liver decreased between 4 h and 24 h. These biodistribution data, obtained with [^{64}Cu]Cu-1C1m-Fc, were compared to the previous results obtained with [^{177}Lu]Lu-1C1m-Fc (conjugated with 1 or 3 DOTA), and close profiles were obtained. Nevertheless, as ^{177}Lu and ^{64}Cu differ in charge, in coordination geometry and number to DOTA, the biodistribution of 1Cm-Fc conjugate radiolabeled with each of these radionuclide may be slightly different [43,44]. The difference of charge between the 3 DOTA conjugates radiolabeled with ^{177}Lu and ^{64}Cu results in a higher uptake for the copper compound in the tumor as described in Grunberg et al. [45].

The blood uptake obtained with [^{64}Cu]Cu-1C1m-Fc was closer to [^{177}Lu]Lu-1DOTA-1C1m-Fc. On the contrary, the hepatic distribution (with an accumulation) of the copper-radiolabeled conjugate is closer to the one of [^{177}Lu]Lu-3DOTA-1C1m-Fc. In this case, we supposed that 3 DOTA conjugate antibody (either radiolabeled with ^{177}Lu or ^{64}Cu) have a similar internalization into the hepatocytes.

Compared to both ^{177}Lu compounds, the % IA/g with [^{64}Cu]Cu-1C1m-Fc was higher in the gastrointestinal tract (stomach, small intestine and colon). The increased uptake can be explained by the hepatobiliary excretion of ^{64}Cu [46]. The absence of excretion from the liver and the gastrointestinal tract between 24 and 48 h could be explained by the transchelation of [$^{64}\text{Cu}^{2+}$] ions from the chelating agent to transport proteins [39]. DOTA-copper complexes have a good thermodynamic stability but seem to be not sufficiently inert under reducing or acidic conditions [47]. For [^{64}Cu]DOTA, our group have already demonstrated that almost all the activity was associated to metalloproteins [48]. Moreover, for 1C1m-Fc, our team previously demonstrated that 44% of the total bound activity is internalized after 24 h [49]. After internalization, ^{64}Cu is recycled through the transport proteins and metabolized. For ^{64}Cu conversely to ^{177}Lu , internalization is involved in recycling and, therefore, in nonspecific binding. Copper ions are described to have an important affinity for the endometrium [50]. Specific chelating agents such as TE1-PA [29,48] or sarcophagine (SAR) [51] have been developed that are able to form more stable copper complexes than DOTA, but, in a theranostic approach, it seems more adequate to use the very same compound for both imaging and therapy.

The possible use of ^{64}Cu -radiolabeled compounds in the imaging step to predict absorbed dose to tumors and dose-limiting organs for the same compound labeled with a therapeutic radioisotope (for instance ^{177}Lu) is of great interest. Thus, absorbed doses obtained experimentally in our previous studies with [^{177}Lu]Lu-1DOTA-1C1m-Fc or [^{177}Lu]Lu-3DOTA-1C1m-Fc [27,28] have been compared to extrapolated ones from the present [^{64}Cu]Cu-1C1m-Fc study.

Extrapolated ^{177}Lu absorbed doses (from ^{64}Cu mice data) for parenchymal organs (such as: liver, lung, spleen and kidneys) provided good predictive dosimetry values (relative differences within 20%) when compared with [^{177}Lu]Lu-1DOTA-1C1m-Fc. We obtained an inferior matching when comparing Lu-extrapolated organ doses with the [^{177}Lu]Lu-3DOTA-1C1m-Fc (up to 80% overestimation in lung). The observed discrepancy correlates with the data obtained in the biodistribution study.

A common feature is the higher extrapolated absorbed doses in the gastrointestinal tract than can be related to the known uptake in these tissues for the ^{64}Cu -radiolabeled compound compared to that of ^{177}Lu , as described previously [46].

^{177}Lu -absorbed dose extrapolations to the tumor and the uterus from the ^{64}Cu -radiolabeled compound are higher compared to published dosimetry data for [^{177}Lu]Lu-1DOTA-1C1m-Fc or [^{177}Lu]Lu-3DOTA-1C1m-Fc (around +50% and +100%, respectively). This overestimation is explained by the lack of later time acquisition points after 50 h for the ^{64}Cu -labeled compounds. For both the tumor and the uterus, the uptake in these TEM-1-expressing tissues is still not decreasing at 50 h postinjection (the last measured time point), and the extrapolation to infinity based on the physical decay of ^{177}Lu overestimates the actual value.

In future developments, it would be interesting to study the combination of TEM-1 and fibroblast-activated protein (FAP) targeting. Indeed, FAP inhibitors (FAPIs) target the tumor stroma, which is enriched in cancer-associated fibroblasts (CAFs), which are essential for proliferation and metastasis [52]. Contrary to FAPIs, radiolabeled 1C1m-Fc can target both microenvironment and tumor TEM-1-positive cells. Nevertheless, if the antibody quantity is too low, 1C1m-Fc could be blocked in the microenvironment, thereby reducing the quantity of anti-TEM-1 in the tumor and the antitumoral efficacy. The usage of these two approaches could thus be synergic. Similarly to 1C1m-Fc, FAPIs present an uptake in the endometrium that have to be taken into account. This uptake increases during the premenopausal and may be linked to the cyclic regeneration as FAPIs accumulate in tissue during the remodeling process [53].

5. Conclusions

In this study, we have demonstrated that [^{64}Cu]Cu-1C1m-Fc permits the visualization of TEM-1 expression with high resolution PET images and allows for the selection of patients who are candidates for [^{177}Lu]Lu-1C1m-Fc therapy. Furthermore, extrapolated dosimetry based on [^{64}Cu]Cu-1C1m-Fc data could be used as an indicator to predict the toxicity in parenchymal organs, as increased tissues-absorbed doses were measured in TEM-1-positive tissues.

1C1m-Fc radiolabeled with ^{64}Cu for imaging would appear as an interesting radionuclide companion for therapeutic application with [^{177}Lu]Lu-1C1m-Fc. In perspective, this work points out the importance of future developments, such as human dosimetry extrapolation studies, aiming at the assessment of treatment safety in patients for radiolabeled compounds targeting TEM-1.

6. Patents

J.K.F. and S.M.D. hold patents in the domain of antibodies and, in particular, on the 1C1m antibody used in this study.

Supplementary Materials: The following are available online at <https://www.mdpi.com/article/10.3390/cancers13235936/s1>, Figure S1: Mass spectra of 1C1m-Fc conjugated with DOTA (a) $\text{DAR}_{\text{avr}} = (0 \times 15 + 1 \times 60 + 2 \times 95 + 3 \times 90 + 4 \times 95 + 5 \times 55 + 6 \times 40 + 7 \times 15 + 8 \times 5) / (15 + 60 + 95 + 90 + 95 + 55 + 40 + 15 + 5) = 3$; (b) $\text{DAR}_{\text{avr}} = (0 \times 8 + 2 \times 80 + 3 \times 100 + 4 \times 75 + 5 \times 70 + 6 \times 70 + 7 \times 50) / (8 + 80 + 100 + 75 + 70 + 70 + 50) = 4$, Figure S2: Biodistribution of [^{64}Cu]Cu-1C1m in BALB/c nude mice bearing TEM-1-positive and negative tumor, group 2, Figure S3: Normalized time-activity curves for the considered source organs (experimental data in blue with respective \pm SD interval). Red lines represent monoexponential fitting curves obtained for source organ nTACs. The coefficient of determination (R^2) of the fit in respect to experimental data (blue dots) is also reported.

Author Contributions: Methodology, J.A.D., A.F.-C., S.G. (Silvano Gnesin) and J.B.; investigation, J.A.D., P.L.S. and S.M.-L.; data curation, J.A.D.; writing—original draft preparation, J.A.D., A.F.-C., S.G. (Silvano Gnesin) and J.B.; writing—review and editing, S.G. (Sébastien Gouard), S.M.D., N.S., M.B., J.K.F. and D.V.; supervision, A.F.-C. and J.O.P.; project administration, J.A.D.; funding acquisition, J.O.P.; N.S. and M.C. All authors have read and agreed to the published version of the manuscript.

Funding: This research was funded with the help of the Alfred and Annemarie von Sick Grant (Zurich, Switzerland) and the Department of Nuclear Medicine and Molecular Imaging, Lausanne University Hospital (Lausanne, Switzerland). This research was also funded in part by grants from the French National Agency for Research, called “Investissements d’Avenir” IRON LabEx n° ANR-11-LABX-0018-01, IGO LabEx n° ANR-11-LABX-0016-01, Siric ILIAD, DHU Oncogreff, ArronaxPlus Equipex n° ANR-11-EQPX-0004 and NExT n° ANR-16-IDEX-0007.

Institutional Review Board Statement: All animal experiments were conducted in compliance either with the Swiss regulations (cantonal authorization VD-2993) and the guidelines of the Lausanne University Hospital or with the French regulations and approved by the local animal ethics committee (APAFIS#6145). In this case, animals were housed under specific pathogen-free conditions in the UTE animal facility (SFR François Bonamy, IRS-UN, University of Nantes, license number: C-44-278).

Informed Consent Statement: Not applicable.

Data Availability Statement: The data presented in this study are available in article or Supplementary Materials here.

Acknowledgments: The authors thank the CIMA imaging facility (Nantes) and the IVIF platform (Lausanne) for expert technical assistance in PET imaging. We thank the Radioactivity platform (SFR Santé), for expert technical assistance. The authors thank the cyclotron Arronax for the supply of copper-64. The authors thank George Coukos (Ludwig Institute for Cancer Research and Department of Oncology, Lausanne University Hospital and University of Lausanne, CH-1011 Lausanne, Switzerland) for supporting this research work and participating in funding acquisition.

Conflicts of Interest: All authors declare that they have no conflict of interest.

References

- Filippi, L.; Chiaravalloti, A.; Schillaci, O.; Cianni, R.; Bagni, O. Theranostic Approaches in Nuclear Medicine: Current Status and Future Prospects. *Expert Rev. Med. Devices* **2020**, *17*, 331–343. [\[CrossRef\]](#)
- Keinänen, O.; Fung, K.; Brennan, J.M.; Zia, N.; Harris, M.; van Dam, E.; Biggin, C.; Hedt, A.; Stoner, J.; Donnelly, P.S.; et al. Harnessing⁶⁴Cu/⁶⁷Cu for a Theranostic Approach to Pretargeted Radioimmunotherapy. *Proc. Natl. Acad. Sci. USA* **2020**, *117*, 28316–28327. [\[CrossRef\]](#)
- Langbein, T.; Weber, W.A.; Eiber, M. Future of Theranostics: An Outlook on Precision Oncology in Nuclear Medicine. *J. Nucl. Med.* **2019**, *60*, 13S–19S. [\[CrossRef\]](#)
- Accorsi, R. Brain Single-Photon Emission CT Physics Principles. *Am. J. Neuroradiol.* **2008**, *29*, 1247–1256. [\[CrossRef\]](#)
- Jadvar, H.; Chen, X.; Cai, W.; Mahmood, U. Radiotheranostics in Cancer Diagnosis and Management. *Radiology* **2018**, *286*, 388–400. [\[CrossRef\]](#) [\[PubMed\]](#)
- Teicher, B.A. CD248: A Therapeutic Target in Cancer and Fibrotic Diseases. *Oncotarget* **2019**, *10*, 993–1009. [\[CrossRef\]](#)
- MacFadyen, J.R.; Haworth, O.; Roberston, D.; Hardie, D.; Webster, M.T.; Morris, H.R.; Panicoc, M.; Sutton-Smith, M.; Dell, A.; van der Geer, P.; et al. Endosialin (TEM1, CD248) is a Marker of Stromal Fibroblasts and is not Selectively Expressed on Tumour Endothelium. *FEBS Lett.* **2005**, *579*, 2569–2575. [\[CrossRef\]](#) [\[PubMed\]](#)
- Tomkowicz, B.; Rybinski, K.; Foley, B.; Ebel, W.; Kline, B.; Routhier, E.; Sass, P.; Nicolaidis, N.C.; Grasso, L.; Zhou, Y. Interaction of Endosialin/TEM1 with Extracellular Matrix Proteins Mediates Cell Adhesion and Migration. *Proc. Natl. Acad. Sci. USA* **2007**, *104*, 17965–17970. [\[CrossRef\]](#) [\[PubMed\]](#)
- Simonavicius, N.; Robertson, D.; Bax, D.A.; Jones, C.; Huijbers, I.J.; Isacke, C. Endosialin (CD248) is a Marker of Tumor-Associated Pericytes in High-Grade Glioma. *Mod. Pathol.* **2008**, *21*, 308–315. [\[CrossRef\]](#)
- MacFadyen, J.; Savage, K.; Wienke, D.; Isacke, C.M. Endosialin Is Expressed on Stromal Fibroblasts and CNS Pericytes in Mouse Embryos and is Downregulated during Development. *Gene Expr. Patterns* **2007**, *7*, 363–369. [\[CrossRef\]](#)
- Davies, G.; Cunnick, G.H.; Mansel, R.E.; Mason, M.D.; Jiang, W.G. Levels of Expression of Endothelial Markers Specific to Tumour-Associated Endothelial Cells and their Correlation with Prognosis in Patients with Breast Cancer. *Clin. Exp. Metastasis* **2004**, *21*, 31–37. [\[CrossRef\]](#)
- O’Shannessy, D.J.J.; Somers, E.B.; Chandrasekaran, L.K.; Nicolaidis, N.C.; Bordeaux, J.; Gustavson, M.D. Influence of Tumor Microenvironment on Prognosis in Colorectal Cancer: Tissue Architecture-Dependent Signature of Endosialin (TEM-1) and Associated Proteins. *Oncotarget* **2014**, *5*, 3983–3995. [\[CrossRef\]](#) [\[PubMed\]](#)

13. Maia, M.; Conway, E. CD248: Reviewing its Role in Health and Disease. *Curr. Drug Targets* **2012**, *13*, 432–439. [[CrossRef](#)]
14. Rouleau, C.; Gianolio, D.A.; Smale, R.; Roth, S.D.; Krumbholz, R.; Harper, J.; Munroe, K.J.; Green, T.L.; Horten, B.C.; Schmid, S.M.; et al. Anti-Endosialin Antibody–Drug Conjugate: Potential in Sarcoma and Other Malignancies. *Mol. Cancer Ther.* **2015**, *14*, 2081–2089. [[CrossRef](#)]
15. Thomas, A.; Teicher, B.A.; Hassan, R. Antibody–Drug Conjugates for Cancer Therapy. *Lancet Oncol.* **2016**, *17*, e254–e262. [[CrossRef](#)]
16. Li, C.; Wang, J.; Hu, J.; Feng, Y.; Hasegawa, K.; Peng, X.; Duan, X.; Zhao, A.; Mikitsch, J.L.; Muzykantov, V.R.; et al. Development, Optimization, and Validation of Novel anti-TEM1/CD248 Affinity Agent for Optical Imaging in Cancer. *Oncotarget* **2014**, *5*, 6994–7012. [[CrossRef](#)]
17. Zhao, A.; Nunez-Cruz, S.; Li, C.; Coukos, G.; Siegel, D.L.; Scholler, N. Rapid Isolation of High-Affinity Human Antibodies Against the Tumor Vascular Marker Endosialin/TEM1, Using a Paired Yeast-Display/Secretory Scfv Library Platform. *J. Immunol. Methods* **2011**, *363*, 221–232. [[CrossRef](#)] [[PubMed](#)]
18. Cicone, F.; Denoel, T.; Gnesin, S.; Riggi, N.; Irving, M.; Jakka, G.; Schaefer, N.; Viertl, D.; Coukos, G.; Prior, J.O. Preclinical Evaluation and Dosimetry of [(111)In]CHX-DTPA-scFv78-Fc Targeting Endosialin/Tumor Endothelial Marker 1 (TEM1). *Mol. Imaging Biol.* **2020**, *22*, 979–991. [[CrossRef](#)]
19. Chacko, A.M.; Li, C.; Nayak, M.; Mikitsch, J.L.; Hu, J.; Hou, C.; Grasso, L.; Nicolaidis, N.C.; Muzykantov, V.R.; Divgi, C.R.; et al. Development of 124I Immuno-PET Targeting Tumor Vascular TEM1/Endosialin. *J. Nucl. Med.* **2014**, *55*, 500–507. [[CrossRef](#)] [[PubMed](#)]
20. Lange, S.E.; Zheleznyak, A.; Studer, M.; O’Shannessy, D.J.; Lapi, S.E.; Van Tine, B.A. Development of 89Zr-Ontuxizumab for in vivo TEM-1/endosialin PET Applications. *Oncotarget* **2016**, *7*, 13082–13092. [[CrossRef](#)] [[PubMed](#)]
21. Grothey, A.; Strosberg, J.R.; Renfro, L.A.; Hurwitz, H.I.; Marshall, J.L.; Safran, H.; Guarino, M.J.; Kim, J.P.; Hecht, J.R.; Weil, S.C.; et al. A Randomized, Double-Blind, Placebo–Controlled Phase II Study of the Efficacy and Safety of Monotherapy Ontuxizumab (MORAb-004) Plus Best Supportive Care in Patients with Chemorefractory Metastatic Colorectal Cancer. *Clin. Cancer Res.* **2018**, *24*, 316–325. [[CrossRef](#)] [[PubMed](#)]
22. Norris, R.E.; Fox, E.; Reid, J.M.; Ralya, A.; Liu, X.W.; Minard, C.; Weigel, B.J. Phase 1 Trial of Ontuxizumab (MORAb-004) in Children with Relapsed or Refractory Solid Tumors: A Report from the Children’s Oncology Group Phase 1 Pilot Consortium (ADVL1213). *Pediatr. Blood Cancer.* **2018**, *65*, e26944. [[CrossRef](#)] [[PubMed](#)]
23. Diaz, L.A.; Coughlin, C.M.; Weil, S.C.; Fishel, J.; Gounder, M.M.; Lawrence, S.; Azad, N.; O’Shannessy, D.J.; Grasso, L.; Wustner, J.; et al. A First-in-Human Phase I Study of MORAb-004, a Monoclonal Antibody to Endosialin in Patients with Advanced Solid Tumors. *Clin. Cancer Res.* **2015**, *21*, 1281–1288. [[CrossRef](#)] [[PubMed](#)]
24. Bourgeois, M.; Bailly, C.; Frindel, M.; Guérard, F.; Chérel, M.; Faivre-Chauvet, A.; Kraeber-Bodéré, F.; Bodet-Milin, C. Radioimmunoconjugates for Treating Cancer: Recent Advances and Current Opportunities. *Expert Opin. Biol. Ther.* **2017**, *17*, 813–819. [[CrossRef](#)]
25. Puvvada, S.D.; Guillen-Rodriguez, J.M.; Yan, J.; Inclan, L.; Heard, K.; Rivera, X.I.; Answer, F.; Mahadevan, D.; Schatz, J.H.; Persky, D.O. Yttrium-90-Ibritumomab Tiuxetan (Zevalin (R)) Radioimmunotherapy after Cytoreduction with ESHAP Chemotherapy in Patients with Relapsed Follicular Non-Hodgkin Lymphoma: Final Results of a Phase II Study. *Oncol. Basel* **2018**, *94*, 274–280. [[CrossRef](#)]
26. Caserta, E.; Chea, J.; Minnix, M.; Poku, E.K.; Viola, D.; Vonderfecht, S.; Yazaki, P.; Crow, D.; Khalife, J.; Sanchez, J.F.; et al. Copper 64-Labeled Daratumumab as a PET/CT Imaging Tracer for Multiple Myeloma. *Blood* **2018**, *131*, 741–745. [[CrossRef](#)]
27. Delage, J.A.; Faivre-Chauvet, A.; Fierle, J.K.; Gnesin, S.; Schaefer, N.; Coukos, G.; Dunn, M.; Viertl, D.S.; Prior, J.O. (177) Lu Radiolabeling and Preclinical Theranostic Study of 1C1m-Fc: An Anti-TEM-1 scFv-Fc Fusion Protein in Soft Tissue Sarcoma. *EJNMMI Res.* **2020**, *10*, 98. [[CrossRef](#)]
28. Delage, J.A.; Faivre-Chauvet, A.; Barbet, J.; Fierle, J.K.; Schaefer, N.; Coukos, G.; Dunn, M.; Viertl, D.S.; Prior, J.O. Impact of DOTA Conjugation on Pharmacokinetics and Immunoreactivity of [(177)Lu]Lu-1C1m-Fc, an Anti TEM-1 Fusion Protein Antibody in a TEM-1 Positive Tumor Mouse Model. *Pharmaceutics* **2021**, *13*, 96. [[CrossRef](#)]
29. Navarro, A.S.; Le Bihan, T.; Le Saec, P.; Bris, N.L.; Bailly, C.; Sai-Maurel, C.; Bourgeois, M.; Chérel, M.; Tripier, R.; Faivre-Chauvet, A. TE1PA as Innovating Chelator for (64)Cu Immuno-TEP Imaging: A Comparative In Vivo Study with DOTA/NOTA by Conjugation on 9E7.4 mAb in a Syngeneic Multiple Myeloma Model. *Bioconjug. Chem.* **2019**, *30*, 2393–2403. [[CrossRef](#)]
30. Mortimer, J.E.; Bading, J.R.; Colcher, D.M.; Conti, P.S.; Frankel, P.H.; Carroll, M.I.; Tong, S.; Poku, E.; Miles, J.K.; Shively, J.E.; et al. Functional Imaging of Human Epidermal Growth Factor Receptor 2-Positive Metastatic Breast Cancer Using (64)Cu-DOTA-trastuzumab PET. *J. Nucl. Med.* **2014**, *55*, 23–29. [[CrossRef](#)]
31. Fierle, J.K.; Abram-Saliba, J.; Brioschi, M.; Detiani, M.; Coukos, G.; Dunn, S.M. Integrating SpyCatcher/SpyTag Covalent Fusion Technology into Phage Display Workflows for Rapid Antibody Discovery. *Sci. Rep.* **2019**, *9*, 1–15. [[CrossRef](#)] [[PubMed](#)]
32. Liu, S.; Li, D.; Park, R.; Liu, R.; Xia, Z.; Guo, J.; Krasnoperov, V.; Gill, P.S.; Li, Z.; Shan, H.; et al. PET Imaging of Colorectal and Breast Cancer by Targeting EphB4 Receptor with 64Cu-Labeled hAb47 and hAb131 Antibodies. *J. Nucl. Med.* **2013**, *54*, 1094–1100. [[CrossRef](#)]
33. Christian, S.; Winkler, R.; Helfrich, I.; Boos, A.M.; Besemfelder, E.; Schadendorf, D.; Augustin, H.G. Endosialin (Tem1) Is a Marker of Tumor-Associated Myofibroblasts and Tumor Vessel-Associated Mural Cells. *Am. J. Pathol.* **2008**, *172*, 486–494. [[CrossRef](#)] [[PubMed](#)]

34. Christian, S.; Ahorn, H.; Koehler, A.; Eisenhaber, F.; Rodi, H.-P.; Garin-Chesa, P.; Park, J.E.; Rettig, W.J.; Lenter, M.C. Molecular Cloning and Characterization of Endosialin, a C-type Lectin-like Cell Surface Receptor of Tumor Endothelium. *J. Biol. Chem.* **2001**, *276*, 7408–7414. [[CrossRef](#)]
35. Qin, C.; Liu, H.; Chen, K.; Hu, X.; Ma, X.; Lan, X.; Zhang, Y.; Cheng, Z. Theranostics of Malignant Melanoma with $^{64}\text{CuCl}_2$. *J. Nucl. Med.* **2014**, *55*, 812–817. [[CrossRef](#)]
36. Chakravarty, R.; Chakraborty, S.; Dash, A. $^{64}\text{Cu}_{2+}$ Ions as PET Probe: An Emerging Paradigm in Molecular Imaging of Cancer. *Mol. Pharm.* **2016**, *13*, 3601–3612. [[CrossRef](#)]
37. Johnbeck, C.B.; Knigge, U.; Loft, A.; Berthelsen, A.K.; Mortensen, J.; Oturai, P.; Langer, S.W.; Elema, D.R.; Kjaer, A. Head-to-Head Comparison of ^{64}Cu -DOTATATE and ^{68}Ga -DOTATOC PET/CT: A Prospective Study of 59 Patients with Neuroendocrine Tumors. *J. Nucl. Med.* **2017**, *58*, 451–457. [[CrossRef](#)]
38. Piccardo, A.; Paparo, F.; Puntoni, M.; Righi, S.; Bottoni, G.; Bacigalupo, L.; Zanardi, S.; DeCensi, A.; Ferrarazzo, G.; Gambaro, M.; et al. $^{64}\text{CuCl}_2$ PET/CT in Prostate Cancer Relapse. *J. Nucl. Med.* **2017**, *59*, 444–451. [[CrossRef](#)]
39. Boschi, A.; Martini, P.; Janevik-Ivanovska, E.; Duatti, A. The Emerging Role of Copper-64 Radiopharmaceuticals as Cancer Theranostics. *Drug Discov. Today* **2018**, *23*, 1489–1501. [[CrossRef](#)] [[PubMed](#)]
40. Wadas, T.; Wong, E.H.; Weisman, G.R.; Anderson, C.J. Coordinating Radiometals of Copper, Gallium, Indium, Yttrium, and Zirconium for PET and SPECT Imaging of Disease. *Chem. Rev.* **2010**, *110*, 2858–2902. [[CrossRef](#)]
41. Dolznig, H.; Schweifer, N.; Puri, C.; Kraut, N.; Rettig, W.J.; Kerjaschki, D.; Garin-Chesa, P. Characterization of Cancer Stroma Markers: In Silico Analysis of an mRNA Expression Database for Fibroblast Activation Protein and Endosialin. *Cancer Immun.* **2005**, *5*, 10.
42. Opavsky, R.; Haviernik, P.; Jurkovicova, D.; Garin, M.T.; Copeland, N.G.; Gilbert, D.J.; Jenkins, N.A.; Bies, J.; Garfield, S.; Pastorekova, S.; et al. Molecular Characterization of the Mouse Tem1/Endosialin Gene Regulated by Cell Density In Vitro and Expressed in Normal Tissues In Vivo. *J. Biol. Chem.* **2001**, *276*, 38795–38807. [[CrossRef](#)] [[PubMed](#)]
43. Rinne, S.S.; Leitao, C.D.; Gentry, J.; Mitran, B.; Abouzayed, A.; Tolmachev, V.; Ståhl, S.; Löfblom, J.; Orlova, A. Increase in Negative Charge of ^{68}Ga /Chelator Complex Reduces Unspecific Hepatic Uptake but does not Improve Imaging Properties of HER3-targeting Affibody Molecules. *Sci. Rep.* **2019**, *9*, 17710. [[CrossRef](#)]
44. Cooper, M.S.; Ma, M.T.; Sunassee, K.; Shaw, K.P.; Williams, J.D.; Paul, R.L.; Donnelly, P.S.; Blower, P.J. Comparison of (^{64}Cu) -Complexing Bifunctional Chelators for Radioimmunoconjugation: Labeling Efficiency, Specific Activity, and In Vitro/In Vivo Stability. *Bioconjug. Chem.* **2012**, *23*, 1029–1039. [[CrossRef](#)]
45. Grunberg, J.; Jeger, S.; Sarko, D.; Dennler, P.; Zimmermann, K.; Mier, W.; Schibli, R. DOTA-Functionalized Polylysine: A High Number of DOTA Chelates Positively Influences the Biodistribution of Enzymatic Conjugated Anti-Tumor Antibody chCE7agl. *PLoS ONE* **2013**, *8*, e60350. [[CrossRef](#)]
46. Capasso, E.; Durzu, S.; Piras, S.; Zandieh, S.; Knoll, P.; Haug, A.; Hacker, M.; Meleddu, C.; Mirzaei, S. Role of $^{64}\text{CuCl}_2$ PET/CT in Staging of Prostate Cancer. *Ann. Nucl. Med.* **2015**, *29*, 482–488. [[CrossRef](#)] [[PubMed](#)]
47. Cai, Z.; Anderson, C.J. Chelators for Copper Radionuclides in Positron Emission Tomography Radiopharmaceuticals. *J. Label. Compd. Radiopharm.* **2014**, *57*, 224–230. [[CrossRef](#)]
48. Frindel, M.; Camus, N.; Rauscher, A.; Bourgeois, M.; Alliot, C.; Barré, L.; Gestin, J.-F.; Tripier, R.; Faivre-Chauvet, A. Radiolabeling of HTE1PA: A New Monopicolinate Cyclam Derivative for Cu-64 Phenotypic Imaging. In vitro and In Vivo Stability Studies in Mice. *Nucl. Med. Biol.* **2014**, *41*, e49–e57. [[CrossRef](#)] [[PubMed](#)]
49. D’Onofrio, A.; Gano, L.; Melo, R.; Mendes, F.; Oliveira, M.C.; Denoël, T.; Schaefer, N.; Viertl, D.; Fierle, J.; Coukos, G.; et al. Biological Evaluation of New TEM1 Targeting Recombinant Antibodies for Radioimmunotherapy: In Vitro, In Vivo and in Silico Studies. *Eur. J. Pharm. Biopharm.* **2021**, *158*, 233–244. [[CrossRef](#)]
50. Pérez-Debén, S.; Gonzalez-Martin, R.; Palomar, A.; Quiñonero, A.; Salsano, S.; Dominguez, F. Copper and Lead Exposures Disturb Reproductive Features of Primary Endometrial Stromal and Epithelial Cells. *Reprod. Toxicol.* **2020**, *93*, 106–117. [[CrossRef](#)]
51. Cai, H.; Li, Z.; Huang, C.-W.; Park, R.; Shahinian, A.H.; Conti, P.S. An Improved Synthesis and Biological Evaluation of a New Cage-Like Bifunctional Chelator, 4-((8-amino-3,6,10,13,16,19-hexaazabicyclo[6.6.6]icosane-1-ylamino)methyl)benzoic acid, for ^{64}Cu Radiopharmaceuticals. *Nucl. Med. Biol.* **2010**, *37*, 57–65. [[CrossRef](#)]
52. Shi, X.; Xing, H.; Yang, X.; Li, F.; Yao, S.; Zhang, H.; Zhao, H.; Hacker, M.; Huo, L.; Li, X. Fibroblast Imaging of Hepatic Carcinoma with ^{68}Ga -FAPI-04 PET/CT: A Pilot Study in Patients with Suspected Hepatic Nodules. *Eur. J. Nucl. Med. Mol. Imaging* **2021**, *48*, 196–203. [[CrossRef](#)]
53. Dendl, K.; Koerber, S.A.; Finck, R.; Mokoala, K.M.G.; Staudinger, F.; Schillings, L.; Heger, U.; Röhrich, M.; Kratochwil, C.; Sathekge, M.; et al. ^{68}Ga -FAPI-PET/CT in Patients with Various Gynecological Malignancies. *Eur. J. Nucl. Med. Mol. Imaging* **2021**, *48*, 4089–4100. [[CrossRef](#)]

